MECHANICAL AND THERMO-PHYSICAL PROPERTIES OF POLYMESODA BENGALENSIS REINFORCED POLYMER-MATRIX COMPOSITES

MAHSHURI BINTI YUSOF

FACULTY OF ENGINEERING
UNIVERSITY OF MALAYA
KUALA LUMPUR

2018

MECHANICAL AND THERMO-PHYSICAL PROPERTIES OF POLYMESODA BENGALENSIS REINFORCED POLYMER-MATRIX COMPOSITES

MAHSHURI BINTI YUSOF

THESIS SUBMITTED IN FULFILMENT OF THE REQUIREMENTS FOR THE DEGREE OF DOCTOR OF PHILOSOPHY

FACULTY OF ENGINEERING
UNIVERSITY OF MALAYA
KUALA LUMPUR

2018

UNIVERSITY OF MALAYA
ORIGINAL LITERARY WORK DECLARATION

Name of Candidate: Mahshuri binti Yusof

Matric No: KHA110019

Name of Degree: The Degree of Doctor Philosophy

Title of Project Paper/Research Report/Dissertation/Thesis ("this Work"): Mechanical and thermo-physical properties of polymesoda bengalensis reinforced polymer-matrix composites

Field of Study: Material Engineering

I do solemnly and sincerely declare that:

(1) I am the sole author/writer of this Work;
(2) This Work is original;
(3) Any use of any work in which copyright exists was done by way of fair dealing and for permitted purposes and any excerpt or extract from, or reference to or reproduction of any copyright work has been disclosed expressly and sufficiently and the title of the Work and its authorship have been acknowledged in this Work;
(4) I do not have any actual knowledge nor do I ought reasonably to know that the making of this work constitutes an infringement of any copyright work;
(5) I hereby assign all and every rights in the copyright to this Work to the University of Malaya ("UM"), who henceforth shall be owner of the copyright in this Work and that any reproduction or use in any form or by any means whatsoever is prohibited without the written consent of UM having been first had and obtained;
(6) I am fully aware that if in the course of making this Work I have infringed any copyright whether intentionally or otherwise, I may be subject to legal action or any other action as may be determined by UM.

Candidate's Signature Date:

Subscribed and solemnly declared before,

Witness's Signature Date:

Name:

Designation:

MECHANICAL AND THERMO-PHYSICAL PROPERTIES OF POLYMESODA BENGALENSIS REINFORCED POLYMER-MATRIX COMPOSITES

ABSTRACT

The main objective of this research is to investigate the effect of including calcium carbonate ($CaCO_3$) from *lokan*, a local clam shell, in varying micron sizes and particle contents to unsaturated polyester (UPE) on the mechanical and thermophysical properties of UPE/$CaCO_3$ composites. The first part of this research involves characterizing the particle of *lokan* clam shell, which is scientifically known as *Polymesoda bengalensis*. The polymorph of the particle is identified by X-ray diffraction (XRD) and its morphology is observed by scanning electron microscope (SEM). The study reveals that the particle consists entirely of $CaCO_3$ of aragonite polymorph. The SEM indicates that the aragonite is in the form of rod-like crystals. The filler used for this study, aragonite $CaCO_3$, is ground and graded into eight different mean sizes, treated with 1 wt% stearic acid, then reinforced into UPE resin. The samples are fabricated through ultrasonication and open molding method at room temperature according to the different filler weight fractions (2, 4, 6 and 8 wt%) and sizes. Tensile, compressive and flexural tests are done according to ASTM D638, ASTM D695 and ASTM D790, respectively. Vickers hardness testing is conducted at 245.2 mN for a 20 seconds indentation period. The Tabor number, or correlation between hardness and ultimate compressive strength, H/σ_y is then measured. The results signify that including aragonite $CaCO_3$ in the UPE matrix greatly improves the tensile modulus, compressive modulus and flexural modulus. The stiffness increases with decreasing filler size and increasing filler content owing to the better particles-networks produced in these conditions. In addition, an increment in tensile and compressive strengths is also achieved as the filler size decreases and filler loading increases. Finer filler provides larger interfacial areas for the particles to withstand higher loads, hence improving the tensile and compressive strengths. However, including aragonite $CaCO_3$ in the UPE matrix is not very helpful in enhancing the flexural strength, except for the smallest filler size (29.84 µm). In all cases, the $CaCO_3$ filler modified with stearic acid improves the mechanical performance of UPE/$CaCO_3$ composites more than untreated filler. In terms of surface hardness, the UPE hardness improves as untreated $CaCO_3$ filler is infused into the matrix. The Tabor number of all samples is found to be lower than 3. The modified $CaCO_3$ filler, however, softens the sample surface, thus reducing the Tabor number. The steady-state thermal conductivity of the samples is measured according to ASTM E1225-99. The thermal conductivity of the UPE/$CaCO_3$ composites increases gradually as the filler size decreases and filler content increases. Adding filler content reduces the filler size and does not make the aragonite helpful in raising the specific heat of UPE/$CaCO_3$ composites. Thermal diffusivity appears better with finer filler size and greater filler content. Treatment with 1 wt% stearic acid is only effective for coarser filler of 206.55 µm and more. In conclusion, this study demonstrates that $CaCO_3$ derived from *lokan* shell waste has great potential to replace commercial $CaCO_3$ owing to its effect of enhancing the mechanical performance and thermal conductivity of particulate-filled polymer matrix composites.

Keywords: Mechanical properties; Thermo-physical properties; Particle-reinforced composites; $CaCO_3$ filler; Stearic-acid coating.

MECHANICAL AND THERMO-PHYSICAL PROPERTIES OF POLYMESODA BENGALENSIS REINFORCED POLYMER-MATRIX COMPOSITES

ABSTRAK

Tujuan utama kajian ini dilakukan ialah untuk melihat sejauh mana keberkesanan memasukkan serbuk kalsium karbonat ($CaCO_3$) yang diperolehi daripada kulit cengkerang ke dalam poliester tak tepu (UPE) dalam pelbagai saiz berjulat mikro dan berlainan nisbah kandungan. Kajian tertumpu kepada ciri-ciri mekanikal dan termo-fisikal bahan komposit tersebut. Bahagian pertama kajian ini melibatkan pencirian serbuk cengkerang *lokan* atau turut dikenali dengan nama saintifik sebagai *Polymesoda bengalensis*. Polimorf serbuk kulit *lokan* telah dikenalpasti melalui teknik pembelaun X-ray (XRD) dan ciri morfologinya diperhatikan melalui mikroskop elektron pengimbas (SEM). Keputusan menunjukkan serbuk cengkerang *lokan* mengandungi $CaCO_3$ daripada jenis kristal (polimorf) aragonite. Pemerhatian melalui SEM pula menunjukkan kristal aragonite tersebut wujud dalam bentuk rod. Butiran penguat yang dipilih dalam kajian ini iaitu $CaCO_3$ aragonite telah dikisar dan digredkan kepada lapan saiz purata yang berbeza, dirawat dengan 1% berat asid stearik, dan kemudian dimasukkan ke dalam matrik UPE. Proses penghasilan sampel ialah melalui gabungan kaedah ultrasonikasi dan acuan terbuka yang dilakukan pada suhu bilik mengikut nisbah pengisi dalam berat (2, 4, 6 dan 8% mengikut berat) dan saiz bahan pengisi yang berlainan. Ujian ketegangan, mampatan dan lenturan telah dilakukan masing-masing mengikut garis panduan seperti yang terkandung dalam ASTM D638, ASTM D695 dan ASTM D790. Ujian kekerasan Vicker pula dijalankan pada 245.2mN selama 20 saat tempoh lekukan. Nombor Tabor atau nisbah kekerasan kepada kekuatan mampatan kemudiannya dikira. Keputusan ujian menunjukkan bahawa memasukkan serbuk $CaCO_3$ aragonite ke dalam medium UPE mampu meningkatkan kekenyalan bahan komposit baik dalam keadaan tegangan, mampatan mahupun lenturan. Kekenyalan komposit meningkat dengan pengecilan saiz dan peningkatan kandungan pengisi. Ini disebabkan dalam keadaan tersebut rangkaian antara bahan penguat amat baik. Di samping itu, kekuatan tegangan dan mampatan turut meningkat sekiranya saiz bahan penguat semakin kecil dan nisbah kandungan bertambah. Semakin kecil saiz bahan penguat, semakin besar luas permukaan partikel tersebut bagi memudahkan proses pemindahan tekanan dan seterusnya meningkatkan nilai kekuatan tegangan dan mampatan bahan komposit tersebut. Walau bagaimanapun, ia tidak membantu dalam meningkatkan kekuatan lenturan kecuali bagi bahan pengisi yang bersaiz paling kecil iaitu 29.84 µm. Dalam semua keadaan, merawat permukaan bahan pengisi dengan 1% berat asid stearik dapat meningkatkan prestasi mekanikal bahan komposit berbanding dengan bahan pengisi tidak dirawat. Dari aspek kekerasan permukaan, kekerasan asal bahan matrik UPE dipertingkatkan sebaik sahaja bahan pengisi $CaCO_3$ yang tidak dirawat dimasukkan ke dalam matriks. Nilai nombor Tabor bagi kesemua sampel didapati lebih rendah daripada nilai 3. Merawat pengisi $CaCO_3$ dengan asid stearik bagaimanapun dapat melembutkan permukaan sampel dan seterusnya mengurangkan lagi nilai nombor Tabor itu. Pengaliran haba sehingga mencapai keadaan stabil bagi sampel tersebut diukur dengan menggunakan kaedah meter aliran haba mengikut garis panduan ASTM E1225-99. Nilai konduksi haba bagi komposit UPE/$CaCO_3$ didapati meningkat dengan pengecilan saiz dan peningkatan kandungan bahan pengisi. Kesimpulannya $CaCO_3$ yang diperoleh daripada bahan buangan daripada sumber makanan laut iaitu kulit cengkerang *lokan* mempunyai potensi yang besar bagi menggantikan $CaCO_3$ komersial. Ini adalah kerana ia menghasilkan kesan positif dalam meningkatkan prestasi mekanikal dan nilai konduksi haba bahan komposit tersebut

Keywords: Ciri-ciri mekanikal; Ciri-ciri termofisikal; Komposit partikel yang diperkuat; Pengisi $CaCO_3$; Rawatan asid stearik.

ACKNOWLEDGEMENTS

In the name of Allah, the Most Gracious and the Most Merciful. Alhamdulillah, all praises to Allah for the strength and His blessing to complete this thesis. Special appreciation to my supervisor, Assoc. Prof. Dr. Amalina Muhammad Afifi for her aspiring guidance, advice and patience. Without her support, this thesis would not have been possible.

My acknowledgement also goes to all the technicians and staff from the Department of Mechanical Engineering for their co-operation. I particularly wish to thank Mr. Asri, Mr. Aziz and Mdm. Hartini for their assistance with my laboratory work.

Sincere thanks to all my friends in Block Q: Syukriyah, Nurin, Rinie, Wahid, Mia, Nad, Pia, Jess, Yuen, Natalina, Chai, Zira, Atikah and Nurul for sharing ideas and for their moral support throughout my study. Thanks for the friendship and memories.

To my beloved husband, Md Hafiz Ahmad, thank you for your love and great help. My deepest gratitude also goes to my beloved parents, Allahyarham Yusof Hj Sapiee and Zubaidah Hj Razali. And not forgetting my beloved children, Faezul Amir, Zahra Sufi, Zahirah Sofea, Hani Fatini and Hana Humaira for their love.

Finally, this research would not have been possible without the financial support from the SLAI scholarship, Universiti Malaysia Sarawak (Unimas) and research grant PV096/2012A (PPP), University of Malaya. Thank you very much for all the contributions.

With love,

Mahshuri Yusof

August, 2018

TABLE OF CONTENTS

LIST OF FIGURES

LIST OF TABLES

LIST OF SYMBOLS AND ABBREVIATIONS

UPE : Unsaturated Polyester

SMC : Sheet Moulding Compound

BMC : Bulk Moulding Compound

PP : Polypropylene

LDPE : Low Density Polyethylene

HDPE : High Density Polyethylene

ABS : Acrylonitrile Butadiene Styrene

HA : Hydroxyapatite

EVA : Ethylene Vinyl Acetate

EPDM : Ethylenepropylene Diene Monomer

PBT : Polybutylene Terephthalate

MEKP : Methyl Ethyl Ketone Peroxide

NPCC : Nano-sized Precipitated Calcium Carbonate

MCC : Micron-sized Calcium Carbonate

H : Hardness

HV : Vickers Hardness number

UTS : Ultimate Tensile Strength

XRD : X-ray Diffraction

SEM : Scanning Electron Microscopy

TEM : Transmission Electron Microscopy

DSC : Differential Scanning Calorimetry

TGA : Thermal Gravimetric Analysis

DTG : Differential Thermal Gravimetric Analysis

BET : Brunauer-Emmett-Teller

EDX	:	Energy Dispersive X-ray Analyser
EDXS	:	Energy Dispersive X-ray Spectroscopy
ASTM	:	American Society for Testing and Materials
O	:	Oxygen
C	:	Carbon
Cu	:	Copper
Zn	:	Zinc
Cd	:	Cadmium
Cr	:	Chromium
Mn	:	Manganese
Hg	:	Mercury
Ni	:	Nickel
As	:	Arsenic
Ag	:	Silver
Pb	:	Plumbum, Lead
Mg	:	Magnesium
Ca	:	Calcium
Co	:	Cobalt
$CaCO_3$	:	Calcium Carbonate
SiO_2	:	Silicon dioxide, Silica
$Mg(OH)_2$	:	Magnesium hydroxide
Al_2O_3	:	Aluminum oxide, Alumina
$wt\%$	:	Weight percent
$vol\%$	:	Volume percent
σ	:	Strength
F	:	Load

σ_y : Yield Strength

σ_{UTS} : Ultimate tensile strength

Pa : Pascal

k_c : Thermal conductivity

Q : Amount of heat transfer

α : Thermal diffusivity

C_p : Specific heat capacity

ρ : Density

T : Temperature

A : Area

V : Volume

m : Mass

T_d : Decomposition temperature

ΔH_R : Heat of reaction

X_c : Degree of crystallinity

LIST OF APPENDICES

CHAPTER 1: INTRODUCTION

1.1 Introduction

A composite is defined as a material that consists of a combination of two or more constituents with an interface separating them; the constituents differ in form and chemical composition and are essentially insoluble in each other (Callister & Rethwisch, 2012). Most composite materials contain two phases. The continuous phase is a matrix while the other phase is the reinforcement, or dispersed phase. The reinforcement can be in three forms, namely particulate, fibrous or structural. Figure 1.1 shows a classification of composite materials.

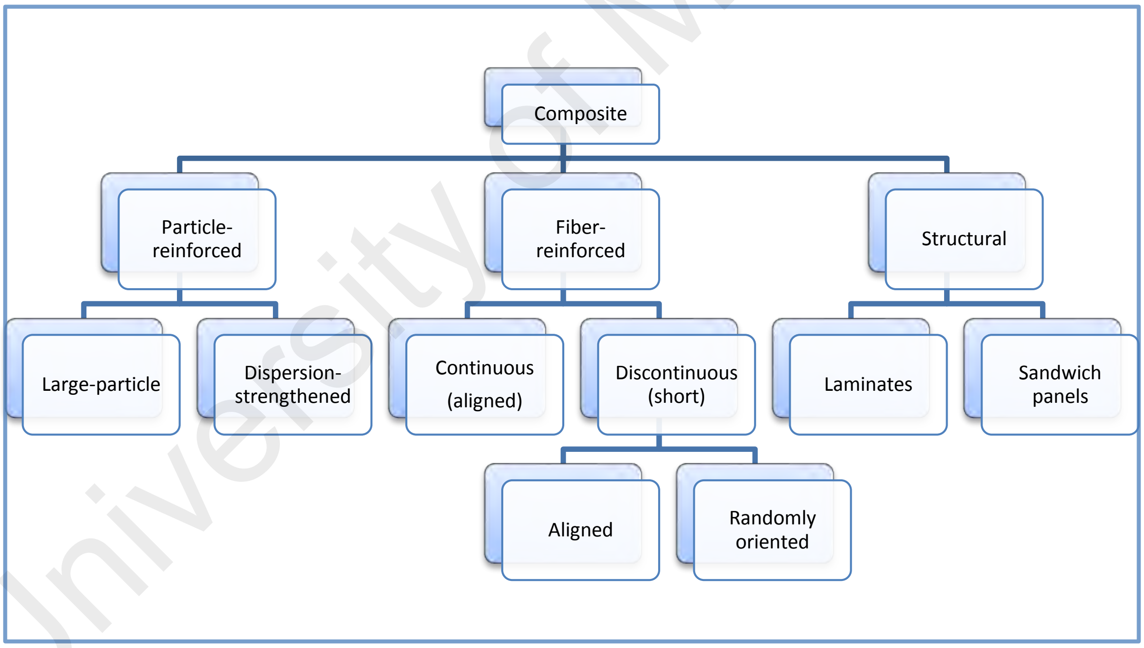

Figure 1.1: A classification of composite materials

(Callister & Rethwisch, 2012)

A particulate polymer composite consists of tiny particles of one material embedded in a polymer matrix. The particles can be categorized into two main groups, large particles and dispersion-strengthened particles (Callister & Rethwisch, 2012). Large particles are those that cannot interact with the matrix at the atomic or molecular levels, whereas dispersion-strengthened particle have diameters between 10 and 100 nm. In this size range, a strengthening mechanism occurs on the atomic or molecular level. Otterstedt and Brandreth (1998) classified particles that act as filler in the matrix phase as ultrafine, fine, medium and coarse filler, depending on the mean diameter of the particles (filler) as shown in Table 1.1.

Table 1.1: Classification of filler by mean diameter size (Otterstedt & Brandreth, 1998)

Filler	**Mean diameter (μm)**
Ultrafine	<0.1
Fine	0.1-1
Medium	1-10
Coarse	>10

In the early days, the main idea behind embedding particles into a polymer matrix was to decrease the cost of the composite. Then the role of particle reinforcement became more practical, for instance in increasing the mechanical properties of composites, such as stiffness and strength, while simultaneously decreasing shrinkage. Today, focus is not only on cost and mechanical properties but also on creating new functional properties not possessed by the matrix polymer, such as flame retardancy or conductivity (Moczo & Pukanszky, 2008).

Particulate composites are used in large quantities in various kinds of applications. In 2004, General Electric, US, used about 270 tons of nanocomposite materials (Stewart, 2004). In 2007, Europe used a vast 4.8 million tons of filler (Rothon, 2007). Table 1.2 shows thirteen different types of filler that were in high demand on European markets in 2007.

Table 1.2: Consumption of particulate fillers in Europe in 2007

(Rothon, 2007)

Filler	**Amount (ton)**
Carbon black	2,000,000
Natural calcium carbonate and dolomite	1,500,000
Aluminium hydroxide	250,000
Precipitated silica	225,000
Talc	200,000
Kaolin and clay	200,000
Fumed silica	100,000
Cristobalite, quartz	100,000
Precipitated calcium carbonate	75,000
Calcined clay	50,000
Magnesium hydroxide	20,000
Wollastonite	20,000
Wood flour and fiber	20,000

Among all fillers, carbon black and calcium carbonate ($CaCO_3$) are the most widely employed. About 95% of the total amount of carbon black is used as filler in rubber and less than 5% in plastics. However, $CaCO_3$ is mostly used as filler in plastics and only relatively little in elastomers (Otterstedt & Brandreth, 1998)

In this research, $CaCO_3$ particles derived from the clam shell locally known as *lokan* were applied as filler in polymer matrix composites. *Lokan*, or *Polymesoda spp.,* is a type of clam that lives in mangrove and muddy areas. Sarawak covers about 173792.00 ha of mangrove forest, not including muddy areas (Hamli et al., 2012). Mangrove regions make the best habitat for the most important taxon of edible bivalves in Sarawak, *Polymesoda spp*. *Polymesoda spp.* is widely distributed in most divisions of Sarawak due to the existence of immense mangrove and muddy areas. This species is an inexpensive protein source for the people of Sarawak. It is mostly utilized for local consumption but is not extensively distributed on large commercial markets.

Polymesoda spp., including *Polymesoda bengalensis,* is currently not listed as a threatened species (Do et al., 2012). The activities of collection or even over-collection of marine shells is not a threat of extinction to marine shells (Wood & Wells, 1995) as long as their habitats are not destroyed or contaminated with industrial and domestic waste (Holme, 1995) and are protected from desiccation (Lent, 1969).

The basic component of a bivalve shell is calcium carbonate ($CaCO_3$). Calcium is separated from the blood by the mantle, one of the seashell's organs, that forms $CaCO_3$ crystals in the bivalve shell. A comparative study on commercial $CaCO_3$ and $CaCO_3$ from bivalve shells was done by Islam et al. (2011). An investigation using an energy dispersive X-ray analyzer (EDX) showed that the element content of cockle shell powder is more calcium carbon than in commercial calcium carbonate, whereas commercial calcium carbonate contains more oxygen. The surface morphology of commercial calcium carbonate is aggregated cubic-like calcite crystal, whereas cockle shell powder contains rod-like aragonite crystals. The specific gravity of calcite is 2.71 and that of aragonite is 2.93.

1.2 Research Motivation

This research focuses on $CaCO_3$ extracted from the *lokan* shell, or *Polymesoda bengalensis*, a local clam, to be used as filler or reinforcement in polymer composites. Rather than disposing of the clam shells in landfills or open spaces, it is recommended to apply and manage this waste as potential filler in polymer matrix composites. It was reported that in 2011, out of about 290 waste disposal sites in Malaysia, 114 were in critical condition as a result of about 30000 tons of waste disposed every day. This means about 1.8 million tons of waste disposed per year (Agamuthu & Fauziah, 2011). Table 1.3 provides a list of the composition of municipal solid waste as published by Chua et al. (2011) and collected from various literatures. Evidently, food and organic waste contributed the most among the various types of waste in Malaysia from 2001 to 2010.

Table 1.3: The composition of municipal solid waste according to various studies and sites

(Chua et al., 2011)

Components	**2001[1]**	**2001[2]**	**2002[3]**	**2003[4]**	**2004[5]**	**2005[6]**	**2005[7]**	**2007[8]**	**2010[9]**
Food waste & organic	68.4	32	56.3	37.4	49.3	45	47.5	42	43.5
Mix plastics	11.8	16	13.1	18.9	9.7	24	-	24.7	25.2
Mix paper	6.3	29.5	8.2	16.4	17.1	7	18.5	12.9	22.7
Textiles	1.5	3.4	1.3	3.4	-	-	2.13	2.5	0.9
Rubber & leather	0.5	2	0.4	1.3	-	-	-	2.5	-
Wood	0.7	7	1.8	3.7	-	-	4.41	5.7	-
Yard wastes	4.6	-	6.9	3.2	-	-	2.72	-	-
Ferrous	2.7	3.7	2.1	2.7	2	6	-	5.3	2.1
Glass	1.4	5.5	1.5	2.6	3.7	3	-	1.8	2.6
Pampers	-	-	-	5.1	-	-	3.81	-	-
Other	2.1	1.9	8.4	5.3	18.2	15	21.93	2.6	1.8
Total	100	100	100	100	100	100	100	100	100

[1] Hassan, M. N., Chong, T. L., Rahman, M., Salleh, M. N., Zakaria, Z., & Awang, M. (2001, October). Solid waste management in Southeast Asian countries with special attention to Malaysia. In *Proceedings Sardinia, 8th International Waste Management and Landfill Symposium, Italy* (pp. 1-5).

[2] Wan Ramle Wan A. Kadir (2001). A comparative analysis of Malaysian and the UK waste policy and institutional framework, Waste Management Conference 2001

[3] Nazeri A.R (2000) A report on solid waste composition from a study conducted at Taman Beringin landfill in 2000

[4] Kathirvale, S., Muhd Yunus, M. N., Sopian, K., & Samsuddin, A. H. (2004). Energy potential from municipal solid waste in Malaysia. *Renewable energy*, *29*(4), 559-567.

[5] JICA. The study on national waste minimisation in Malaysia. July 2004-June 2006

[6] As published by Ministry of Housing and Local government's website based on 2005

[7] Sampling by Bukit Tagar Sanitary Landfill 2005

[8] Muhammad Abu Eusuf, Che Musa Che Omar, Shamzani Affendi Mohd. Din, Mansor Ibrahim An Overview on Waste Generation Characteristics in some Selected Local Authorities in Malaysia, Proceedings of the International Conference on Sustainable Solid Waste Management, 5 - 7 September 2007, Chennai, India. pp.118-125

[9] Siti Rohana M. Yatim. Household solid waste characteristics and management in low cost apartment in Petaling Jaya, Selangor, 2010

The current method of waste disposal is not sustainable, and consequently, the Department of National Solid Waste Management proposed some actions the government should adopt to minimize this problem. Among the suggestions are the installation of incinerators for safe and efficient disposal, upgrading non-sanitary landfills, and implementing waste reduction through 3R (reduce, reuse, recycle). In Sarawak, the *lokan* shell is abundant, has no eminent use and is commonly regarded as waste. Reusing the clam shell and converting it into a useful material is one way to minimize such food waste and therefore decrease the amount of waste disposed in landfills.

Japan is an example country where unused disposed shell (calcium carbonate) waste is converted into calcium oxide to be used practically in a range of areas, such as agriculture (fertilizer), the fishing industry (extermination of red tide), the food industry (food additive) and the health industry (natural mineral supply) (www.asada-shokai.co.jp/eng/in3c.html). In terms of particulate-filled composite material, using $CaCO_3$ extracted from local resource waste can possibly reduce the cost of particle reinforcement and hence lessen the cost of composite material. Furthermore, utilizing unused disposable seashells can also reduce the dependence on $CaCO_3$ resources from limestone quarries.

1.3 Objectives

The aim of the current research is to investigate the mechanical and thermophysical properties of untreated and stearic acid-treated *lokan*-filled unsaturated polyester matrix composites with different filler sizes and loadings. The specific objectives of this research are as follows:

1. To identify the elemental content and crystal structure of *lokan* shell particle.
2. To investigate the effect of including $CaCO_3$ particle from *lokan* shell-filled unsaturated polyester (UPE) composites of varying sizes and filler concentration on the mechanical and thermophysical properties.
3. To investigate the effect of treating $CaCO_3$ surface with 1 wt% stearic acid on the mechanical and thermophysical properties of UPE/$CaCO_3$ composites.

In Malaysia, studies on applying $CaCO_3$ from the *lokan* clam shell as filler in polymer matrix composites are not well established. Therefore, a study on the characterization of the clam shell and its particle should be initially done. An investigation of the mechanical properties effects on the stiffness and strength of tensile, compression and flexural loadings as well as surface hardnessis also done. Regarding thermophysical properties, three properties are studied: heat conductivity, heat diffusivity and specific heat content. The effect of treating $CaCO_3$ particle with stearic acid under both mechanical and thermal properties is compared with untreated $CaCO_3$-filled UPE composites. Comparisons are also done according to filler weight fraction and filler size. The filler weight fractions were 2 wt%, 4 wt%, 6 wt% and 8 wt%. The particles ranged in size: 636.87 µm, 574.81 µm, 485.84 µm, 297.94 µm, 206.55 µm, 46.30 µm, 35.06 µm and 29.84 µm. Subsequently, the mechanical and thermophysical properties are studied to evaluate the suitability as a substitute to existing, conventional $CaCO_3$ particulate-filled polymer matrix composites. A comparative study will be carried out against published literature.

Unsaturated polyester (UPE) is chosen as a matrix because it has good mechanical properties, and it is low cost and easy to use (Horrocks & Price, 2001). It is currently the most used thermosetting polymer and is also expected to be in highest demand on the global market by 2015 (Kandelbauer et al., 2014).

1.4 Scope of research and limitations

The scope of this research is limited to the infusion of $CaCO_3$ particle from *lokan* shells at weight fractions of 2 wt%, 4 wt%, 6 wt% and 8 wt%. In some literature, it has been reported that infusing low fractions of filler in the polymer resin can produce better mechanical properties than higher filler fractions. For example, 4 wt% filler content is the best amount to achieve optimum mechanical properties, such as tensile strength (Ou et al., 1998), compressive strength and modulus (He et al., 2011), flexural strength (He et al., 2011), fracture toughness (Lauke, 2015) and hardness (Lam et al., 2005). The maximum tensile strength was gained at 5 wt% by nano-UPE/$CaCO_3$ compared to 7 wt% and 9 wt% filler loadings due to uniform particle distribution (Baskaran et al., 2011) and the capability to resist and deflect crack failure (Dong et al., 2011). Large numbers of tiny cracks developed in the composites as more than the optimum amount of particles were added (Baskaran et al., 2011).

Another limitation of this research is treating the $CaCO_3$ particle with 1 wt% stearic acid. $CaCO_3$ surface modification with stearic acid yields better mechanical properties than untreated $CaCO_3$ (Deshmukh et al., 2010a). This amount of stearic acid was used because it attains the maximum contact angle of water and hydrophobicity (Jeong et al., 2009).

In terms of methodology, the process of producing clam shell particles is limited to utilizing mortar and pestle, and blender. This technique is selected for high volumes of clam shell particle production. It has also been applied by researchers including Awang-Hazmi et al. (2007), Islam et al. (2012) and Kamba et al. (2013) to produce particle from cockle shells. The authors applied a Los Angeles abrasive machine for high volume particle production but the particle deteriorated with other elements, which may be from sticky dust on the surface of the drum and steel balls. The authors also tried a centrifugal ball mill but the production rate was very low.

1.5 Outline of the thesis

This thesis consists of 6 chapters, covering the introduction, a literature review, research methodology, results and discussion, potential applications, and conclusions and recommendations. The thesis is organized as follows:

Chapter 1 presents the background and motivation of the study. The aims and objectives of the research are also presented.

Chapter 2 documents the details of *lokan*, or *Polymesoda bengalensis*, as well as the mechanical and thermal properties of particulate-filled polymeric composites. The effects of particle size and particle content on the composites' strength and stiffness under tensile, compression and flexural loadings are reviewed. Besides, the effects on surface hardness, thermal conductivity, specific heat content and thermal diffusivity of the composites are also reviewed.

Chapter 3 describes in detail the procedures done to determine the particle from raw clam shells, sample fabrication, mechanical testing and thermophysical testing. Mechanical testing covers tensile, compressive, flexural and surface hardness where as thermophysical testing covers thermal conductivity testing and differential scanning calorimetry (DSC) testing.

Chapter 4 presents the experimental results and discussion. The data are grouped into two parts: untreated and stearic acid-treated *lokan*-filled UPE composites. For each group, the data are categorized according to particle size and particle content as infused in the UPE matrix composites.

Chapter 5 recommends some potential applications of using $CaCO_3$ particle from *Polymesoda bengalensis* shell particle as the filler in the composites. The recommendations are based on the comparison of the information which is collected from other literature and from previous work done by the researcher.

Chapter 6 presents the conclusions and recommendations for future work.

CHAPTER 2: LITERATURE REVIEW

2.1 Introduction

As fillers are added to a polymer matrix, filler characteristics such as particle size, particle distribution and specific surface area greatly affect the performance of the composites. For particulate-filled polymer composite systems, particle content or particle fraction influences the composite's performance. For better performance, fillers are treated with chemicals. The purpose of treating the filler surface is to produce filler that is chemically compatible with the polymer matrix. The interaction between such treated filler and its corresponding surfactant may produce either strong filler-matrix bonding and/or promote homogeneous dispersion of the filler in the matrix. Surface treatment can be categorized into two main groups: non-reactive and reactive treatment. The performance of the surface treatment is dependent on the interaction between the inorganic surface and matrix polymer (Thio et al., 2004) and the amount of surfactant (Jeong et al., 2009). Filler with inactive surfaces, such as talc, cannot be treated by either reactive or non-reactive treatment.

2.2 *Lokan (Polymesoda bengalensis)*

Lokan, also known by the scientific name *Polymesoda bengalensis*, is one of the largest mangrove bivalve species distributed in mangrove swamps, which can grow up to 10 cm in diameter (Poutiers, 1998). This large, heavy bivalve was formerly known as *Genolia bengalensis*. It is originally from Bangladesh, India, Malaysia, Philippines, Thailand and Vietnam. However, it is currently widely distributed along coastal east Indian states and Myanmar (Do et al., 2012). The general Corbiculidae characteristics along with height, length and width measurements are shown in Figure 2.1. Height is the distance from the bottom of the shell hinge to the top of the shell. Length is the widest part across the shell at 90 degrees to the height, and the width or hinge width (inflation) is measured at the thickest part.

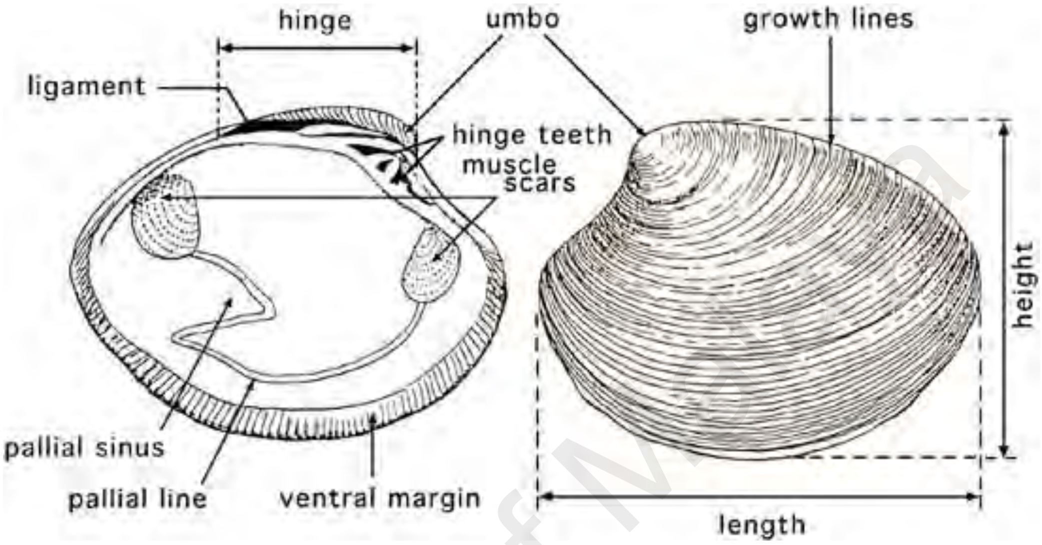

Figure 2.1: Main features of a bivalve shell

(Poutiers, 1998)

Bivalves including *Polymesoda bengalensis* are extraordinary organisms. They can adapt successfully in the extreme environment of mangroves by changing their behavior and physiological features (Pechenik, 2005), such as closing their hard shells to prevent dehydration. This species is well adapted to its habitat, being able to tolerate long periods of low tide and continue to rapidly filter-feed when inundated (Ng & Sivasothi, 1999). It was reported that this species is currently not listed as a threatened species (Do et al., 2012). However, acidic environments, meaning low pH values, may cause erosion to the external shell (Plaziat, 1984). In addition, any activities related to the destruction of mangrove areas may affect its existence in future.

Hamli et al. (2012) conducted a study on the distribution of edible bivalves in eight divisions of Sarawak. Through the study it was found that the diversity of edible bivalves seemed highest in Kuching and Bintulu compared to the other six divisions. *Polymesoda spp*. and other bivalves provide an essential source of protein in the diet of the local community in Sarawak. Table 2.1 shows the distribution of *Polymesoda* species in eight selected divisions of Sarawak (Hamli et al., 2012) while Table 2.2 presents the habitat and morphological characteristics of *Polymesoda spp*.

Table 2.1: Availability of *Polymesoda spp.* in Sarawak, Malaysia (Hamli et al., 2012)

Family	**Species**	**Kuching**	**Sarikei**	**Sibu**	**Mukah**	**Bintulu**	**Miri**	**Limbang**	**Lawas**
Corbiculidae	*Polymesoda bengalensis*	+	+	+	-	+	+	+	-
	Polymesoda erosa	-	-	+	+	+	+	+	+
	Polymesoda expansa	-	-	-	-	+	+	+	+

(+)=present, (-)=absent

Table 2.2: Characteristics of *Polymesoda spp.* in Sarawak, Malaysia (Hamli et al., 2012)

Species	**Lokal Name**	**Habitat**	**Characteristic**
Polymesoda bengalensis	Lokan bakau	Brackish water	Hard and thick sub-trigonal, eroded umbo, dark green
Polymesoda erosa	Lokan apung	Brackish water	Hard and thick sub-rhomboidal, eroded umbo, green
Polymesoda expansa	Lokan selam	Brackish water	Hard and thick, trigonal ovate, eroded umbo, yellow

Not much research has been done on the composition of the *lokan* shell and its usage. Most literature reports on the utilization of different types of mollusks and determining the concentrations of heavy metals in water as molluscs tend to accumulate metals in their body tissue (Yap & Cheng, 2009). Heavy metal contamination may be retained in water bodies and taken up by plankton, molluscs, and fish before being transferred to humans via food consumption. Molluscs such as clams, mussels, cockles and oysters are widely reported in literature as biomonitors or indicators for heavy metal pollution in estuaries and coastal water due to their abundance, sedentary nature, easy collection, and weight (Yap & Cheng, 2009). Yusoff and Long (2011) used *lokan* as one of the molluscs to assess environmental contamination, especially to determine the concentrations of heavy metals such as Cd, Cr, Cu, Zn and Mn in the estuary of Sungai Sematan, Sarawak. They found *lokan* to be the best biomonitor because it can accumulate the highest amount of Cd, Zn and Mn compared to other mollusks (Yusoff & Long, 2011).

The mollusc shell has several functions. Its main functions are as a skeleton for the attachment of muscles, and to support and protect the clam inside the shell against predators. Mangroves are generally exposed to changes in physiochemical characteristics such as salinity, dissolved oxygen content, pH and temperature, due to tidal fluctuations (Pechenik, 2005). In order to survive in harsh conditions, bivalves have developed an outer layer, or shell, to protect them from dehydration during low tide, attacks by predators and high temperatures (Hashim, 1993). Therefore, bivalves can survive for long periods as long as they are protected from desiccation (Lent, 1969).

The main component of the mollusc shell is calcium carbonate. Calcium is obtained from the diet or taken up from seawater. Carbonate is derived from the CO_2/bicarbonate pool in the animal’s tissue. Calcium carbonate is formed by the deposition of salt crystals in an organic matrix of protein called conchiolin. The shells of bivalves are made of three layers: an outer periostracum, a middle prismatic layer and an inner calcareous layer (Gosling, 2003). The three layers are described as follows:

i) Periostracum layer: This thin layer consists of horny conchiolinthat often becomes thinner due to mechanical abrasion, fouling organisms, parasites or disease.

ii) Prismatic layer: This layer contains calcium carbonate with a polymorph, either aragonite or calcite.

iii) Nacreous layer: The surface of this layer is smooth and provides a comfortable space for the clam inside. Depending on the species, the texture of this layer can be dull or iridescent mother of pearl.

The calcareous shells of bivalves are multilayered and consist of two intermixed phases (Wilbur, 1964): an organic matrix, and crystalline calcium carbonate in the form of calcite or aragonite. Most bivalve shells have different layers composed of calcite and aragonite. However, some bivalves like the oyster may contain more calcite than aragonite, while others may have only aragonite. Those phases can exist in a number of recurrent patterns occurring in discrete shell layers. Six types that have been differentiated are shown in Figure 2.2. The followingis a brief explanation of the six types of patterns in the shell layers (Taylor & Layman, 1972).

(i) Simple prismatic structure with columnar polygonal calcite or aragonite prisms

(ii) Composite prismatic structure with tiny radiating acicular crystals

(iii) Nacreous structure in which tabular sheets of aragonite are found resembling a brick wall when cut in sections. These are usually found in middle and inner shell layers

(iv) Foliated structure of lath-like calcitic crystallites arranged in sheets

(v) Cross-lamellar structure, which is normally aragonitic. Here the shell is made of closely spaced lamellae, each of which contains thin, stacked plates of aragonite; the plates of adjacent lamellae are inclined in opposite directions to one another. In some cases, intergrowths of blocks of crystals are found (complex crossed lamellar structure) with four principal orientations.

(vi) Homogeneous structure with small granular anhedral crystals.

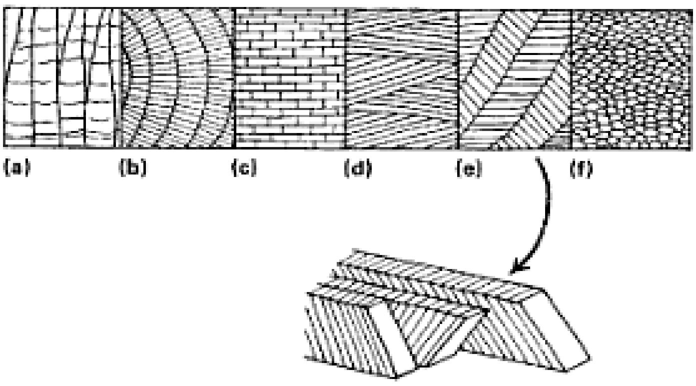

Figure 2.2: Morphology of a bivalve shell layer: (a) a simple prismatic, (b) compound prismatic, (c) sheet nacreous, (d) foliated, (e) crossed lamellar with inset showing disposition of stacked aragonite lamellae, (f) homogeneous

(Taylor & Layman, 1972)

2.3 Unsaturated Polyester

Unsaturated polyester (UPE) resin is the most widely used cross-linkable polymer for composites owing to its benefits in terms of design flexibility, chemical resistance, thermal and dimensional stability, low density and cost-benefit balance (Unal et al., 2006). It makes up approximately 80% of all thermoset resins. The remainder 20% comprises epoxies, phenolics, acrylics, imides, and urethanes. It is expected that the global market volume for UPE demand may reach 5.8 billion USD by 2015 (Kandelbauer et al., 2014). This includes the major consumption in the wind-energy, marine, pipe and tank, transportation and construction sectors. The high demand for UPE resin is mainly due to the possibility of being highly filled and easily processed (Penczek et al., 2005). Table 2.3 shows the mechanical and thermophysical properties of unsaturated polyester resin. The properties of UPE resin are depend on the additional materials used and the conditions of curing. Figure 2.3 shows the main areas of UPE consumption and approximate market shares of UPE consumed in Japan, Europe, and the USA.

Many filler types are compatible for infusion in UPE resin. Most filler applied in UPE resin are inorganic and of mineral origin. Liquid UPE resin allows for large filler loading. The filler may able to decrease curing shrinkage, increase composite hardness, decrease tensile elongation, and decrease impact strength. Table 2.4 summarizes some common filler materials and their functions.

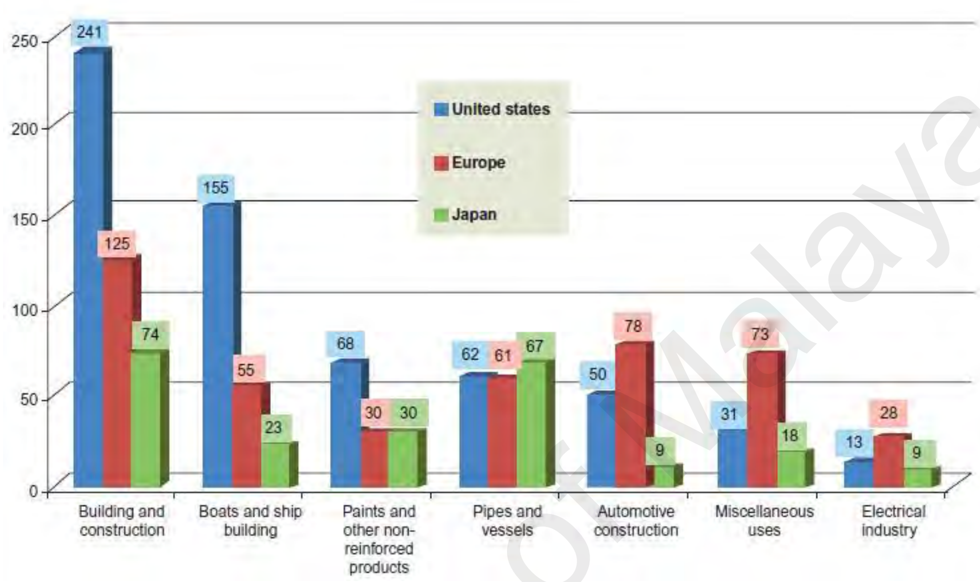

Figure 2.3: Expected market shares in several industrial sectors for unsaturated polyester resin in Japan, Europe and the USA (Numbers are given as 10^3)

(Krämer, 1992)

Table 2.3: Mechanical and thermophysical properties of unsaturated polyester resin

(Reis, 2012; Jones & Ashby, 2012)

Property	**Value**	**Resistance to chemical**	
Viscosity at 25 °C	250-350	Dilute acid	Good
Density (gcm^{-3})	1.1-1.4	Dilute alkalis	Good
Heat distortion temperature (°C)	54	Oils and greases	Moderate
Modulus of elasticity (GPa)	1.3-4.5	Aliphatic hydrocarbon	Poor
Flexural strength (MPa)	45	Aromatic hydrocarbon	Poor
Tensile strength (MPa)	45-85	Halogenated hydrocarbon	Poor
Maximum elongation (%)	1	Alcohols	Good
Glass temperature (K)	340		
Specific heat (Jkg^{-1}K^{-1})	1200-2400		
Thermal conductivity (Wm^{-1}K^{-1})	0.2-0.24		
Thermal coefficient (MK^{-1})	50-100		

Table 2.4: General fillers infused in unsaturated polyester and vinyl ester resins, and their purposes

(Zaske & Goodman, 1986)

Filler	Typical Applications
Calcium carbonates	Synthetic marble, SMC, BMC, matched die molding, building panels, autobody putty, mine bolt grouts
Clays	Molding compounds, SMC, BMC
Talcs	Autobody putty, gel coats
Alumina trihydrate	Synthetic onyx, flame retardant SMC, BMC and molding compounds, flame retardant construction composites
Dolomites	SMC, BMC, matched die molding
Glass and ceramic microballoons	Synthetic marble, bowling ball cores, low density SMC, deep submergence vehicles
Phenolic microballoons	Deep submergence vehicles
Glass microspheres	SMC, gel coats
Nepheline syenite	Building panels
Silica sand	Polymer concrete

2.4 Mechanical Properties

Basically, pure polymer has low strength and low stiffness. Fillers are induced in the polymer to produce better composite materials, which combine the advantages of their constituent phases. This, however, results in the improvement of some mechanical properties but the reduction of others. For particulate-filled polymer composites, the reduction is mostly caused by weak filler-matrix interface and the inhomogeneous dispersion of filler in the composites as a result of filler agglomeration. Filler size, filler loading and interfacial adhesion are among the factors affecting the mechanical properties of composites.

2.4.1 Tensile modulus

Tensile modulus, or Young's modulus, is determined by the slope of the tensile stress-strain curve up to the elastic limit. The stiffness of the composites increases as filler loading increases (Mareri et al., 1998; Ou et al., 1998) and particle size decreases (Mishra et al., 2005; Vollenberg & Heikens, 1989). Better stiffness attained with particulate-filled polymer composites is attributable to better filler "bridges" or percolation networks (He & Jiang, 1993) produced by homogeneously distributed filler in the polymeric composites.

2.4.1.1 Effect of particle size

Embedding rigid inorganic fillers, which normally have higher stiffness than a polymer matrix either in micro or nano-size may enhance the stiffness of the neat polymer matrix (Radford, 1971; Spanoudakis & Young, 1984). Many researchers have found that particle size affects the tensile modulus of particulate polymer composites, while others have claimed that particle size has no significant effect on tensile modulus.

It has been reported in some literature that the tensile modulus of particulate-filled polymer composites increases as filler size decreases. Chisholm et al. (2005) infused micro and nano-size silica particles in an epoxy matrix and found that higher elastic modulus was attained in nanocomposites. Similar outcome was achieved by Douce et al. (2004), as shown in Figure 2.4, where significant improvement is evident at high particle loading. Mishra et al. (2005) observed that $CaCO_3$/PP composites containing smaller particles (21 nm) are stiffer than composites with larger nanoparticles (39 nm) as demonstrated in Figure 2.5.

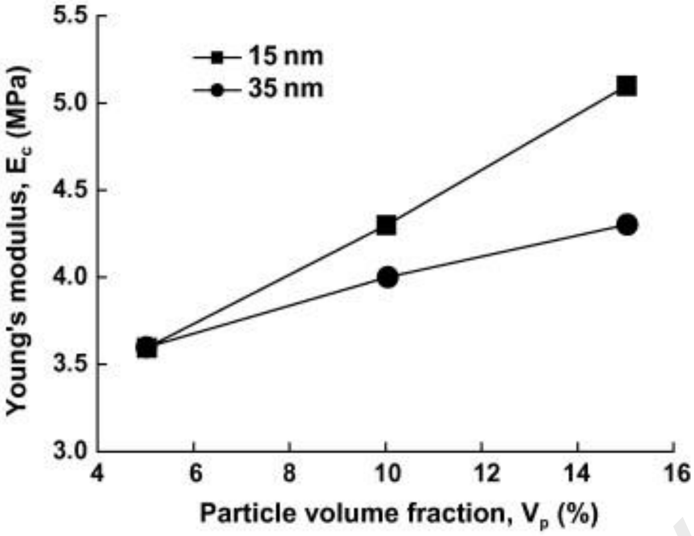

Figure 2.4: Effect of different silica particle sizes and content of polysiloxane nanocomposite on composite stiffness

(Douce et al., 2004)

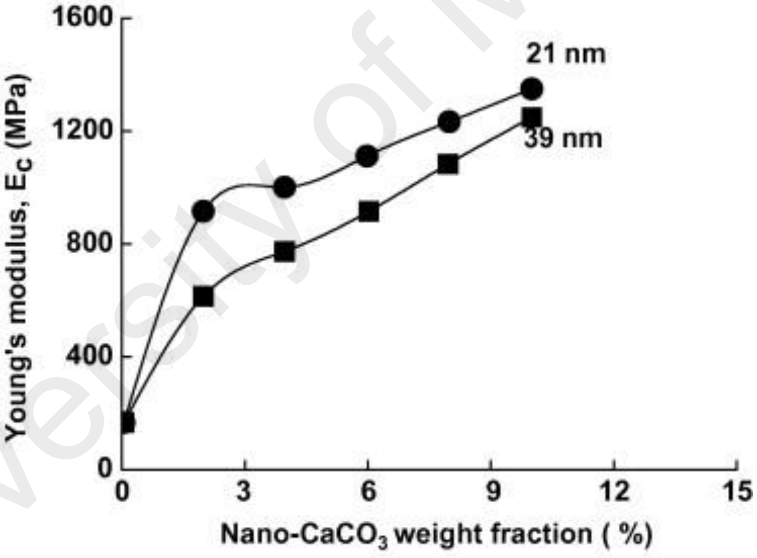

Figure 2. 5: Tensile stiffness of 21 nm and 39 nm $CaCO_3$/PP composites with different filler content

(Mishra et al., 2005)

The performance of Young's modulus depends on the critical size of the filler (Cho et al., 2006). The effect of tensile modulus is more significant when the filler size is below a critical size value. For sizes ranging from 0.5 μm to 15 nm of spherical alumina and glass bead particles infused in vinyl ester resin, no significant changes in the composite's Young's modulus were detected. Stiffness enhanced as the size of alumina reduced to 50 and 15 nm in diameter. Ji et al. (2002) predicted that 30 nm is the critical particle size. Obvious effects on the modulus were found when particle size was lower than the critical size, as illustrated in Figure 2.6.

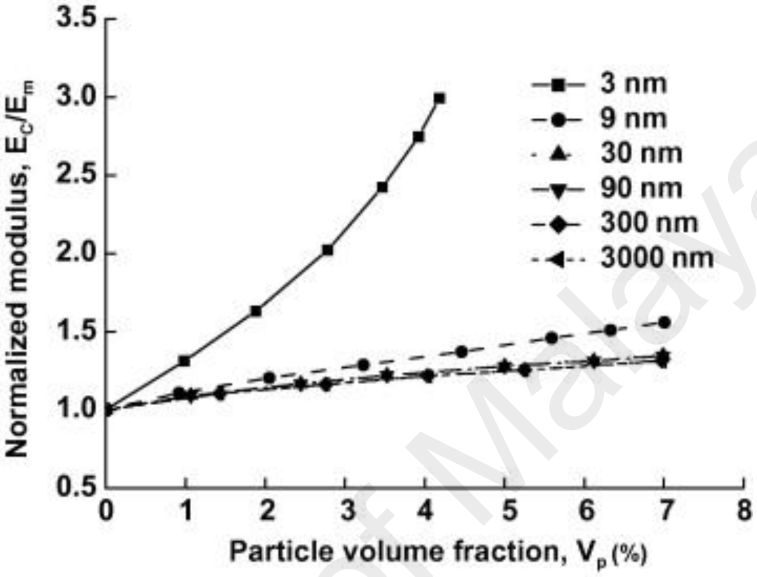

Figure 2.6: The predicted stiffness of different spherical particle size-filled polymer composites at constant particle-to-matrix modulus ratio of $\frac{E_p}{E_m} = 40$

(Ji et al., 2002)

Other researchers reported that particle size does not affect the modulus of particulate polymer composites. Nakamura et al. (1992) conveyed that the modulus of spherical and irregular-shaped silica particles with sizes ranging from 2-30 µm in a silica matrix remained constant with increasing particle size. The elastic modulus of $CaCO_3$ for filler sizes of 1, 5 and 20 µm filled polybenzoxazine composites increased with filler content but did not depend on particle size (Suprapakorn et al., 1998). The same observation was made by Singh et al. (2002), whereby the modulus of aluminum particle/polyester composite was unaffected by particle sizes of 100 nm, 3.5 µm and 20 µm. Particle alumina trihydrate particle with sizes of 1-12 µm filling an epoxy matrix did not affect the modulus of the composite (Lange & Radford, 1971). Identical results were found by Spanoudakis and Young (1984) on epoxy/spherical glass bead particle composite, as shown in Figure 2.7. The tensile modulus was not greatly affected by particle sizes in the range of 4.5-62 μm for 10-18 vol% spherical glass particles.Verbeek (2003) found that particle size has no significant effect on the modulus of low density polyethylene (LDPE)/phlogopite composites (Figure 2.8).

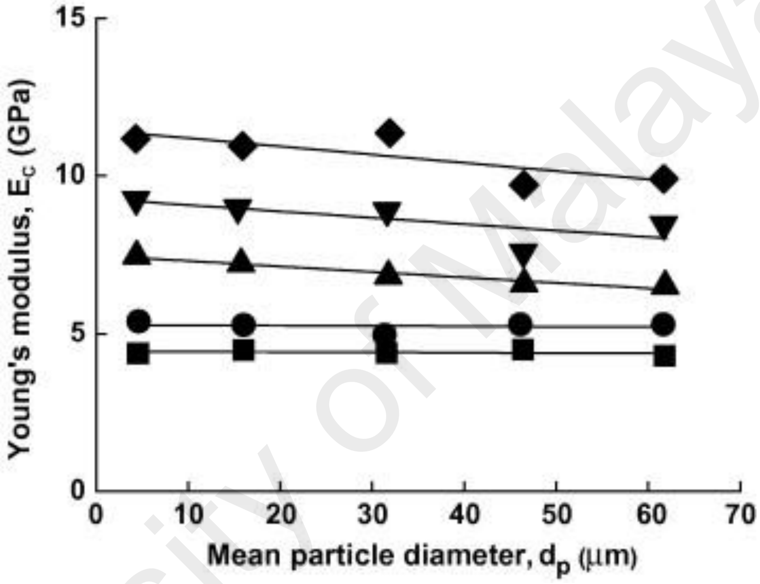

Figure 2.7: Effect of filler size and filler content on the stiffness of glass bead-filled epoxy composites (■ 10%; ● 18%; ▲30%; ▼ 40%; ♦ 46%)

(Suprapakorn et al., 1998)

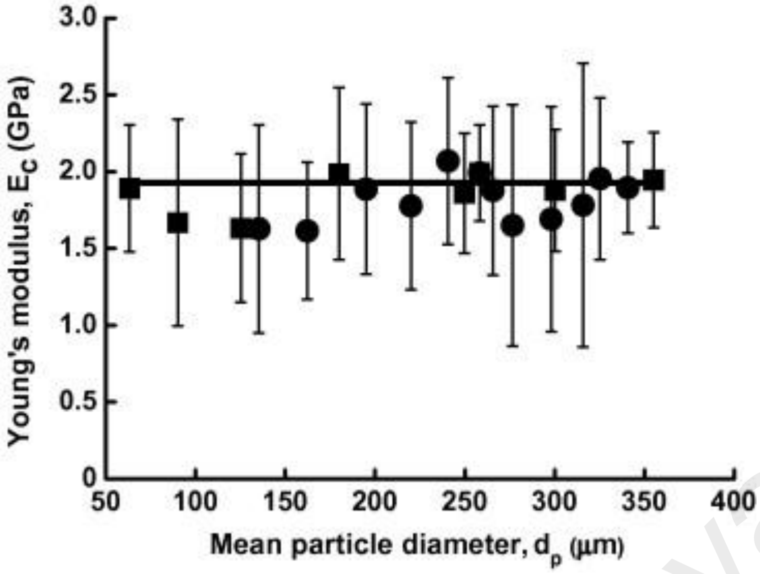

Figure 2.8: Variation in Young's modulus with particle size and size distribution of phlogopite, at constant aspect ratios for narrow (■) and wide (●) distribution. The predicted values using the equation are shown as a solid line

(Verbeek, 2003)

Contradictory results were reported by Jiang et al. (2005), as micron-sized $CaCO_3$ particles in acrylonitrile butadiene styrene (ABS) had higher modulus than neat ABS and nano-sized $CaCO_3$ (Figure 2.9). This was due to the formation of particle agglomeration of nano-sized $CaCO_3$ rather than micro-$CaCO_3$ particles in the ABS matrix as observed through EDXS mapping by SEM (Figure 2.10). Another reason was the calculation of the modulus at the strain, which was less than 1.5%. At this value, the stress is not high enough to break the bonding between the particles and ABS. Even though nano particles have greater interfacial area, at this low strain value, this did not contribute to modulus enhancement.

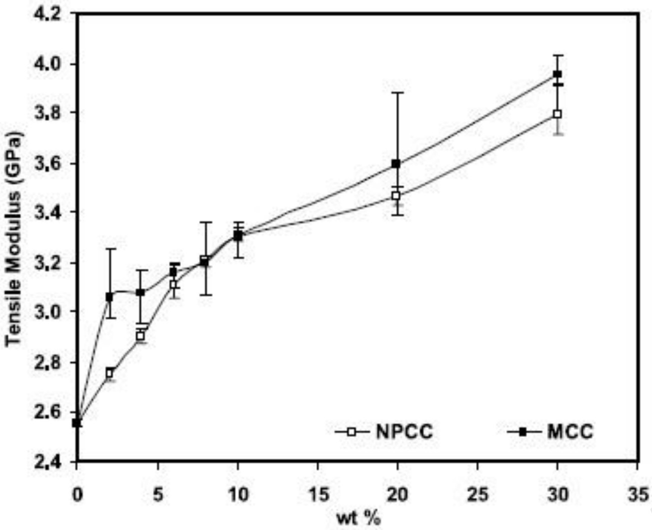

Figure 2.9: Young's modulus of nano-$CaCO_3$/ABS (NPCC) and micro-$CaCO_3$/ABS (MCC) composites with different filler content

(Jiang et al., 2005)

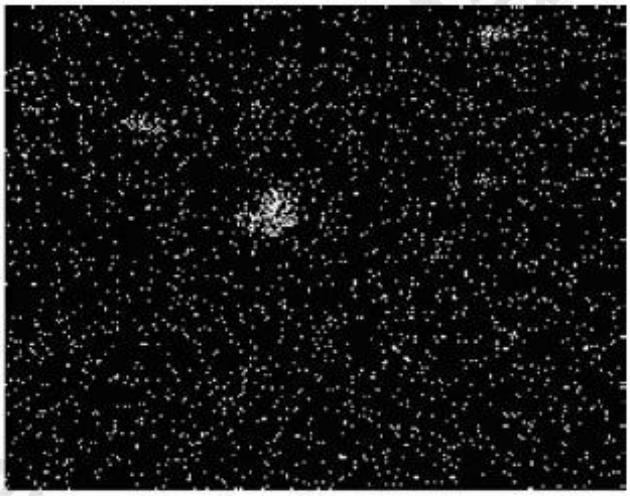

Figure 2.10: Agglomeration of nano-$CaCO_3$ in acrylonitrile-butadiene-styrene (ABS) resin by EDXS mapping

(Jiang et al., 2005)

He and Jiang (1993) explained the relationship between particle size and composite stiffness through a phenomenon called a percolation network. As the filler infuses the liquid resin, stress zones are produced in the matrix around the particles. These zones join to produce percolation networks, or filler "bridges". For very fine and well-dispersed particles, the total volume affected is bigger and the distance between particles is shorter. This leads to an improvement in the composite's modulus (He & Jiang, 1993).

2.4.1.2 Effect of particle loading

Most studies have shown the positive effect of increasing particle loading on Young's modulus. The stiffness of $CaCO_3$-filled polypropylene (Demjén et al., 1998) and $CaCO_3$-filled acrylonitrile-butadiene-styrene (Jiang et al., 2005) increases as filler content increases. Infusing 10 vol% of hydroxyapatite (HA) particulate-filled high density polyethylene (HDPE) increases the tensile modulus of the composites by over 50% (Wang et al., 1998). Similar results were found, whereby the tensile moduli of nylon 6/silica nanocomposites (Ou et al., 1998), glass bead-filled epoxy composites (Suprapakorn et al., 1998), and nano silica-filled polysiloxane composites (Douce et al., 2004) increased with increasing filler loading. The increment in tensile modulus as silica content increases in nylon 6 is shown in Figure 2.11.

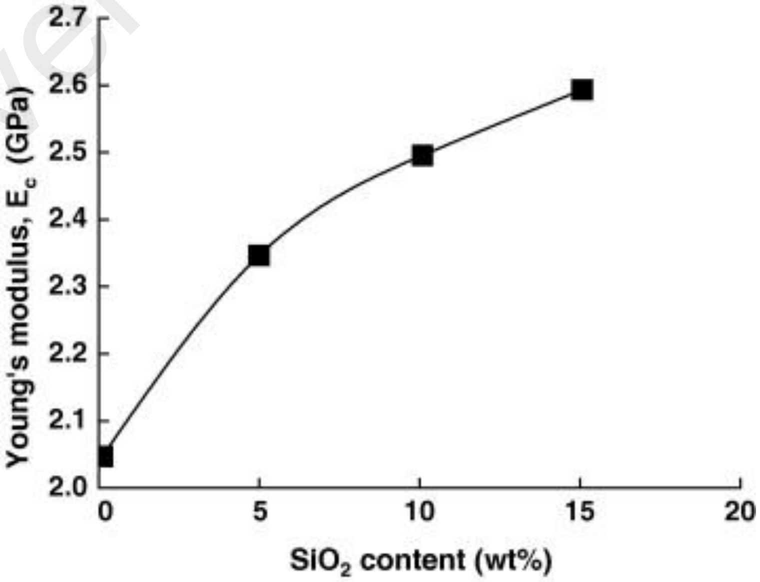

Figure 2.11: Tensile modulus of SiO_2/nylon 6 nanocomposites at various filler content (Ou et al., 1998)

2.4.2 Tensile strength

The strength of a material is the maximum stress the material can sustain under uniaxial tensile loading. Many researchers agree that particle size and particle loading influence the properties of particulate-filled polymeric composites. Basically, in most cases, a decrease in filler size may improve the tensile strength of the composites. Smaller particle sizes provide wider surface areas for the stress transfer mechanism, thus increasing the amount of stress that the particles can sustain. However, beyond a certain extent, the filler tends to agglomerate and thus weaken the composite.

2.4.2.1 Effect of particle size

Particle size has significant effect on the strength of particulate-filled polymer composites. The tensile strength of particulate-filled polymer composites increases as particle size decreases (Pukanzsky, 1995). At the same filler content, nano-sized $CaCO_3$/ABS exhibits higher tensile strength compared to micron-sized $CaCO_3$/ABS composites, as illustrated in Figure 2.12 (Jiang et al., 2005). Pukanszky and Vörös (1993) found that for spherical calcium carbonate filler with sizes of 10 nm, 80 nm, 1.3 μm and 58 μm embedded in polypropylene matrix, the yield strength will increase with decreasing particle size (Figure 2.13). A similar pattern was found by Cho et al. (2006) as shown in Figure 2.14, where the strength of 5 vol% glass bead particles embedded in a vinyl ester matrix increases as the filler size decreases. The opposite results were found for 3 vol% of alumina particles due to the poor dispersion of nanoparticles in the vinyl ester matrix.

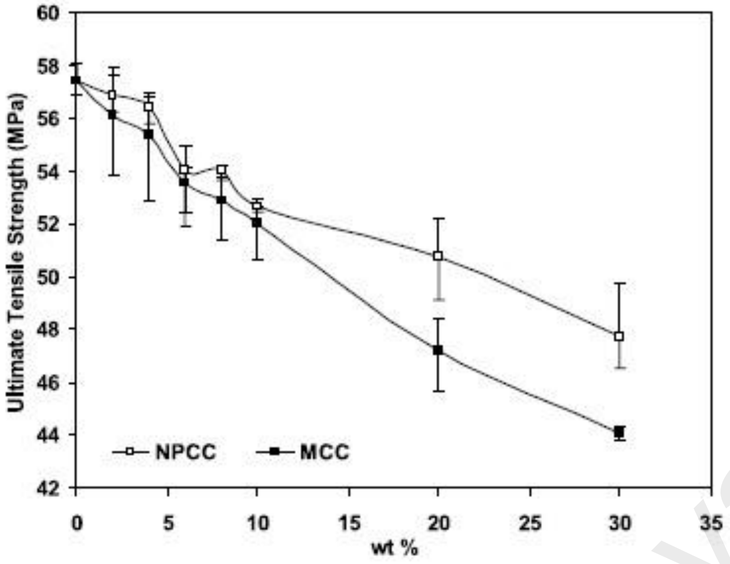

Figure 2.12: Tensile strength of nano-sized (NPCC) and micro-sized (MCC) $CaCO_3$/ABS composites with different filler content

(Jiang et al., 2005)

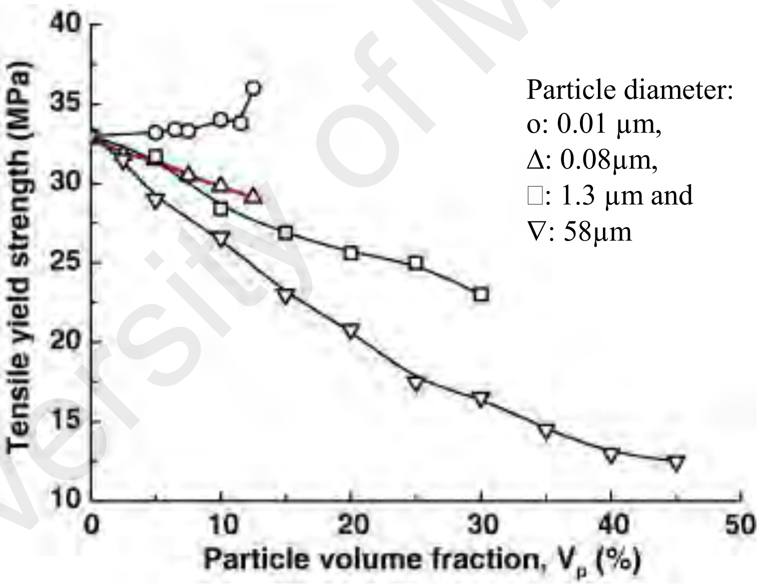

Figure 2.13: Tensile strength of spherical $CaCO_3$/PP composites with different filler sizes and filler content

(Pukanszky & Vörös, 1993)

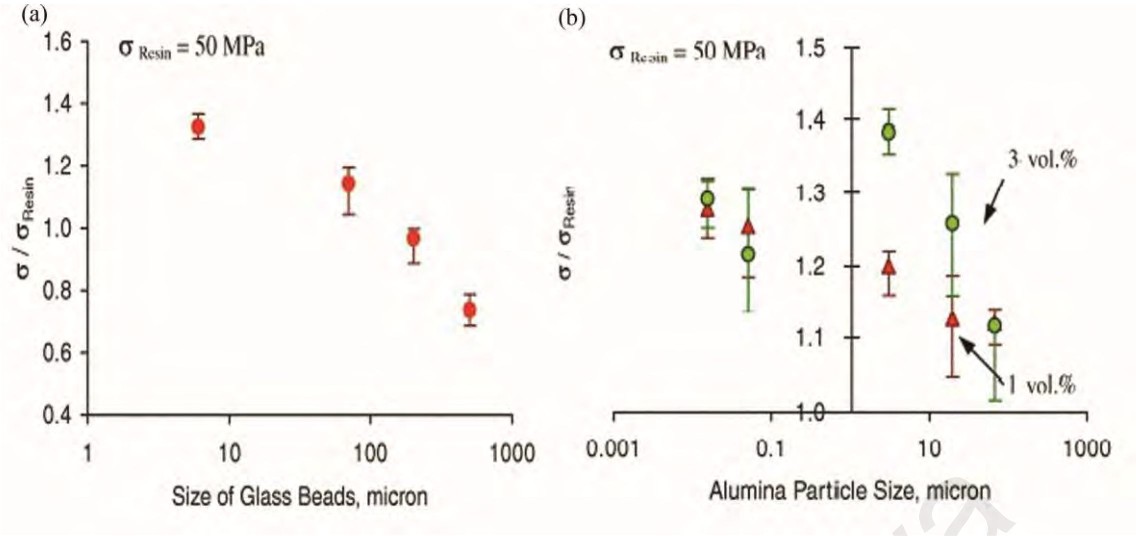

Figure 2.14: Effect of particle size of (a) 5 vol% glass beads, and (b) 1 and 3 vol% alumina particles on the tensile strength of composites

(Cho et al., 2006)

Nakamura et al. (1993) investigated the effect of including various sizes of micro-scale silica particles in epoxy polymer on the tensile strength of that polymer composite. As seen in Figure 2.15, they found a large improvement in tensile strength as the particle size was decreased. A similar trend was observed for micro-scale sized alumina trihydrate-filled epoxy polymer matrix at the same particle loading (10 vol%) (Radford, 1971) as shown in Table 2.5. Zhang et al. (2004) indicated that nano-$Mg(OH)_2$/ethylenepropylene diene monomer (EPDM) has higher tensile strength compared to micro-$Mg(OH)_2$ embedded in the same polymer at the same particle loading (Figure 2.16). Ghari and Jalali-Arani (2016) found that the use 10 parts per hundred rubber of nano $CaCO_3$ can increase about 350% tensile strength.

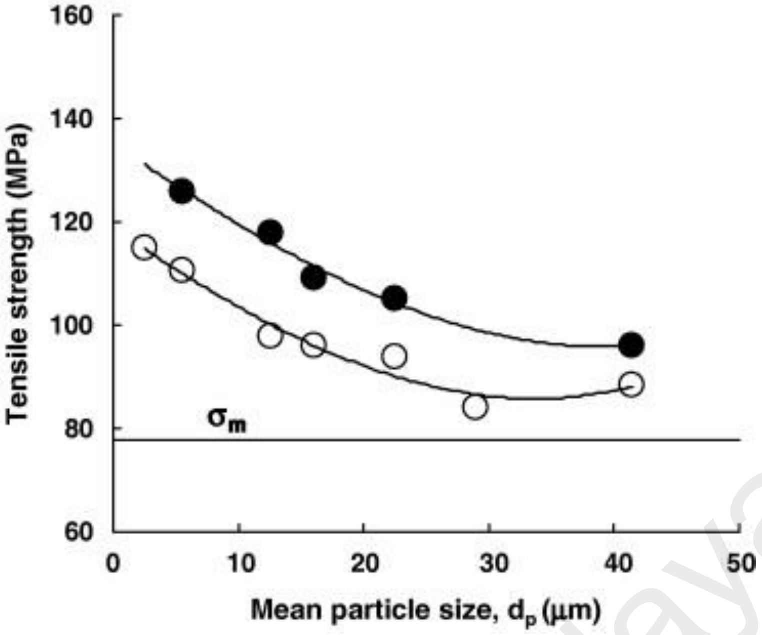

Figure 2.15: Tensile strength of different filler sizes and filler content of spherical silica/epoxy composites

(Nakamura et al., 1992)

Table 2.5: Tensile strength of alumina trihydrate-filled epoxy composites

(Radford, 1971)

Particle size (μm)	Volume fraction (%)	Tensile strength (MPa)
Unfilled	0	75.9 ± 8.8
1	10	58.0 ± 3.4
8	10	29.9 ± 1.7
12	10	27.2 ± 2.4

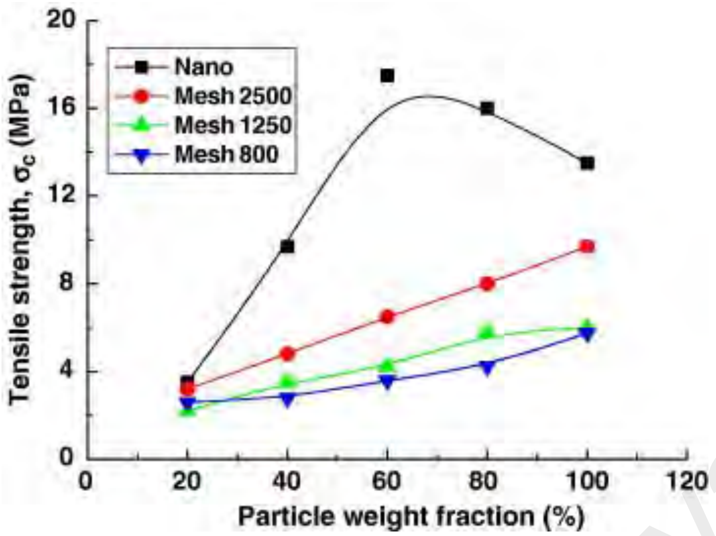

Figure 2.16:Tensile strength of different filler sizes and filler loading of $Mg(OH)_2$-filled EPDM composites (Nano= 50/100 nm, 2500 mesh=2.03 µm, 1250 mesh=2,47 µm, 800 mesh= 2.93 µm)

(Zhang et al., 2004)

Smaller particles are required to maximize the effect of the filler in the polymer matrix. Large surface-to-volume ratio of the filler produces composites with superior properties. Higher tensile strength is gained as the filler size decreases. Smaller particles have a greater total surface area, thus improving the efficiency of the stress transfer mechanism (Jiang et al., 2005; Pukanszky & Vörös, 1993). Although in some cases the tensile strength drops, which is not expected. This may due to particle agglomeration and poor bonding (debonding) between matrix and particles.

The main problem with decreasing the size of the filler is the increment of surface energy through the van der Waals force. At the same particle loading, fine fillers result in higher surface area thus increasing the surface energy (Lam et al., 2005). As a result, the tendency of the particle-particle interaction will also increase, promoting the agglomeration or clustering of small particles. Particle agglomeration is one of the main issues addressed with regards to the failure of nano-sized particulate-filled matrix composites. It was found that no matrix-particle debonding was observed in nano-sized filler or nanoparticle clusters due to the very strong interfacial bonding between the nanoparticles and matrix (Al Robaidi et al., 2011).

In particulate-filled matrix composites, debonding easily occurs between the matrix and large filler. The failure of micron-sized filler in the polymer matrix mostly originates in the form of particle-matrix debonding (Cho et al., 2006; Gent, 1980). Particle-matrix debonding leads to ineffective stress transfer (Fu et al., 2008). At this point, the particles cannot carry any more loads, leading to declining composite strength. Debonded particle-matrix interfaces can still transfer compressive stress through the particle-matrix contact but not tensile stress due to particle-matrix separation.

2.4.2.2 Effect of particle loading

The tensile strength of particulate-filled polymer composites increases as the filler content increases (Nakamura et al., 1992; Zhang et al., 2004). With increasing filler content, additional loads transferred to the filler, resulting in higher composite tensile strength. However, in some cases tensile strength reduction was found as more filler was infused into the polymer resin (Pukanszky, 1995). The contradiction of these results may be due to the particle/matrix interfacial adhesion, which plays a significant role in improving the tensile strength of the particulate polymer composite. Poorly bonded particulate-matrix interfaces may contribute to the inefficient stress transfer between the components. This may lead to discontinuity of stress distribution and therefore particle-polymer debonding. Particles can ultimately not carry any extra load and any additional particle loading may not contribute to any tensile strength improvement.

The reduction of particulate-filled polymer composite tensile strength is also due to the particles clustering or agglomerating. The addition of fine filler to the polymer matrix leads to the formation of particle agglomerate. At low filler loading, the particles are distributed homogenously. Lam et al. (2005) found that the agglomeration size of nanoclay particles increases as the filler loading increases. It was reported that for 4 wt% nanoclay/epoxy composites the average agglomeration size is 125 nm while for 15 wt% nanoclay/epoxy composites the average agglomeration size is 400 nm. Clustering is produced because of the reduction of free volume and increase of cross-link density. The addition of fine particles may reduce the free volume in the matrix, thus restricting particle movement. In addition, as the particles increase, the fine filler's inertia toward the cluster may also increase, hence contributing to the larger agglomeration. In most literature it has been found that nanoparticle clustering might occur at 4 wt% filler loading and below (Chan et al., 2011; Dong et al., 2011; Lam et al., et al., 2005). Figure 2.17 illustrates the formation of aggregate and agglomerate according to nano filler cluster size (Al Robaidi et al., 2011).

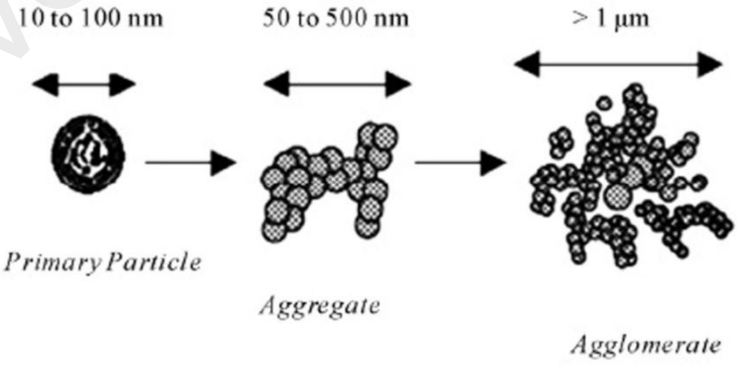

Figure 2.17: Aggregate and agglomerate formation from primary particles (Al Robaidi et al., 2011)

2.4.3 Compression properties

It was observed in a study that compressive yield stress increases as the amount of filler is increased (Suwanprateeb, 2000). In compressive loading, the presence of voids or cracks in the particulate-filled polymer composites does not influence the composites' performance. This is because a debonded particle-matrix interface can still transfer compressive stress through the particle-matrix contact but not tensile stress due to particle-matrix separation (Teng, 2010) as shown in Figure 2.18.

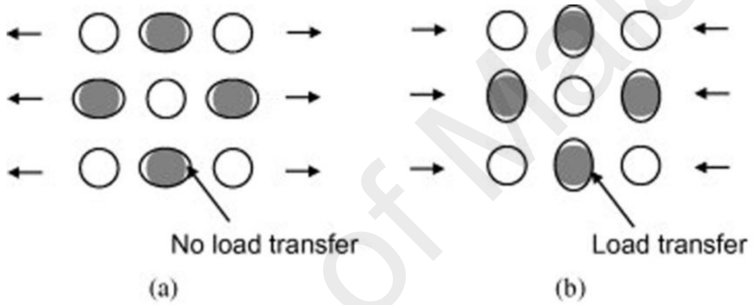

Figure 2.18: Particle-matrix debonding in particulate-filled polymer composite responds differently to (a) tension and (b) compression loading

(Teng, 2010)

He et al. (2011) found that the maximum compressive properties, such as compressive strength, compressive modulus, and compressive displacement during break and fracture work are achieved at 4 wt% $CaCO_3$. The values are higher than at 6 wt% and 8 wt% as shown in Table 2.6. Observation under TEM (Figure 2.19) shows that good dispersion and good interfacial particle-matrix interaction were attained at 4 wt% $CaCO_3$, which is why the maximum compressive strength was achievable at this ratio. Particle agglomeration was observed at 8 wt% $CaCO_3$/epoxy, which explains the occurrence of the tremendous drop in compressive strength.

Table 2.6: Compressive properties of epoxy and $CaCO_3$/epoxy composites from TGA and DTG curves

(He et al., 2011)

Sample	**Compressive strength (MPa)**	**Compressive modulus (GPa)**	**Compressive displacement at break (mm)**	**Fracture work (J)**
0 wt% nano-$CaCO_3$	107.41 ± 2.23	2.15 ± 0.13	1.07 ± 0.06	3.97 ± 0.19
2 wt% nano-$CaCO_3$	110.99 ± 4.33	2.17 ± 0.09	1.08 ± 0.04	3.31 ± 0.17
4 wt% nano-$CaCO_3$	121.95 ± 3.13	2.28 ± 0.11	1.86 ± 0.08	8.19 ± 0.23
6 wt% nano-$CaCO_3$	111.08 ± 3.65	2.16 ± 0.08	1.75 ± 0.06	7.09 ± 0.31
8 wt% nano-$CaCO_3$	74.77 ± 4.12	2.09 ± 0.16	2.09 ± 0.07	4.35 ± 0.24

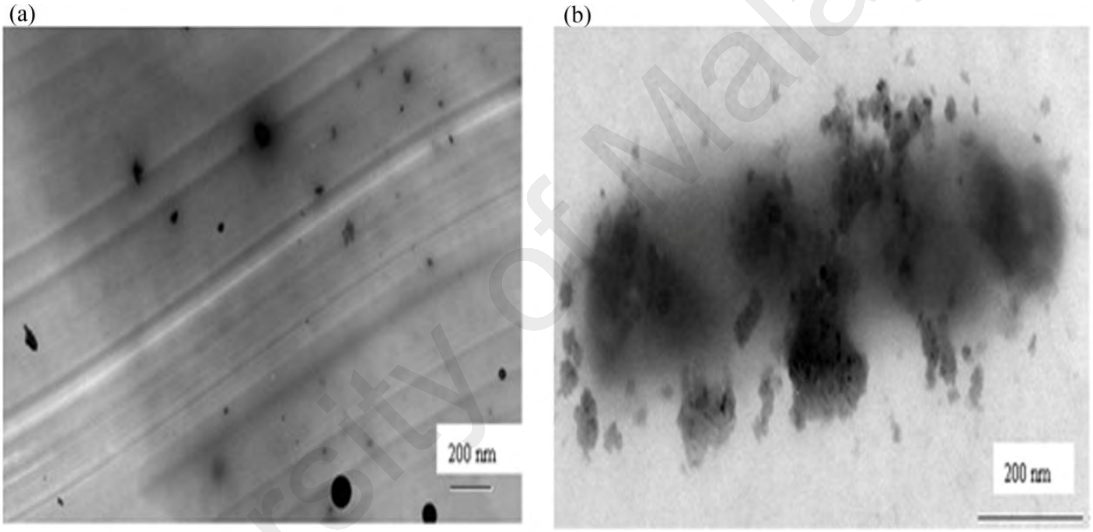

Figure 2.19: TEM images showing better dispersion of (a) 4 wt% than in (b) 8 wt% nano-$CaCO_3$ in epoxy resin

(He et al., 2011)

2.4.4 Flexural Properties

Flexural strength is the highest stress experienced within materials at the moment of rupture. Flexural modulus is the ratio of stress to strain in flexural deformation. In particulate-filled polymer composites, both flexural strength and flexural modulus are affected by particle size and particle loading.

He et al. (2011) found that at low filler content, the flexural strength increases as the particle content increases. The maximum flexural strength is achieved at 4 wt% $CaCO_3$ and it gradually decreases as filler is added to the epoxy resin matrix (Figure 2.20). Good particle dispersion at this filler loading maximizes the interfacial interactions between particles and matrix.

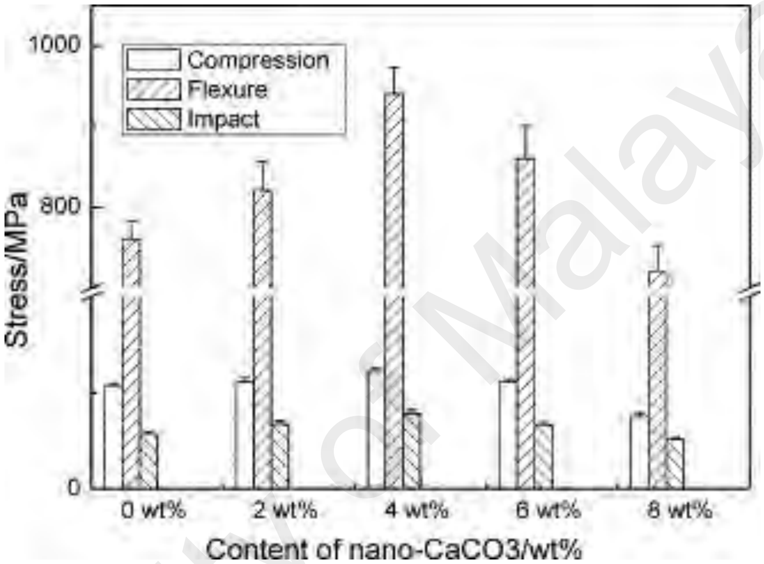

Figure 2.20: Mechanical properties of pure epoxy resin and nano-$CaCO_3$/epoxy composites at different filler loadings

(He et al., 2011)

Yang et al. (2006) studied the effect of different $CaCO_3$ filler loadings in three different types of polypropylene (PP). The results show that the flexural strength and flexural modulus increase with increasing filler loading. The agglomeration of nano-$CaCO_3$ at high loading does not greatly affect flexural strength and flexural modulus. Table 2.7 shows the results for flexural strength and flexural modulus of the $CaCO_3$/PP nano composites.

Table 2.7: Flexural properties of $CaCO_3$/PP nanocomposites

(Yang et al., 2006)

Composition (weight ratio)		**PP1**		**PP2**		**PP3**	
PP	**CC007**	**Flexural strength (MPa)**	**Flexural modulus (MPa)**	**Flexural strength (MPa)**	**Flexural modulus (MPa**	**Flexural strength (MPa)**	**Flexural modulus (MPa**
100	0	35.4	1386.7	23.7	905.4	27.8	1082.3
98	2	35.4	1420.8	23.7	927.2	27.9	1100.6
96	3	35.6	1451.4	23.9	954.0	28.3	1132.6
94	6	35.8	1469.4	24.0	971.4	28.6	1166.3
92	8	36.1	1485.1	24.3	982.8	29.2	1189.4
90	10	36.4	1536.3	24.4	1023.4	30.0	1221.5
80	20	37.5	1722.4	25.2	1144.5	31.4	1346.8
70	30	38.3	1868.5	27.6	1277.0	32.7	1562.8
60	40	39.2	2085.9	30.1	1468.6	34.2	1694.2

PP1 is homopolymer polypropylene, PP2 is polypropylene copolymer and PP3 is the mixture of PP1 and PP2 at 1:1 weight ratio.

Not all nano-sized particles infused in polymer resin exhibit excellent flexural properties compared to micro-sized particles. Dong et al. (2011) investigated the effect of embedding micro and nano-sized particles into epoxy resin. Three different types of particles embedded in the epoxy resin were platelet-like alumina particles (~300 nm in thickness), spherical zinc oxide (average size of 30 nm) and nanoclay powders. The results revealed that micro-sized platelet-like alumina particles resulted in the highest improvement in flexural modulus (at 8 wt%), flexural strength (at 3 wt%) and flexural strain at break (at 3 wt%) as compared to epoxy/zinc oxide and epoxy/nanoclay composites. The results are presented in Table 2.8.

Table 2.8: Flexural properties of micro and nano-sized particulate-filled epoxy composites

(Dong et al., 2011)

Sample	**Particle content (wt%)**	**Flexural modulus (GPa)**	**SD**	**Flexural strength (MPa)**	**SD**	**Flexural strain at break (%)**	**SD**
Neat epoxy	0	2.73	0.208	104.6	10.14	N/A[b]	N/A
Epoxy/alumina composites	1	3.02	0.144	101.3	12.85	3.8	0.9
	3	3.11	0.097	111.3	5.98	5.1	1.2
	5	3.34	0.105	99.6	17.88	3.7	1.0
	8	3.46	0.144	81.8	11.28	2.7	0.5
Epoxy/zinc oxide composites	1	2.94	0.049	101.3	6.61	3.9	0.6
	3	3.11	0.063	104.8	13.95	4.3	0.9
	5	3.27	0.070	94.6	4.57	3.2	0.2
	8	3.07	0.175	100.9	6.63	3.9	0.5
Epoxy/nanoclay composites	1	2.85	0.187	78.0	5.61	3.1	0.2
	3	3.02	0.107	86.5	6.01	3.2	0.3
	5	2.82	0.100	72.5	3.29	2.9	0.19
	8	3.07	0.242	75.6	4.53	2.8	0.21

[a] SD-Standard deviation. [b] Flexural strength was reached at 5% flexural strain prior to the sample breaking according to ASTM D790

Dong et al. (2011) explained the reduction of the flexural modulus of zinc oxide-reinforced epoxy composites at 8 wt%. Breakage occurred through the particle agglomerates, especially at 5 wt% and 8 wt%. At 8 wt% zinc oxide content, the agglomerate tended to easily break compared to 5wt% zinc oxide because of the crack propagation path that passes through both the epoxy matrix and particle agglomerates without changing direction. However, at 5 wt% zinc oxide loading, the agglomerates were harder to break and were capable of resisting and deflecting crack failure, as shown in Figure 2.21 where the crack was deflected either downwards or upwards.

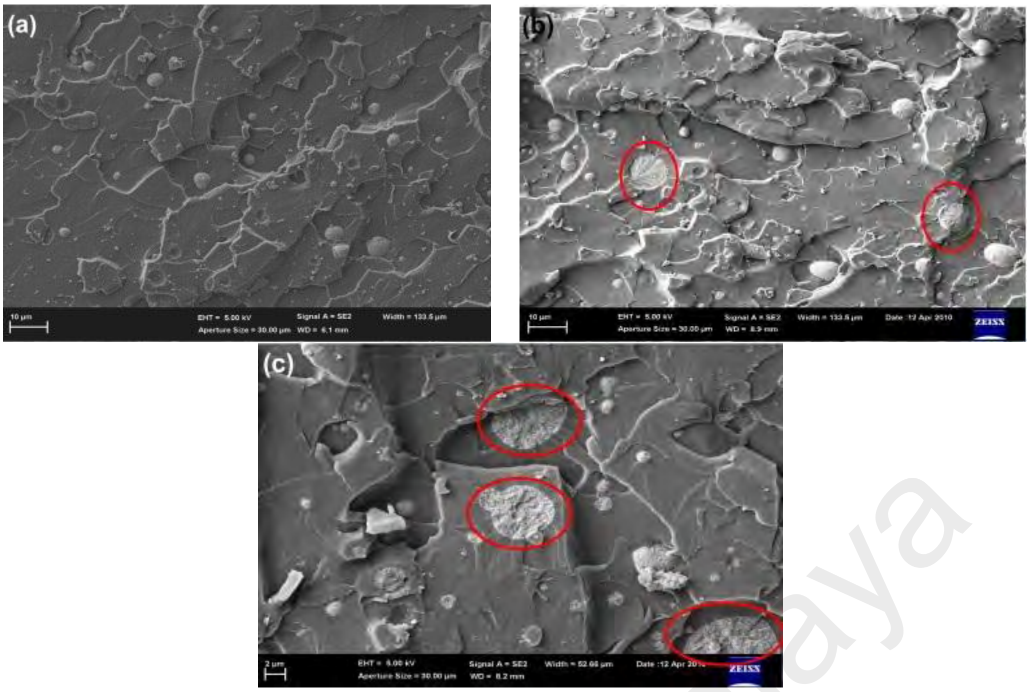

Figure 2.21: SEM images showing the fracture surface of different filler content at (a) 3 wt%, (b) 5 wt% and (c) 8 wt% zinc oxide-filled epoxy composites

(Dong et al., 2011)

2.4.5 Hardness and Tabor's correlation

Hardness is defined as the resistance of a material to the formation of indentation on its surface. Hardness is well established for characterizing metals and ceramics (Askeland et al., 2011). Hardness testing for characterizing polymers has not been used much but is increasingly being employed in recent years for quality assurance tests and determining changes in morphology and microstructure of polymers and polymer blends (Baltá Calleja & Fakirov, 1997). For particulate-filled polymer composites, surface hardness depends on filler size (Schwartz & Söderholm, 2004) and filler content (Lam et al., 2005).

A composite with finer filler showed higher surface hardness than coarser filler (Schwartz & Söderholm, 2004). This is because finer filler has shorter inter-particle spacing and larger total surface area, thus improving matrix protection. Matrix protection from greater hardness of inorganic fillers therefore increases the total surface area hardness of composites.

Lam et al. (2005) proved that nanoclay hardness increases with increasing nanoclay filler, up to a maximum limit at 4 wt% as shown in Figure 2.22. At maximum hardness, no plastic deformation was found on the stress-strain curve. However, above the maximum content limit, the filler might retard the chemical reaction, causing an incomplete curing process of the composites, and thus softening the composites. Therefore, the surface becomes softer as filler is added beyond this limit. Another reason for the reduction of surface hardness is particle agglomeration. Curing polymer resin at low temperatures may cause the agglomeration of particles since the particles cannot be easily dispersed despite being subjected to sonication. As the particle content increases, the free volume allows for the particles to move around more, and so the agglomeration cannot be easily separated by mechanical stirring and ultrasonic separation (sonication) at room temperature. Then agglomeration size also increases with increasing filler content (Figure 2.23). Besides, the formation of agglomerate clusters is found as filler content increases due to the increment of cross-link density.

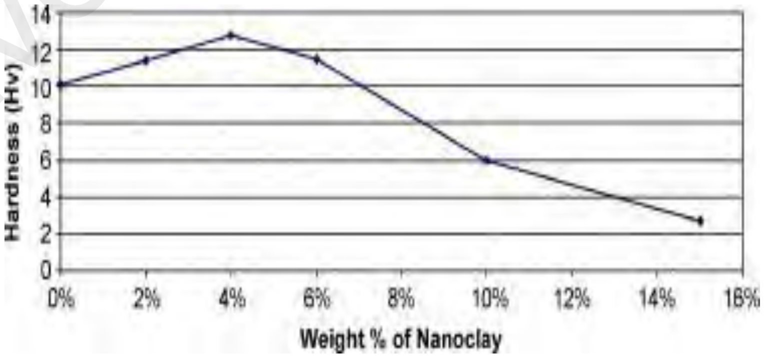

Figure 2.22: Effect of filler content on the surface hardness value of nanoclay/epoxy composites

(Lam et al., 2005)

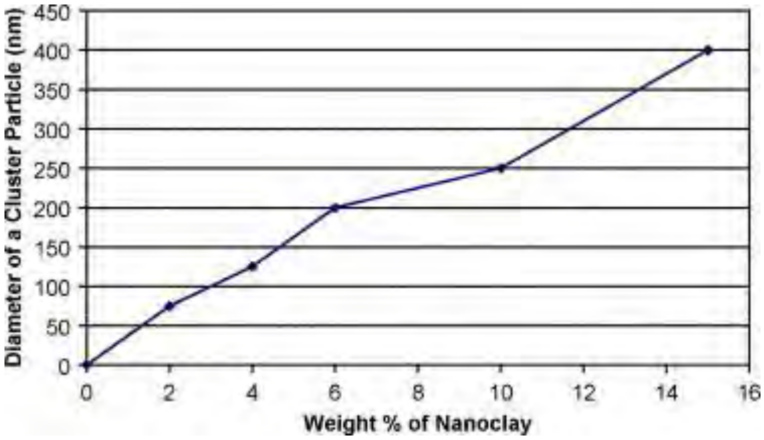

Figure 2.23: The increase of particle cluster size with the increase of nanoclay content in epoxy matrix composites

(Lam et al., 2005)

Tabor's correlation is the correlation between hardness and yield stress of materials (Suwanprateeb, 2000) by assuming the metal as rigid perfectly plastic solids as shown in Figure 2.24. It can be related as a simple equation, $H \approx C\sigma_y$, where σ_y is yield stress and C is a constant of approximately 3 (Tabor, 1951). The relationship between the ultimate tensile strength (σ_{UTS}) and Vickers hardness (H_v) is $H_V = 3.\sigma_{UTS}$ (Boyer & Gall, 1985).

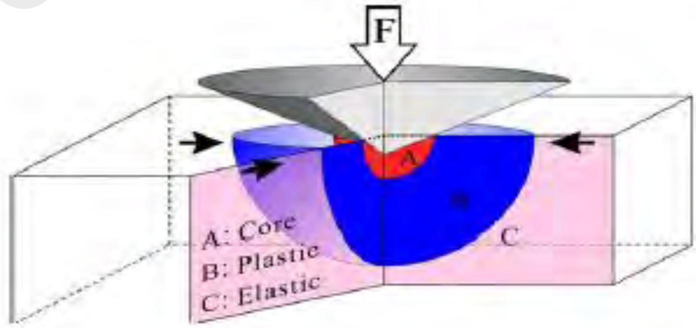

Figure 2.24: Idealized cavity model of elastic-plastic indentation

(Zhang et al., 2011a)

Zhang et al. (2011a) claimed that Tabor's analyses (Tabor, 1951) were not suitable for all materials. The correlation between hardness and strength can be classified into four types: type I ($3\sigma_y < H_V < 3\sigma_{UTS}$), type II ($H_V \approx 3\sigma$), type III ($H_V < 3\sigma$), and type IV ($H_V > 3\sigma$). Figure 2.25 shows Tabor's correlation of all four classes of relationships between strength and hardness. Type I is normally experienced by high-ductility materials. Type II is ideally suitable for plastics (Tabor, 1951) and only valid for materials without, or with low work-hardening ability and that are difficult to normally crack (Zhang et al., 2011a). Type III always exhibits shear deformation behavior under either tension or compression. Type IV is experienced by very brittle materials.

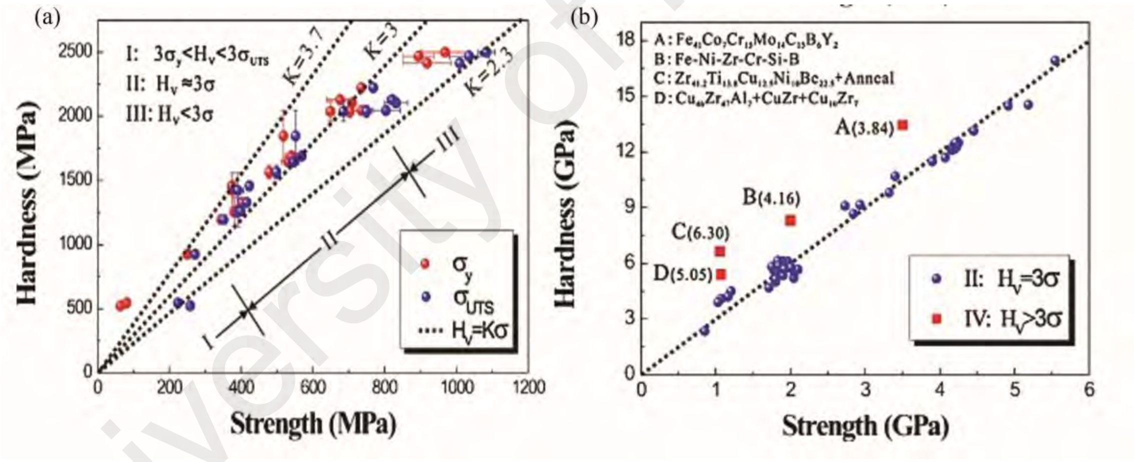

Figure 2.25: Correlation between strength and hardness in (a) Cu and Cu-Zn alloys with different pretreatment; and (b) metallic glass

(Zhang et al., 2011)

Tabor (1951) claimed that materials with different indentation morphologies always exhibit different relationships between hardness and strength. The geometry of indentations could be classified into three types: sink-in, pile-up and crack (Figure 2.26). Materials with good ductility exhibit "sink-in" morphology after hardness testing because they are easily deformed by the effortless nucleation and dislocation movement and they cannot fully harden during the hardness test. This is the reason why one third of hardness is always lower than ultimate tensile strength (UTS). Materials that can easily harden up to their UTS allow for shear deformation to gradually increase and hence the hardness approximately equals 3 times the yield stress or UTS. Thus, "pile-up" morphology will be exhibited due to sufficient hardening. This normally occurs in micron-grained, ultra-fine grained and nano-crystalline materials. For brittle materials, hardness-to-strength ratio larger than 3 occurs due to the limitation of the materials as shear deformation tends to be extremely problematic and cleavage cracking becomes much easier.

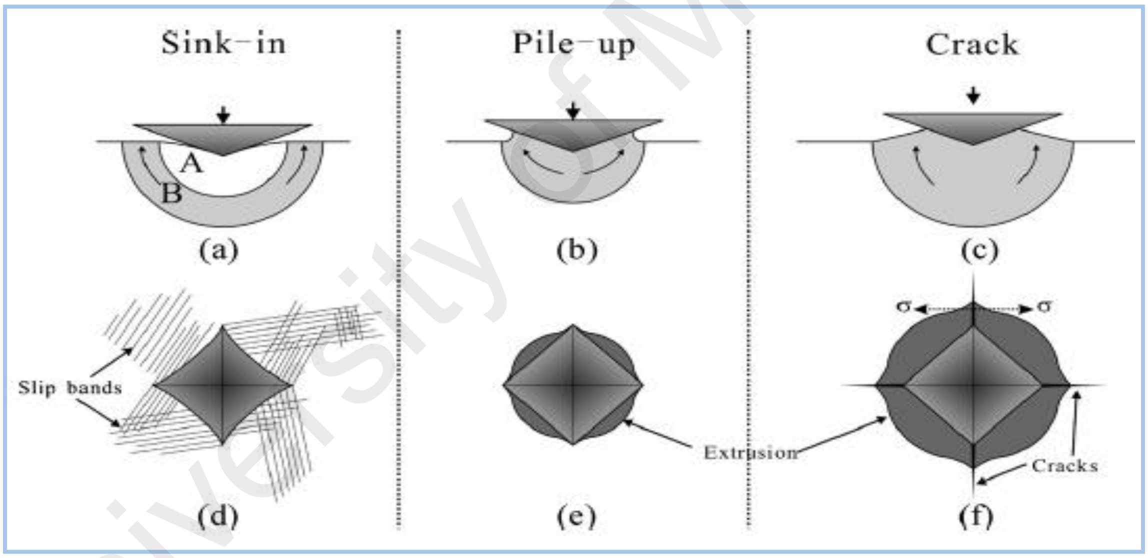

Figure 2.26: Three types of indentation morphology: sink-in, pile-up and crack (Zhang et al., 2011a)

Tabor's correlation is influenced by the interfacial bonding between the filler and polymer matrix (Kaymakci & Ayrilmis, 2014). Excellent filler-matrix interfacial bonding produces better Tabor's correlation values. The correlation increases as the filler loading increases up to an optimum value. Then, adding filler beyond the maximum value leads to a weak correlation. At this point, the amount of polymer matrix is not sufficient for the filler-matrix attachment.

2.4.6 Microscopic observation of the failure process

Ahmad et al. (2008) studied the effect of silica mineral particle shape on the tensile properties of epoxy composite. They found that the higher the aspect ratio of the filler, the greater the strength and modulus of the composite. The aspect ratio of a filler particle is the ratio between the particle's largest and smallest dimensions. The result showed that elongated silica mineral composites have the highest strength and modulus while the lowest trend is shown by angular silica mineral composites. High aspect ratio provides a great surface area, or more contact area between the filler and the matrix, thus providing high potential to reinforce the matrix. High aspect ratio also leads to higher levels of stress transferability, hence increasing the flexural modulus of composites. Figure 2.27 shows a micrograph of elongated and angular silica-filled epoxy composites. Obviously, there is weak interfacial bonding between the angular particle surface and epoxy matrix. This may be associated with the stress concentration factors at the edge of the particles.

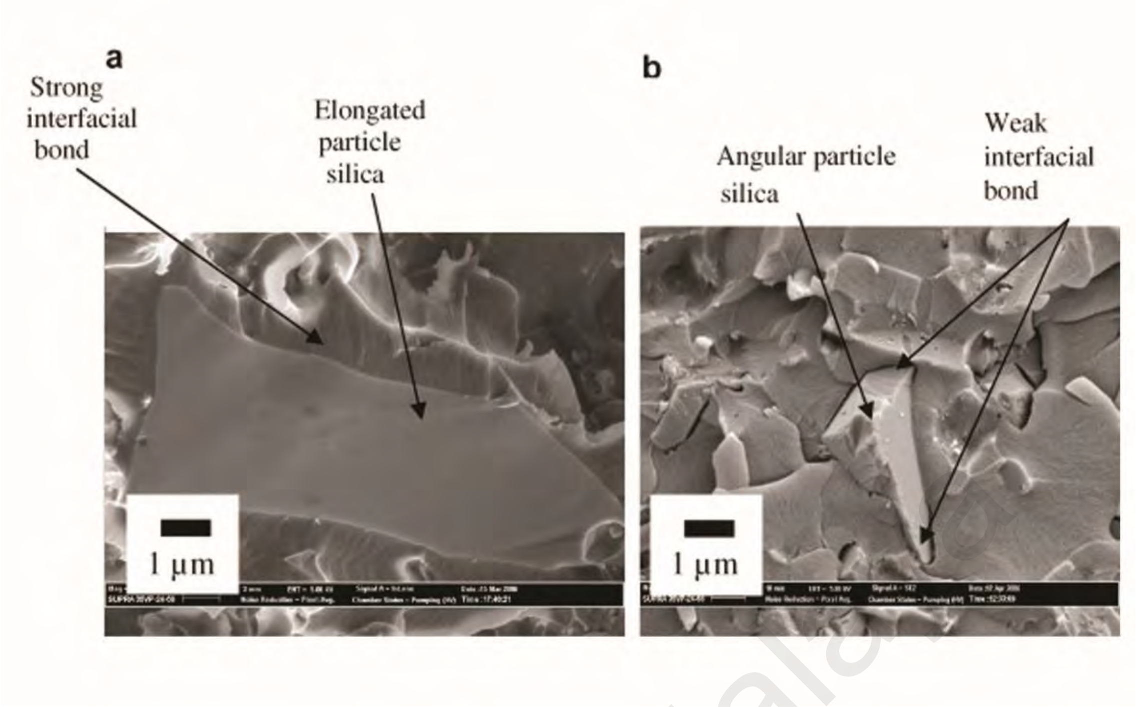

Figure 2.27: SEM images showing weaker interfacial bonding between angularparticles than elongated particles

(Ahmad et al., 2008)

Dong et al. (2011) illustrated the failure mechanism of different shapes and sizes of filler and filler loading in polymer composites. According to the study, for similar filler loading, the shape and size of the filler influences the flexural modulus value. Micro-sized and platelet-like filler, such as alumina would exhibit better flexural modulus and strength compared to nano-sized and sphere-shaped filler, such as zinc oxide, at similar filler loading. Figure 2.28 shows that small (1-10 µm) platelet-shaped particles of alumina display good particle dispersion and are well-embedded into the epoxy resin. More and bigger defects in terms of interfacial bonding are observed for larger alumina particles (equal to or more than 10 µm) due to the clustering effect that results in high stress concentrations around their edges.

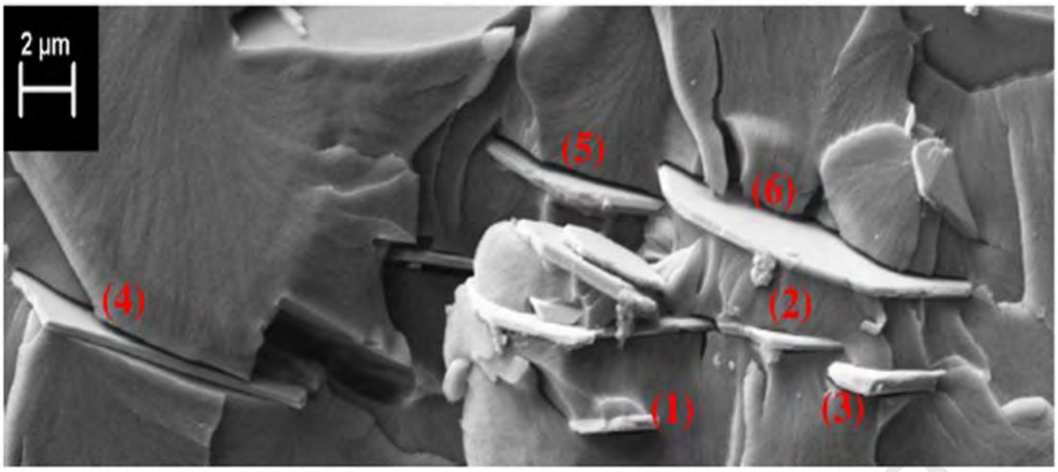

1, 2 and 3: Small alumina particles
4, 5 and 6: Large alumina particles

Figure 2.28: SEM micrograph showing weaker interfacial bonding between larger particles of alumina-reinforced epoxy at 8 wt% alumina

(Dong et al., 2011)

For spherical shaped filler, flexural failure mostly occurs due to the agglomeration of several filler particles and it can generally be classified into two mechanisms: (i) breakage through the agglomerates and (ii) breakage adjacent to or touching a few of the agglomerates. Agglomeration can still be found in the composite although the samples undergo ultrasonication. Figure 2.29 shows the breakage mechanism of large and rigid zinc oxide filler agglomerates in epoxy matrix composite. At low filler loading (in this case 5 wt%), the crack propagation direction rapidly changes and touches only a small area of the agglomerates. This is because of the agglomerates' ability to resist and deflect crack failure. However, on certain surface areas, the crack is capable of breaking the agglomerates. For higher filler loading (8 wt%), the crack rapidly propagates without changing direction in the polymer matrix or breaking the agglomerates. Charpy impact resistance for particulate-filled polymeric composites can be adversely affected by three main factors: the size of agglomerates, particles' aspect ratio and particle shape (Dong et al., 2011). Large agglomerates can be crack initiators. High particle aspect ratio with possible edges may contribute to great stress concentrations, thus initiating and propagating failure. Irregular particle shapes with angularities and edges may also facilitate impact failure.

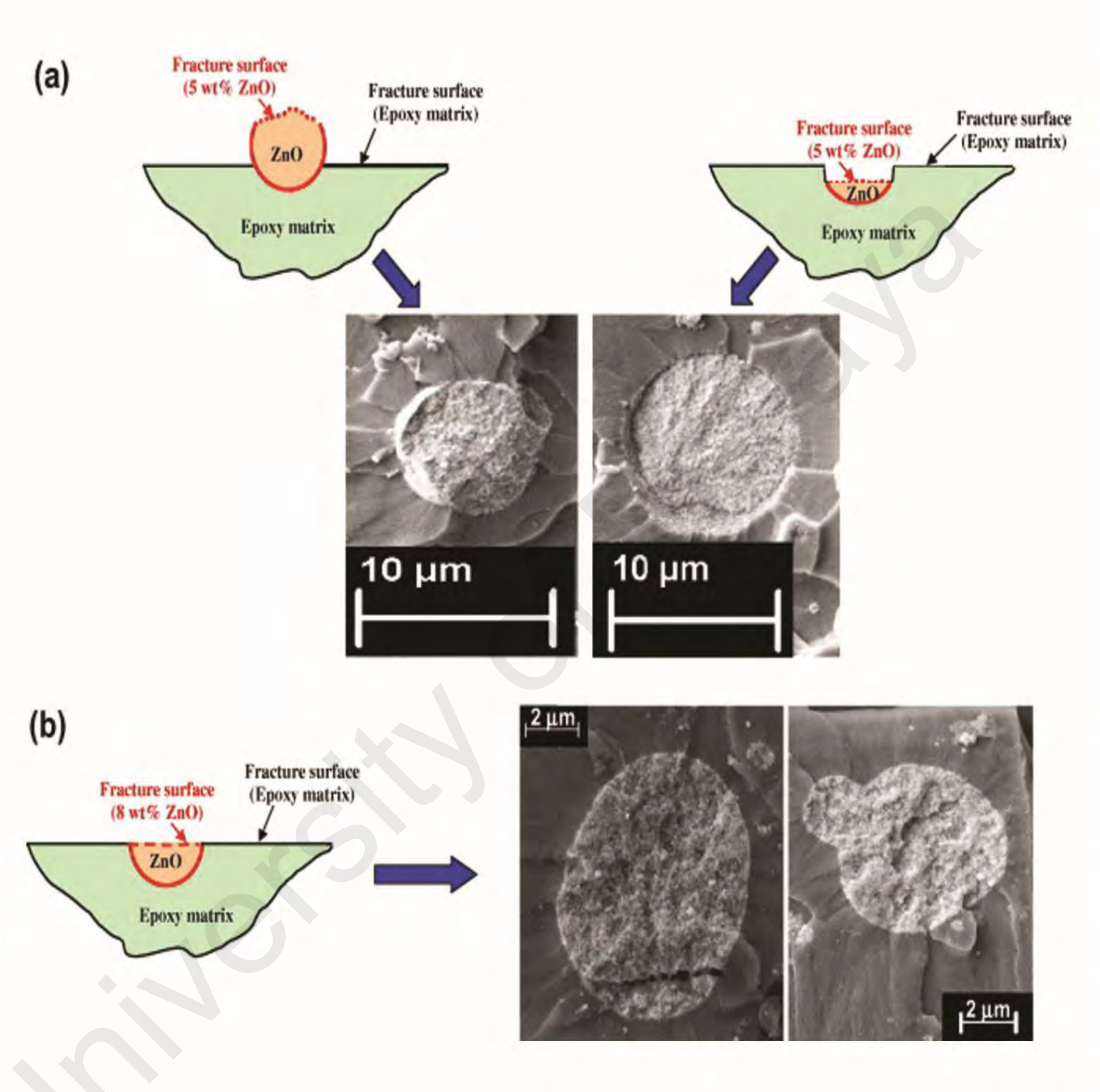

Figure 2.29: Breakage mechanisms of zinc oxide agglomerates at (a) 5 wt% and (b) 8 wt% of zinc oxide/epoxy composites

(Dong et al., 2011)

Cho et al. (2006) investigated the failure modes of macro and nano-scale 5 vol% glass beads, and 1 and 3 vol% alumina (Al_2O_3, aluminum dioxide) particles in vinyl ester resin by uniaxial loading direction. Sonication was applied to prevent agglomeration of the particles and subsequently, dispersing additive was used to prevent re-agglomeration. It was noted that debonding initiation appeared mostly at one pole of the particles in the direction of the applied tension. Two different failure modes were found:one for small particles with diameters less than 70 µm and when the particle diameter was more than 200 µm.

For small particles with diameters below 70 µm, the debonding area was first observed at one pole and it grew to a certain size before stopping (Figure 2.30). Then, at the opposite pole of the particles, de-bonding started to initiate and grew up to 80-90% of failure stress when it reached debonding anglesof 52-62°, which were measured from the pole to the front of the debonded area (Figure 2.31). Thin lines or micro-cracks kinking with angles of 40-45° were also observed to have initiated from the debonding sites (Figure 2.32). The angle was measured from the crack to the tangential line on the interface at the interfacial crack tip. Before fracture, cracks on the composite surface of the specimen were also observed. Noticeable debonding appeared at 70% failure stress or at the stress-strain curve where nonlinearity appeared to start. The curves in Figure 2.33 indicate that as the size of particles embedded in the polymer composite decreased, there were higher stress levels that caused a noticeable extent of debonding or curve nonlinearity.

For large particles with more than 200 µm diameter, debonding was only observed when stress was above 90% of failure stress. Besides, no surface cracks and only little nonlinearity appeared in the stress-strain curves due to the lower failure stresses.

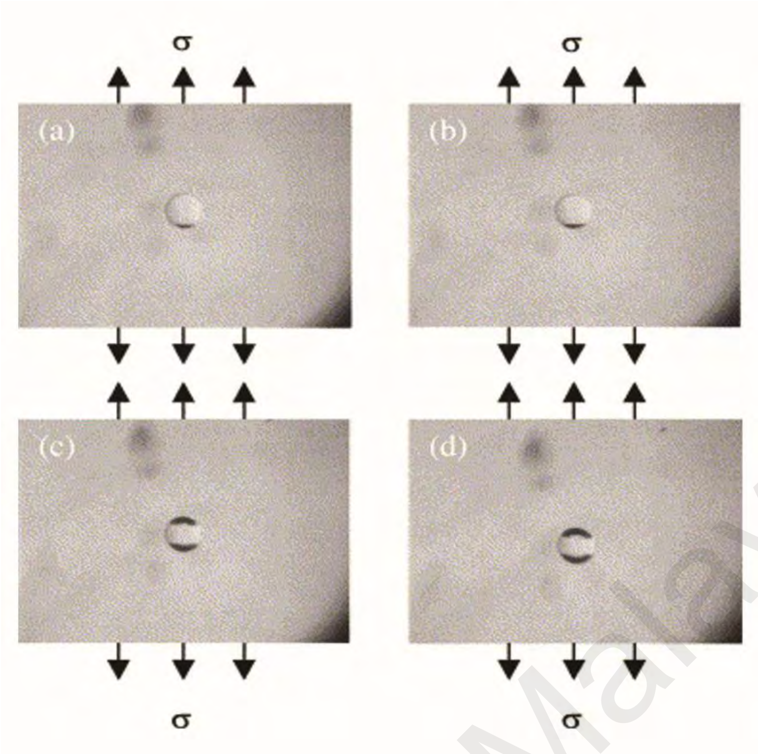

Figure 2.30: Mechanism of failure growth: (a) start of particle-matrix debonding at one pole of the particle, (b) debonding grows, (c) debonding emerges at the opposite pole, (d) debonding fully extended

(Cho et al., 2006)

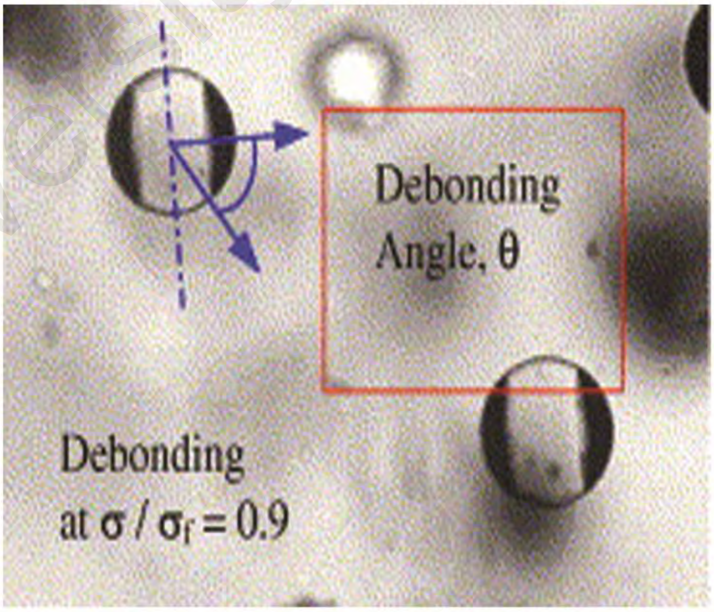

Figure 2.31: Debonding angle and partially debonded particles in composite

(Cho et al., 2006)

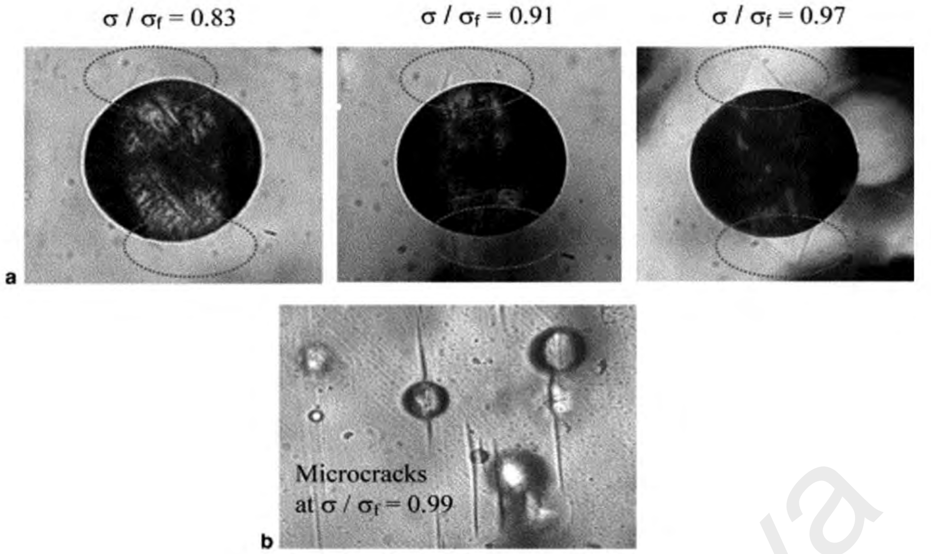

Figure 2.32: Cracks in matrix material before failure: (a) micro-cracks kinking from debonding crack; (b) cracks on composite specimen surface

(Cho et al., 2006)

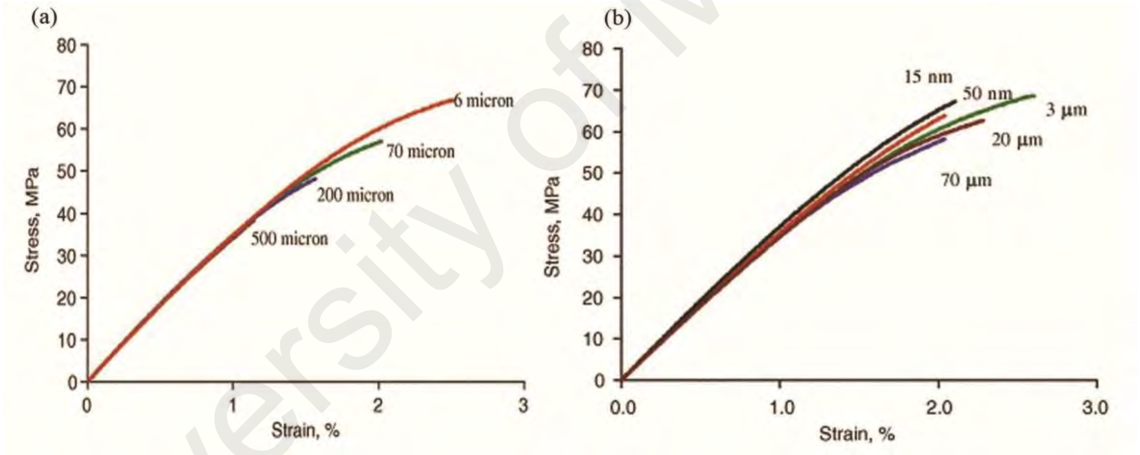

Figure 2.33: Stress-strain curves for different sizes of (a) glass bead particles at 5 vol% and (b) alumina particles at 3 vol% in vinyl ester resin

(Cho et al., 2006)

Suwanprateeb (2000) investigated the effect of tensile loading of $CaCO_3$ powder with average size of 5 μm filling high density polyethylene (HDPE). The result presented in Figure 2.34 shows that tensile yield stress decreases with increasing filler volume fraction. The tensile properties of materials are determined from flaws and submicroscopic cracks. The rigid $CaCO_3$ surface acts as a defect in the HDPE matrix and leads to complete debonding at the interface as observed under SEM (Figure 2.35).

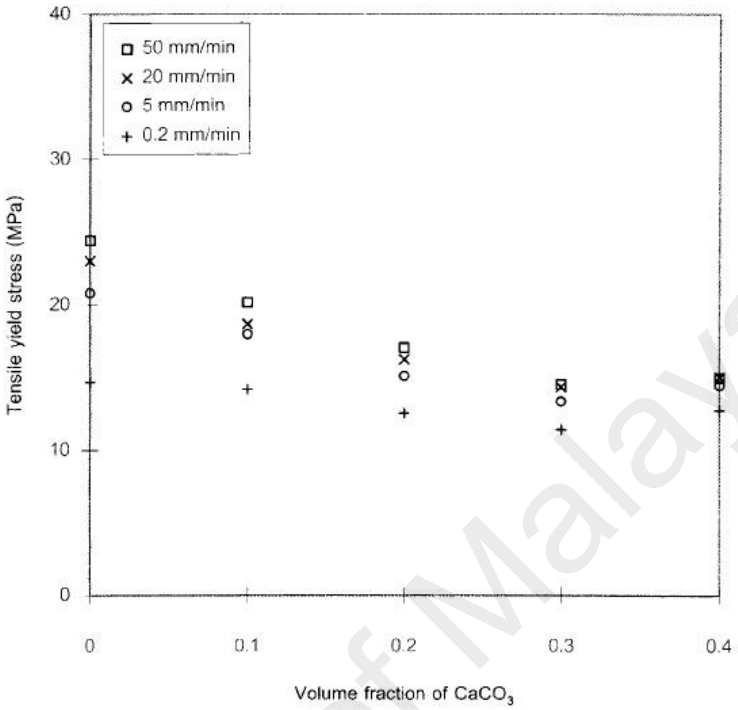

Figure 2.34: Effect of $CaCO_3$ particle content on the tensile yield stress of composites (Suwanprateeb, 2000)

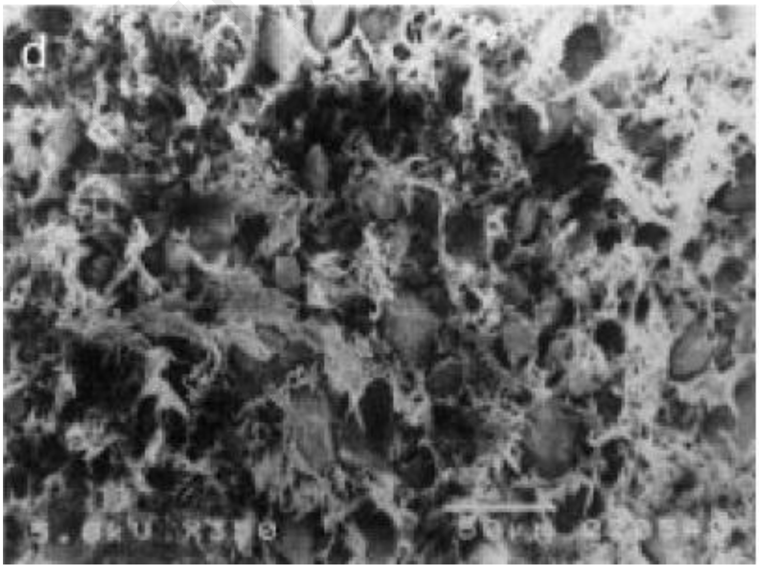

Figure 2.35: SEM image showing the detachment of the polyethylene matrix from the calcium carbonate surface

(Suwanprateeb, 2000)

2.4.7 Effect of surface treatment

Surface treatment can be categorized into two main groups: reactive and non-reactive treatment. The purpose of reactive treatment is to produce excellent bonding between particles and the matrix. It is also known as a coupling agent. In reactive treatment, one end of the surfactant molecules reacts with the inorganic surface to produce covalent bonds, which produce stronger bonding than non-reactive treatment (Thio et al., 2004). An example of reactive treatment is with silane. The purpose of the non-reactive treatment is to promote homogenous filler dispersion in the matrix by covering the filler surface with a small molecular weight organic compound (Fekete et al., 2004). Non-reactive treatment methods typically involve molecules with polar hydrophilic groups associated with the inorganic filler, while the hydrophobic groups interact with the polymer matrix (Thio et al., 2004). Two types of forces involved are van der Waals and polar-polar forces. An example of non-reactive treatment for $CaCO_3$ filler is with stearic acid (Móczó et al., 2002). Surface treatment performance is dependent on the interaction between the inorganic surface and matrix polymer (Thio et al., 2004) and the amount of surfactant (Jeong et al., 2009). Fillers with an inactive surface such as talc cannot be treated by either reactive or non-reactive treatment. The composites also can be treated without using the chemical. Heat treatment for example can improve the mechanical properties of the composites by improving the rigidity of the amorphous polymer results in improvement of elastic modulus (do Nascimento et al., 2016)

2.4.7.1 Characterization of surface treatment

Jeong et al. (2009) studied the characteristics of ground $CaCO_3$ powder treated with stearic acid. From the hydrophobicity test, the surface of ground $CaCO_3$ powder was generally hydrophilic but changed to hydrophobic surface when coated with stearic acid. The optimal amount of stearic acid to modify the ground $CaCO_3$ powder surface was 1.0 mass%, because the contact angle and hydrophobicity shown in Figures 2.36 and 2.37 yielded from this amount are similar to a complete monolayer. $CaCO_3$ also can be treated using 2% of dodecyl dihydrogen phosphate to change the surface property from hydrophilic to hydrophobic (Zhao et al., 2016)

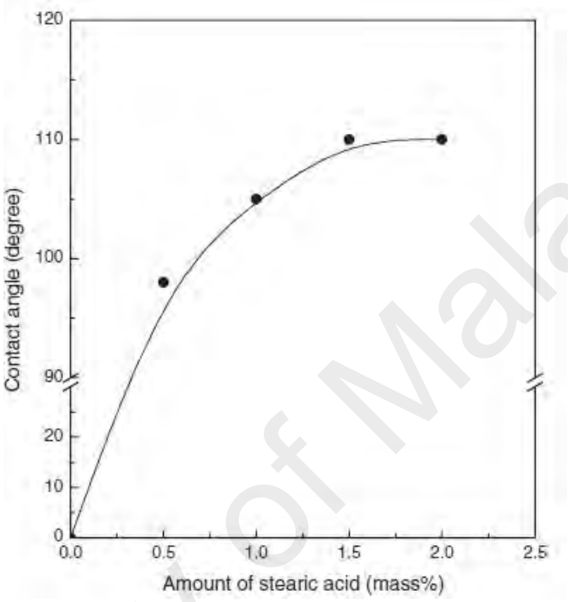

Figure 2.36: Contact angle of water atvarious amounts of stearic acid coated on the surface ofground $CaCO_3$

(Jeong et al., 2009)

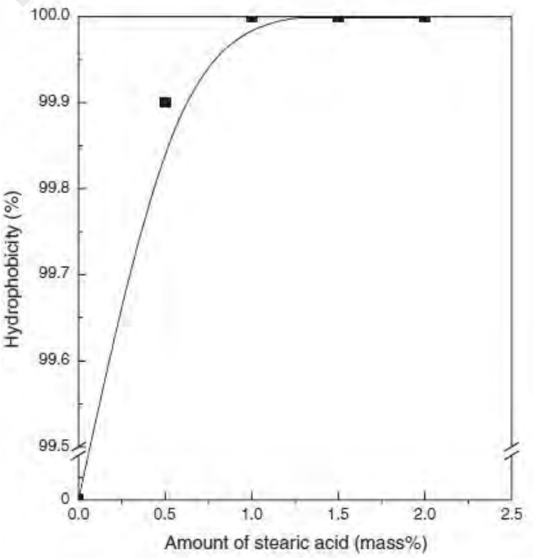

Figure 2.37: Hydrophobicity at various amounts of stearic acid coated on the surface of ground $CaCO_3$

(Jeong et al., 2009)

Treating $CaCO_3$ with stearic acid can also decrease the particle size, hence increasing the specific surface area as shown in Table 2.9. Kiss et al. (2007) found that using stearic acid leads to a significant decrease in surface tension, which results in decreased interaction between the filler as well as limited aggregation.

Table 2.9: Physical properties and surface properties of untreated and stearic acid-treated ground $CaCO_3$ (GCC)

(Jeong et al., 2009)

	Sample	**Max diameter** (μm)	**Min diameter** (μm)	**Average diameter** (μm)	**Specific surface area** (m^2/g)
Physical properties	Untreated GCC	30.20	0.36	5.24	2.18
	Treated GCC with 1.0 mass% stearic acid	26.30	0.36	5.20	2.20
Surface properties		**Contact angle**	**Hydrophobicity**	**Surface free energy,** $\boldsymbol{\gamma_s^D}$ (mJ/m^2)	
	Untreated GCC	0°	0%	93.3	
	Treated GCC with 0.5 mass% stearic caid	98±3°	99.9%		
	Treated GCC with 1.0 mass% stearic acid	105±3°	100%	34.8	
	Treated GCC with 1.5 mass% stearic acid	110±3°	100%		
	Treated GCC with 2.0 mass% stearic acid	110±3°	100%		

2.4.7.2 Effect of surface treatment on the mechanical properties

Treating $CaCO_3$ with stearic acid enables increasing the tensile strength of the composites compared to untreated $CaCO_3$-filled polymer composites. According to Demjen et al. (1998) tensile strength is significantly affected by chemical treatment. Deshmukh et al. (2010a) discovered that composites containing uncoated $CaCO_3$ have lower tensile strength than those coated with stearic acid, for up to 20 wt% $CaCO_3$ filler content (Table 2.10). More than 20 wt% filler exhibits a decrease in tensile strength. The increase is due to the hydrophobic feature produced by the stearic acid coating, which enhances dispersion between the phases and promotes good $CaCO_3$ particle-PBT matrix adhesion. Evidence of poor adhesion and strong particle-particle of the uncoated $CaCO_3$-PBT matrix was observed through SEM (Figure 2.38).

Table 2.10: Tensile yield strength of uncoated and stearic acid-coated $CaCO_3$/PBT composites

(Deshmukh et al., 2010a)

Sample	**Tensile yield (MPa) for uncoated $CaCO_3$**	**Tensile yield (MPa) for coated $CaCO_3$**
Pure PBT	56.408	
5 wt% $CaCO_3$	51.166	52.711
10 wt% $CaCO_3$	51.362	53.297
20 wt% $CaCO_3$	53.299	58.938
30 wt% $CaCO_3$	50.406	50.235

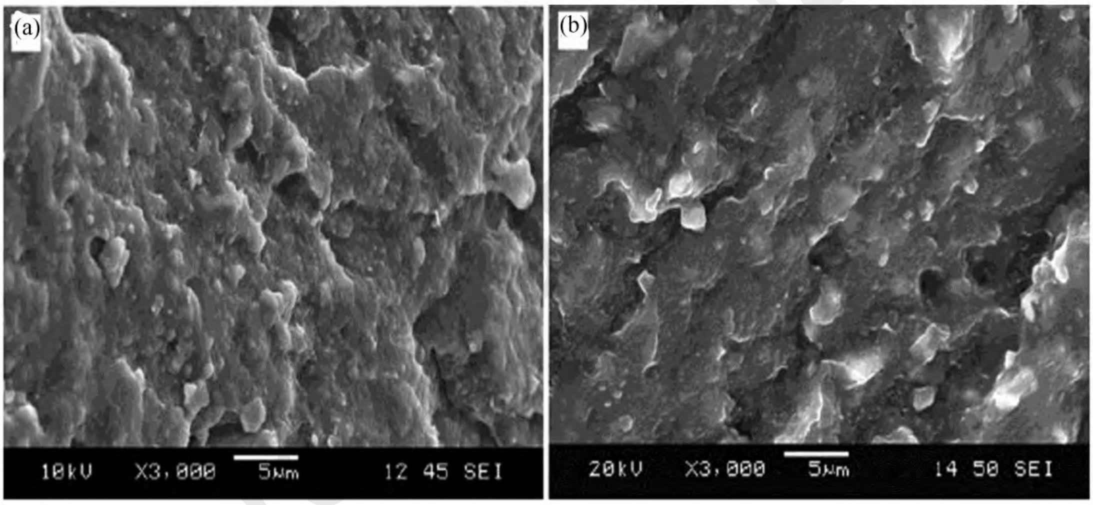

Figure 2.38: SEM images showing (a) the strong interaction among uncoated $CaCO_3$ particles and (b) better dispersion of stearic acid-coated $CaCO_3$ in $CaCO_3$/PBT composites

(Deshmukh et al., 2010)

The growth in the specific area of the filler (Pukanszky, 1990) produces higher tensile strength and tensile modulus of particulate-filled polymer composites, as shown in Figure 2.39. The tensile strength of uncoated filler composite increases intensely with increasing specific surface area up to 6 m^2/g, above which the strength declines due to the formation of aggregates. Clustering of small aggregates that form bigger clusters encourages the easy debonding and fracture of aggregates. For $CaCO_3$ filler coated with stearic acid, the tensile strength increases continuously as the size of the particles decreases (specific surface area increases) but the tensile strength value is always smaller than for uncoated $CaCO_3$ particle PP composites at similar specific surface areas. Figure 2.40 shows better filler distribution when the $CaCO_3$ is treated with stearic acid. However, this treatment does not guarantee superior tensile strength and tensile modulus.

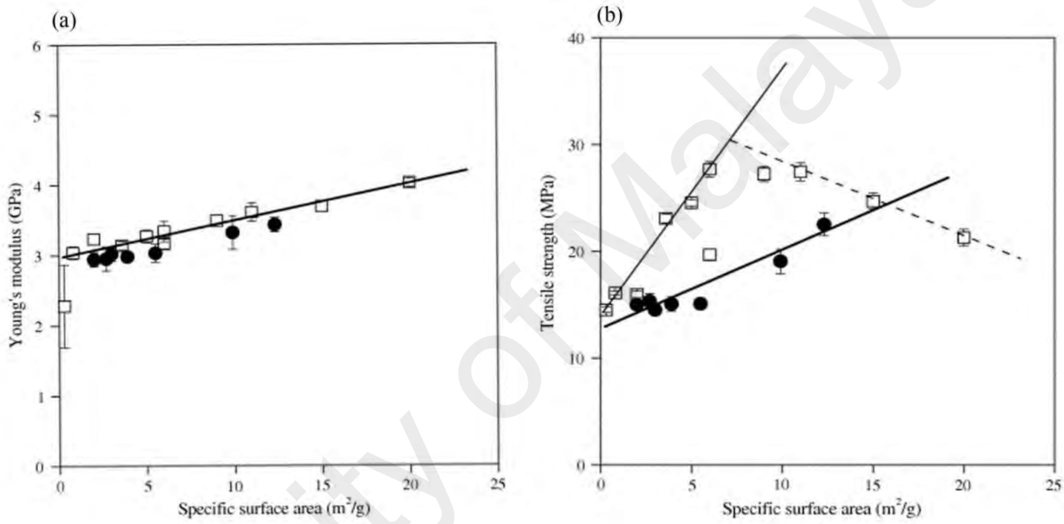

Figure 2.39: Effect of filler coating and specific surface area on (a) the stiffness and (b) the tensile strength of $CaCO_3$/PP composites (□Uncoated, •coated)

(Kiss et al., 2007)

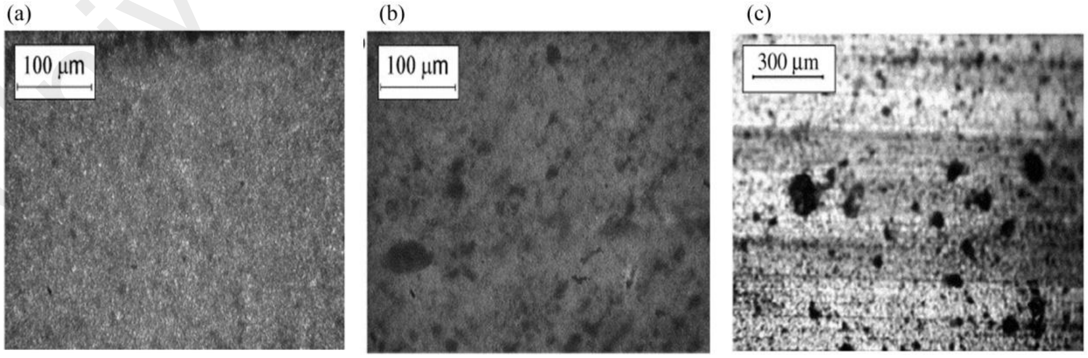

Figure 2.40: Optical microscopy images showing better distribution of coated $CaCO_3$ filler in $CaCO_3$/PP composites: (a) coated filler with specific surface area of 2.0 m^2/g at 30 vol% filler, and (c) uncoated filler with specific surface area of 9.0 m^2/g at 20 vol% filler

(Kiss et al., 2007)

The tensile strength of the composite depends on the effectiveness of stress transfer between matrix and filler. Particle-matrix interfacial adhesion plays a significant role in affecting the strength of particulate composites. Effective stress transfer produced by excellent particle-matrix bonding may contribute to high-strength composites (Fu et al., 2008). Poor bonding between matrix and particles leads to ineffective stress transfer. Therefore, the particles cannot carry any additional load and at this point, the composite strength decreases with increasing particle loading.

Interfacial adhesion has little effect on the stiffness of the particulate-filled polymer composites (Fu et al., 2008). Better filler dispersion produces a stiffening effect of the composite. However, as treatment is introduced to the polymer on the filler surface, a concentration gradient around the particles is also introduced, thus resulting in competition between the ‘stiffening’ effect of better dispersion and the ‘softening’ effect of the treatment agent. This may explain why in some cases, treatment may not help to increase the composite’s modulus.

2.5 Thermophysical Properties

Thermophysical properties are defined as including all material properties affecting the transfer and storage of heat that vary with the state variables’ temperature, pressure and compositions and other relevant variables, without altering the material’s chemical identity. These properties include thermal conductivity and diffusivity, heat capacity, thermal expansion and thermal radiative properties, viscosity and mass, thermal diffusion coefficient, speed of sound, surface and interfacial tension in fluids. In this study, only three thermal properties were investigated: thermal conductivity, thermal diffusivity, and specific heat content.

2.5.1 Thermal conductivity

Thermal conductivity is the ability of a substance to transfer heat. It represents the quantity of heat passing per unit of time per unit area at a temperature drop of one degree Celsius per unit length. Thermal conductivity, k can be expressed in a mathematical equation as follows:

$$\mathbf{k} = \frac{\mathbf{Qx}}{\mathbf{A\Delta T}} \tag{2.1}$$

Where Q is amount of heat transfer through the material (J/s or W), A is the area of the body (m^2) and ΔT is change in temperature (K).

For composite materials, the effective thermal conductivity is dependent on the conductivity of individual constituents. The common fillers for enhancing the thermal conductivity of polymers are listed in Table 2.11.

Table 2.11: Thermal conductivity of some fillers

(Fischer & Gogotsi, 2006; Pierson, 1993; Wypych, 2016)

Material	Thermal conductivity at 25° C (W/mK)
Graphite	100~400 (on-plane)
Carbon black	6~174
Carbon Nanotubes	2000~6000
Diamond	2000
PAN-based Carbon fibre	8~70 (along the axis)
Pitch-based Carbon fibre	530~1100 (along the axis)
Copper	483
Silver	450
Gold	345
Aluminum	204
Nickel	158
Boron nitride	250~300
Aluminum nitride	200
Beryllium oxide	260
Aluminum oxide	20~29

For particulate-filled polymer composites, the degree of crystallinity (%crystallinity) affects the thermal conductivity of the composites. The degree of crystallinity increases with $CaCO_3$ particles infusing PBT resin because it acts as a nucleating agent. The rise in % crystallinity leads to the increase in the composites' thermal conductivity. This is, however different for stearic acid-coated $CaCO_3$. Stearic acid-coated $CaCO_3$ is not a strong nucleating agent owing to the reduction in surface energy (Papirer et al., 1984). Hence, the degree of crystallinity of stearic acid-coated $CaCO_3$-filled polymer composites is lower and results in reduced ability to transfer heat (Deshmukh et al., 2010a). Smaller filler leads to greater improvement of % crystallinity (Frormann et al., 2008).

Thermal conductivity is also affected by the amount of filler added to the polymer matrix (Ebadi-Dehaghani et al., 2014; Patnaik et al., 2010). For 80 wt% silver-coated wollastonite infused in EVA resin, the increment is about 10 times compared to neat EVA (Table 2.12) (Krupa et al., 2008). Both experimental results and theoretical modeling agree that the thermal conductivity of the composites increases as the amount of filler increases (Azeem & Zain-ul-Abdein, 2012; Kumlutaş et al., 2003). Higher filler content facilitates greater crystallization of the polymer composites (Zhao & Li, 2006).

Table 2.12: Thermal conductivity of neat EVA and silver-coated wollastonite fiber/EVA composites

(Krupa et al., 2008)

w_f	v_f	$w_{f(Ag)}$	$v_{f(Ag)}$	**k (W/mK)**
0	0	0	0	0.13±(0.01)
0.1	0.019	0.068	0.007	0.14±(0.01)
0.2	0.041	0.136	0.015	0.16±(0.01)
0.3	0.068	0.204	0.025	0.19±(0.01)
0.4	0.102	0.272	0.038	0.29±(0.01)
0.5	0.146	0.340	0.054	0.42±(0.01)
0.6	0.204	0.408	0.075	0.73±(0.01)
0.7	0.285	0.476	0.105	1.14±(0.01)
0.8	0.406	0.544	0.150	1.32±(0.01)

Note: w_f and v_f are weight and volume fractions of fillers in composites, respectively
W_f(Ag) and v_f(Ag) are weight and volume fractions of silver in composites, respectively.

Besides, smaller filler size is more effective for transferring heat than coarser filler. This is because smaller filler has a larger surface area for contact with more resin molecules for heat transfer (Frormann et al., 2008). With the same filler content, finer filler tends to be well-dispersed and it fulfills the free volume in the matrix phase. The smaller the particles, the more easily they diffuse into the polymer network. This leads to smaller distances between the filler (Ebadi-Dehaghani & Nazempour, 2012) for better thermal conductive “bridges.” Therefore, efficient heat conduction can be improved by reducing the filler size.

Different values of thermal conductivity are produced by different shapes of similar fibers. Fibrous shaped copper produces higher thermal conductivity compared to prismatic and spherical shape, when infused in nylon resin (Tekce at al., 2007). This is due to better interaction among the fibrous shaped fillercompared to other filler shapes.

Weidenfiller et al. (2004) expressed particle “chains” as particle interconnectivity. Particles with poor thermal conductivity may produce better thermal conductivity if they exhibit better interconnectivity in the polymer matrix. Copper particle-filled polymer matrix composite is expected to have higher thermal conductivity than talc because the thermal conductivity of copper is approximately 40 times higher than talc. However, the opposite result was observed, as the thermal conductivity of talc/PP at 30 vol% was twice as high as Cu/PP composite. This was due to the higher interconnectivity of talc than copper (Figure 2.41).

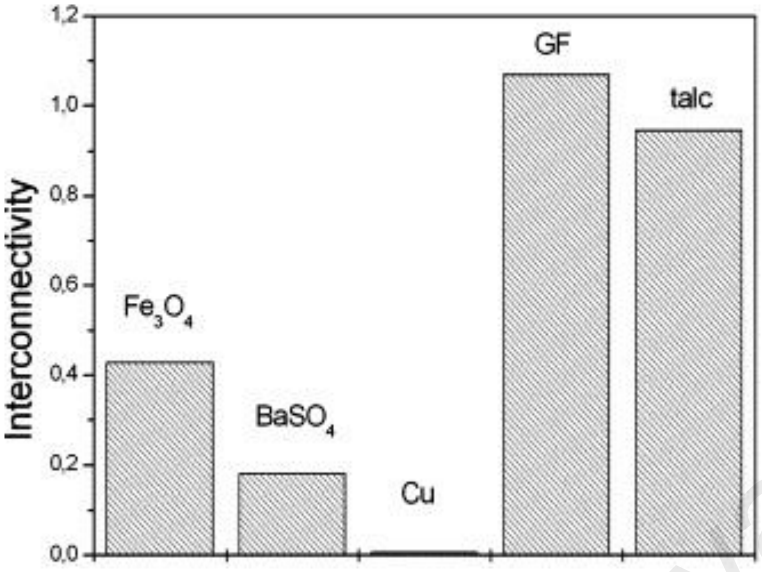

Figure 2.41: Interconnectivity of 30 vol% particulate-filled PP at room temperature (Weidenfeller et al., 2004)

2.5.2 Specific heat content

Specific heat is defined as the amount of energy required to raise a unit temperature of a unit mass of a substance. Specific heat capacity depends on the molecular structure and its phase. The higher the specific heat, the higher the material can absorb heat to raise 1°C of 1 kg of the material. Specific heat, C_p can be expressed in a mathematical equation as follows:

$$\mathbf{C_p = \frac{\Delta Q}{m\Delta T}} \tag{2.2}$$

Where C_p is specific heat capacity (J/kg°C), ΔQ is change in heat (J), m is mass (kg) and ΔT is change in temperature (°C or K).

Specific heat content of particulate-filled polymer composites is affected by weight filler fraction (Weidenfeller et al., 2004). At low filler loading, the measured specific heat is linearly dependent on filler content up to a maximum level. Then as filler is added, the filler disperses non-homogeneously in the polymer matrix, leading to non-liner homogeneity. For ethylene vinyl acetate copolymer (EVA) filled with wollastonite fibers and coated with silver, a linear decrease of specific heat content was observed as filler was added up to 70 wt% (Krupa et al., 2008). Then the addition of wollastonite fibers produced non-homogeneous fiber distribution in the polymer composite, resulting in the increase of specific heat content as shown in Figure 2.42.

For metal powder-filled polymer matrix composites, the specific heat is very low. The addition of zinc, copper and iron particles to the HDPE matrix up to 25 vol% produces an insignificant decrease of specific heat content of the composites (Sofian et al., 2001).

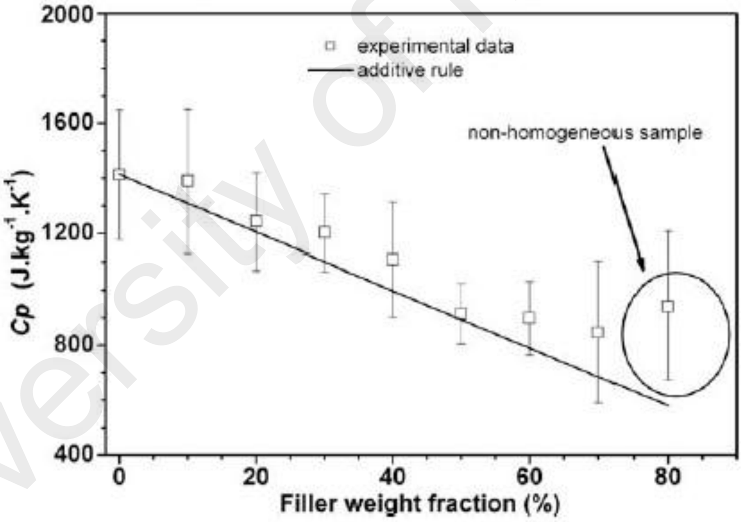

Figure 2.42: Specific heat capacity $C_p$of various filler weight fractionsof EVA/W-Ag composites

(Krupa et al., 2008)

2.5.3 Thermal diffusivity

Thermal diffusivity is a measure of the way heat flows through a material to the other side. It can also be expressed as the rate of temperature change in a transient heat transfer process. The higher the value of thermal diffusivity, the higher the rate of temperature propagation the substance has. Thermal diffusivity, α is measured in m^2s^{-1} and can be determined mathematically as follows:

$$\boldsymbol{\alpha} = \frac{\mathbf{k}}{\boldsymbol{\rho}\mathbf{C_p}} \tag{2.3}$$

Where α is thermal diffusivity m^2s^{-1}, ρ is sample density (kgm^{-3}), k is thermal conductivity (Wm^{-1}K^{-1}) and C_p is specific heat (Jkg^{-1}K^{-1}).

Thermal diffusivity of particulate-filled polymer composites is also affected by filler content. Thermal diffusivity increases as talc content increases in HDPE resin (Mehrjerdi et al., 2013). A nonlinear increase of thermal diffusivity was observed as the filler content increased (Krupa & Chodák, 2001; Sofian et al., 2001). Composite thermal diffusivity can be grouped into two zones: at low and high filler loading. At low filler loading thermal diffusivity slowly increases whereas rapid increase in thermal diffusivity is observed at higher filler loading. Thermal diffusivity significantly improves when the filler content of the metal powder reinforced in a HDPE matrix is above 16 vol% (Sofian et al., 2001).

Particle size also influences the performance of heat transport, or heat diffusivity. Smaller particles produce higher thermal diffusivity than coarse particles. At similar filler concentrations, smaller graphite particles yield higher thermal diffusivity than coarser particles (Krupa &Chodák, 2001).

Enhanced thermal diffusivity of the composites is due to the rising crystallinity of the matrix. Semicrystalline matrices have higher thermal diffusivity than amorphous matrices because they are able to transport heat (Krupa &Chodák, 2001). For particulate-filled polymer matrix composites, the degree of crystallinity rises as particles reinforce the matrix because it acts as a nucleating agent (Papirer et al., 1984). High amounts of small particles lead to particle aggregation. Higher particle aggregation might improve heat transport in the material, hence improving the heat diffusivity of the composites (Krupa &Chodák, 2001).

Similar with thermal conductivity, thermal diffusivity of particulate-filled polymer composites is also influenced by the particles' interconnectivity. Better particle interconnectivity achieved at 30 vol% of talc particles in PP resin resulted in higher thermal diffusivity compared to copper particles in the same matrix (Weidenfeller et al., 2004).

2.6 Summary

Filler characteristics are greatly affecting the performance of particulate polymer matrix composites. Those characteristics include the particle size and distribution, specific surface area and surface energy, filler shape and other characteristics such as chemical composition or purity of the fillers, also hardness and thermal properties. Generally, the mechanical properties of the composites increase as the filler size decreases and filler loading increases.

Finer filler has a large surface to volume ratio. Theoretically this can produce composites with superior properties due to its excellent ability for stress transfer. Nano-sized particles for example generally perform better mechanical properties than coarser particles because it provides wider surface area for stress transfer mechanism. Adding more fine filler thus increase the mechanical properties. However, in real condition finer filler tend to agglomerate due to higher surface energy. The clustering of nanoparticles may form particles agglomeration to micron size. Adding more filler may increase the amount or size of the agglomeration. Micron size agglomerations promote failure due to the particle-matrix debonding and fracture of the aggregates. The agglomeration also reduces the stiffness of the composites due to homogenous dispersion of particles in the polymer matrix.

To reduce the amount of surface energy, the particles is commonly treated with chemical. Stearic acid is the popular chemical to treat the surface of $CaCO_3$ particles. The treatment can change the surface of $CaCO_3$ to be hydrophobic, improve compatibility between filler and increase the dispersion of particles in the matrix. However, the treatment does not eliminate aggregation completely.

Adding filler into polymer matrix also affect the thermophysical properties of the composites. Metallic fillers such as silver, copper and nickel are among the most common fillers embedded in the polymer matrix composites to increase the thermal conductivity. However, adding nonconductive particles also able to increase the thermal conductivity. Adding talc powder with excellent interconnectivity in polymer matrix yields higher thermal conductivity than copper even though copper has 40 times thermal conductivity than talc.

Particle size also influences the performance of thermal conductivity and thermal diffusivity. At similar filler content, finer particles produce higher thermal diffusivity and thermal conductivity because it has high surface area to conduct heat. Finer filler with better filler dispersion can easily build filler bridges. Good filler connections then improve the thermal conductivity and thermal diffusivity.

CHAPTER 3: METHODOLOGY

3.1 Introduction

This chapter explains the procedures to determine the objectives of this study. It consists of the process of raw material preparation into particle form, determining the particle density, composite production, mechanical testing and thermophysical testing.

3.2 Raw material preparation

About 30 kg of marsh clam shells were washed and scrubbed to remove the dirt from the shells. Then the shells were boiled in water for about 10 to 15 minutes to allow the shell and flesh to separate easily. Again, the shells were scrubbed, cleaned thoroughly with distilled water and rinsed gently to remove any remaining pollutants that had clogged the shells. After the cleaning process, the shells were placed under the sun to dry for 3 hours. Next, the shells were dried in an oven at 85°C for 7-8 hours. The cleaned and dried shells were crushed using a manual mortar and pestle to produce smaller aggregate. The small pieces of aggregate were then ground into particle form using a blending machine. The particle was sieved through aperture sizes of 850 µm, 600 µm, 500 µm, 300 µm, 212 µm, 150 µm, 75 µm, and 63 µm. The sieves were stacked on top of one another with increasing aperture size from the bottom to the top, and at the very bottom there was a round receiver. The particle was then dried again for 1 hour at 75°C before being packed and sealed in polyethylene plastic bags. The process of *lokan* particle production is attached in Appendix A.

3.3 Sieving technique

In this research, the clam shell particle was graded according to mean size diameter by using sieves made from stainless steel (Endecott Ltd, made in London, England), available in the Geology Lab, Department of Civil Engineering, University of Malaysia Sarawak. Through this technique, the particle size distribution of round or nearly round aggregate can be assessed. It involves nested column sieves with wire mesh screen or cloth. The sieves were stacked on top of one another with increasing aperture size from bottom to top, and at the most bottom part was a round receiver as shown in Figure 3.1. In this experiment, eight standard sieve sizes were chosen to distribute the particle sizes, which were 850 μm, 600 μm, 500 μm, 300 μm, 212 μm, 150 μm, 75 μm, and 63 μm. The column was placed in a mechanical shaker which shakes the column by tapping. This method allows the sieves to move in a horizontal, circular motion, as characterized by hand sieving. This movement may produce a higher degree of sieving for denser particles. For each series of experiments, 100 g of clam shell particle was poured into the top of the sieve and the shaking process was done for about 30 minutes. The sieved particle was then stored in sealed bags according to the particle size range at room temperature.

Figure 3.1: Sieve column and mechanical shaker, and different sieve mesh sizes

3.4 Particle mean size measurement

The particle size distribution of graded *lokan* shell particle was determined by Malvern Mastersizer 2000 particle size analyzer, which is available at the Geology Lab, Faculty of Science, University of Malaya. This particle size analyzer can measure particle sizes in the range of 0.05-1000 µm. 5 g of clam shell particle was stirred in 100 ml of distilled water to avoid particle settling. The mean diameter size of the particle was then measured by laser diffraction method and analyzed according to distribution width. The mean size was taken at 50% distribution and the average of 3 data was recorded.

Figure 3.2: Malvern Mastersizer 2000 particle size analyzer

3.5 Surface modification of $CaCO_3$ particles

The surface of $CaCO_3$ from clam shell particle was treating with stearic acid at a constant amount of 1 wt%. This amount was selected because previous studies reported that the contact angle for water that reached a maximum value was at 1 wt% stearic acid (Jeong et al., 2009). The modification procedure was published by Gomari et al. (2006) and also applied by Mihajlović et al. (2009). 1 wt% of stearic acid solution was prepared by dissolving 1 g of stearic acid into 99 g of chloroform. At the same time, 10 g of $CaCO_3$ was dispersed in 100 ml of warm distilled water at 50°C. Then 10 ml of stearic acid solution was added to the mixture of $CaCO_3$ and warm distilled water. It was then stirred at 450 rpm for 15 minutes. Finally, the suspension was washed with distilled water and dried at 50°C for 4 hours. Table 3.1 presents the characteristics of stearic acid used in this study.

Table 3. 1: Characteristics of stearic acid

Name	Stearic acid
Molecular formula	$C_{18}H_{36}O_2$
Molecular weight, g/mol	284.48
Assay (GC) (as methyl ester)	>97.0%
Identify IR spectrum	passes test
Melting range 67-69°C	67-69 °C
Iodine number	<4.0
Acid value	194-212
Heavy metal (as Pb)	<0.001%
Mineral acids	Passes test
Sulfate ash (600°C)	<0.1%

3.6 Characterization of the clam shells

The shell particle was characterized by X-ray diffraction (XRD) using a PANalytical X'Per PRO powder diffractometer at the Geology Laboratory, Faculty of Science, University of Malaya. The quantities of different polymorphs were measured by semi-quantitative peak analysis software. The surface morphology of the shells and their particle were studied by Scanning Electron Microscope (SEM) Hitachi S3400N model with gold sputtered coating, which was available at the UKM-MTDC Technology Centre. An elemental study was performed using an energy dispersive X-ray analyzer (EDX-Horiba EMAX model) that was connected to the SEM. For each different part of the shell sample (inner, cross-section and outer part), three spectrums were obtained in three different spots. The elements of each spot were then tabulated. Figure 3.3 shows the inner and outmost surface of the *lokan* or *Polymesoda bengalensis* shell.

Figure 3.3: The inner and outmost surface of the *Polymesoda bengalensis* shell

3.7 Specific surface area measurement

Brunauer-Emmett-Teller (BET) theory is applied to measure specific surface area of the material. Gas such as nitrogen is commonly employed to adsorp on the surface of the solid sample because it does not chemically react with material surface. The multilayer adsoption process by the gas happens on the sample surface. The BET equation is then used to measure specific surface area. Refer Appendix E for more information. The following hypotheses are applied in order to extend the theory of monolayer molecular adsorption to multilayer adsorption:

1. Gas molecules physically adsorp on a solid in layer infinitely
2. Gas molecules only interact with adjacent layers, and
3. The Langmuir theory can be applied to each layer.

The specific surface areas of the untreated and stearic acid-treated $CaCO_3$ particles were measured by nitrogen adsorption (BET method) using Autosorb 1 apparatus, which is available at the Powder Laboratory, Faculty of Engineering, University of Malaya. 24 hours before measurement, the samples were degassed at 100°C and 10^{-5} mmHg pressure.

3.8 Fabrication of samples

The unsaturated polyester (UPE) resin GP862T is a thixotropic premix that served as the matrix in this study. The curing agent employed was Butanox$^{(R)}$M-60, or in chemical terms, methyl ethyl ketone peroxide (MEKP), manufactured by Akzo Nobel Industrial Chemicals B.V. with a density of 1.170 g/cm^3. Both resin and curing agent were supplied by Portal Trading, Pulau Penang, Malaysia.

2, 4, 6 and 8 wt% of clam shell were mixed with unsaturated polyester (UPE). Each mixture was blended mechanically for 5 minutes before being soaked in an ultrasonic bath for 15 minutes. Then, 1 wt% of curing agent was added into the mixture for rapid curing. Next, the mixture was poured into a mold, stirred for 5 minutes, degassed for 30 minutes and cured at room temperature for 24 hours. It was then followed by post-curing at 70^{o}C for 3 hours. Unfilled UPE was also processed similarly but without ultrasonication as a control mixture. The samples were then cut according to ASTM standard dimensions. The cut sections were polished to produce smooth surfaces for better dimension readings. The specimens were prepared according to the required dimensions by ASTM-D standards as shown in Table 3.2. Figure 3.4 shows the schematic diagram of the tensile, compression and flexural test specimens according to the ASTM standards mentioned in Table 3.2. The overall process of sample preparation is attached in Appendix B.

Table 3.2: Standards and dimensions of the test specimens

(www.intertek.com)

Testing	ASTM-D standard	Cross head speed (mm/min)	Length (mm)	Width (mm)	Span length (mm)	Depth (mm)	Gauge length (mm)
Tensile	ASTM D638	2	150	10	-	4	80
Compression	ASTM D695	2	12.7	12.7	-	25.4	-
Flexural	ASTM D790	2	125	12.7	64	3.2	-

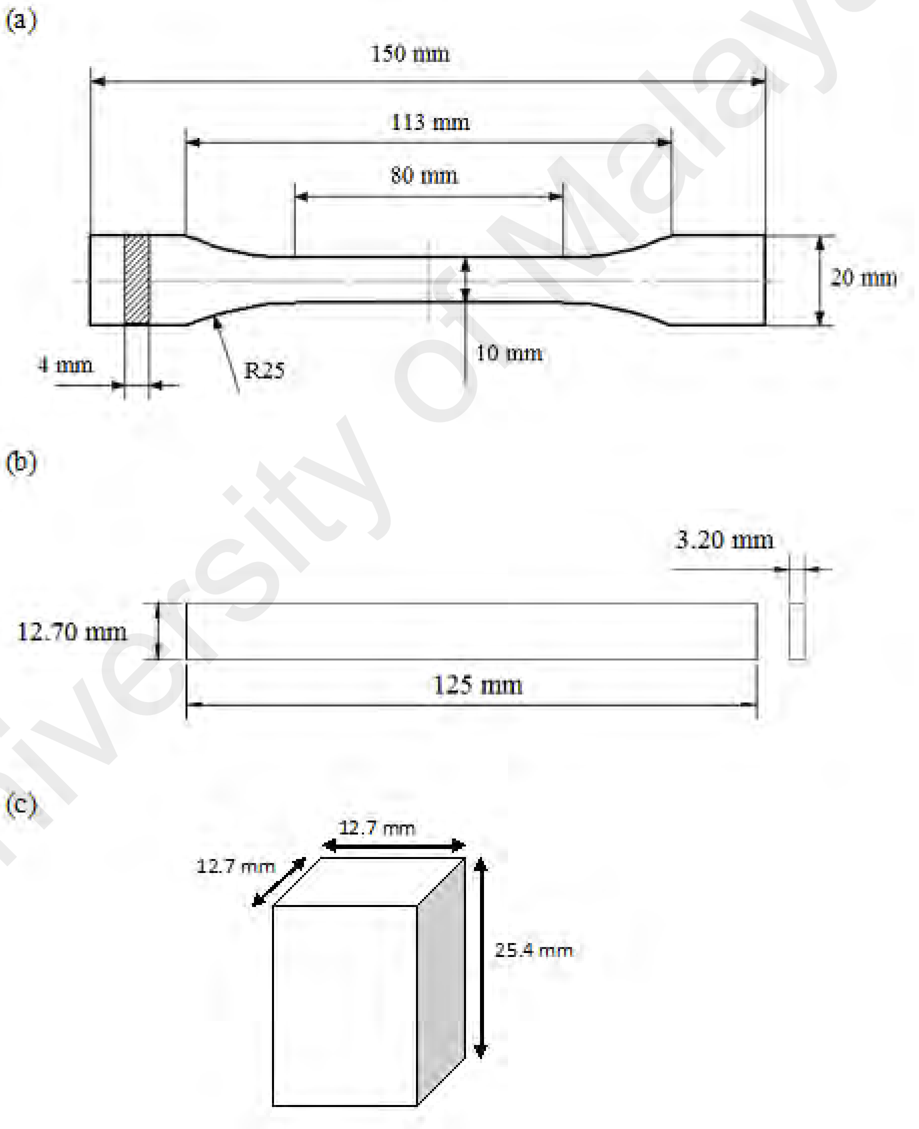

Figure 3.4: The schematic diagram of the tensile, compression and flexural test specimens

3.9 Mechanical testing

Four different mechanical tests were done in this research, namely tensile, compression, flexural, and hardness tests. The pictures of equipment and samples is attached in Appendix C. The results were compared in terms of different mean sizes and mass fractions of $CaCO_3$, as well as different surface modifications. For each parameter, the average of ten readings was measured. Then the standard deviation (SD) was determined by equation 3.1. It is an index of how closely the individual data points close around the mean or the variability between the data of each parameter. Finally, the standard error of the mean (SE) was measured by using equation 3.2. Standard error is uncertainty of how the data mean represents the parameter mean.

$$SD = \sqrt{\frac{\sum_{i=1}^{N}(x_i - \bar{x})^2}{N-1}} \tag{3.1}$$

$$SE = \frac{SD}{\sqrt{N}} \tag{3.2}$$

Where x_i is the result of the i^{th} experiment for each trial, $\bar{x}$ is the mean value of the results, and N is the repetition number of each trial.

3.9.1 Tensile testing

A tensile test is one of the most basic types of material testing method that is normally done on a material to evaluate how the material reacts to tension forces by pulling on the material until it fractures. The sample elongates at constant rate until it fractures. The amount of force and elongation results from tensile test are used to determine mechanical properties such as stress and strain. Plotting stress-strain curve gives us the values of Young's modulus, yield strength, tensile strength, strain at break and stress at break. Young's modulus is represented by the slope at the first portion of the graph which behaves elastically. Tensile strength is obtained at the maximum point (stress) of the curve. Yield strength is the stress corresponding to the intersection of 0.002 strain offset line and stress-strain curve.

Tensile properties were measured with a universal testing machine according to ASTM D638 Standard Test Method for Tensile Properties of Plastic. The samples were cut into dog bone shapes 150 mm long, with the center sections 10 mm width x 4 mm thick x 80 mm long. The test was performed using an Instron 4469 universal testing machine with a 50 kN load cell attached at 2 mm/min cross-head speed. The averages of 10 data for tensile modulus and tensile strength were recorded.

3.9.2 Flexural testing

A three-point bending test or a flexural test is a mechanical test to obtain the values of flexural stress, flexural strain and flexural stress-strain response of a material. A simply supported beam is supported on two outer points and deformed by driving a third central point downwards. When the bending force is applied to the specimen, the specimen experiences both elongation and compressive forces. The elongation zone of the specimen would experience tensile stresses as the molecules are pulled apart. The compressed zone experiences the compressive stresses. The maximum stress is located at the centre of the specimen.

The flexural tests were performed according to ASTM D790 using an Instron 4469 universal testing machine with a 50 kN load cell attached. This test was conducted at Basic Material Science Laboratory, Department of Mechanical Engineering, University of Malaya. A three-point bending test was conducted at 2 mm/min cross-head speed and at room temperature. The specimen dimensions were 3.2 x 12.7 x 125 mm and the span-to-thickness ratio was 16:1. Finally, the average of 10 readings for flexural modulus and flexural strength was recorded. The samples'surface morphology was studied by scanning electron microscope (SEM) Hitachi S3400N model with gold sputter coating.

3.9.3 Compression testing

A compression test is a method for determining the behaviour of materials under a compressive load. The test is conducted by loading the test specimen between two plates, and then applying a force to the specimen by moving the crossheads together. During the test, the specimen is compressed, and applied load versus deformation is recorded. A stress-strain curve can be plotted from the data obtained through a compression test to analyze the result or performance of the material being tested in terms of compressive modulus and compressive strength.

For the compression test, the samples were cut into rectangular blocks of 12.7 x 12.7 x 25.4 mm according to the ASTM D695 Standard Test Method for Compressive Properties of Rigid Plastics. The test was performed with an Instron 4469 universal testing machine with a 50 kN load cell attached at 2 mm/min cross-head speed. The average of 10 readings for compressive modulus and compressive strengths was recorded.

3.9.4 Hardness testing

Hardness test is applied to measure a material's resistance to localized plastic deformation. The indenter, which is harder than the sample is forced into the surface of the sample, under controlled load and rate of application. The indenter can be made from steel, tungsten carbide and diamond. The hardness number is measured by applying the value of depth or size of the indented area.

Hardness testing was performed using a Vickers hardness tester with a square-base diamond pyramid indenter with an angle of 136° between opposite faces of the pyramid. The test was conducted using a Shimadzu micro hardness tester, which is available at Surface Engineering Laboratory, Department of Mechanical Engineering, University of Malaya, at 245.2 mN for a 20 sec indentation period. The specimen surface was carefully polished using high-grade 2000 grit sandpaper prior to testing. A total of 10 indentation points were measured on the samples' surfaces. The Vickers hardness numbers (H_V) were then recorded and converted into Pascals (Pa) unit. This was done by converting the applied force from kgf to newtons. The conversion can be done by applying the following equation.

$$\boldsymbol{H_V = 1.854\,\frac{F}{d^2}} \tag{3.3}$$

Where F is load in kgf and d is an arithmetic mean of the two diagonals.

3.10 Thermophysical Testing

Two tests were done in this research to determine the thermophysical properties of untreated and stearic acid-treated UPE/$CaCO_3$ composites with different particle sizes and fractions. The tests were to determine the specific heat and the effective thermal conductivity of the composites. The specific heat of the $CaCO_3$ particle and UPE/$CaCO_3$ composites was measured by differential scanning calorimetry (DSC) method. This method is also applicable to measuring the degree of the composites'crystallinity. The effective thermal conductivity of the composites was measured by P.A. Hilton Heat Conduction Unit H-940 machine. The measurements were conducted up to steady-state condition, where the temperature change was not more than $\pm 1^{o}C/min$. Finally, thermal diffusivity was calculated by substituting the values of density, specific heat capacity and thermal conductivity in the formula.

3.10.1 Determination of density

The density of the samples, ρ was determined by applying equation (3.4). The mass of the samples was measured by using electronic balance. The length, width and thickness were measured by using a vernier caliper.

$$\boldsymbol{\rho = \frac{m}{V}} \tag{3.4}$$

Where m is mass and V is volume of the sample.

The theoretical density of the composites, ρ_c was calculated using rule-of-mixture of particle-reinforced composite material as shown in equation (3.5).

$$\boldsymbol{\rho}_{c} = \frac{\mathbf{1}}{\left(\frac{m_f}{\rho_f} + \frac{m_m}{\rho_m}\right)} \tag{3.5}$$

Where m_m is mass of matrix, m_f is mass of particle, ρ_m is density of matrix and ρ_f is density of particle.

3.10.2 Determination of thermal conductivity

The thermal conductivity was measured by P.A. Hilton H-940 (Figure 3.5) machine using the guarded heat flow method according to ASTM E1225-99 standard test method for thermal conductivity of solids by means of comparative longitudinal heat flow technique (Figure 3.5 and 3.6). This machine is available at Heat Transfer and Thermodynamics Laboratory, Mechanical Engineering, University of Malaya. A cylindrical shape specimen with 25 mm diameter and 3 mm thickness was placed in the two brass terminals of the conduction unit. A constant heat flux of 10W was supplied from a hot terminal, while the cooling process was done by water circulating at a constant rate of 4 L/min at a cold terminal. The temperatures at the hot terminals ($T1$, $T2\ and\ T3$) and cold terminals ($T4,\ T5\ and\ T6$) were measured by thermocouples every 30 minutes up to 3 hours. Then the temperature readings were taken every 15 minutes due to the near steady-state condition. Steady-state is achieved when the temperature change is not more than $\pm 1\ °C/min$ (Azeem et al., 2012). The temperatures at the interfaces of hot (Th) and cold (Tc) ends of the specimens were calculated by extrapolating the values of $T1 - T6$. The effective thermal conductivity of the composite samples, k_c can be calculated with the following steps.

Heat flow in hot zone:

$$\mathbf{q_h} = \boldsymbol{k}_{\mathbf{brass}}\mathbf{A}\frac{[\mathbf{T_1} - \mathbf{T_3}]}{[\mathbf{Z_1} - \mathbf{Z_3}]} \tag{3.6}$$

Heat flow in cold zone:

$$\mathbf{q_c} = \boldsymbol{k}_{\mathbf{brass}}\mathbf{A}\frac{[\mathbf{T_4} - \mathbf{T_6}]}{[\mathbf{Z_4} - \mathbf{Z_6}]} \tag{3.7}$$

Substitute heat flow in hot and cold zones to determine the average heat input:

Average heat input:

$$\mathbf{Q_{avg}} = \frac{\mathbf{q_h} + \mathbf{q_c}}{\mathbf{2}} \tag{3.8}$$

Therefore, thermal conductivity, k_c:

$$\boldsymbol{k_c} = \frac{\boldsymbol{Q_{avg}\Delta Z_c}}{\boldsymbol{A \cdot \Delta T_c}} \tag{3.9}$$

Where

$\Delta Z_c = the\ length\ (m) of\ the\ composite\ sample,$

$\Delta T_c = T_h - T_c = temperature\ (K)\ difference\ across\ composite\ sample,$ and

$Area, A = 4.91x10^{-4}m^2$

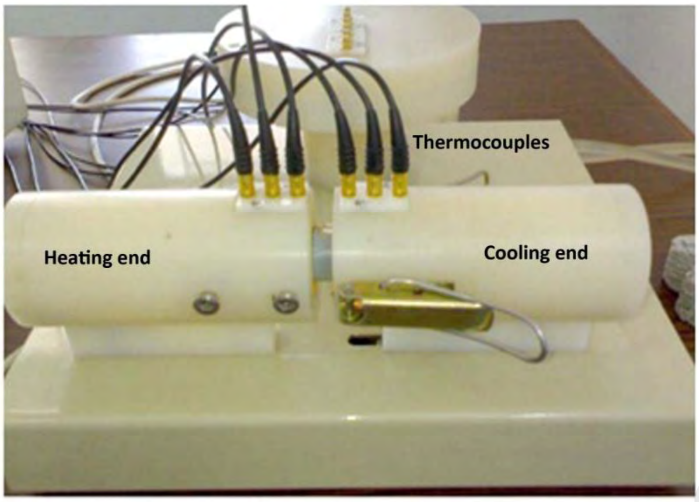

Figure 3.5: P.A. Hilton Heat Conduction Unit H-940 for heat conduction measurement.

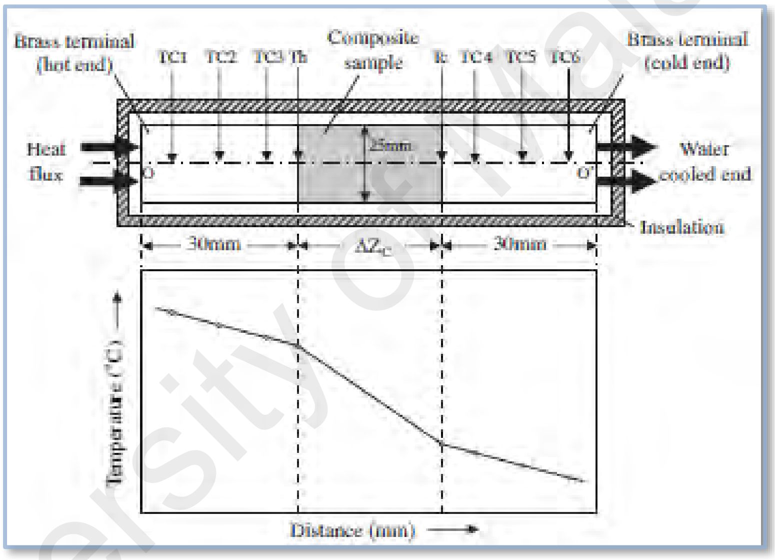

Figure 3.6: Experimental setup and temperature measurement

(Azeem et al., 2012)

3.10.3 Determination of specific heat and degree of crystallinity

DSC is applied to study thermal behaviour of the material such as glass transitions, melting transition, specific heat capacity, crystallinity and many more. The temperature in DSC is designed to be increases linearly as a function of time throughout the experiment. The reference sample must have well-defined heat capacity over the range of temperature. The difference of amount of heat to increase both sample and reference is measured. The normalized DSC curve which is heat flux versus temperature or versus time can be used to calculate enthalpies of transitions.

The specific heat values of $CaCO_3$ particle and the untreated and stearic acid-treated UPE/$CaCO_3$ composites were measured by differential scanning calorimetry (DSC) (Model: Mettler Toledo) which is available at Analysis Research Laboratory, Chemical Engineering, University of Malaya. DSC is a technique to measure heat flow into and out of a sample as a function of temperature or time. This method was chosen because it has lower inaccuracy (1-10%), easier sample preparation and wider temperature range (100-1000 K) (Verdonck et al., 1999) than other techniques.

About 2-3 mg of samples in the form of $CaCO_3$ particle and UPE/$CaCO_3$ with different filler fractions were placed in an Aluminum pan while an empty pan served as reference. The tests were carried out at a heating rate of 10°C/min in the temperature range of 20-500°C in nitrogen atmosphere. The samples' heat capacity values were taken at 23°C. Specific heat capacity, C_p is calculated using equation 3.10.

$$\boldsymbol{C_p = \frac{1({}^{\delta Q}/_{dt})}{m({}^{\delta T}/_{dt})}} \tag{3.10}$$

Where $({}^{\delta Q}/_{dt})$ is the heat flux given by the DSC curve, m is the sample mass and $({}^{\delta T}/_{dt})$ is the heating rate of the sample.

The decomposition temperature (T_d) and heat of reaction (ΔH_R) of the samples were measured from DSC. Then the degree of crystallinity (X_c) of the UPE/$CaCO_3$ composites was calculated by taking the value of reaction heat for 100% crystalline polyester resin (ΔH_R^0) as 400 J/g (Severini & Gallo, 1985) as reference. The degree of crystallinity (X_c) was then calculated according to the formula below:

$$\boldsymbol{X_c = \frac{H_R \times 100}{\Delta H_R^o \times w}} \tag{3.11}$$

Where ΔH_R is heat of reaction of the sample, ΔH_R^0 is heat of reaction for 100% crystalline polyester resin and w is mass fraction of the UPE in the composites.

3.10.4 Determination of thermal diffusivity

Lastly, the thermal diffusivity was determined using an equation by substituting the values of density, specific heat capacity and thermal conductivity. The thermal diffusivity, or α value of the sample, was determined with the following equation:

$$\boldsymbol{\alpha = \frac{k_c}{\rho C_p}} \tag{3.12}$$

Where k_c is thermal conductivity ($W/m \cdot K$), C_p is specific heat capacity ($J/kg°C$) and ρ is density (kg/m^3).

CHAPTER 4: RESULTS AND DISCUSSION

4.1 Introduction

This chapter presents the experimental results achieved from three main activities: clam shell characterization and shell particle tests, determining the mechanical properties of clam shell particle-filled unsaturated polyester composites and identifying the thermo-physical properties of clam shell particle-filled unsaturated polyester composites. The shell and particle were identified by X-ray diffraction (XRD) analysis and energy dispersive X-ray (EDX) analysis, whereas the morphology was observed by scanning electron microscope (SEM). The ground particle sizes were measured by particle size analysis and the results were presented in terms of mean particle size. The mechanical properties of UPE/$CaCO_3$ (aragonite) composites, including stiffness and strength in the form of flexural, tensile and compressive loadings were determined experimentally by Instron 4469 universal testing machine attached with a 50kN load cell. The surface hardness of the composites was measured by a Shimadzu microhardness tester. In terms of thermophysical properties, the thermal conductivity, thermal diffusivity and specific heat content of the composites were also evaluated. The thermal conductivity was measured by P.A. Hilton Heat Conduction Unit H-940. The specific heat content was determined with Differential Scanning Calorimetry (DSC - model Mettler Toledo). The thermal diffusivity was calculated using a mathematical equation. Then the effects of 1 wt% stearic acid treatment on the mechanical and thermophysical properties were compared with untreated particles.

4.2 Characterization of *Lokan* (*Polymesoda bengalensis)* clam shell

The first objective of this research was to investigate the characteristics of the *lokan* (*Polymesoda bengalensis)* shell and its particle. The particle was obtained by grinding and sieving to less than 63 µm. For the characterization process, the polymorph of *lokan* shell particle underwent XRD analysis. The polymorph's morphology was identified by SEM. The elemental content at three different regions on the shell was recognized by EDX connected with SEM.

4.2.1 Identification of clam shell polymorph by XRD analysis

X-ray diffraction (XRD) is a sensitive instrument applied to identify the crystalline phase of inorganic compounds. Figure 4.1 illustrates the XRD patterns of the *lokan*, or *Polymesoda bengalensis* shell particle. The XRD pattern (Pokroy et al., 2007) shows that all peaks matched with calcium carbonate ($CaCO_3$). The *lokan* particle peaks were measured from 0° to 80° of 2θ, thus no peaks were detected at over 80°. The peaks were then compared with calcite and aragonite polymorphs. The XRD patterns in Figure 4.1 demonstrate that the crystalline component of $CaCO_3$ is aragonite. The strongest peaks observed in XRD show the characteristic peaks of aragonite at 2θ values of 26.192°, 27.46°, 33.090° and 45.823°, which correlate with (hkl) indices of (111), (102), (201) and (122). Other peaks were also observed at 36.056°, 37.841°, 38.418°, 48.336°, 50.206° and 52.384°. Only three peaks out of 64 correspond with calcite, which were at 36.009°, 48.306° and 76.957° (Reference Code 98-002-0179). Thus, it can be concluded from the XRD analysis that *Polymesoda bengalensis* shell contains mostly aragonite (Reference Code 98-015-7995).

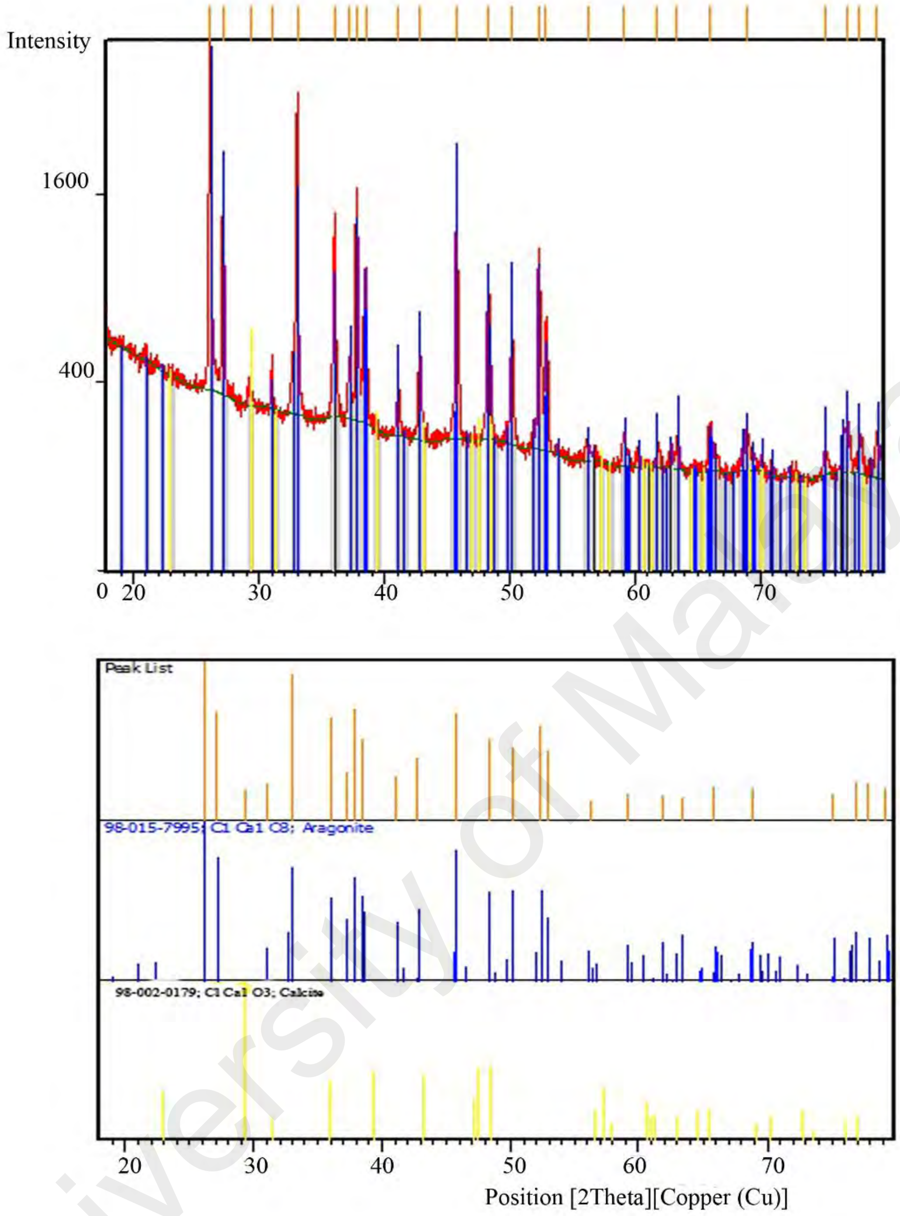

Figure 4.1: XRD patterns of *Polymesoda bengalensis* clam shell particle

4.2.2.1 Surface morphology by SEM

The scanning electron microscope (SEM) is an instrument for examining microstructural morphology. The morphology of raw clam shell and its particle was examined by SEM. Then the element detected was analyzed using energy dispersive X-ray (EDX).

4.2.2.1 Surface morphology of the *Polymesoda bengalensis* clam shell particle

Figure 4.2 (a) shows an image of the outmost and inner *Polymesoda bengalensis* shell surfaces. The outer surface, or the periostracum layer of the shell is rough and displays concentric rings. The green color is darker at the ventral part of the shell where an eroded umbo surface is also present. At the inner surface, or nacreous layer, a yellow area is detected in the dorsal region where the muscles are attached, whereas the other part is white in color. Figures 4.2 (b-f) illustrate the morphology of three different parts of the clam shell. The sectional part of the shell reveals aragonite layers arranged in a cross-lamellar structure. A porous surface is detected in the ventral region (Figure 4.2 (c)) of the outmost shell layer, whereas the dorsal part has a finer structure (Figure 4.2 (d)). Different aragonite sizes are found in the inner part of the shell. Courser aragonite polymorph (Figure 4.2 (e)) is identified in the yellow dorsal part of the inner surface rather than the white surface region (Figure 4.2 (f)) of the shell.

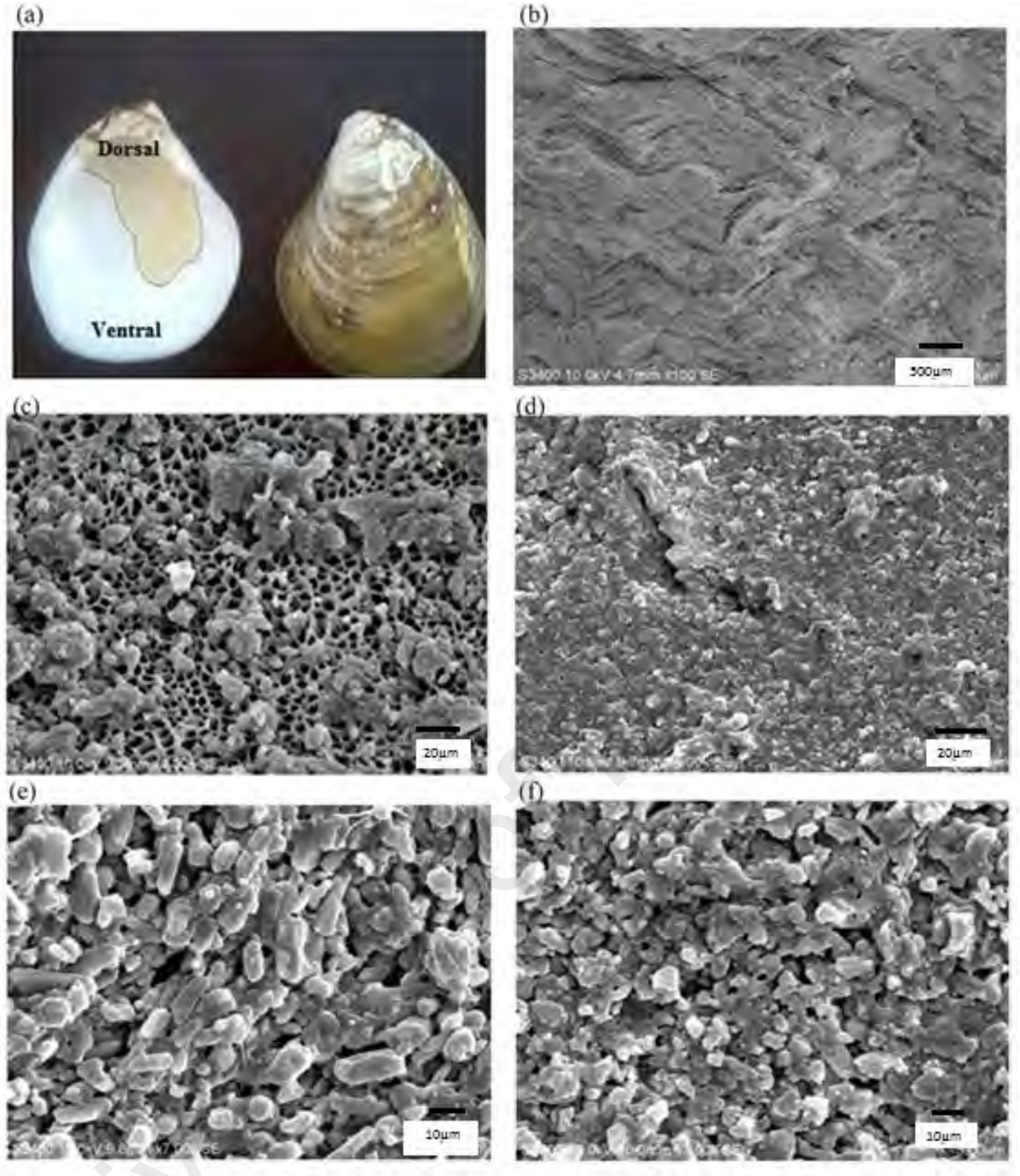

Figure 4.2: Image of (a) inner and outmost surfaces, and SEM images of the (b) cross-sectional area, (c) ventral part of the outmost surface, (d) dorsal part of the outer surface, (e) yellow area of the dorsal part at the inner surface, and (f) white area of the dorsal part at the inner surface of the *Polymesoda bengalensis* shell

4.2.2.2 Surface morphology of the *Polymesoda bengalensis* clam shell particle

Figure 4.3 reveals the clam shell particle surface morphology by SEM. Micron-sized aragonite particles are detected in the particle. The rod-like aragonite crystal particles appear to attract each other and produce clustering among many particles, while the particles are arranged in a similar orientation. This may be due to high surface energy, which results in greater attraction among particles. The particle-particle interaction phenomenon has also been addressed by several authors (He at al., 2011; Zhang et al., 2011b) and it normally occurs in untreated calcium carbonate particle due to the Van der Waal force of small particles. Besides, short rod particles are also detected. These may be produced from the long rod aragonite particles that were partly destroyed during the shell powdering process. The morphology of different sizes of *Polymesoda bengalensis* clam shell particle are attached in Appendix D.

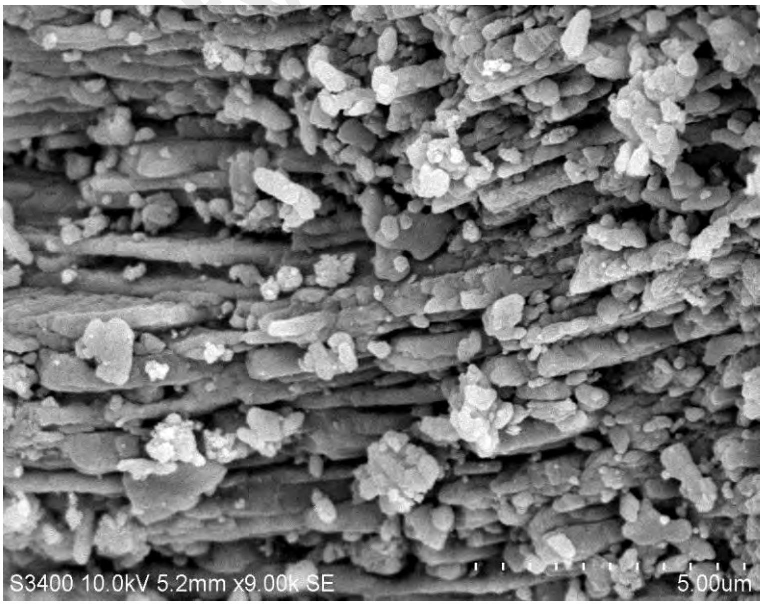

Figure 4.3: SEM image of the surface morphology of *Polymesoda bengalensis* clam shell particle

Morphologic changes occurred as the particle was treated with 1 wt% stearic acid. Figure 4.4 displays the untreated and stearic-acid treated $CaCO_3$ particle morphology from *Polymesoda bengalensis* clam shell. The untreated particle is originally in rod-like form. Treating the particle with 1 wt% stearic acid shortens the particle length, thus reducing the aspect ratio. Stearic acid reacts with $CaCO_3$ by releasing carbon dioxide and Ca^{2+}. Releasing Ca^{2+} ion from $CaCO_3$ surface might reduce the aspect ratio of the $CaCO_3$ because this process rapidly occurs at the tip of the particle (Fontana, 2005). The chemical process is as follow:

$$CaCO_3 + 2H^+ \rightarrow Ca^{2+} + CO_2 + H_2O$$

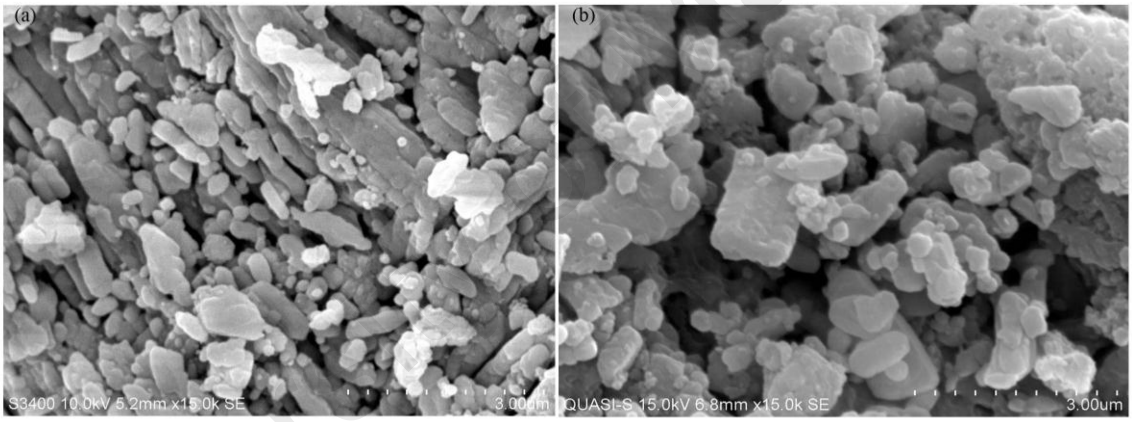

Figure 4.4: SEM images of (a) untreated and (b) stearic acid-treated $CaCO_3$ particle from *Polymesoda bengalensis* clam shell

4.2.3 Elemental analysis by EDX

The chemical composition of the *lokan* clam shell particler was analyzed using energy dispersive X-ray spectroscopy (EDX). EDX revealed the presence of individual elements in the sample. Figure 4.5 shows the clam shell locations from where the particle was taken for EDX analysis. Table 4.1 displays the EDX results of the elemental content of particle derived from *lokan* shell obtained from three different places. The findings indicate that particle of less than 63 µm contains pure $CaCO_3$ with no trace elements and it is rich in oxygen and calcium.

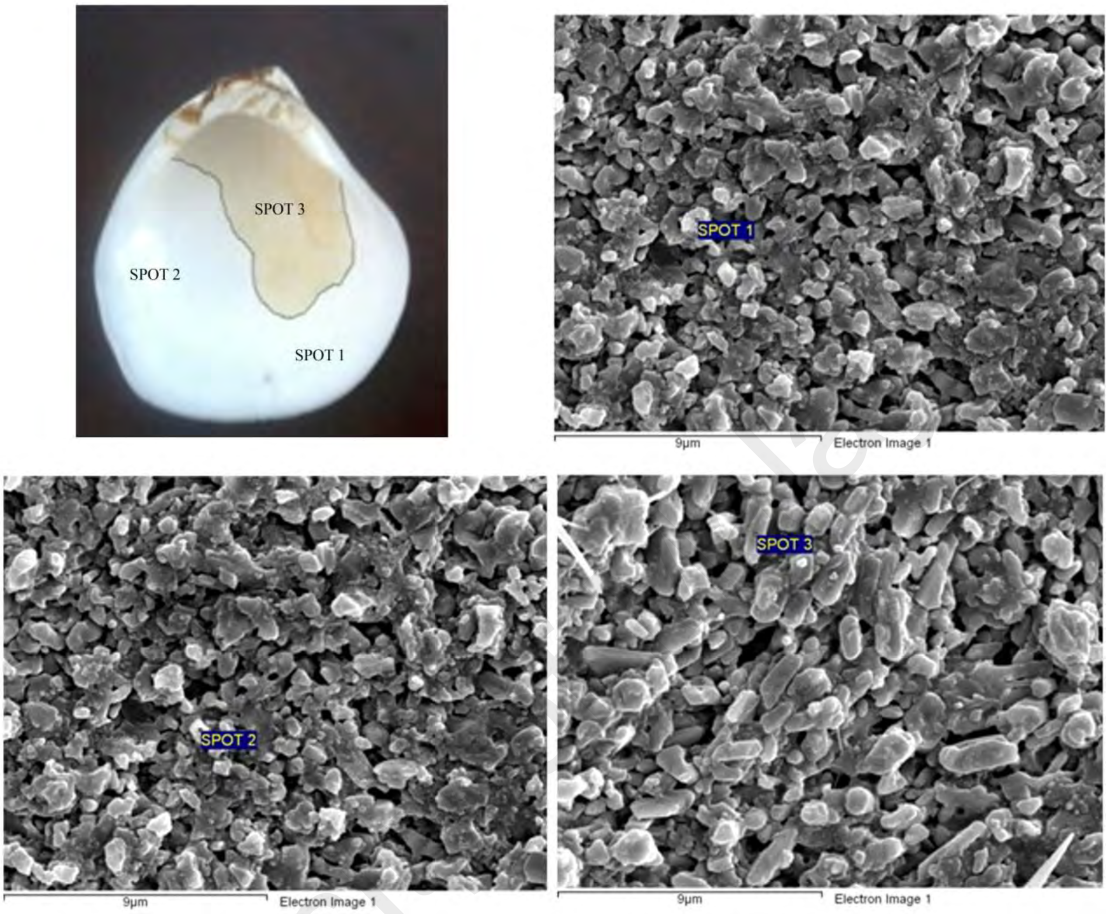

Figure 4.5: Locations of particle taken from the *lokan* or *Polymesoda bengalensis* clam shell for elemental composition detection by EDX

Table 4.2: Elemental content of particle derived from *Polymesoda bengalensis* clam shell

Spectrum	**C (%)**	**O (%)**	**Ca (%)**	**Total (%)**
Spectrum 1	11.23	33.69	55.08	100
Spectrum 2	15.94	50.63	33.43	100
Spectrum 3	15.38	45.37	39.25	100
Mean	14.18	43.23	42.59	
Std. Deviation	2.58	8.67	11.20	
Max	15.94	50.63	55.08	
Min	11.23	33.69	33.42	

4.2.4 Mean particle size of clam shell particle

The particle size distribution is the average number of particles within a given size class of width for a unit volume of suspension. Table 4.2 summarizes the mean particle size of ground clam shell particle as determined by Malvern Mastersizer 2000 particle size analyzer. Each group represents the average size of clam shell particles that pass through a certain sieve aperture. The sieves were stacked one on top of another with decreasing aperture size from top to bottom: 850, 600, 500, 300, 212, 150, 75, and 63 µm. For each mean particle size, the data was the average of three readings. One of the readings taken from the particle size analyzer is shown in Figure 4.6. The mean particle size was taken at 50% distribution, which is denoted as D(v, 0.5) in the analysis table shown in the Figure 4.6.

Table 4.2: Mean particle size of the filler

Clamshell particle through sieve size (µm)	Reading 1 (µm)	Reading 2 (µm)	Reading 3 (µm)	Average (µm)
850	650.98	580.91	678.72	636.87
600	570.85	575.61	577.96	574.81
500	494.02	482.26	481.23	485.84
300	309.29	289.86	294.66	297.94
212	208.04	206.18	205.44	206.55
150	46.05	46.84	46.02	46.30
75	35.13	34.41	35.64	35.06
63	29.91	29.63	29.99	29.84

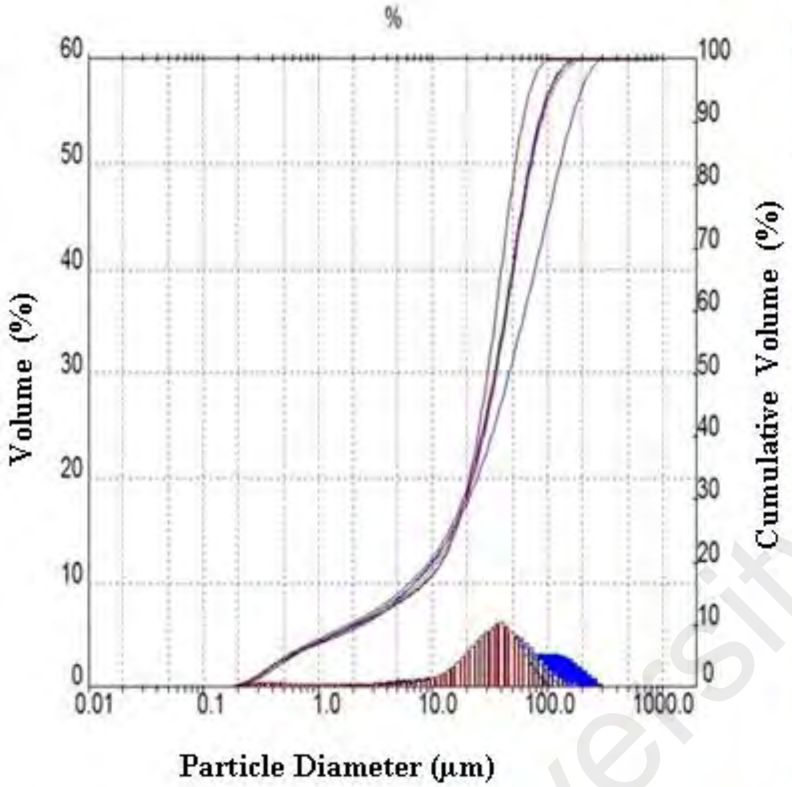

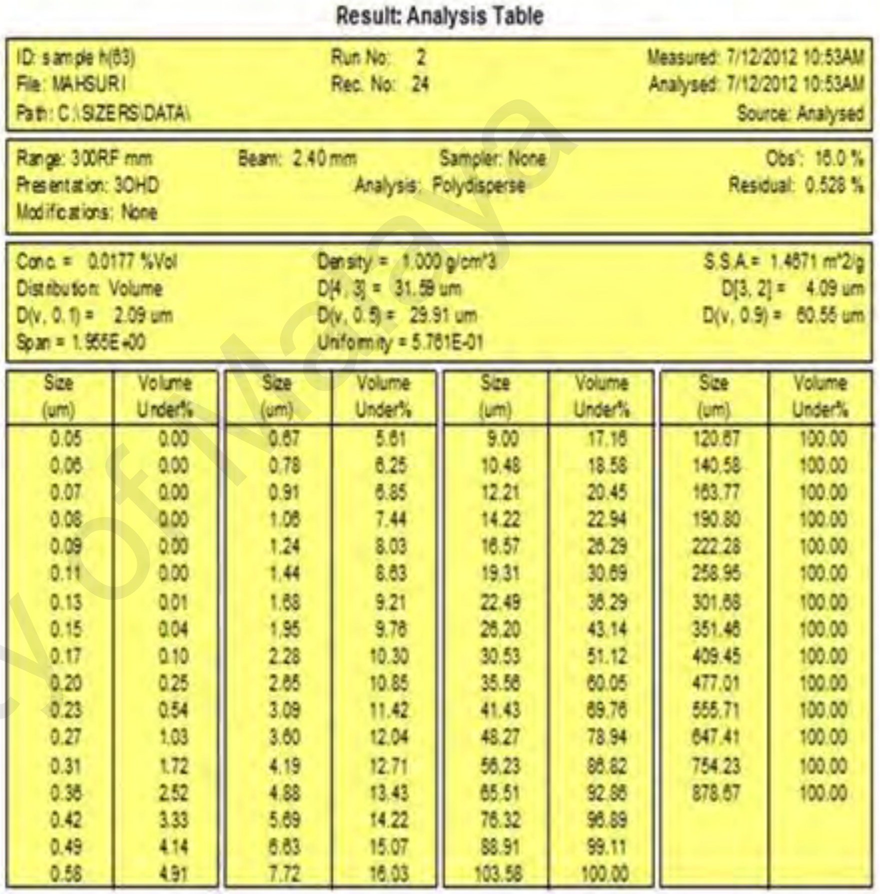

Result: Analysis Table

ID: sample h(63) Run No: 2 Measured: 7/12/2012 10:53AM
File: MAHSURI Rec. No: 24 Analysed: 7/12/2012 10:53AM
Path: C:\SIZERS\DATA\ Source: Analysed

Range: 300RF mm Beam: 2.40 mm Sampler: None Obs': 16.0 %
Presentation: 3OHD Analysis: Polydisperse Residual: 0.528 %
Modifications: None

Conc. = 0.0177 %Vol Density = 1.000 g/cm^3 S.S.A.= 1.4671 m^2/g
Distribution: Volume D[4, 3] = 31.59 um D[3, 2] = 4.09 um
D(v, 0.1) = 2.09 um D(v, 0.5) = 29.91 um D(v, 0.9) = 60.56 um
Span = 1.955E+00 Uniformity = 5.761E-01

Size (um)	Volume Under%	Size (um)	Volume Under%	Size (um)	Volume Under%	Size (um)	Volume Under%
0.05	0.00	0.67	5.61	9.00	17.16	120.67	100.00
0.06	0.00	0.78	6.25	10.48	18.58	140.58	100.00
0.07	0.00	0.91	6.85	12.21	20.45	163.77	100.00
0.08	0.00	1.06	7.44	14.22	22.94	190.80	100.00
0.09	0.00	1.24	8.03	16.57	26.29	222.28	100.00
0.11	0.00	1.44	8.63	19.31	30.69	258.95	100.00
0.13	0.01	1.68	9.21	22.49	36.29	301.68	100.00
0.15	0.04	1.95	9.76	26.20	43.14	351.46	100.00
0.17	0.10	2.28	10.30	30.53	51.12	409.45	100.00
0.20	0.25	2.65	10.85	35.56	60.05	477.01	100.00
0.23	0.54	3.09	11.42	41.43	69.76	555.71	100.00
0.27	1.03	3.60	12.04	48.27	78.94	647.41	100.00
0.31	1.72	4.19	12.71	56.23	86.82	754.23	100.00
0.36	2.52	4.88	13.43	65.51	92.86	878.67	100.00
0.42	3.33	5.69	14.22	76.32	96.89		
0.49	4.14	6.63	15.07	88.91	99.11		
0.56	4.91	7.72	16.03	103.58	100.00		

Figure 4.6: Particle size distribution analysis of *lokan* (*Polymesoda bengalensis*) clam shell particle determined with the particle size analyzer

4.2.5 Surface area by BET analysis

The specific surface area of the particle is the ratio of the total particle surface area per unit mass. In this study, six samples in particle form were taken for specific surface area measurement: three different mean particle sizes of untreated CaO_3 particle (29.84, 35.06 and 46.30 µm) and three different mean particle sizes of stearic acid-treated $CaCO_3$ particle (29.84, 35.06 and 46.30 µm). Table 4.3 presents the specific surface area of untreated and stearic acid-treated $CaCO_3$ particle determined by Brunauer-Emmett-Teller (BET) method.

Table 4.3 Particle sizes and specific particle surface areas of the investigated particle

Particle size (µm)	**Specific surface area (m^2/g) of untreated particle**	**Specific surface area (m^2/g) of stearic acid-treated particle**
29.84	7.143	1.419
35.06	2.217	1.174
46.30	0.589	0.540

Table 4.3 signifies that the specific surface area of the particle increases with finer particle size. Reducing the particle size from 35.06 to 29.84 µm increases the specific surface area from 2.217 to 7.143 m^2/g for untreated particle compared to 1.174 to 1.419 m^2/g for stearic acid-treated particle. The result from this work is similar to other studies in the literature (Jeong et al., 2009; Kiss et al., 2007). There is an obvious increment in the untreated particle compared to stearic acid-treated particle. Theoretically, smaller particles have agreater surface area. For particulate-filled composites, a large surface area is very important for adhesion at the matrix-filler interface. However, this also leads to increasing surface energy, which encourages the finer particles to agglomerate. Coating $CaCO_3$ with stearic acid leads to a significant decrease in the specific surface area of similar-size particle, especially for fine particle (Kiss et al., 2007). In all cases, treated particle has lower specific surface area than untreated particle. Particle with

46.30 µm mean diameter reduces the specific surface area by approximately 8.3% from 0.589 m^2/g to 0.540 m^2/g as the particle is treated with 1 wt% stearic acid. A more significant reduction of approximately 80% in specific surface area is observed as 29.84 µm mean diameter particles are treated with stearic acid. The decrease is from 7.143 m^2/g to 1.419 m^2/g for untreated and stearic acid-treated particle, respectively. Reduced specific surface area may reduce particle-particle interactions, resulting in better filler dispersion through the polymer matrix.

4.3 Mechanical properties

In general, the effect of adding rigid particles to polymer is to enhance mechanical properties, such as the stiffness and strength of particulate-filled polymer composites. The positive effects are due to the good compatibility between the particles and the matrix. Good compatibility was determined as the particles were well-distributed in the polymer matrix and there was good adhesion quality between the particles and matrix. In this section, the mechanical properties are evaluated in terms of stiffness and strength, upon subjecting UPE/$CaCO_3$ composites to tensile, compressive and flexural loadings. The effects of particles size, particle content and stearic acid treatment on the stiffness and strength of the composites are discussed.

4.3.1 Tensile properties

In general, adding $CaCO_3$ particles in UPE resin would improve the mechanical properties of the composites. Figure 4.7 represents the stress-strain curves of 29.84 µm mean size of $CaCO_3$ filler infused in UPE polymer matrix composites at four different weight fractions of fillers; 2 wt%, 4 wt%, 6 wt% and 8 wt%.

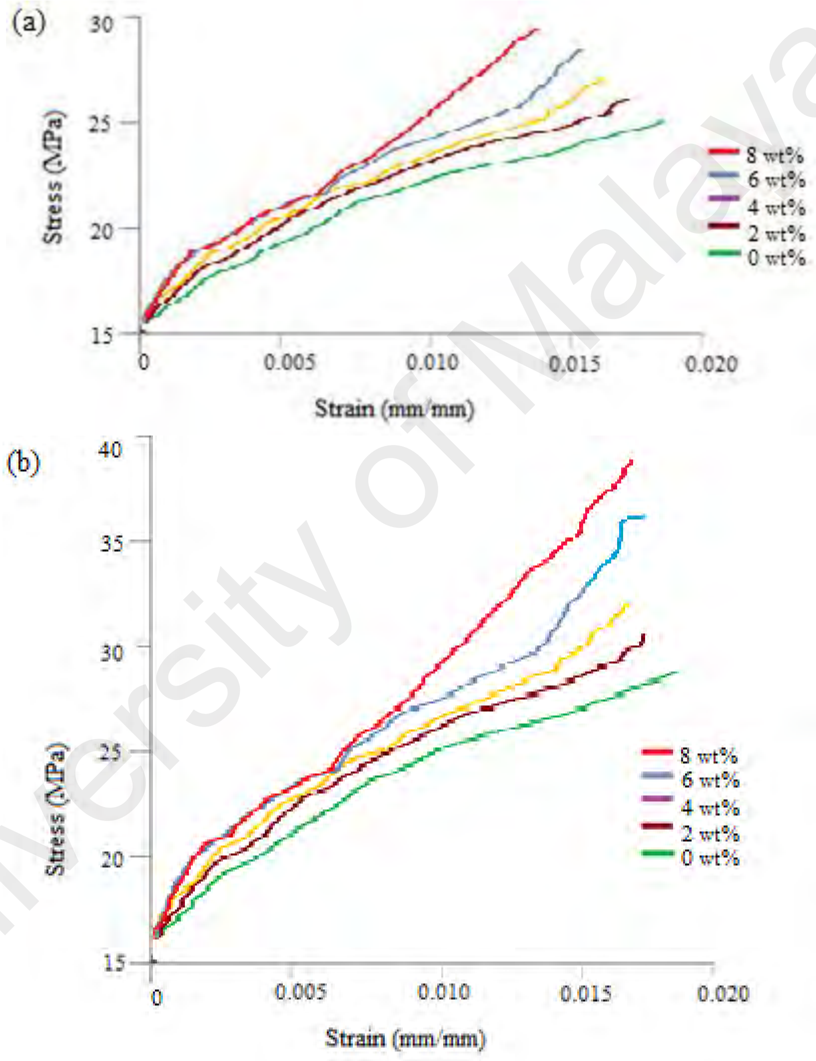

Figure 4.7: Tensile stress-strain curve of (a) untreated and (b) stearic acid treated of 29.84 µm mean diameter size of $CaCO_3$ at different filler fraction in UPE/$CaCO_3$ composites

The curves show the tensile strength and the stiffness of the UPE polymer are increase as the $CaCO_3$ filler is added in the UPE resin. The improvement of

UPE/$CaCO_3$ composites are tremendously observed by the highest filler fraction which is 8 wt%. Treating the filler with 1 wt% stearic acid improves both Young's modulus and tensile strength for all samples at similar filler loading compared to untreated UPE/$CaCO_3$ composites. However, the drawback of the inclusion of $CaCO_3$ filler in UPE polymer matrix is the reduction of strain at break. Including the $CaCO_3$ filler which is stiffer than UPE resin reduce the strain at break. The more $CaCO_3$ filler infused in the UPE matrix, the shorter the strain at break the composites would be. This result is also similar with Ahmad et al. (2007). This reflects that the ductility of the composites is also decreased as the amount of $CaCO_3$ filler is increased. The ductility is defined as the percentage of the strain of break. According to Wypych (2016), the elongation at break is normally inversely proportional to the tensile strength. In the composites, the presence of particle decreases the amount material toughness thus, results in the deduction of elongation at break. Figure 4.8(b) shows the fracture surface of the sample under tensile loading. It shows the failure is in the form of brittle fracture because the direction of the crack is nearly perpendicular to the direction of the tensile loading and the fracture surface is smooth (Jones & Ashby, 2012).

Figure 4.8: The specimen (a) before tensile test and (b) after tensile test (at the fracture surface)

4.3.1.1 Tensile modulus

The tensile modulus, also known as Young's modulus, is the slope of the stress-strain curve up to the elastic limit. It reflects the performance of both filler and matrix interface materials in transferring elastic deformation in instances of small strain without interface fracturing. The average values from ten readings of the tensile modulus of pure unsaturated polyester (UPE) resin and UPE/$CaCO_3$ (aragonite) composites are given in Figure 4.9. The stiffness of neat UPE resin is 1578.90 MPa. As 2 wt% untreated coarse filler with 636.87 µm size is introduced into the UPE resin, the tensile stiffness sharply drops to 515.62 MPa, which is approximately 67.32% reduction. This indicates that reinforcing untreated coarse filler in the matrix resin has a negative influence on the tensile stiffness of aragonite UPE/$CaCO_3$ composites. Poor interfacial bonding was found between particle-matrix by coarse filler or big size of particles' cluster. This is due to the high stress concentrations around their edges (Dong et al., 2011). The particle-matrix debonding not only reduce the tensile strength of the composites but also the elasticity (Al Robaidi et al., 2011)

The stiffness of the composites appears to slowly increase as the filler content increases and the filler size decreases. The increase continues up to a maximum value of 8 wt% filler content with the finest filler size of 29.84 µm, which is 1982.10 MPa. These results are similar to other researchers' works, such as Mishra et al. (2005), Chisolm et al. (2005) and Douce et al. (2004), who found that composite stiffness improves with decreasing particle size and increasing particle content.

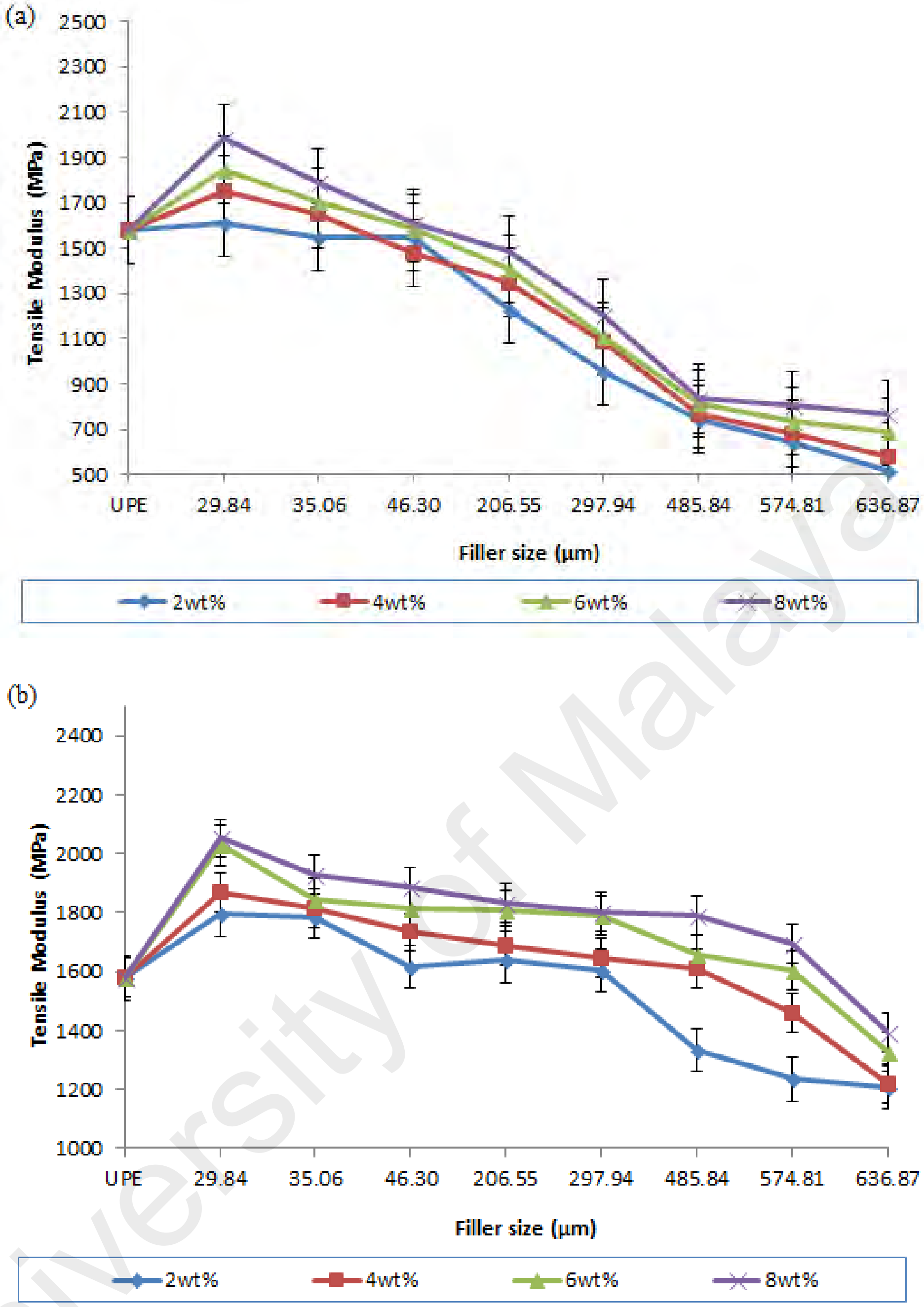

Figure 4.9: Tensile modulus of (a) untreated, and (b) stearic acid-treated UPE/$CaCO_3$ (aragonite) composites with different sizes and filler contents

For untreated $CaCO_3$ particle-filled polymer composites, the improvement in tensile modulus is influenced more by filler size than filler loading. The change in tensile stiffness is much more noticeable with lower filler size than higher filler content. As illustrated in Figure 4.9, for similar filler sizes, there is no obvious difference in composite stiffness upon infusing the fillers into the UPE matrix in the range of 2-8 wt% except for the finest filler of 29.84 µm. The values are close to each other. For example, adding 297.94 µm filler in the UPE matrix in the amounts of 2, 4, 6 and 8 wt% produces 956.73, 1085.50, 1112.42 and 1207.79 MPa, respectively. However, reducing the filler size from 297.94 µm to 206.55 µm increases the stiffness from 956.73 MPa to 1226.67 MPa at 2 wt% filler loading. Coarser fillers tend to deposit on the bottom surface of the sample due to gravitational force during the curing process as shown in Figure 4.8, resulting in inhomogeneous filler dispersion. Adding more coarse filler may not help much to increase the tensile modulus for the same reason. The specific gravity of aragonite $CaCO_3$ is 2.93 and that of liquid UPE resin is 1.13. Higher specific gravity fillers tend to deposit at the bottom of the mixture (Figure 4.10) due to their motion through the polymer resin during curing process. This leads to inhomogeneous dispersion of the filler in the UPE matrix, hence reducing the stiffness of the composites. Figure 4.10 also shows that finer particles dispersed in the mixture, not deposit at the bottom because finer filler can diffuse more easily into the polymer liquid during curing process compared to coarse filler.

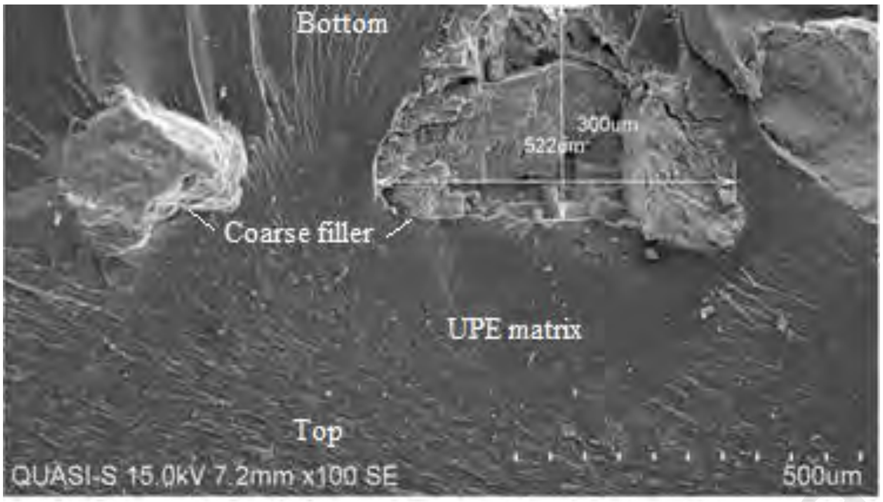

Figure 4.10: Coarse particles with 574.81 µm mean size tend to deposit at the bottom of the sample due to gravitational force during the curing process

In addition, adding more untreated filler also encourages the formation of agglomerate, which is lead to the inhomogeneous filler dispersion in the UPE matrix as shown in Figure 4.11. The circles show the areas where the agglomeration are found. However, the finest filler size of 29.84 µm disperses better in the composite, although particle agglomeration is still observed. Adding more $CaCO_3$ filler which is stiffer than unsaturated matrix would increase the stiffness of the composites. As a result, adding more fine filler up to 8 wt% in the UPE resin yields good improvement in tensile modulus.

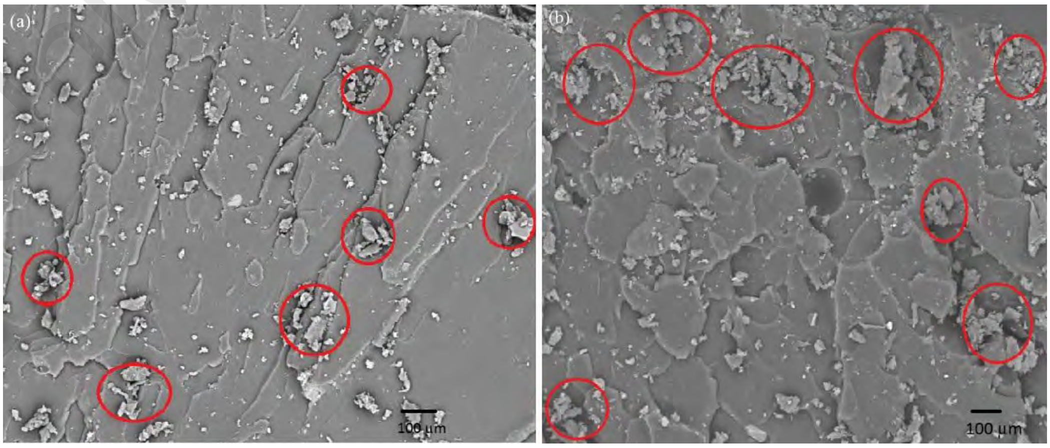

Figure 4.11: Better filler dispersion by finer filler in UPE polymer composites with (a) 29.84 µm and (b) 35.06 µm particle size distribution

The improvement in composite's stiffness is obvious when the filler is treated with 1 wt% stearic acid. At the same filler fraction and filler size, the treated filler composites produce higher stiffness values than untreated filler composites. Such improvement is due to the fact that the treatment reduces the surface energy of the $CaCO_3$ filler, hence encouraging the homogeneous dispersion of the filler in the matrix. Well-dispersed filler in the matrix produces an excellent filler interconnection that is useful for improving the stiffness of the composites. A particle network is produced by the interconnection between the stress concentration zone and the filler. Besides, at similar filler content, treated clam shell particle composites exhibit a higher modulus of elasticity compared to untreated composites. This increment indicates that treating clam shell particle with 1 wt% stearic acid produces stiffer composites that can withstand higher stress at the same strain rate. In this study, the maximum Young's modulus value was obtained at 8 wt% filler content with 29.84 μm mean particle size $CaCO_3$ filler. The treated UPE/$CaCO_3$ produced 2053.02 MPa, which is 70.93 MPa higher than untreated UPE/$CaCO_3$ composites.

Reinforcing filler in the neat resin may introduce stress concentration around the filler. If the filler is not well-dispersed, the interconnections of the stress concentration zones are disturbed. In this case, the stiffness would be low. However, for well-dispersed filler, the stress concentration zones would be well-interconnected, thus yielding higher stiffness. Figure 4.9 shows that introducing very coarse filler with 636.87 μm size reduces the tensile modulus of the UPE/$CaCO_3$ (aragonite) composites even if the filler is treated with stearic acid. The most pronounced reduction is when 2 wt% coarse filler with 636.87 μm size is introduced into the UPE resin, whereby the tensile stiffness sharply reduces to approximately 67.32% and 23.48% for untreated and treated fillers, respectively.

Generally, the stiffness of the particulate-filled polymer composites is greater than pure resin due to the formation of a particle interconnection (He & Jiang, 1993) and the "stiffening effect" (Mareri et al., 1998) as a result of particle reinforcement. Finer filler can diffuse more easily into the polymer liquid, thus producing a greater affected volume with a shorter distance between the fillers. This would produce excellent stress zone interconnections. Therefore, finer fillers normally generate greater stiffness. As shown in the graphs, the tensile stiffness of UPE/$CaCO_3$ (aragonite) composites increases steadily as smaller fillers are infused into the UPE matrix. A better particle interconnection network produced by finer filler generates stiffer composites. In the 2-8 wt% range of $CaCO_3$ particles, the maximum Young's modulus is achieved with 29.84 µm filler at 8 wt% for both untreated and stearic acid-treated composites. However, for smaller filler size, the surface energy would be higher. The fillers tend to agglomerate, distorting the filler "bridges" and hence reducing the particulate-filled composites' stiffness. The non-reactive treatment, which is with stearic acid for $CaCO_3$ (Móczó et al., 2002) would reduce the filler's surface energy. Therefore, a more homogeneous filler distribution is produced in the treated particulate-filled polymer composite, which leads to greater tensile stiffness.

Non-reactive treatment can reduce the filler's surface energy by producing monolayer on the surface of the filler (Jeong et al., 2009). This monolayer change the filler surface behavior to be more hydrophobic by increasing the surface contact angle. In the case of $CaCO_3$ filler treated by stearic acid, the optimum surface contact angle is achieved when fatty acid was adsorbed as a complete monolayer on the surface of $CaCO_3$. Any addition of the stearic acid more than the amount to obtain the optimum surface angle would not affect any increment on the hydrophobicity (Jeong et al., 2009).

The treatment also results in a competition between the “stiffening” effect of better filler dispersion and the “softening” effect of the treatment agent (Mareri et al., 1998). In this study, the enhanced Young’s modulus as the filler is treated with 1 wt% stearic acid indicates that the “stiffening” effect is more dominant than the “softening” effect. Figure 4.12 illustrates the more homogeneous filler dispersion and better particle-matrix bonding in stearic acid-treated than untreated with 29.84 µm filler size and 8 wt% filler content. Table 4.4 represents a list of the tensile modulus of untreated and stearic acid-treated aragonite $CaCO_3$ with different filler sizes and filler contents. All data are the average of ten readings.

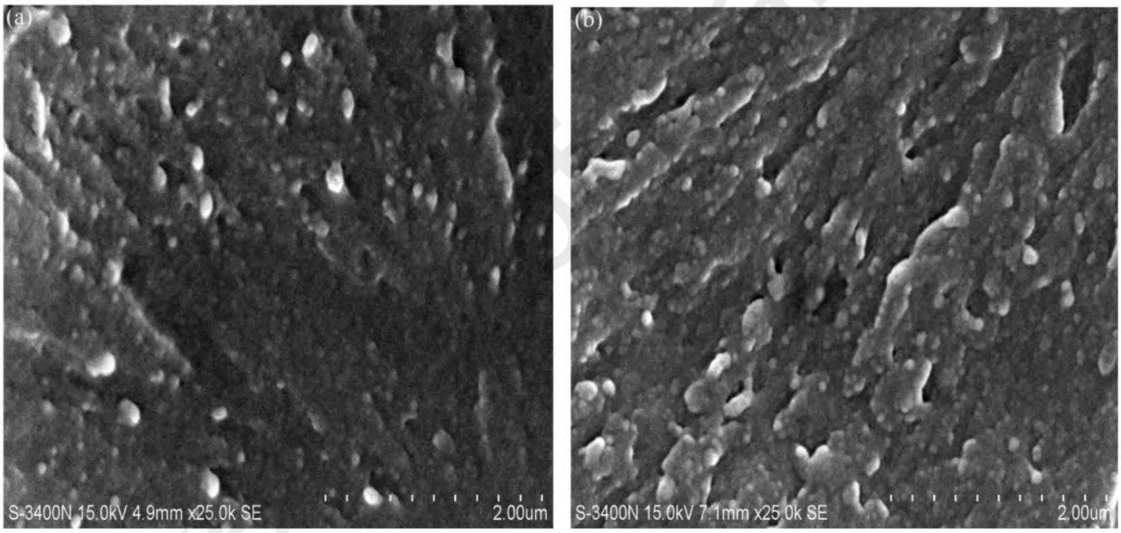

Figure 4.12: SEM images of fracture surface of (a) poorly bonded particle-matrix and poor filler distribution in untreated composite and (b) better particle-matrix bonding and homogeneous filler distribution in stearic acid-treated UPE/$CaCO_3$ (aragonite) composites with 29.84 µm mean particle size and 8 wt% filler content.

Table 4.4: Tensile modulus of untreated and stearic acid-treated UPE/$CaCO_3$ (aragonite) with different sizes and filler loadings

Tensile modulus of untreated UPE/$CaCO_3$ composites (MPa) ± Standard error (MPa)								
Size (µm) Weight fraction (wt%)	**29.84**	**35.06**	**46.30**	**206.55**	**297.94**	**485.84**	**574.81**	**636.87**
2 wt%	1611.46 ±4.95	1544.67 ±4.16	1544.67 ±4.64	1226.67 ±5.77	956.73 ±3.96	741.64 ±6.06	643.48 ±5.40	515.62 ±7.68
4 wt%	1754.53 ±6.18	1651.68 ±6.32	1478.54 ±5.17	1348.41 ±5.47	1085.50 ±3.09	766.02 ±7.01	678.45 ±5.20	578.47 ±7.05
6 wt%	1845.19 ±5.22	1701.11 ±4.73	1585.68 ±6.30	1404.56 ±7.41	1112.42 ±6.16	812.62 ±4.71	733.25 ±3.49	686.85 ±8.15
8 wt%	1982.10 ±6.47	1786.70 ±3.83	1609.01 ±4.91	1486.58 ±5.61	1207.79 ±6.63	834.05 ±6.26	802.62 ±6.55	764.53 ±8.18
Tensile modulus of stearic acid-treated UPE/$CaCO_3$ composites (MPa) ± Standard error (MPa)								
2 wt%	1794.30 ±7.89	1787.78 ±9.40	1617.64 ±10.74	1638.66 ±10.89	1603.30 ±9.07	1333.69 ±8.93	1235.75 ±9.46	1207.42 ±5.72
4 wt%	1870.78 ±9.72	1815.48 ±8.98	1733.83 ±8.82	1689.19 ±8.95	1648.60 ±10.28	1610.09 ±6.40	1460.52 ±10.35	1218.48 ±9.02
6 wt%	2029.35 ±9.84	1847.74 ±10.34	1812.61 ±9.22	1806.82 ±9.59	1791.58 ±8.02	1657.51 ±10.22	1606.46 ±9.88	1327.73 ±9.70
8 wt%	2053.02 ±11.22	1927.59 ±9.77	1885.76 ±10.28	1831.36 ±12.19	1804.74 ±7.04	1789.47 ±6.57	1694.77 ±8.87	1392.77 ±8.23

Tensile modulus of neat unsaturated polyester (UPE) resin: 1578.90±7.85 MPa

4.3.1.2 Tensile strength

Tensile strength is the maximum stress that the material can sustain under uniaxial tensile loading and it is strongly associated with interfacial failure behavior. The average values from ten readings of the tensile strength of neat UPE and UPE/$CaCO_3$ (aragonite) are illustrated in Figure 4.13.

The tensile strength of unfilled UPE resin is 17.81 MPa. The inclusion of coarse $CaCO_3$ filler is not very useful in improving the tensile strength of the composites. At 2 wt% untreated filler content with 636.87 µm filler size, the drop is about 35%. For untreated filler, replacing 8 wt% and less of the UPE matrix weight with aragonite $CaCO_3$ filler of greater than 46.30 µm exhibits a negative influence on the tensile strength of UPE/$CaCO_3$ composites. Filler smaller than 46.30 µm exhibits higher tensile strength than unfilled UPE resin. The tensile strength, however, increases gradually as the finer filler is added to the UPE matrix. The increase in tensile strength is due to the ability of $CaCO_3$ filler, which is finer than 46.30 µm, to sustain stresses transmitted from the UPE matrix. For all filler sizes, the 8 wt% filler displays better tensile strength than lower filler fractions.

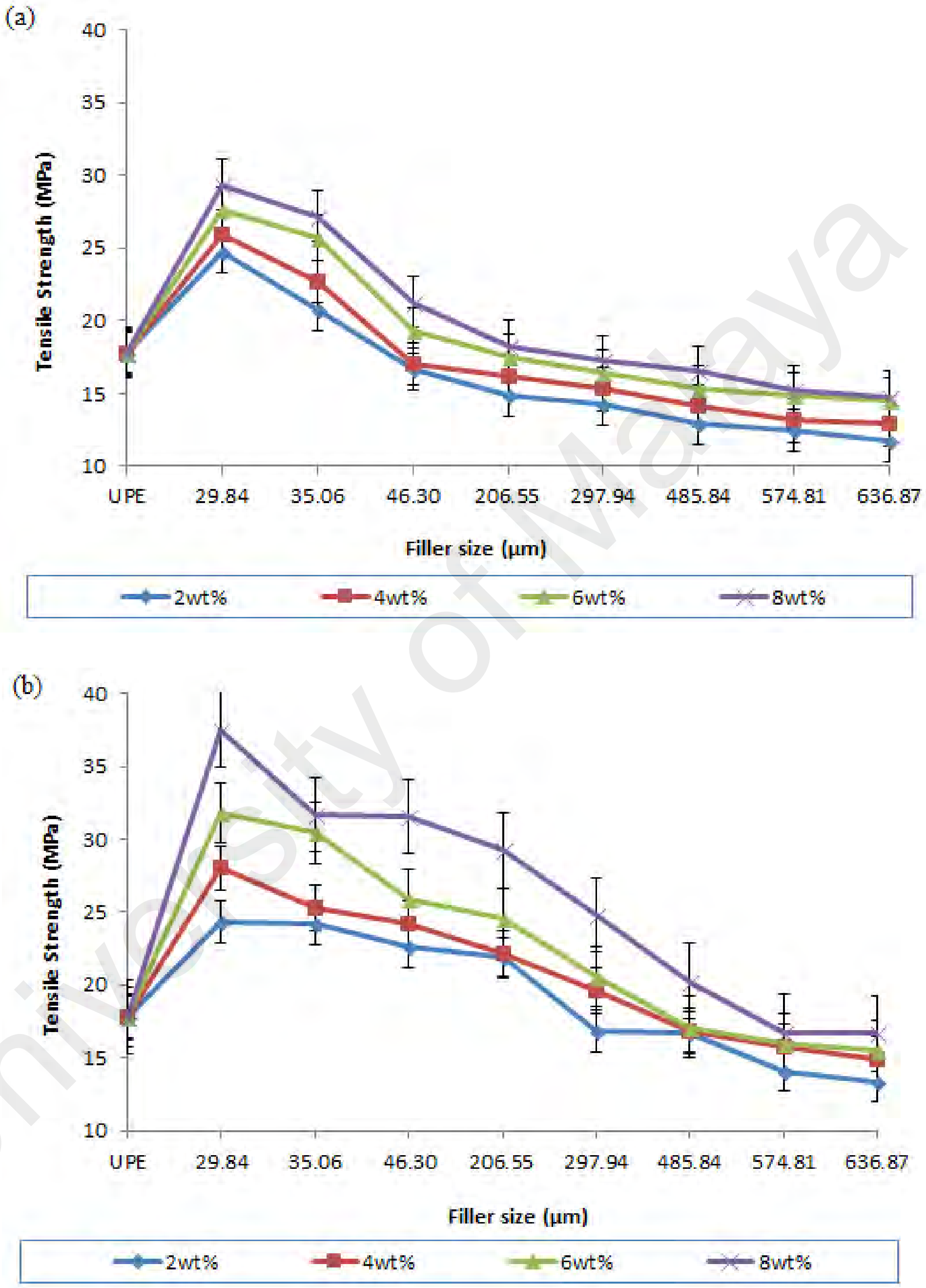

Figure 4.13: Tensile strength of (a) untreated and (b) stearic acid-treated UPE/$CaCO_3$ (aragonite) composites with different sizes and filler contents

Generally, the drastic drop in the tensile strength of untreated UPE/$CaCO_3$ composites is for two main reasons: flaws and poor adhesion between particles and the matrix. Figure 4.14 shows flaws detected in the composites before the tensile test. No voids are detected in the neat UPE resin. Once the $CaCO_3$ particles are introduced in the UPE resin, which is initially in viscous liquid form, voids in the form of air bubbles are produced in the matrix phase. The formation of air bubbles in the liquid is facilitated by solid particles (Marschall et al., 2003) due to the presence of macroscopic stress (Uddin, 2009) during sonication. Sound waves in a sonication environment may introduce stress in the liquid, which can prevent particle agglomeration. However, if the stress from the sound waves exceeds the tensile strength of the liquid, cavities may be created starting at the solid-liquid boundary (Marschall et al., 2003) because this area is where the stress is concentrated, and the stress level is greater than the bulk liquid itself. The cavities are then released in the liquid in the form of air bubbles. The solid-liquid boundaries in the sonication environment may act as surfaces for 'seeding' the cavitation. In the current study, the vacuum pump cannot efficiently remove all air bubbles in the viscous liquid resin during sample fabrication. The filler content also affects the generated void size. At low filler content of 2 wt% and 46.30 µm filler size as shown in Figure 4.14(c), voids of approximately 18.3 – 40.2 nm are generated in the composites. Adding more filler content up to 8 wt% reduces the size of voids to 15.5–35.8 nm, but their numbers increase as illustrated in Figure 4.14(d). This phenomenon was explained by Michler and von Schmeling (2013). At constant void volume fraction, the number of voids will increase as the size of the voids decreases. The voids were also found in other composites as shown in Appendix G (Ichetaonye et al., 2016; Shi et al., 2017; Gittings et al., 2009).

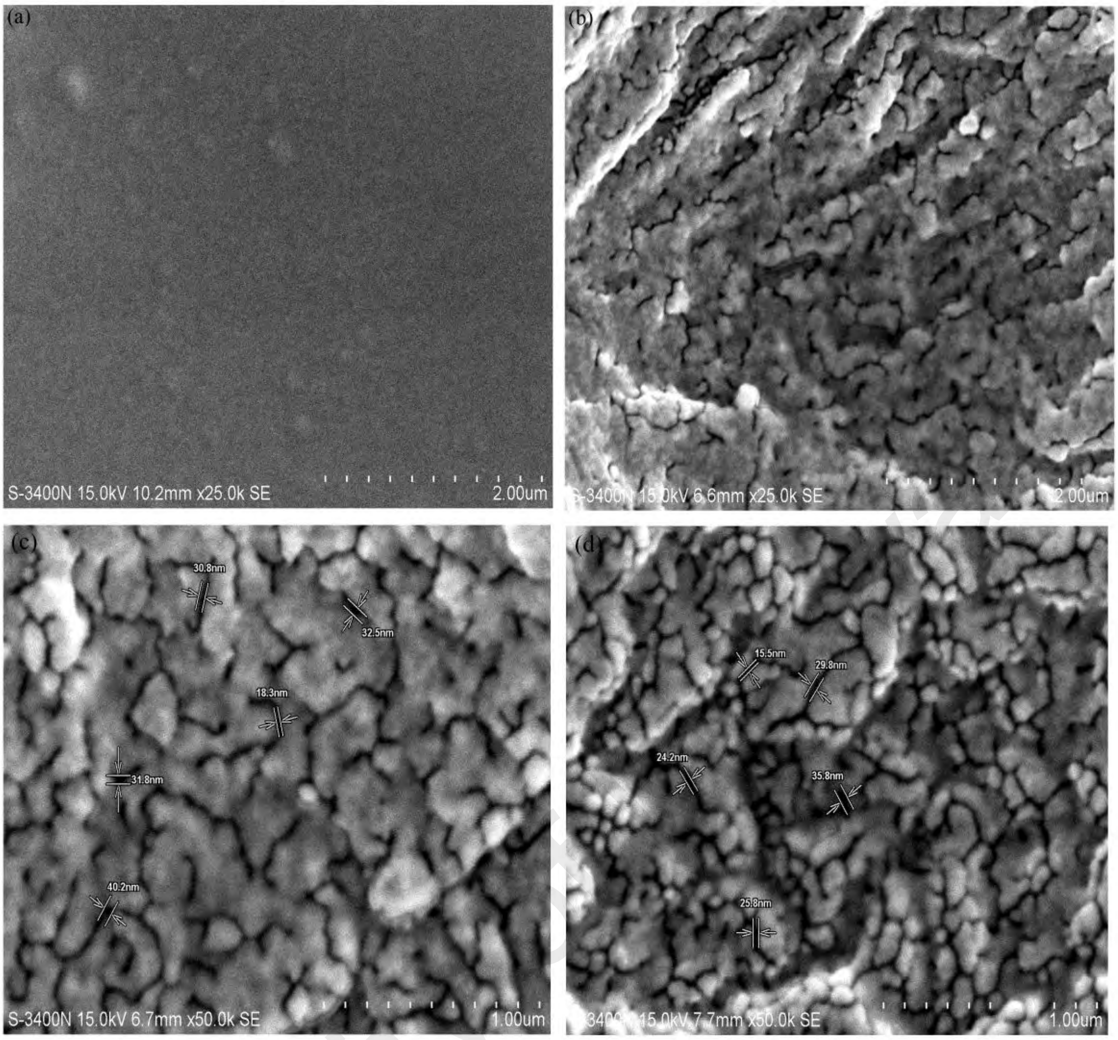

Figure 4.14: SEM images of (a) pure unsaturated polyester (UPE) resin and (b) flaws found at 2 wt%, (c) measurement of voids at 2 wt% and (d) measurement of voids at 8 wt% $CaCO_3$ with 46.30 µm size infused in the UPE matrix before mechanical testing

Flaws or voids act as defects or weak points in the composites. As the sample is pulled apart, failure is initiated at the flaws in the composites. The extensive initiation of flaws under tensile loading may reduce the matrix's capability to transfer the load to the reinforcement, thus decreasing the tensile strength of the composites. However, as explained by Michler and von Schmeling (2013), the size of the voids generated in the composites affects the mechanical properties. Nano-sized voids have a positive effect on the composites' mechanical properties. This is because nanovoids can initiate the same energy absorbing mechanisms as microvoids, but with a much lower risk of premature fracturing (Michler & von Schmeling, 2013). However, as the void size increases to the micron scale, this would eliminate the positive effects of the nanometer-scale voids. Thus, in the current study, adding particles to the UPE resin can increase the tensile strength.

Weak interaction between particles and the matrix can also lead to particle-matrix debonding when the composites are subjected to external loading. Figure 4.15 reveals the fracture surface following tension testing. Introducing 2 wt% of 574.81 µm $CaCO_3$ filler in the UPE resin creates particle-matrix debonding in the composite materials. Figure 4.15(a) illustrates that the particle-matrix debonding size measured in 574.81 µm-filled UPE composites is 207 µm. The fracture surface without the presence of an unsaturated polyester layer indicates the matrix has debonded completely from the untreated $CaCO_3$ particles by breaking the interface. This particle-matrix debonding produced remarkable reduction in the tensile strength of the composites. The debonded particle-matrix interface cannot efficiently transfer tensile stress due to particle-matrix separation (Teng, 2010), as shown in Figure 4.15. Tensile stress enhancement as finer fillers are added to the resin is obtained owing to the size reduction of the particle-matrix debonding in the composites. As seen in Figure 4.15 (a), including 574.81 µm $CaCO_3$ produces particle-matrix debonding of 54 µm, while infusing 297.94 µm filler decreases the particle-matrix debonding size to 10.3 µm. This signifies that finer filler is attached to the matrix more strongly, thus reducing the possibility of matrix-filler debonding. Particle-matrix debonding can form more easily in stiff polymers such as unsaturated polyester (UPE) than in soft polymers (Sudar et al., 2007).

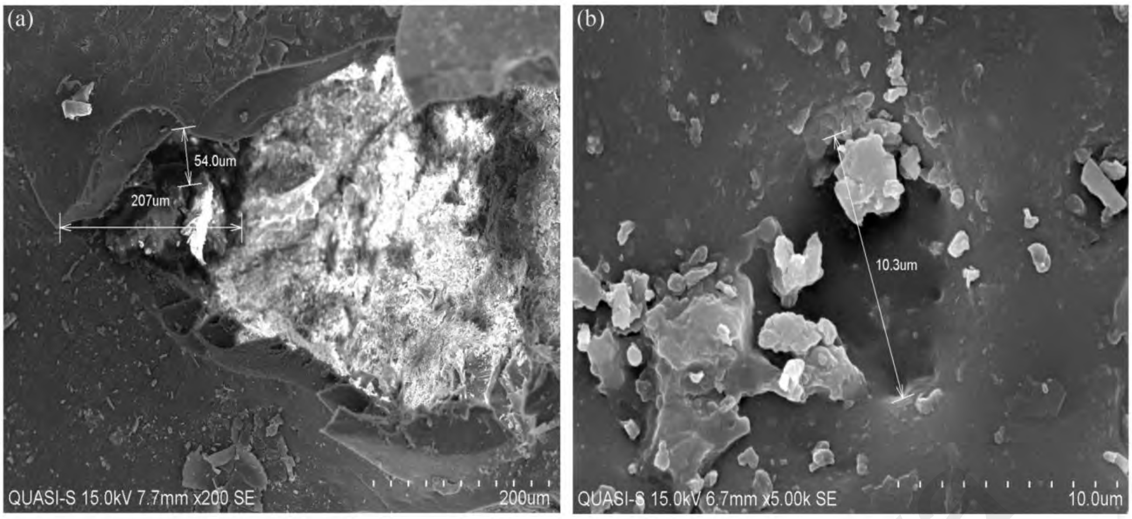

Figure 4.15: SEM fractographs displaying the size reduction in particle-matrix debonding as finer filler is infused in the UPE matrix: (a) 2 wt% of 574.81 μm $CaCO_3$ and (b) 2 wt% of 297.94 μm untreated $CaCO_3$

Treating aragonite $CaCO_3$ with 1 wt% stearic acid has positive effects in terms of the composites' tensile strength. In all cases, the stearic acid-treated UPE/$CaCO_3$ samples yield higher tensile strength than untreated UPE/$CaCO_3$ composites. For example, 8 wt% of treated 485.84 μm filler produces 20.26 MPa tensile strength, whereas untreated filler produces 16.52 MPa as the filler is incorporated into the UPE resin. Good particle-matrix bonding is a key factor contributing to this enhancement. This effect is on account of the good adhesion between stearic acid-treated $CaCO_3$ particles and the UPE matrix (Figure 4.16 (b)). The resin is still attached on the surface of the filler after the tension test. Compared to untreated filler composites, the filler is completely debonded from the matrix as illustrated in Figure 4.16 (a). In a stiff matrix such as UPE resin, almost the entire filler is separated from the matrix when subjected to external loading (Sudar et al., 2007). However, this weakness can be reduced by modifying the aragonite $CaCO_3$ surface with 1 wt% stearic acid. Stearic acid is basically used to produce better filler dispersion (Móczó et al., 2002) in the matrix. However, in the current study, it is also able to strengthen the particle-matrix adhesion.

Treating $CaCO_3$ with stearic acid can improve the filler dispersion by reducing the particle-particle interactions. Monolayer of stearic acid on the $CaCO_3$ particle surface decreases the particles adhesion by increasing the hydrophobicity and contact angle of the particles (Semakina et al., 2015). Treating $CaCO_3$ with 1 wt% stearic acid can improve the hydrophobicity to be 100% from 0% of untreated $CaCO_3$ (Jeong et al., 2009). As a result, the surface energy is lowered thus, allows better dispersion of fillers in polymer matrix.

The treatment also can improve the particle-matrix adhesion. Basically, the chemical structure of stearic acid consists of hydrophilic head and hydrophobic long tail (Garrett &Grisham, 2005). As the $CaCO_3$ particles treat with stearic acid, the hydrophobic hydrocarbon group at the long tail of the stearic acid absorb perpendicularly onto the $CaCO_3$ surface to form the monolayer (Hu et al, 2009). This reaction happens because the surface of $CaCO_3$ which was positively charged can easily be attracted to negatively charge stearic acid (Shi et al., 2011). Meanwhile, the hydrophilic carboxyl group will be bonded to the surface of polymer matrix (Hu et al., 200). This chemical reaction results in the improvement of particle-polymer matrix bonding. Besides, the treatment also able to reduce the electrostatic forces of attraction among the agglomerate particles due to ultrasonication (Shimpi et al., 2015).

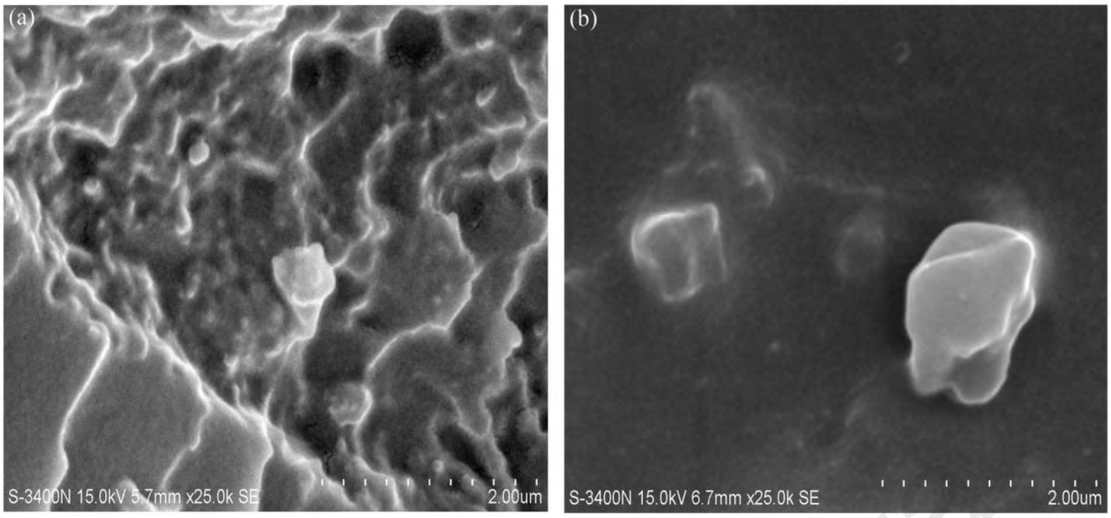

Figure 4.16: SEM images of fracture surface of (a) poor particle-matrix adhesion in untreated composites and (b) better particle-matrix adhesion in stearic acid-treated 46.30 µm $CaCO_3$ particles at 8 wt% filler loading

Similar to untreated filler, adding finer treated particles to the UPE resin can increase the tensile strength. Infusing particles finer than 297.94 µm may enhance the tensile strength of the UPE resin further. Particle size has a significant impact on the tensile strength of particulate-filled polymer composites. Similar trends were also reported in various publications (Cho et al., 2006; Nakamura et al., 1992; Zhang et al., 2004). Smaller particles have a greater total surface area, thus improving the efficiency of the stress transfer mechanism. In addition, a larger interfacial area of smaller particles leads to particles being able to carry higher loads. As more filler is infused into the polymer matrix, more particles with larger surface area can carry more loads, hence expanding the composites' tensile strength. An efficient stress transfer mechanism between small particles with large surface area and the resin will be take placed if both phases are adhered well. The tensile strength values of all untreated and stearic acid-treated UPE/$CaCO_3$ composite samples with different filler sizes and loadings are listed in Table 4.5.

Table 4.5: Tensile strength of untreated and stearic acid-treated UPE/$CaCO_3$ (aragonite) with different sizes and filler loadings

Tensile strength of untreated UPE/$CaCO_3$ composites (MPa) ± Standard error (MPa)								
Size (µm) Weight fraction (wt%)	**29.84**	**35.06**	**46.30**	**206.55**	**297.94**	**485.84**	**574.81**	**636.87**
2	24.79 ±0.61	20.76 ±0.61	16.68 ±0.60	14.84 ±2.39	14.25 ±0.49	12.93 ±0.73	12.41 ±0.54	11.70 ±0.66
4	25.91 ±0.54	22.67 ±0.59	17.03 ±0.47	16.22 ±0.93	15.29 ±0.71	14.14 ±0.37	13.12 ±0.30	12.90 ±0.50
6	27.58 ±0.59	25.73 ±0.54	19.35 ±0.67	17.55 ±0.93	16.42 ±0.64	15.33 ±0.34	14.85 ±0.33	14.49 ±0.34
8	29.32 ±0.59	27.18 ±0.62	21.28 ±0.71	18.27 ±0.61	17.26 ±0.44	16.52 ±0.52	15.21 ±0.47	14.77 ±0.65
Tensile strength of stearic acid-treated UPE/$CaCO_3$ composites (MPa) ± Standard error (MPa)								
2	24.31 ±1.15	24.22 ±1.16	22.58 ±0.70	21.88 ±0.71	16.84 ±0.64	16.76 ±1.20	14.11 ±0.82	13.38 ±0.68
4	28.02 ±1.47	25.29 ±0.95	24.19 ±0.88	22.14 ±1.50	19.60 ±0.57	16.84 ±0.53	15.76 ±0.62	14.94 ±1.39
6	31.79 ±2.42	30.44 ±1.04	25.86 ±1.09	24.52 ±1.32	20.56 ±1.49	17.14 ±0.81	15.96 ±0.48	15.53 ±0.41
8	37.53 ±2.48	31.67 ±1.30	31.54 ±2.21	29.22 ±2.96	24.81 ±1.72	20.26 ±0.79	16.78 ±0.49	16.69 ±0.61

Tensile strength of neat unsaturated polyester (UPE) resin: 17.81±0.10 MPa

4.3.2 Flexural properties

In general, adding $CaCO_3$ particles in UPE resin would improve the flexural properties such as the flexural modulus and flextural strength. of the composites. Figure 4.17 represents the stress-strain curves of 29.84 µm mean size of $CaCO_3$ filler infused in UPE polymer matrix composites at four different weight fractions of fillers; 2 wt%, 4 wt%, 6 wt% and 8 wt%.

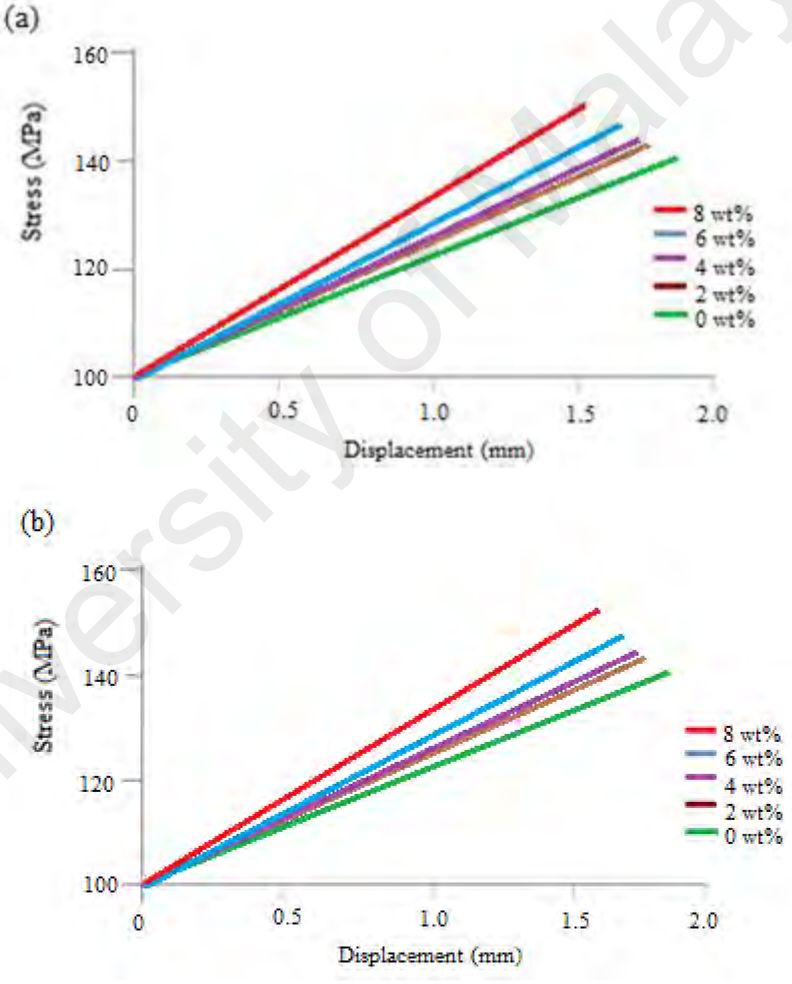

Figure 4.17: Flexural stress-displacement curve of (a) untreated and (b) stearic acid treated of 29.84 µm mean diameter size of $CaCO_3$ at different filler fraction in UPE/$CaCO_3$ composites

The curves show that infusing $CaCO_3$ particle improves the flexural strength and flexural modulus of the samples. The enhancement is gained as the filler content is increases up to 8 wt%. However, as the filler content increases, the displacement or deflection of the sample under flexural loading become shorter. The combination of stiff particles which is $CaCO_3$ in UPE matrix does not helpful to increase the deflection of composites. This is because the interface bond between the matrix and filler is weak due to compressive and tensile force. The sample subjected to bending is prone to both tensile and compression loadings. Treating the filler with 1 wt% stearic acid improves both flexural modulus and flexural strength for all samples at similar filler loading compared to untreated UPE/$CaCO_3$ composites. Figure 4.18 shows the fracture surface of the sample under flexural loading. The specimen fails due to brittle failure because the direction of the crack is nearly perpendicular to the direction of the loading and the fracture surface is smooth (Jones & Ashby, 2012).

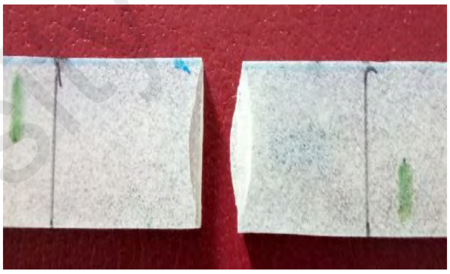

Figure 4.18: The fracture surface of the specimen after flexural test

4.3.2.1 Flexural modulus

Flexural modulus is a measure of how a material will strain or bend under flexural deformation. The flexural modulus of untreated and stearic acid-treated aragonite UPE/$CaCO_3$ composites with different filler sizes and filler contents is shown in Figure 4.19. In contrast to the trend recorded for tensile modulus, there is an overall increase in flexural modulus as UPE resin is filled with $CaCO_3$ clam shell particles, except for 2 wt% 636.87 μm untreated filler. Both untreated and stearic acid-treated $CaCO_3$ particulate-filled UPE composites increase almost linearly with finer filler size and higher filler content. The improvement is distinctly better for stearic acid-treated filler than the untreated counterpart.

The flexural modulus of unfilled UPE resin was initially 1578.90 MPa. Adding 2 wt% of 636.87 μm untreated aragonite $CaCO_3$ decreases the modulus to 3120.26 MPa, or a 1.3% loss. However, a positive effect is noted as filler of the same size is added. At 8 wt% the flexural stiffness is 3478.71 MPa, which is a 10% increment. A significant enhancement is observed as the UPE resin is filled with finer filler in higher amounts. About 50% improvement is obtained as 8 wt% of 29.84 μm untreated filler is infused into the UPE resin. Thus, it can be concluded that the flexural modulus of UPE/$CaCO_3$ composites is significantly affected by both filler size and filler content.

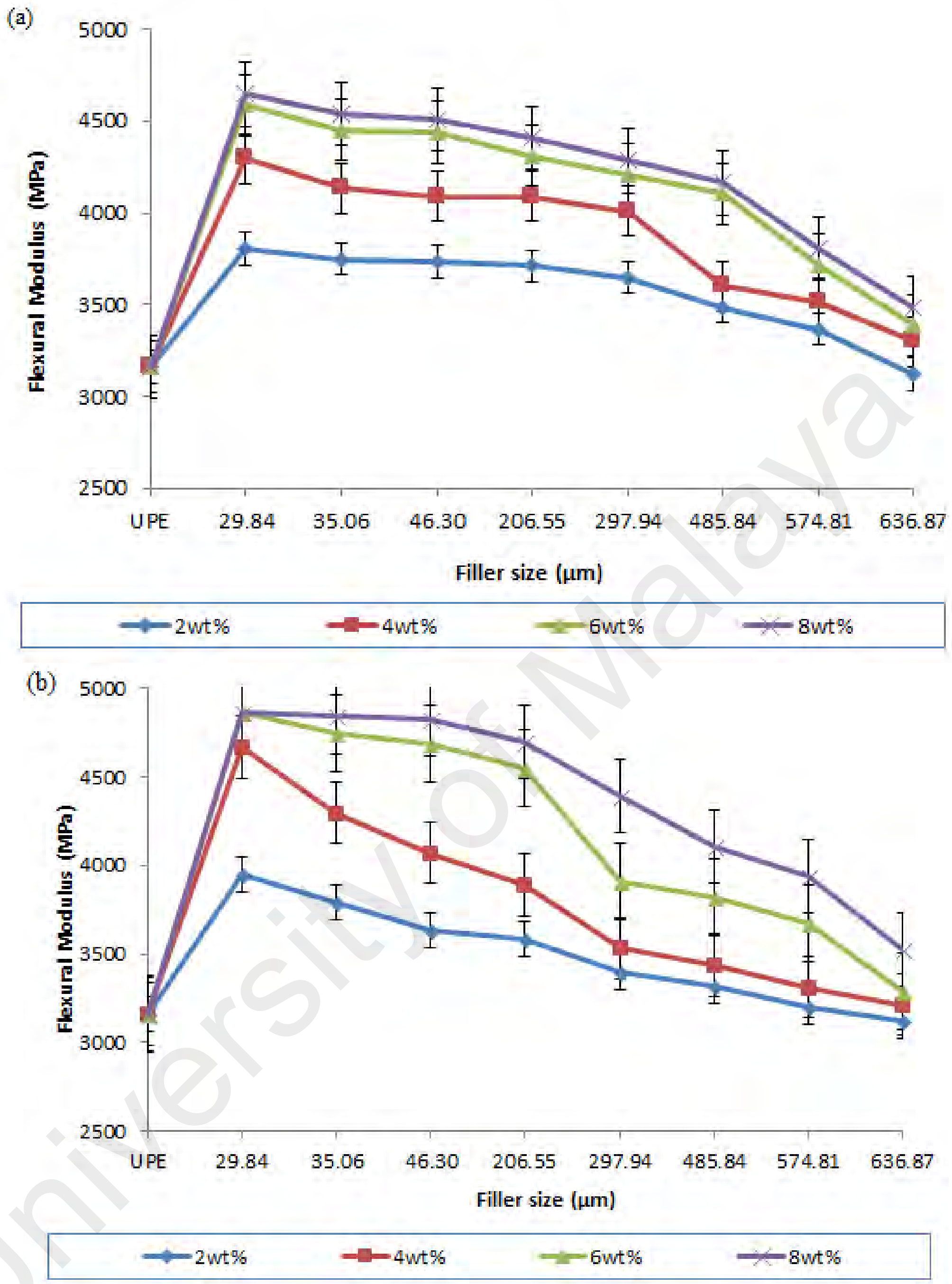

Figure 4.19: Flexural modulus of (a) untreated and (b) stearic acid-treated UPE/$CaCO_3$ (aragonite) composites with different sizes and filler contents.

Generally, treating $CaCO_3$ particles with stearic acid produces stiffer composites than untreated filler, except at low filler loading (2 wt%). More significant improvement is achieved at higher filler loading. At 2 wt% filler with 297.94 µm size, the moduli of untreated and treated filler composites are 3647.74 MPa and 3398.69 MPa, respectively. For identical filler sizes, increasing the filler content to 8 wt% produces a stiffer matrix of 4282.8 MPa with untreated filler and 4391.48 MPa with treated filler.

The increase in flexural modulus can be attributed to the composites' enhanced brittleness and stiffness. For both untreated and treated fillers, the flexural moduli of the composites appear to increase with decreasing filler size up to a maximum value at 8 wt% filler loading. Other than particle size, material stiffness is also affected by the filler dispersion in the matrix. Homogeneous filler dispersion might contribute to greater composite stiffness. As the particles infuse into the matrix, a stress concentration is also introduced around each particle. The stress concentration zones are interconnected, forming a particle interconnection network. For very fine and well-dispersed particles, the total volume affected is larger and the distance between particles becomes shorter. This phenomenon leads to an excellent particle interconnection network that produces a high modulus of particulate-filled polymer composites. This phenomenon was described by He and Jiang (1993) and applied by other authors to explain their results of the effect of particle-filled polymer matrix on the stiffness of composites (Mareri et al., 1998; Švehlová & Polouček, 1994). However, as the filler size decreases, the surface energy would increase (Jiang et al, 2005), attracting the filler to start clustering and thus distorting the continuous percolation network formation. Therefore, at 8 wt%, the flexural modulus is very close to 6 wt% as the filler size decreases. Figure 4.20 (a) illustrates an SEM image of agglomerate in 6 wt% filler content of stearic acid-treated $CaCO_3$ filler with 29.84 µm mean particle size. The agglomerate present in 8 wt% filler content of stearic acid-treated $CaCO_3$ as shown in

Figure 4.20 (b) indicates that this treatment cannot eliminate the formation of particle agglomeration, especially as the filler content increases. Larger agglomerates form at higher filler content.

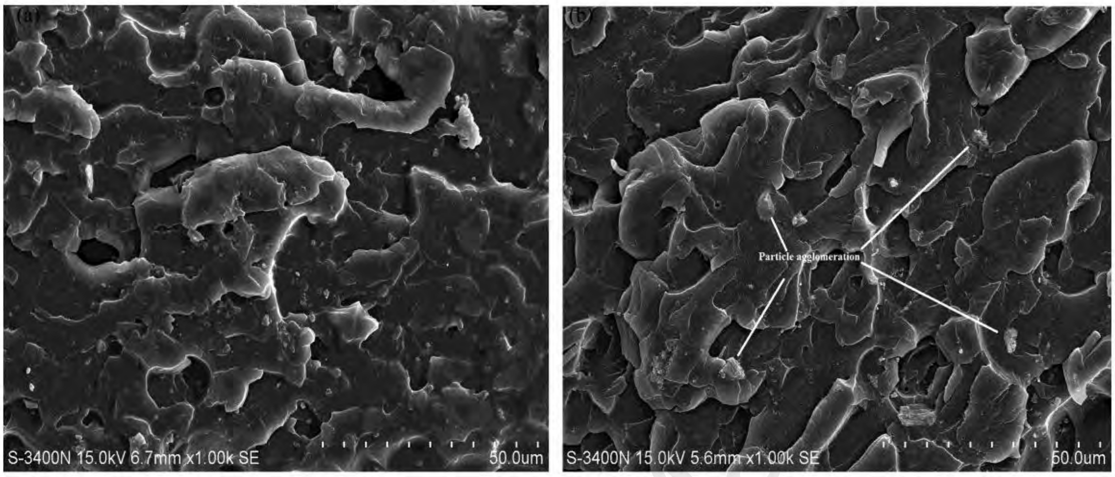

Figure 4.20: SEM images of fracture surface illustrating agglomerates present at (a) 6 wt% and (b) 8 wt% of 29.84 µm stearic-treated UPE/$CaCO_3$ (aragonite) composite.

Figure 4.21 illustrates the dispersion of untreated and stearic acid-treated aragonite $CaCO_3$ filler in the UPE matrix. Stearic-treated $CaCO_3$ filler appears more homogeneously dispersed than the untreated filler composite. This leads to greater flexural modulus yield in the treated samples. Table 4.6 shows the flexural modulus values of all samples of untreated and stearic acid-treated UPE/$CaCO_3$ composites with different filler sizes and filler loadings.

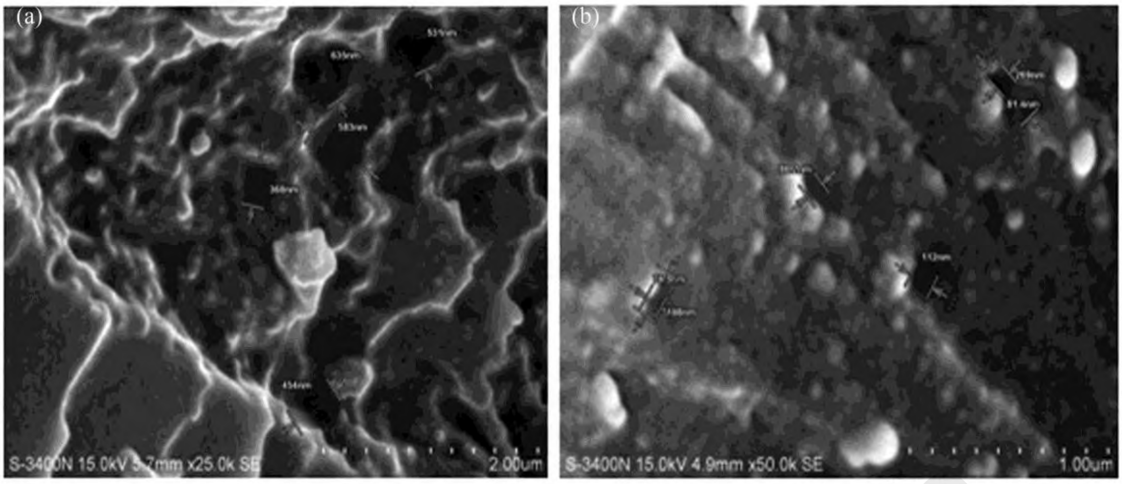

Figure 4.21: SEM images showing better filler dispersion in (a) stearic acid-treated filler than (b) untreated filler for 8 wt% filler content with 35.06 µm mean particle size UPE/$CaCO_3$ (aragonite) composites

Table 4.6: Flexural modulus of untreated and stearic acid-treated UPE/$CaCO_3$ (aragonite) with different sizes and filler loadings

Flexural modulus of untreated UPE/CaCO₃ (MPa) ± Standard error (MPa)								
Size (µm) Weightfraction (wt%)	**29.84**	**35.06**	**46.30**	**206.55**	**297.94**	**485.84**	**574.81**	**636.87**
2	3803.56 ±11.82	3748.47 ±12.22	3733.22 ±15.99	3709.45 ±11.35	3647.74 ±11.04	3487.28 ±8.92	3365.29 ±9.78	3120.26 ± 2.76
4	4294.27 ±10.52	4131.64 ±15.46	4090.13 ±14.77	4089.63 ±11.40	4010.44 ±4.19	3600.68 ±4.35	3509.91 ±5.98	3298.45 ±4.98
6	4585.6 ±7.02	4452.59 ±14.92	4438.56 ±15.09	4311.29 ±9.84	4211.22 ±5.57	4102.75 ±4.76	3715.35 ±5.09	3388.75 ±5.83
8	4644.48 ±13.30	4538.16 ±10.68	4506.77 ±7.38	4405.16 ±7.72	4282.8 ±4.69	4162.73 ±4.76	3802.3 ±5.77	3478.71 ±6.09
Flexural modulus of stearic acid-treated UPE/CaCO₃ (MPa) ± Standard error (MPa)								
2	3946.56 ±11.08	3793.43 ±6.75	3632.10 ±14.92	3584.25 ±5.86	3398.69 ±9.19	3317.47 ±10.57	3196.65 ±7.38	3122.24 ±2.10
4	4671.34 ±10.20	4298.37 ±6.59	4071.45 ±9.66	3893.65 ±12.25	3530.70 ±12.29	3438.46 ±9.62	3313.14 ±9.42	3214.80 ±5.91
6	4865.80 ±11.17	4742.77 ±6.94	4690.80 ±7.79	4545.59 ±14.09	3906.71 ±9.45	3817.63 ±12.14	3668.40 ±13.69	3289.25 ±10.97
8	4866.71 ±10.73	4840.97 ±14.26	4827.64 ±9.70	4695.20 ±6.98	4391.48 ±7.02	4107.12 ±12.89	3938.45 ±12.36	3539.40 ±8.98

Flexural modulus of neat unsaturated polyester (UPE) resin: 3160.51±16.6739 MPa

4.3.2.2 Flexural strength

Flexural strength is the maximum stress that a material can sustain under flexural loading or bending. The deflected sample is subjected to a combination of compression and tension. The maximum compressive stress is at the concave face or the inside of the beam at the edge of the deflected sample, while the maximum tensile stress value is at the convex face or the outside of the beam. Figure 4.22 shows the flexural strength of UPE/$CaCO_3$ (aragonite) composites with different sizes and filler contents. Each point represents the average value of ten flexural strength readings. Adding aragonite $CaCO_3$ to the neat UPE resin is not helpful for enhancing the flexural strength. Deformation in the flexural loading exhibits a sharp decrease in flexural strength once coarser filler of 636.87 µm is introduced in the UPE matrix at all filler contents. Then the flexural strength gradually increases as the filler size decreases. The maximum flexural strength is achieved with the finest particle size and with filler content of 2 wt% and 8 wt% for untreated and stearic acid-treated composites, respectively. The decrease in flexural strength with mean filler size of over 29.84 µm is attributed to the inability of the filler to support the stress transferred from the polymer matrix due to poor interfacial bonding generated by partial spaces between filler and matrix. The result also reveals that flexural strength is strongly dependent on filler size. As the filler size gets smaller, the interfacial area for particle-matrix adhesion is larger. Bigger interfacial areas enable the transfer of higher amounts of stress from the polymer.

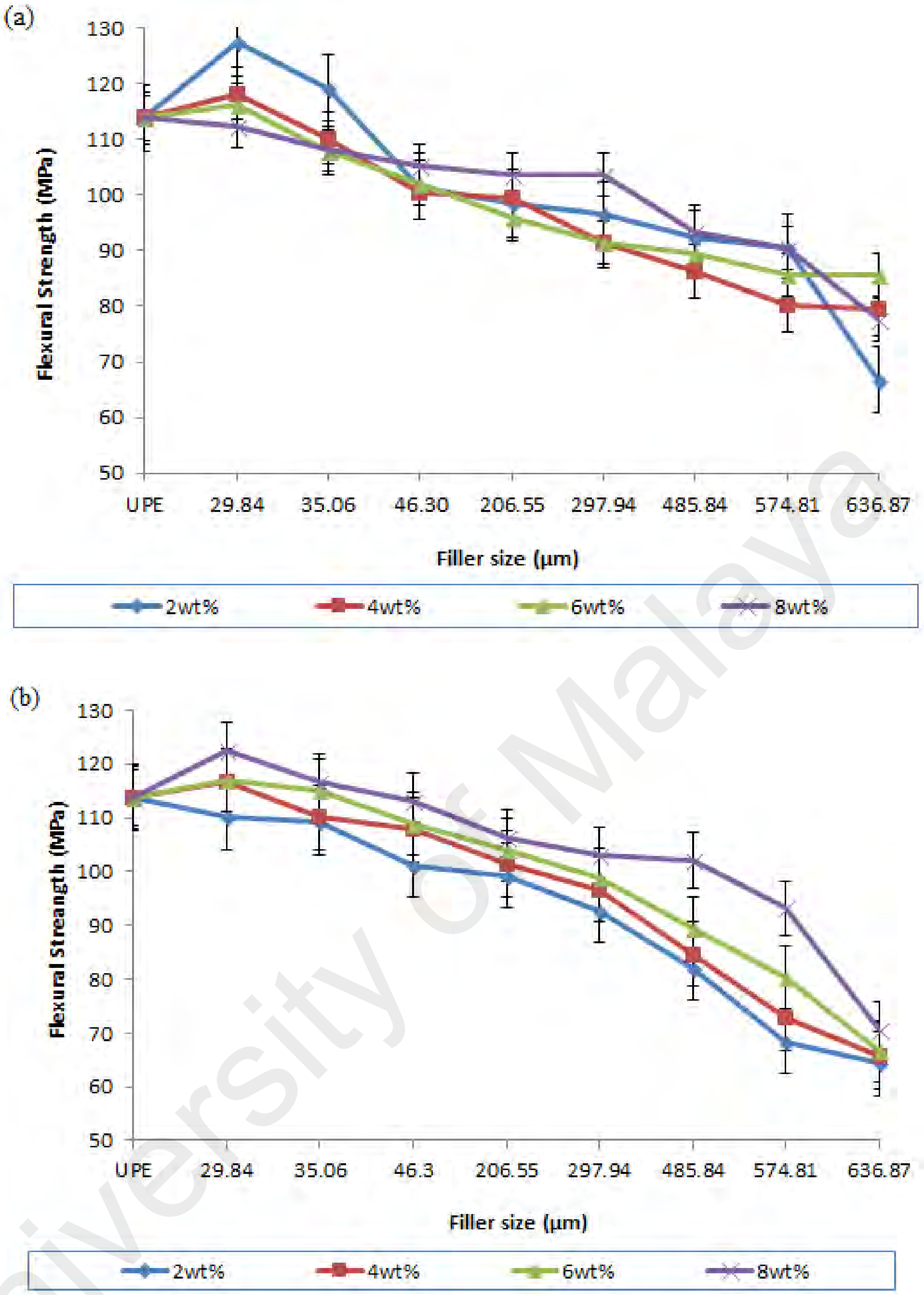

Figure 4.22: Flexural strength of (a) untreated and (b) stearic acid-treated UPE/$CaCO_3$ (aragonite) composites with different sizes and filler contents.

Poor interfacial adhesion between particles and matrix leads to particle-matrix debonding when subjected to external loading. Debonding is strongly related to particle size (Jerabek et al, 2010) and it is easily formed between the matrix and large filler, especially micron-size filler (Cho et al., 2006). In addition, particle-matrix debonding can easily occur in matrices with high stiffness rather than soft polymers (Sudar et al., 2007). In this study, UPE is a thermosetting polymer with high stiffness. Figure 4.23 shows the poor interfacial adhesion between particles and matrix that causes particle-matrix separation. Figure 4.23 (a) displays severe particle-matrix separation observed for 8 wt% of 46.30 µm mean particle size $CaCO_3$ in the UPE resin that results in reduced flexural strength. Particle-matrix separation is also observed at the smallest filler size of 29.84 µm with similar filler, but a higher number of fillers remain attached to the UPE resin. The image in Figure 4.23 (b) proves that finer fillers can become strongly attached to the matrix, thus reducing the possibility of matrix-filler debonding. This explains why smaller particles can maximize the effect of the filler in the polymer matrix. The flexural modulus values of all samples of untreated and stearic acid-treated UPE/$CaCO_3$ composites with different filler sizes and filler loadings are listed in Table 4.7.

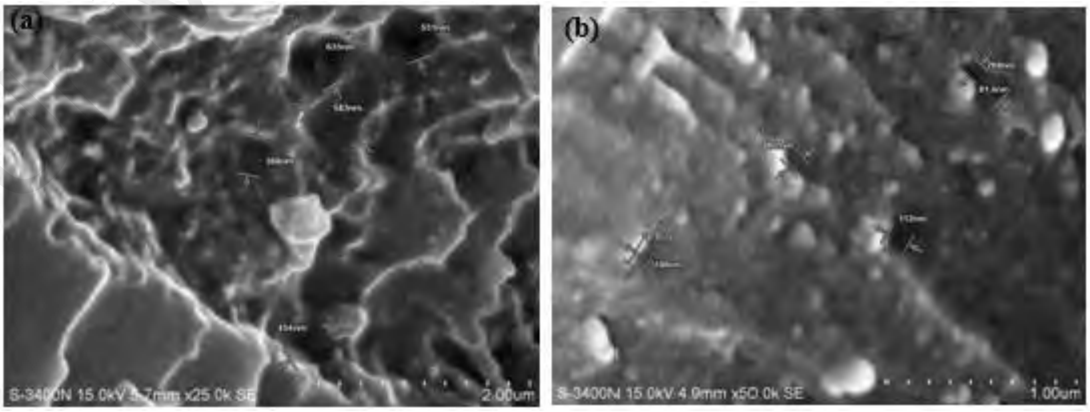

Figure 4.23: SEM images showing the reduced separation of particles from the matrix at 8 wt% filler content with (a) 46.30 µm mean particle size and (b) 29.84 µm mean particle size of $CaCO_3$-filled UPE matrix composites

Table 4.7: Flexural strength of untreated and stearic acid-treated UPE/$CaCO_3$ (aragonite) with different sizes and filler loadings

Size (µm) Weight fraction (wt%)	29.84	35.06	46.30	206.55	297.94	485.84	574.81	636.87
Flexural strength of untreated UPE/$CaCO_3$ (MPa) ± Standard error (MPa)								
2	127.39 ±2.84	119.22 ±3.66	101.52 ±1.59	98.47 ±5.04	96.46 ±3.97	92.33 ±1.52	90.48 ±4.32	66.69 ±7.19
4	118.27 ±2.53	110.23 ±6.79	100.31 ±2.77	99.33 ±5.90	91.57 ±2.51	86.33 ±1.54	80.19 ±1.60	79.62 ±1.19
6	116.13 ±3.67	107.73 ±3.05	102.14 ±3.82	95.79 ±2.98	91.42 ±2.50	89.42 ±1.63	85.62 ±5.68	85.54 ±4.20
8	112.25 ±3.04	108.31 ±3.80	105.26 ±2.32	103.58 ±2.68	103.57 ±2.64	93.24 ±2.15	90.44 ±2.23	77.60 ±2.39
Flexural strength of stearic acid-treated UPE/$CaCO_3$ (MPa) ± Standard error (MPa)								
2	110.43 ±2.02	106.83 ±1.75	101.35 ±2.50	99.21 ±2.04	92.88 ±5.15	82.06 ±4.69	68.67 ±3.88	64.25 ±2.90
4	116.42 ±4.39	110.35 ±2.01	107.33 ±2.15	101.58 ±5.61	96.64 ±3.37	84.64 ±3.51	72.55 ±2.07	65.72 ±4.81
6	117.30 ±3.00	115.39 ±2.41	108.68 ±2.82	104.18 ±3.58	98.74 ±3.87	89.39 ±3.84	80.25 ±3.63	66.49 ±2.25
8	122.42 ±1.70	116.40 ±4.00	113.86 ±3.95	106.25 ±1.98	102.97 ±2.46	102.46 ±5.16	93.17 ±3.25	70.42 ±4.27

Flexural strength of neat unsaturated polyester (UPE) resin: 113.80±3.59 MPa

4.3.3 Compression properties

Figure 4.24 represents the stress-strain curves of 29.84 µm mean size of $CaCO_3$ filler infused in UPE polymer matrix composites at four different weight fractions of fillers; 2 wt%, 4 wt%, 6 wt% and 8 wt%. Pure UPE has a compressive strength of 101.56 MPa. Infusing $CaCO_3$ filler in the UPE matrix improves the compressive strength and compressive modulus of the composites. The significant improvements for both compressive strength and compressive modulus are obtained at the highest filler content which is at 8 wt%. Again, the disadvantage of $CaCO_3$ filled into UPE matrix is the reduction of compressive strain. The more $CaCO_3$ added the shorter the compressive strain experienced by the composites. Figure 4.25 shows the sample before and after the compression test. It shows that most of the sample maintain the shape after the test even the crack was found at the middle of the sample.

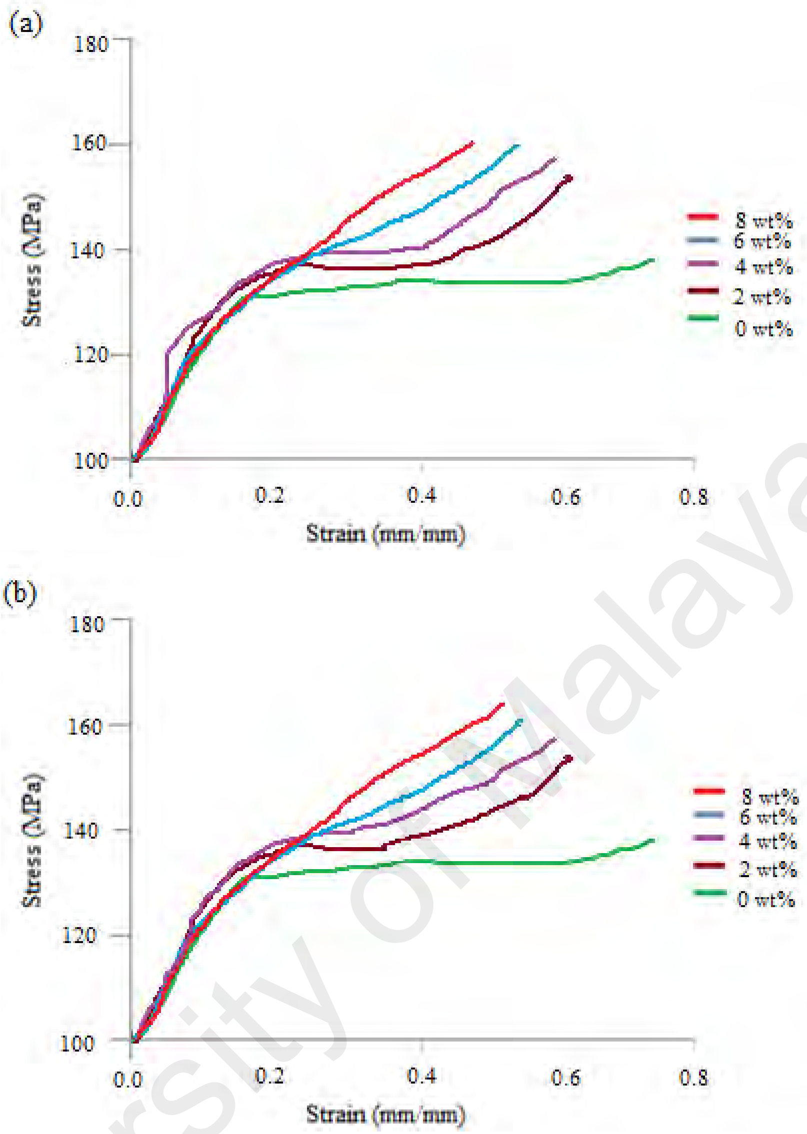

Figure 4.24: Compression stress-strain curve of (a) untreated and (b) stearic acid-treated of 29.84 µm mean diameter size of $CaCO_3$ at different filler fraction in UPE/$CaCO_3$ composites

Figure 4.25: The specimen (a) before and (b) after compression test

4.3.3.1 Compressive modulus

Compressive modulus is the ratio of compressive stress to compressive strain below the proportional limit. The average values from ten readings of the compressive moduli of unfilled UPE resin and UPE/$CaCO_3$ (aragonite) composites are shown in Figure 4.26. The figure presents the compressive modulus of untreated and stearic acid-treated UPE/$CaCO_3$ (aragonite) composites of different sizes and filler contents. For untreated $CaCO_3$ particulate-filled polymer composites, the compressive modulus improvement is influenced by filler size and filler loading. The compressive modulus of unfilled UPE resin is 3012.94 MPa. Similar to tensile modulus, the compressive modulus decreases sharply to 2107.60 MPa, or a 30% decrease when 2 wt% untreated $CaCO_3$ with 636.87 µm filler size is infused in the UPE resin. Beyond this filler fraction, the compressive modulus increases slowly as filler content increases for all filler sizes. However, the increase does not exceed the initial modulus of unfilled UPE resin except for 46.30 µm (6-8 wt%), 35.06 µm (4-8 wt%) and 29.84 µm (2-8 wt%) filler sizes. This signifies that adding coarse, untreated filler from *lokan* shell particle has a negative influence on compressive stiffness. At a similar filler loading, finer filler slightly improves the compressive modulus. At 4 wt% filler fraction, the compressive moduli gained by 297.94 µm, 206.55 µm and 46.30 µm sizes are 2698.11 MPa, 2810.83 MPa and 2902.15 MPa, respectively. For untreated filler, the best compressive modulus of 3598.05 MPa is achieved at 8 wt% with 29.84 µm filler size. This value represents a 19.4% increment compared to unfilled UPE resin.

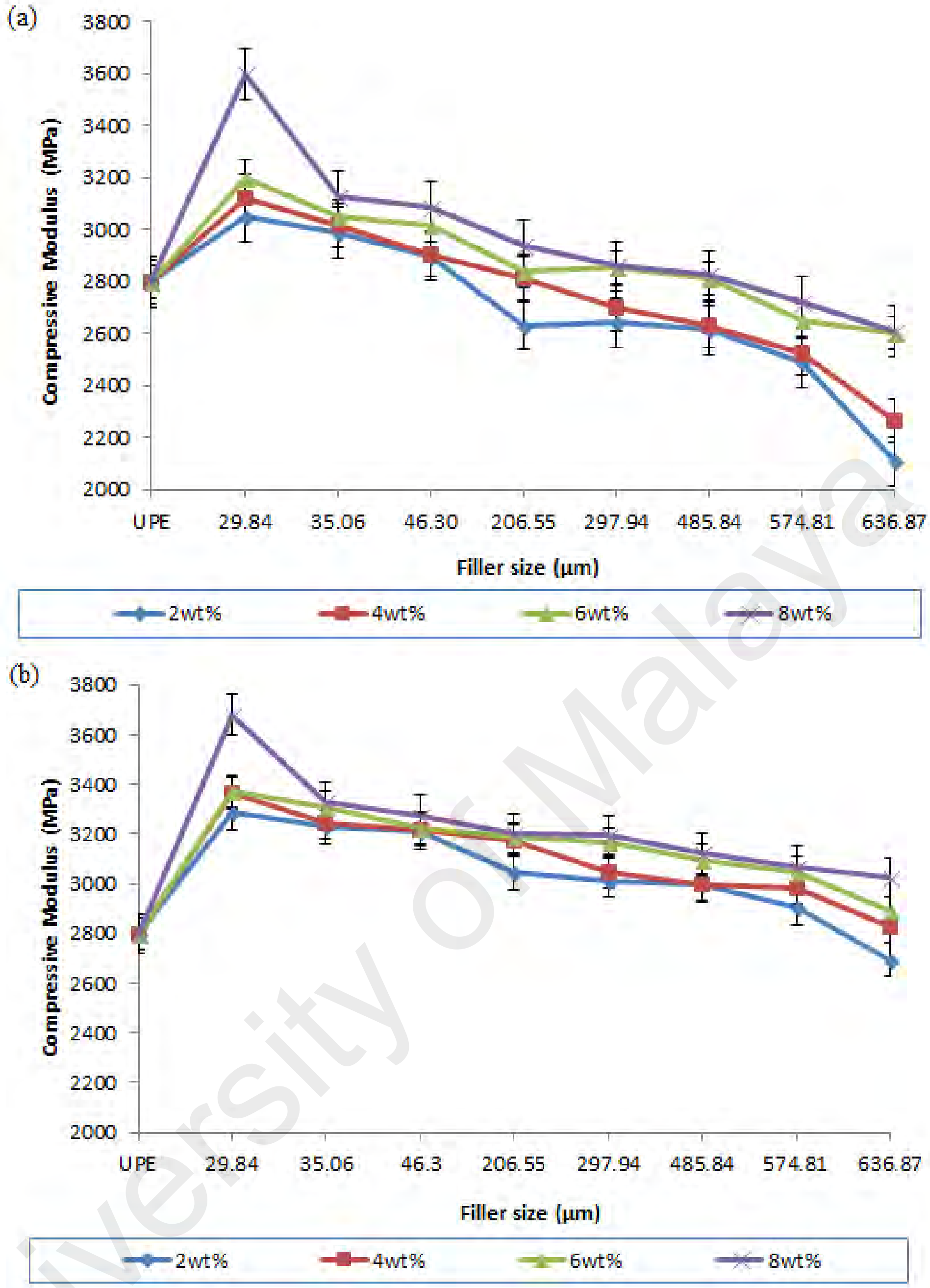

Figure 4.26: Compressive modulus of (a) untreated and (b) stearic acid-treated UPE/$CaCO_3$ (aragonite) composites with different sizes and filler contents.

The stiffness of the untreated UPE/$CaCO_3$ composites is influenced by the particle interconnection network of the filler in the resin. Better filler dispersion in the matrix (Švehlová & Polouček, 1987; He & Jiang, 1993) leads to greater modulus. Better interconnection of the stress zones produced around the finer filler in the matrix resin results in higher compressive modulus gained by the finer filler at higher content. Since the specific gravity of aragonite $CaCO_3$ is 2.93 is higher than liquid UPE resin, which is 1.13, coarse filler tends to settle at the bottom of the sample during the curing process. Sonication is not able to prevent the deposition of coarse filler at the bottom of the mixture due to gravitational force. As a result, coarse filler does not disperse well in the matrix. Finer filler can spread easily into polymer liquid. No filler deposition is observed at the bottom of the sample. Well-dispersed filler in the matrix may provide a small distance between the filler, allowing the zones to join and form a particle interconnection network. A continuous particle interconnection network may increase the modulus of the composites. Therefore, better filler dispersion of finer filler results in higher compressive modulus in the fine particulate-filled polymer composites. Moreover, adding more fine particles to the resin increases the compressive modulus of the composites.

Modifying $CaCO_3$ with 1 wt% stearic acid can successfully improve the compressive modulus of the sample by producing a bigger value than untreated UPE/$CaCO_3$ composites. At 4 wt% with 46.30 μm filler size, untreated filler and stearic acid-treated filler produce 2902.15 MPa and 3214.58 MPa, respectively. This 312 MPa difference is attributed to filler treatment. However, the compressive modulus enhancement is not greatly influenced by filler size and filler content. As shown in Figure 4.26(b), the change in compressive modulus is not obvious by reducing the filler size rather than adding filler content. Higher compressive modulus attained by treated UPE/$CaCO_3$ composites is due to the well-dispersed filler in the matrix. Stearic acid is a non-reactive treatment for $CaCO_3$ (Móczó et al., 2002). This treatment changes the behavior of particles, in that it forms much looser aggregates with a larger diffused interface than untreated particles (Farris, 1968). The change in compressive modulus is not very noticeable as the finer filler size and content increase, because this treatment does not eliminate aggregation completely (Deshmukh et al., 2010a; Deshmukh et al., 2010b). Adding more filler to the matrix generates more agglomerate but of smaller size than untreated particle composites. Figure 4.21 reveals the dispersion of aragonite $CaCO_3$ filler in an unsaturated polyester matrix. Treated filler disperses more homogeneously than its untreated counterpart. The interconnection filler network appears to be disturbed by the formation of agglomerate in both untreated and treated fillers.

The results also show that treating $CaCO_3$ particles with 1 wt% stearic acid stiffens the composites. For treated filler-filled polymer composites, the stiffness is the result of a competition between the "stiffening" effect of better dispersion and the "softening" effect of the treatment agent (Mareri et al., 1998). At low filler content of 8 wt% and below, stearic acid treatment has a greater "stiffening" effect than "softening." Table 4.8 is a list of the compressive moduli of untreated and stearic acid-treated aragonite $CaCO_3$ with different filler sizes and filler contents. All data are the average of ten readings.

Table 4.8: Compressive modulus of untreated and stearic acid-treated UPE/$CaCO_3$ (aragonite) with different sizes and filler loadings

Compressive modulus of untreated UPE/$CaCO_3$ (MPa) ± Standard error (MPa)								
Size (µm) Weight fraction (wt%)	**29.84**	**35.06**	**46.30**	**206.55**	**297.94**	**485.84**	**574.81**	**636.87**
2	3047.55 ±9.19	2986.54 ±15.55	2897.63 ±6.59	2630.14 ±13.28	2641.42 ±10.69	2613.89 ±12.35	2486.71 ±7.84	2107.60 ±9.40
4	3123.32 ±10.51	3014.60 ±15.47	2902.15 ±9.24	2810.83 ±11.68	2698.11 ±10.44	2632.44 ±11.21	2526.59 ±7.58	2264.42 ±8.56
6	3201.39 ±12.03	3050.14 ±12.26	3016.36 ±18.11	2838.74 ±7.28	2851.22 ±16.20	2814.84 ±8.58	2651.70 ±12.09	2599.43 ±10.20
8	3598.05 ±7.42	3130.57 ±7.33	3086.46 ±9.00	2937.51 ±7.82	2857.68 ±14.12	2822.87 ±8.03	2721.06 ±10.52	2608.07 ±8.86
Compressive modulus of stearic acid-treated UPE/$CaCO_3$ (MPa) ± Standard error (MPa)								
2	3284.18 ±15.45	3228.34 ±13.27	3207.70 ±5.66	3044.59 ±16.57	3010.96 ±13.42	2993.64 ±10.83	2902.94 ±16.09	2693.49 ±11.41
4	3363.29 ±11.95	3243.28 ±12.36	3214.58 ±11.99	3172.54 ±12.75	3046.51 ±11.12	2997.07 ±11.09	2985.28 ±10.93	2823.99 ±15.61
6	3370.18 ±11.93	3309.55 ±9.06	3225.12 ±13.58	3185.33 ±12.81	3164.23 ±13.03	3094.69 ±8.91	3046.73 ±14.49	2887.49 ±15.60
8	3678.56 ±7.33	3326.65 ±14.65	3274.41 ±13.32	3200.11 ±11.53	3194.29 ±12.00	3120.69 ±6.75	3070.32 ±14.44	3026.11 ±11.96

Compressive modulus of neat unsaturated polyester (UPE) resin: 3012.94±9.82 MPa

4.3.3.2 Compressive strength

Compressive strength is the maximum stress that a material can sustain under uniaxial compressive loading. The average values from ten compressive strength readings of neat UPE resin and UPE/$CaCO_3$ (aragonite) are illustrated in Figure 4.27. It shows the compressive strengths of UPE/$CaCO_3$ (aragonite) composites with different sizes and filler contents. Initially, the compressive strength of pure UPE resin is 101.56 MPa. Including micron-size aragonite $CaCO_3$ filler generally improves the compressive strength of composites except for 2 wt% untreated filler with 636.87 µm size. The decrease is of about 8.5% compared to unfilled UPE resin.

Generally, the deformation in compression loading exhibits an increase in compressive strength as the filler is induced in the UPE matrix. The filler acts as a barrier to dislocation in the composites, hence improving the compressive strength of particulate-filled polymer composites. A small improvement is gained as the filler size decreases, as shown in Figure 4.27. The highest compressive strengths for both untreated and treated $CaCO_3$ fillers are obtained with the finest filler at 8 wt%. This result indicates that compressive strength depends on filler size. Finer filler provides a larger interfacial area for efficient stress transfer. As a result, greater loads can be carried by the smaller particles. However, the higher filler content does not significantly affect the compressive strength. This is because as the filler content increases, the filler tends to cluster and form bigger agglomerates. The agglomerates lead to further reduction of the interfacial area, hence reducing the effectiveness of stress transfer. In addition, as the filler content increases, the free volume that allows the particles to move around will decrease. Besides, the effectiveness of composite strengthening is also reduced as the distance between the clusters is shorter (Lam et al, 2005). Although sonication is applied to promote better filler dispersion in the matrix, the particles still cannot be homogeneously dispersed as the UPE resin is cured at room temperature. Therefore, the compressive strength isquite similar when the filler size reduces to 46.30 µm for untreated and 574.8 µm for treated $CaCO_3$ filler at all filler loadings.

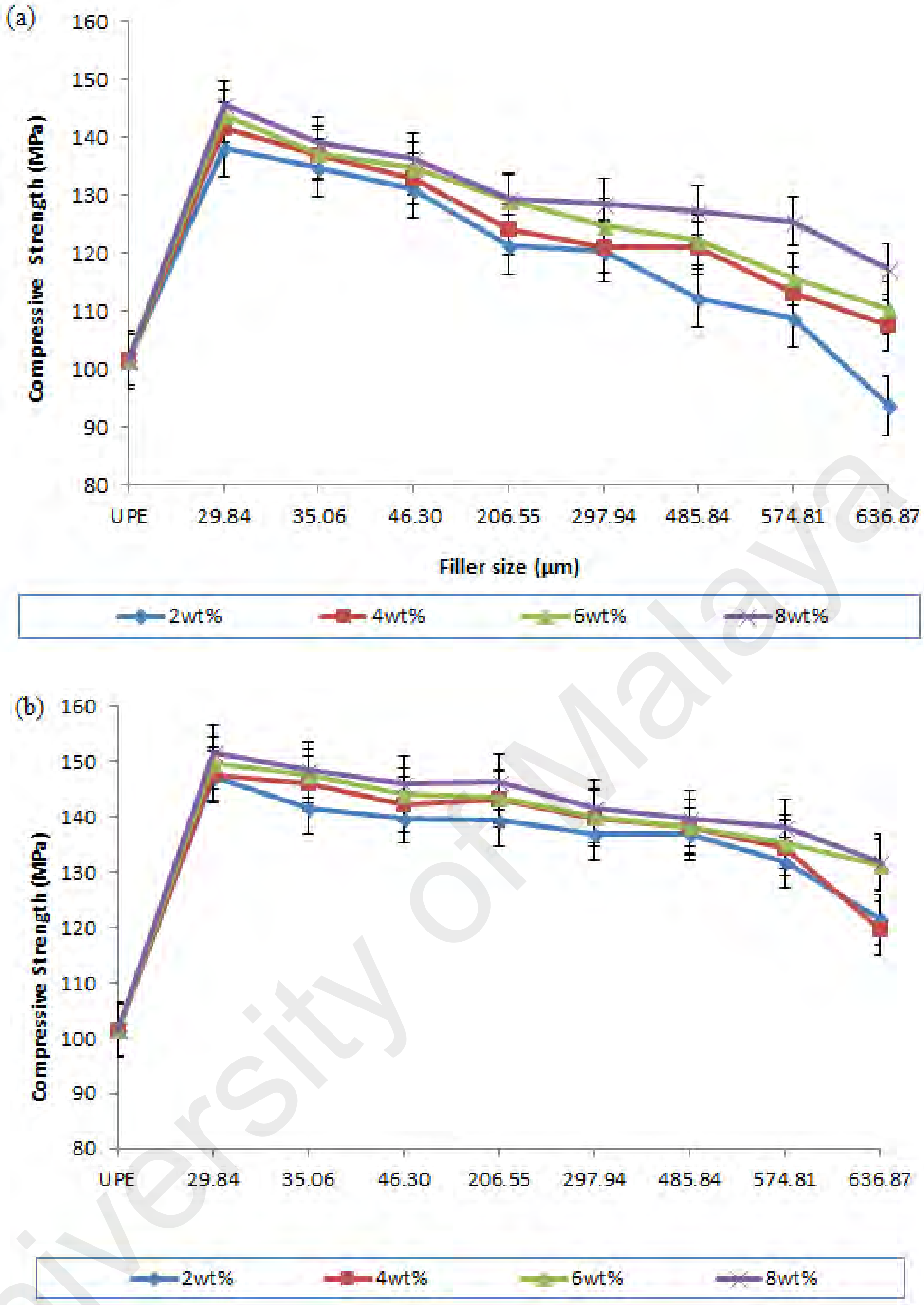

Figure 4.27: Compressive strength of (a) untreated and (b) stearic acid-treated UPE/$CaCO_3$ (aragonite) composites with different sizes and filler contents

As noted previously, a weak interaction is observed between the particles and matrix that leads to particle-matrix debonding when the samples are subjected to tensile loading. Therefore, under tensile loading the tensile strength drops tremendously. This weak interaction between the particles and matrix does not, however cause any drop in compressive strength. This is because the debonded particle-matrix interface is still able to transfer compressive normal traction through the particle-matrix contact compared to tensile loading. Cracks between the particles and matrix, as well as voids due to the presence of air bubbles trapped in the matrix do not have such a significant role in compression testing because the applied stresses tend to close rather to open them. Although interface failure occurs due to load-induced movement of $CaCO_3$ particles through the matrix, void enlargement is limited since the force tends to close the voids. As a result, the compressive strength values are higher than tensile strength. In addition, compared to tensile strength, which is influenced by material flaws more, the compressive strength appears to be influenced by the polymer characteristics more. UPE resin with high compressive strength will produce better composites as it contains rigid $CaCO_3$ filler dispersed in the UPE resin.

Treating aragonite $CaCO_3$ with 1 wt% stearic acid yields a positive effect on the compressive strength of the composites. At the same filler content and filler size, the compressive strength of treated filler is higher than untreated particle-filled UPE composites. For example, at 8 wt% of 29.84 μm aragonite $CaCO_3$ filler, the compressive strength is 145.56 MPa and 151.55 MPa for untreated and stearic acid-treated filler, respectively. Better filler dispersion is a key factor contributing to this enhancement. Homogeneous filler distribution in the polymer matrix reduces the distance between the fillers, thus resulting in higher effectiveness of composite strengthening. Modifying the $CaCO_3$ particles' surface with stearic acid may enhance the compressive strength by reducing the surface energy of the particles. As a result, the agglomerate size is reduced after treatment, as shown in Figure 4.28. Table shows the compressive strength values of all samples of untreated and 1 wt% stearic acid-treated UPE/$CaCO_3$ composites with different filler sizes and filler loadings.

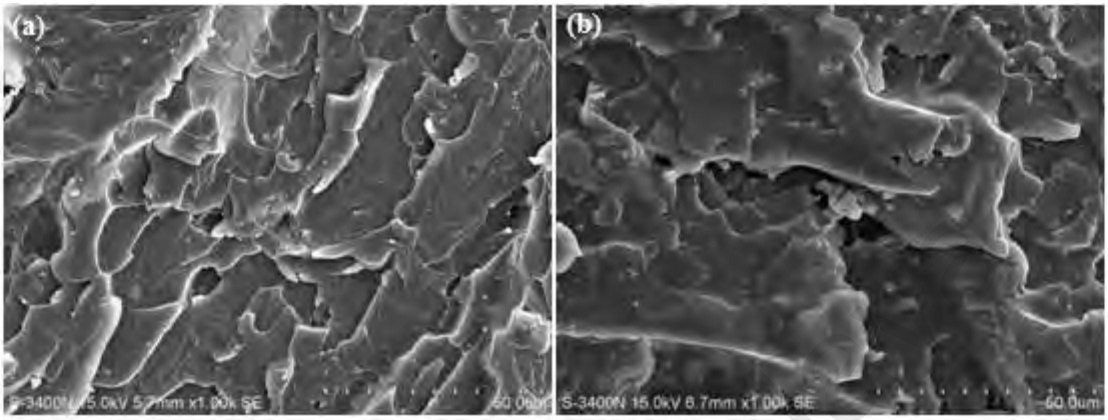

Figure 4.28: SEM images of 8 wt% filler loading in unsaturated polyester (UPE) resin with 46.30 µm filler size for (a) filler agglomerate in untreated sample and (b) filler agglomerate in stearic acid-treated sample

Table 4.9: Compressive strength of untreated and stearic acid-treated UPE/$CaCO_3$ (aragonite) with different sizes and filler loadings

Compressive strength of untreated UPE/$CaCO_3$ (MPa) ± Standard error (MPa)								
Size (µm) Weight fraction (wt%)	**29.84**	**35.06**	**46.30**	**206.55**	**297.94**	**485.84**	**574.81**	**636.87**
2	138.13 ±1.80	134.78 ±2.17	131.08 ±2.34	121.36 ±2.00	120.18 ±3.05	112.23 ±3.17	108.81 ±2.90	93.62 ±1.60
4	141.53 ±1.60	136.87 ±2.44	132.83 ±1.36	124.14 ±2.09	121.08 ±3.97	120.87 ±3.13	113.19 ±2.26	107.58 ±3.63
6	143.62 ±1.58	137.29 ±1.95	134.55 ±1.99	128.97 ±2.33	124.80 ±2.55	122.22 ±1.75	115.55 ±2.49	110.37 ±2.48
8	145.56 ±2.23	139.19 ±2.16	136.21 ±1.37	129.49 ±2.26	128.55 ±1.88	127.32 ±2.05	125.48 ±1.95	117.23 ±2.85
Compressive strength of stearic acid-treated UPE/$CaCO_3$ (MPa) ± Standard error (MPa)								
2	147.33 ±1.45	141.47 ±2.55	139.86 ±3.92	139.27 ±1.94	136.93 ±1.55	136.91 ±1.56	131.76 ±3.43	121.50 ±4.11
4	147.64 ±3.02	146.09 ±1.85	142.14 ±0.88	143.11 ±1.22	139.76 ±2.31	138.18 ±1.63	134.42 ±1.23	119.83 ±1.53
6	149.74 ±1.09	147.52 ±2.22	144.05 ±0.74	143.64 ±1.57	140.13 ±1.12	138.23 ±0.84	135.44 ±3.58	131.32 ±2.23
8	151.55 ±2.73	148.63 ±2.36	146.13 ±1.07	146.16 ±1.85	141.48 ±1.93	139.82 ±2.50	138.13 ±1.61	131.88 ±4.35

Compressive strength of neat unsaturated polyester (UPE) resin: 101.56±1.72 MPa

4.3.4 Hardness

Hardness is a measure of how resistant the sample is to various kinds of permanent shape changes when a constant compressive force is applied. The average values from ten readings of the pure UPE resin and the UPE/$CaCO_3$ (aragonite) composites' surface hardness are shown in Figure 4.29. Originally, the unfilled UPE resin surface has a surface hardness of 206.46 MPa. Adding 2 wt% of 636.87 μm untreated $CaCO_3$ filler reduces the surface hardness. The small increment is attained as the filler size decreases and the filler content increases. Further enhancement in the filler for all sizes does not leave any significant effect on hardness, except for 8 wt% 29.84 μm mean particle size filler. It is suspected that adding more $CaCO_3$ filler to the UPE resin may retard the chemical reaction, thus contributing to an incomplete curing process of the composites (Lam et al., 2005). The maximum hardness value is achieved at 8 wt% filler content with the finest filler size of 29.84 μm.

For filler treated with stearic acid, adding more filler does not help increment the surface hardness compared to unfilled UPE resin except for the 29.84 μm filler size. The optimum hardness is obtained at 6 wt%. The "softening" effect from chemical treatment and also the incomplete curing process might be the biggest factors contributing to the deduction in the surface hardness of stearic acid-treated UPE/$CaCO_3$ composites (Lam et al., 2005). The "softening" effect is very obvious at the sample's surface, which results in low surface hardness of the stearic acid-treated sample. Adding stearic acid-treated $CaCO_3$ particles requires a longer time for solidification because $CaCO_3$ particles might retard the chemical reaction, results in the complete solidification process takes longer time (Lam et al., 2005). The treated samples' surface is relatively soft compared to untreated samples. Even if the load applied is compressive loading, the "softening" effect is more dominant in surface hardness than compressive strength. This is due to the fact that the material indented in the hardness test is constrained by the surrounding matrix, whereas the compressed material does not experience such hydrostatic component.

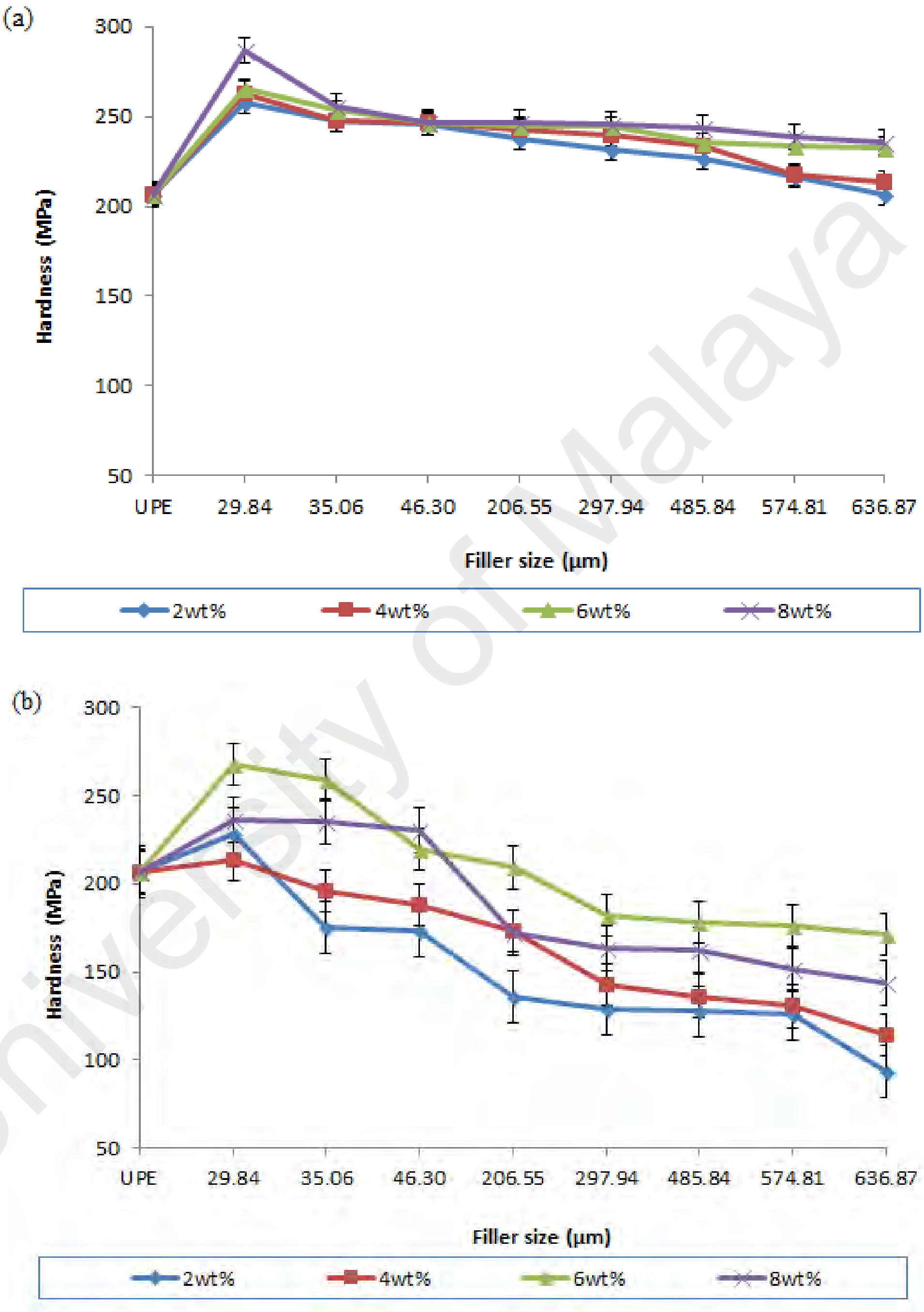

Figure 4.29: Vickers hardness of (a) untreated and (b) stearic acid-treated UPE/$CaCO_3$ (aragonite) composites with different sizes and filler contents

For all composite samples, when an indenter penetratesa sample, the slip bands could nucleate easily and extend to a large area. This results in “pile-up” morphology at the indented surface, as shown in Figure 4.30. The indentation shape is not square $(d_1 \neq d_2)$ because the edge is not a straight line, but it is bend at the center (Lau et al., 2003). Table 4.10 shows the average values of ten hardness readings for untreated and stearic acid-treated UPE/CaCO3 (aragonite) composites with different filler loadings and filler sizes.

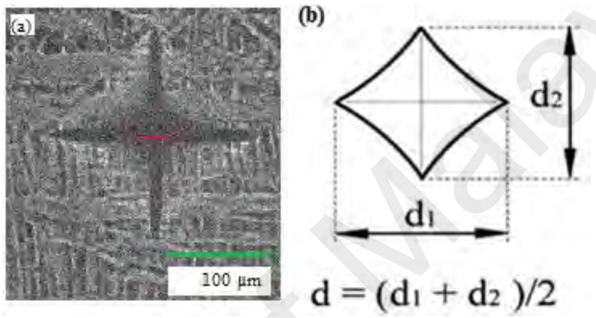

Figure 4.30: “Pile-up” morphology in the indented area of UPE/$CaCO_3$ composites (a) in current study and (b) as sketched by Lau et al. (2003)

Table 4.10: Surface hardness of UPE/$CaCO_3$ (aragonite) with different sizes and filler loadings

Surface hardness of untreated UPE/CaCO3 (MPa) ± Standard error (MPa)								
Size (µm) Weight fraction (wt%)	**29.84**	**35.06**	**46.30**	**206.55**	**297.94**	**485.84**	**574.81**	**636.87**
2	257.33 ±5.21	247.52 ±1.75	245.39 ±3.21	237.82 ±1.99	231.35 ±1.62	226.66 ±2.80	216.65 ±1.87	206.60 ±4.11
4	263.16 ±3.09	248.13 ±4.52	246.24 ±1.48	242.52 1.46	239.76 ±2.50	234.11 ±3.35	217.28 ±2.26	213.79 ±1.96
6	265.37 ±3.71	253.42 ±3.06	246.76 ±1.88	244.49 ±2.01	244.20 ±3.34	235.67 ±1.39	233.80 ±2.85	233.08 ±3.32
8	286.94 ±5.83	255.26 ±3.12	246.85 ±1.96	246.65 ±2.23	245.57 ±1.80	244.01 ±2.37	238.59 ±3.00	235.38 ±5.67
Surface hardness of stearic acid-treated UPE/CaCO3 (MPa) ± Standard error (MPa)								
2	228.34 ±5.86	175.34 ±1.56	173.10 ±2.38	135.66 ±1.64	128.70 ±1.40	127.50 ±0.88	125.53 ±0.64	93.14 ±0.98
4	213.80 ±2.35	195.85 ±0.55	187.89 ±0.98	173.19 ±2.18	142.74 ±1.38	135.94 ±1.24	130.64 ±3.27	114.18 ±1.13
6	267.75 ±3.76	258.90 ±6.36	219.66 ±4.82	209.17 ±1.16	181.93 ±1.96	178.46 ±1.78	176.28 ±0.94	170.90 ±1.29
8	236.34 ±4.78	235.10 ±5.34	230.25 ±4.11	172.42 ±1.07	163.38 ±2.04	162.55 ±2.11	151.04 ±1.14	143.52 ±1.66

Surface hardness of neat unsaturated polyester (UPE) resin: 206.46±2.57 MPa

4.3.5 Tabor’s relation

Figure 4.31 shows the correlation between the compressive strength and hardness, which is also called the Tabor number, of different sizes of $CaCO_3$ particle extracted from *Polymesoda bengalensis* clam shell filled with UPE matrix composites. Originally, according to Tabor’s relation, the hardness value for homogeneous materials is about three times larger than their yield stress. This indicates that the hardness value must be approximately three times greater to initiate yield in tensile loading. However, the results show that Tabor’s relations for all samples are less than 3, which contradict this Tabor’s relation. Similar results were also obtained by other authors for high density polyethylene (HDPE) (Henderson & Wallace, 1989) and some work-hardened materials (Zhang et al., 2011a). According to Zhang et al. (2011a), this discrepancy may be due to the greater complex deformation process in polymer matrix composites compared to metal. The value of Tabor’s number describes the pressure employed in the hardness test to start yielding in tension or compression loading, depending on the type of loading applied. For all samples, the plastic deformation produced by micro hardness indentation is in the form of “pile-up” morphology, as shown in Figure 4.30. This morphology forms due to the decrease in the ductility that occurred because of the limitation with nucleation and movement of dislocations.

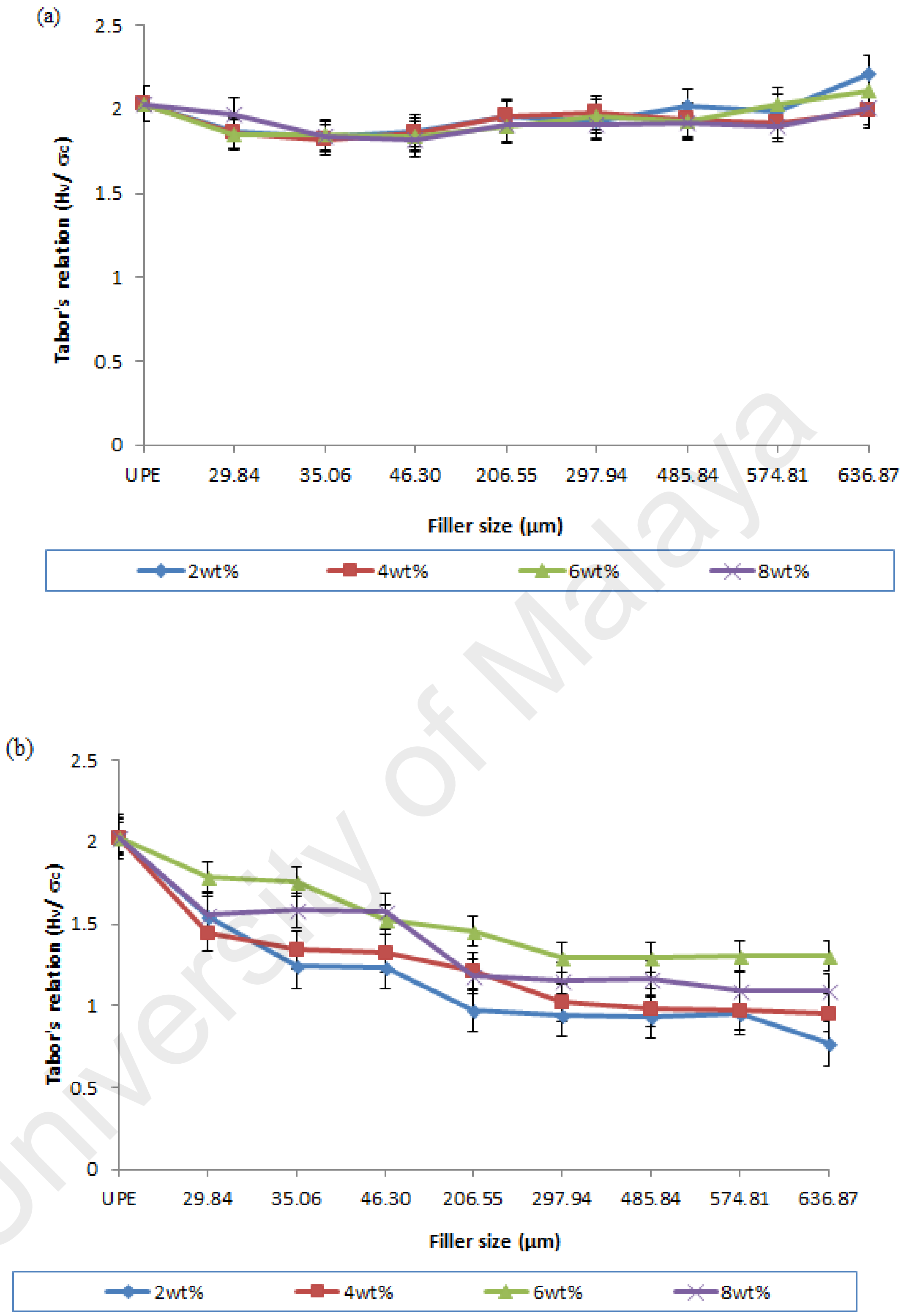

Figure 4.31: Tabor's relation (H_v/σ_c) of (a) untreated and (b) stearic acid-treated UPE/$CaCO_3$ (aragonite) composites with different sizes and filler contents

The results reveal that the pressure is higher in the ranges of 1.81-2.21 and 0.77-1.79 times to start yielding in compression loading for untreated and stearic acid-treated samples, respectively. Therefore, it can be concluded that aragonite $CaCO_3$ modified with stearic acid might soften the composites' surface, hence reducing the pressure for plastic indentation more than unfilled UPE resin. Table 4.11 presents the values of Tabor's relation for untreated and 1 wt% stearic acid-treated UPE/$CaCO_3$ composites with different filler sizes and filler loadings.

Table 4.11: Hardness and compressive strength correlation (Tabor's relation) of UPE/$CaCO_3$ (aragonite) with different sizes and filler loadings

Tabor's relation (H_v/σ_c) of untreated UPE/$CaCO_3$ composites								
Size (µm) Weight fraction (wt%)	**29.84**	**35.06**	**46.30**	**206.55**	**297.94**	**485.84**	**574.81**	**636.87**
2	1.86	1.84	1.87	1.96	1.92	2.02	1.99	2.21
4	1.86	1.81	1.85	1.95	1.98	1.94	1.92	1.99
6	1.85	1.85	1.83	1.90	1.96	1.93	2.02	2.11
8	1.97	1.83	1.81	1.90	1.91	1.92	1.90	2.01
Tabor's relation of stearic acid-treated UPE/$CaCO_3$ composites								
2	1.55	1.24	1.24	0.97	0.94	0.93	0.95	0.77
4	1.45	1.34	1.32	1.21	1.02	0.98	0.97	0.95
6	1.79	1.76	1.52	1.46	1.30	1.29	1.30	1.30
8	1.56	1.58	1.58	1.18	1.15	1.16	1.09	1.09

Tabor's relation of neat unsaturated polyester (UPE) resin: 2.03

4.3.6 Comparative study with commercial calcium carbonate particle-filled unsaturated polyester (UPE) matrix composites

In this section, the results obtained from the current study are compared with other UPE polymer composites that also contain $CaCO_3$ as a reinforcement as reported in published articles. Since the mechanical property values of neat UPE samples vary among articles, the comparison is done in terms of percentage (%) gain or loss as the fillers were reinforced in the UPE resin. This comparison method has also been used by other researchers, such as Chisholm et al. (2005) and Huda et al. (2006). Data from other research works are compared with the best results from the current study that were obtained with stearic acid-treated $CaCO_3$ filler for 29.84 µm composites. The gain or loss in the composites' modulus and strength are determined with the following equations.

$$Gain\ or\ loss\ of\ modulus = \frac{Composite\ modulus - Neat\ UPE\ modulus}{Neat\ UPE\ modulus} \times 100\% \qquad 4.1$$

$$Gain\ or\ loss\ of\ strength = \frac{Composite\ strength - Neat\ UPE\ strength}{Neat\ UPE\ strength} \times 100\% \qquad 4.2$$

Nano UPE/$CaCO_3$ composites vs Micro UPE/$CaCO_3$ composites

Baskaran et al. (2011) investigated the effect of applying nano-sized $CaCO_3$ particulate-filled UPE on the mechanical properties of composites. The fillers were commercial $CaCO_3$ particles in cubic form. The samples were prepared in a similar way to this study, with filler weight fractions of 1, 3, 5, 7 and 9 wt%. Their results are reported in Table 4.12. Table 4.12 provides the mechanical properties of the calcite nano-UPE/$CaCO_3$ composites reported by Baskaran et al. (2011) and 29.84 µm stearic acid-treated UPE/$CaCO_3$ (aragonite), respectively. A comparison was done according to the percentage gain or loss due to the mechanical property values in terms of the tensile, compressive and flexural strength and modulus of neat UPE resin. The values in Baskaran et al.'s study (Baskaran et al., 2011) are not the same as in the current study. This signifies that including $CaCO_3$ particles either at the micron or nano-scale increases the composites' strength and stiffness. At similar filler sizes, the properties are influenced by the weight ratio of the filler in the UPE resin matrix.

Maximum improvement of 8.6% and 37.0% was observed for calcite $CaCO_3$ at 9 wt% regarding tensile strength and tensile modulus, respectively. However, the more rapid increment occurred as aragonite $CaCO_3$ derived from *Polymesoda bengalensis* shell was infused into the UPE resin. At 8 wt%, maximum improvement of 110.7% and 30.1% was attained for tensile strength and tensile modulus, respectively. Micron-sized aragonite $CaCO_3$ had better tensile strength than nano-sized calcite $CaCO_3$. These results are contradictory to reports that the mechanical properties of composites filled with micron-sized filler particles are inferior to those filled with nanoparticles of the same filler (Sumita et al., 1983). In terms of flexural properties, the $CaCO_3$ from *Polymesoda bengalensis* shell again displays a higher gain of flexural modulus by 54.1% at 8 wt%, whereas nano UPE/$CaCO_3$ composites improved by 37.0% at 9 wt% filler content. However, nano UPE/$CaCO_3$ composites exhibited better improvement in terms of flexural strength. The author suggests that the variation may due to the different geometries or shapes of the particles. It is expected that reducing the $CaCO_3$ particles from *Polymesoda bengalensis* shell may lead to great improvement.

Particle shapes with low or high aspect ratio may affect the properties of particulate-filled polymer composites. Anisometric particles with different lengths versus widths are more effective as reinforcement than particles with similar length and width dimensions (isometric particles). Filler with a higher aspect ratio provides a large surface area per volume (Ahmad et al., 2008) and leads to higher stress transferability. Aragonite $CaCO_3$, which has rod-like crystals, has a higher aspect ratio than commercial calcite $CaCO_3$, which is in cubic-like crystals. Therefore, the micron-size UPE/$CaCO_3$ (aragonite) composites in the current study yielded a higher improvement in tensile strength and tensile modulus than the nano-sized calcite UPE/$CaCO_3$ composites reported by Baskaran et al. (2011). Other fillers with lower aspect ratios, such as spherical $CaCO_3$/PP composites (Pukanszky & Vörös, 1993), spherical glass beads/vinyl ester composites (Cho et al., 2006) and spherical silica/epoxy composites exhibit tensile strength loss compared to unfilled resin.

UPE/$CaCO_3$ composites vs Micro UPE/$CaCO_3$ composites

Hanna et al. (2011) investigated the effect of infusing $CaCO_3$ filler in UPE composites. However, filler size is not mentioned. Since only certain data were revealed, other data were estimated by observing the provided curves. It is assumed that Hanna et al. (2011) used nano $CaCO_3$ as filler in the UPE composites because the samples for biomedical applications are normally nano-sized. Table 4.12 shows the superior enhancements gained in terms of tensile modulus, flexural strength and flexural modulus. Applying an electrical vibrator to remove any residual bubbles and guarantee the distribution of the cast inside the mold may be helpful to produce better UPE/$CaCO_3$ composites. Since there are no morphological observations on the sample before and after the tests, it cannot be concluded that this method contributes to the enhancement of mechanical properties.

Table 4.12: Comparison of mechanical properties between untreated UPE/$CaCO_3$ and stearic acid-treated UPE/$CaCO_3$ composites with nano-UPE/$CaCO_3$

Sample		**Nano UPE/$CaCO_3$ (Baskaran et al., 2011)**						**UPE/$CaCO_3$ the filler size was not mentioned) (Hanna et al., 2011)**						**Stearic acid-treated UPE/$CaCO_3$ composites (8 wt% of 29.84 µm mean diameter size filler)**				
Filler fraction (wt%)		**0**	**1**	**3**	**5**	**7**	**9**	**0**	**3**	**6**	**9**	**12**	**15**	**0**	**2**	**4**	**6**	**8**
Tensile properties	Tensile strength (MPa)	58	62	67	70	66	63	37.47	57.68	*51.00	*49.80	*50.50	*48.00	17.81	24.31	28.02	31.79	37.53
	Gain or loss strength [%]	-	+6.9	+15.5	+20.7	+13.8	+8.6	-	+53.9	+36.1	+32.9	+34.8	+28.1	-	+36.5	+57.3	+78.5	+110.7
	Tensile modulus GPa)	2.7	2.8	3.0	3.2	3.35	3.7	2.401	*4.900	*4.780	*4.950	*5.100	5.71	1.578	1.794	1.870	2.029	2.053
	Gain/loss modulus [%]	-	+3.7	+11.1	+18.5	+24.1	+37.0	-	+104.1	+99.1	+106.2	+112.4	+137.8	-	+13.7	+18.5	+28.6	+30.1
Flexural properties	Flexural strength (MPa)	98	101	104	107	105	103	34.19	*84.00	90.00*	*92.00	94.00*	97.86	113.80	110.43	116.42	117.30	122.42
	Gain/loss strength [%]	-	+3.1	+6.1	+9.2	+7.1	+5.1	-	+145.7	+163.2	+169.1	+174.9	+186.2	-	-3.0	+2.3	+3.1	+7.6
	Flexural modulus GPa)	2.7	2.8	3.0	3.2	3.4	3.7	2.57	*3.90	*3.50	*3.60	*3.80	4.89	3.16	3.95	4.67	4.87	4.87
	Gain/loss modulus [%]	-	+3.7	+11.1	+18.5	+25.9	+37.0	-	+51.8	+36.2	+40.1	+47.9	+90.3	-	+25.0	+47.8	+54.1	+54.1
Compression properties	Compressive strength (MPa)	-	-	-	-	-	-	100.36	*123.50	*124.00	124.10	*112.00	*111.00	101.56	147.33	147.64	149.74	151.55
	Gain/loss strength [%]	-	-	-	-	-	-	-	+23.1	+23.6	+23.7	+11.6	+10.7	-	+45.1	+45.4	+47.4	+49.2
Fabrication process	Stirring	2000 rpm for 45 minutes Ultrasonication for 6 hours						20 minutes Electrical vibrator						500 rpm for 5 minutes Ultrasonication for 15 minutes				
	Curing agent	Methyl ethyl ketone peroxide and cobalt naphthenate						Name of accelerator and hardener were not mentioned.						Methyl ethyl ketone peroxide				
	Curing process	Curing for 24 hours at room temperature followed by post-curing at 70 °C for 3 hours.						Curing for 24 hours at room temperature followed by post-curing over night at 45 °C.						Curing for 24 hours at room temperature followed by post-curing at 70 °C for 3 hours.				

*Estimated value taken from the graph or curve

4.4 Thermophysical properties

4.4.1 Density of the composites

Incorporating micron-sized $CaCO_3$ into the UPE matrix affects its density (Figure 4.32). The theoretical density values for unfilled and particulate-filled $CaCO_3$ unsaturated polyester composites are calculated using the rules for mixtures stated in equation 3.4. The data for both theoretical and measured density values and void fractions are presented in Table 4.13

Figure 4.32 demonstrates that the theoretical density values are generally higher than experimentally measured density values. For example, the theoretical density of unfilled UPE is 1.220 gcm^{-3} (Tae & Choi, 2012), whereas the experimental density is 1.208 gcm^{-3}, or approximately 1% less than the theoretical value. Infusing 2 wt% $CaCO_3$ particles with 29.84 μm size increases the matrix density to $1.221\,gcm^{-3}$and $1.225\,gcm^{-3}$ for untreated and stearic acid-treated composites, respectively. Any further addition, however, decreases the composites' density, which is contradictory to the rules for mixtures. This trend is similar for nano $CaCO_3$-filled unsaturated polyester (Baskaran et al., 2011), and silica carbide (SiC)-filled short glass fiber in unsaturated isophthalic polyester resin (Kaundal et al., 2012). Cao et al. (2016) found that treating $CaCO_3$ particles by stearic acid reduce the number of voids thus, results in more tightly packed composites than other methods. The composite reduction with the addition of filler is due to void formation or air entrapment in the UPE matrix during mechanical stirring. Solid particles produce macroscopic stress in the liquid resin, resulting in the formation of air bubbles (Uddin, 2009). Therefore, adding more filler creates more voids in the matrix, making it more difficult to escape from the UPE matrix. The unreleased air then remains in the liquid resin and forms voids in the cured polymer matrix.

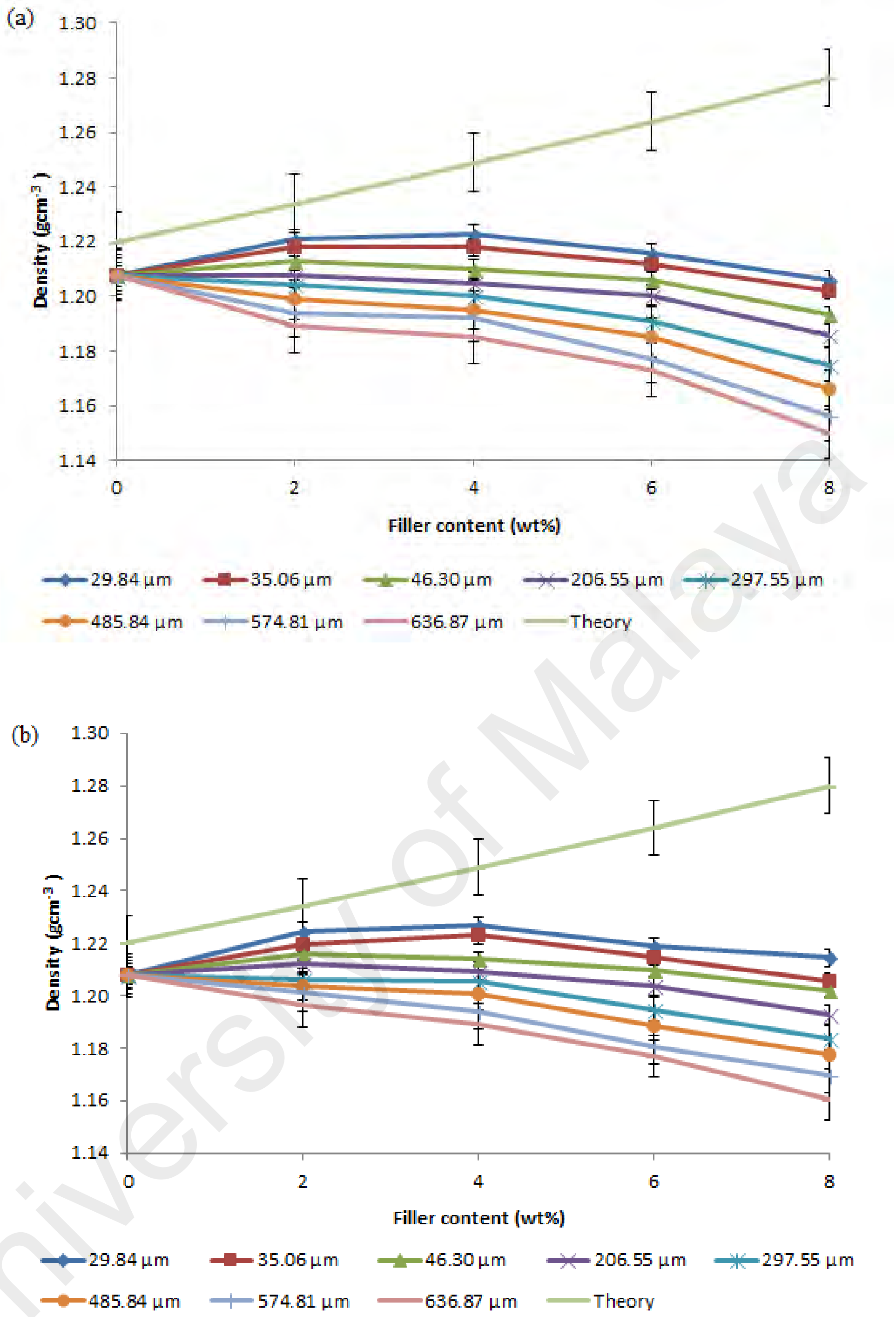

Figure 4.32: Effect of different filler sizes and filler contents of (a) untreated and (b) stearic acid-treated $CaCO_3$ on the density of UPE.

Adding more filler also encourages the formation of agglomerate. The agglomeration of particles at higher loading leads to the formation of voids in the matrix. Consequently, at similar filler sizes, the void fraction in the composites increases with filler content. The results also signify that at similar filler loadings, the void fraction increases with bigger filler size. The same result was reported by Collings (2006), that with increasing particle size, the size of the cavity generated increases as well. Thus, adding coarse filler might increase the void fraction in the composites and result in density reduction.

The theoretical and experimentally measured density values of neat UPE resin, untreated and stearic acid-treated $CaCO_3$-filled UPE composites, and the measured void fractions are presented in Table 4.13. Treating $CaCO_3$ particles with 1 wt% stearic acid produces a higher density than untreated filler. A lower void fraction is measured as treated particles are introduced in the UPE resin compared to untreated filler with similar filler sizes and loadings. Treating the filler with stearic acid leads to a significant decrease in surface tension, which results in decreased interaction between the filler and matrix (Kiss et al., 2007). Reduced surface tension limits the clustering of the filler and finally retards the formation of voids. According to the results, the maximum voids are 10.2% at 8 wt% untreated $CaCO_3$ with 636.87 μm mean diameter size. The void content in the current study is lower than in Kaundal et al. (2012) work, where 19% of voids were found in 10 wt% SiC-glass fiber polyester composites. As the filler size decreased to 29.84 μm, the void content was reduced to 5.8% and 5.2% for untreated and stearic acid-treated composites, respectively. It is expected that by reducing the filler size to the nano-scale, the void content would decrease. This was reported by Baskaran et al. (2011) who found that the void content was 5.8% at 9 wt% nano-$CaCO_3$-filled UPE resin.

Table 4.13: Theoretical and experimental densities and void fractions of untreated and stearic acid-treated UPE/$CaCO_3$ (aragonite) composites with different sizes and filler loadings

Density of untreated UPE/$CaCO_3$ composites(gcm^{-3})									
Size (µm) Weight fraction (wt%)	**Theoretical values**	**Experimental Values**							
		29.84	**35.06**	**46.30**	**206.55**	**297.94**	**485.84**	**574.81**	**636.87**
0	1220	1208	1208	1208	1208	1208	1208	1208	1208
2	1234	1221	1218	1213	1208	1204	1199	1194	1189
4	1249	1223	1218	1210	1205	1200	1195	1192	1185
6	1264	1216	1212	1206	1200	1191	1185	1177	1173
8	1280	1206	1202	1193	1186	1175	1166	1156	1150
Void fraction (%)									
0	-	1.0	1.0	1.0	1.0	1.0	1.0	1.0	1.0
2	-	1.1	1.3	1.7	2.1	2.4	2.8	3.2	3.6
4	-	2.1	2.5	3.1	3.5	3.9	4.3	4.6	5.1
6	-	3.8	4.1	4.6	5.1	5.8	6.3	6.9	7.2
8	-	5.8	6.1	6.8	7.3	8.2	8.9	9.7	10.2
Density of stearic acid-treated UPE/$CaCO_3$ composites (gcm^{-3})									
Size (µm) Weight fraction (wt%)	**Theoretical values**	**Experimental Values**							
		29.84	**35.06**	**46.30**	**206.55**	**297.94**	**485.84**	**574.81**	**636.87**
0	1220	1208	1208	1208	1208	1208	1208	1208	1208
2	1234	1225	1220	1216	1212	1206	1204	1201	1196
4	1249	1227	1223	1214	1209	1205	1200	1194	1189
6	1264	1219	1215	1210	1204	1195	1188	1181	1177
8	1280	1214	1206	1202	1193	1184	1177	1170	1161
Void fraction (%)									
0	-	1.0	1.0	1.0	1.0	1.0	1.0	1.0	1.0
2	-	0.7	1.1	1.5	1.8	2.3	2.4	2.7	3.1
4	-	1.8	2.1	2.8	3.2	3.5	3.9	4.4	4.8
6	-	3.6	3.9	4.3	4.7	5.5	6.0	6.6	6.9
8	-	5.2	5.8	6.1	6.8	7.5	8	8.6	9.3

4.4.2 Differential Scanning Calorimetry (DSC)

DSC measurements were performed to characterize the thermal behavior of neat UPE, untreated and stearic acid-treated UPE/$CaCO_3$ composites. The various thermal characteristics, such as decomposition temperature (T_d), heat of reaction (ΔH_R) and degree of crystallinity(X_c) of the UPE and UPE/$CaCO_3$ composites were determined.

Figure 4.33 displays a thermogram showing the thermal behavior of neat UPE and untreated $CaCO_3$ from *Polymesoda bengalensis* shell filled in UPE resin. An endothermic peak was observed during the temperature scan for each specimen. An endothermic peak or negative peak corresponds to heat absorption during the process. The enthalpy of the heat of reaction (ΔH_R) process is given by the area under the peak and is denoted as “normalized” in the curve, whereas the decomposition temperature (T_d) is denoted by “onset temperature.” Details of the decomposition behavior of untreated $CaCO_3$ recorded by the DSC for different filler sizes (at a constant filler loading of 8 wt%) are given in Figure 4.34. The values of decomposition temperature and enthalpy of neat UPE, and untreated and stearic acid-treated UPE/$CaCO_3$ composites with different filler sizes and 8 wt% filler loading are listed in Table 4.13.

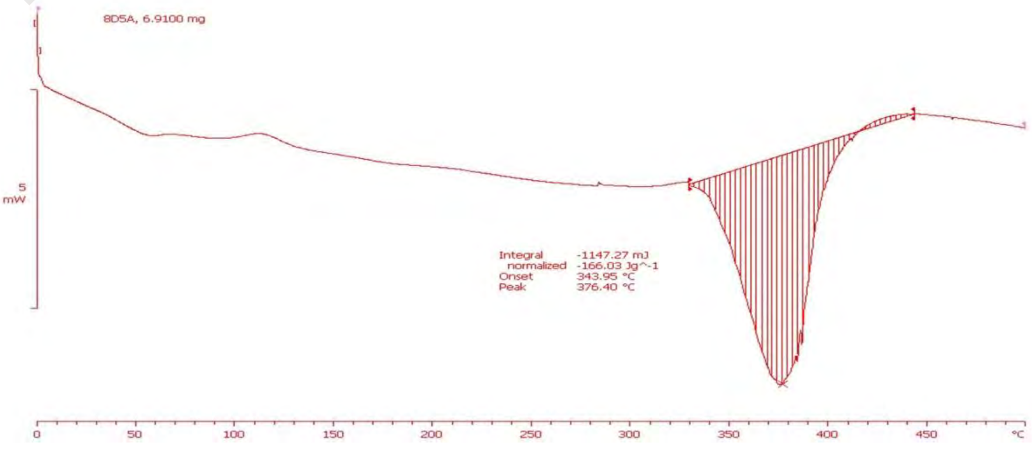

Figure 4.33: DSC thermogram of UPE/$CaCO_3$ (aragonite) composites

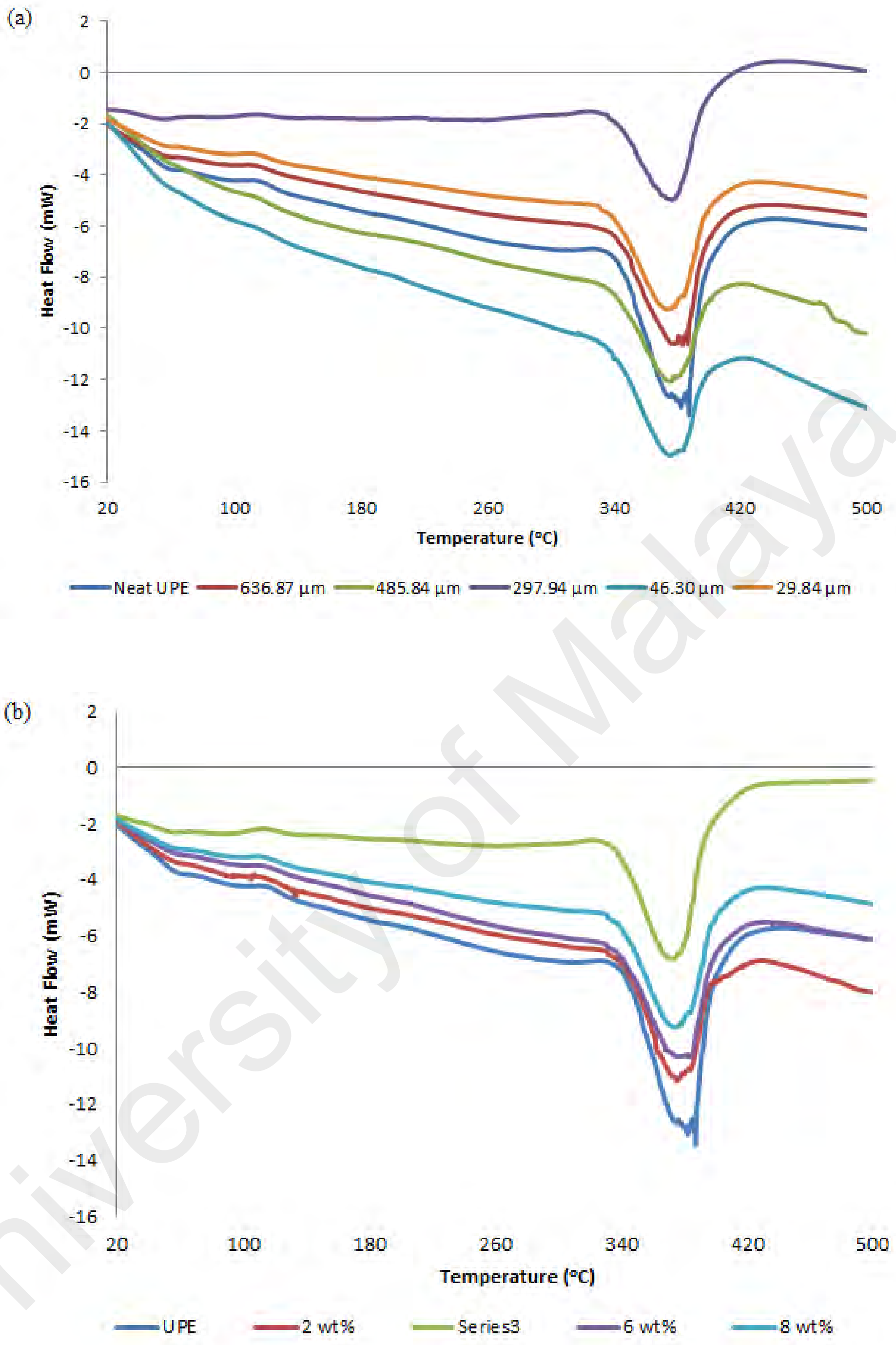

Figure 4.34: DSC curves for decomposition for (a) different sizes (8 wt% filler content) and (b) different filler loadings (with mean diameter size of 29.84 µm) of untreated UPE/$CaCO_3$ composites

The degree of crystallinity, $X_c(\%)$ is an important parameter of crystalline polymers. In this work, the enthalpy, or heat of fusion of the composites was recorded to measure the degree of crystallinity. The degree of crystallinity was calculated by applying equation 3.11 and assuming that the heat of fusion for 100% crystalline polyester resin is 400 J/g (Severini & Gallo, 1985). Figure 4.35 shows the degree of crystallinity for both untreated and stearic acid-treated UPE/$CaCO_3$ composites.

Figure 4.35 (a) presents the degree of crystallinity of various micron-size untreated and stearic acid-treated UPE/$CaCO_3$ (aragonite) composites at 8 wt%. The degree of crystallinity (% crystallinity) of neat UPE is 34.78%. The % crystallinity of both untreated and stearic acid-treated UPE/$CaCO_3$ composites was found to be greater than virgin UPE. Adding 8 wt% coarse filler with 636.87 μm mean diameter increased the % crystallinity to 42.26 and 41.10 for untreated and stearic acid-treated composites, respectively. At the same filler loading, adding finer filler to the polymer composites increased the % crystallinity. Adding 8 wt% with 29.84 μm mean diameter size $CaCO_3$ enhanced the % crystallinity to 51.31 and 47.73 for untreated and stearic acid-treated composites, respectively. Figure 4.35(b) indicates that at the same filler size of 29.84 μm (untreated), the % crystallinity increased with increasing filler content. Adding 2 wt% with 29.84 μm mean diameter size filler increased the degree of crystallinity from 34.78% neat UPE to 42.95%. The degree of crystallinity then continued increasing to 45.12%, 48.01% and 51.31% for 4 wt%, 6 wt% and 8 wt%, respectively. This trend was similar up to 10 wt% $CaCO_3$ in HDPE (Elleithy et al., 2010). Therefore, it can be concluded that the % crystallinity of $CaCO_3$ from *Polymesoda bengalensis* shell particle incorporated into UPE resin increases as the filler size decreases.

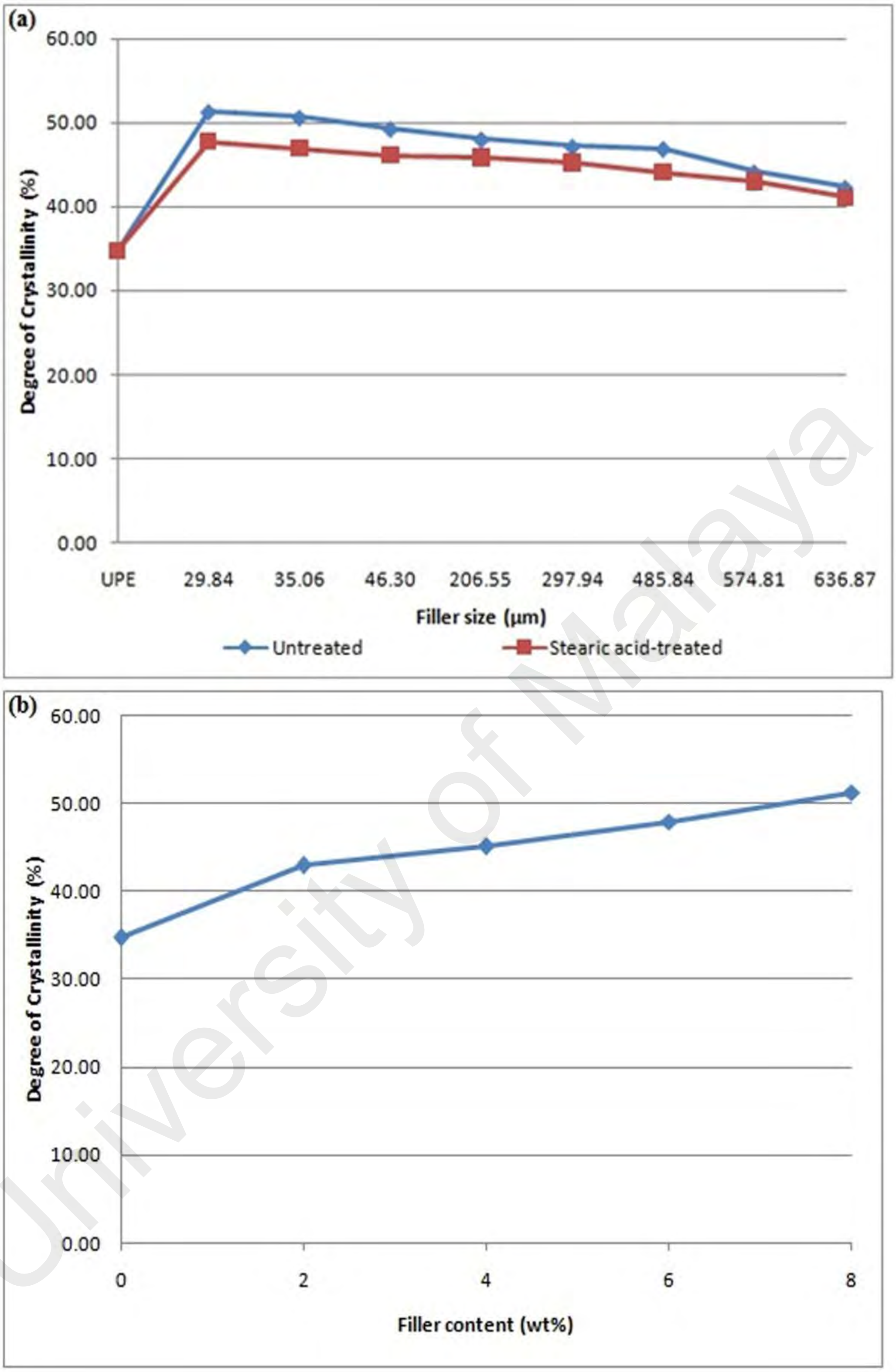

Figure 4.35: Degree of crystallinity of (a) various filler sizes of untreated and stearic acid-treated composites at 8 wt% and (b) various filler contents with 29.84 μm mean diameter of untreated UPE/$CaCO_3$ (aragonite) composites

The result also indicates that $CaCO_3$ acts as a nucleating agent during the crystallization of composites. It is explained by the increasing degree of crystallinity once $CaCO_3$ filler was incorporated into the UPE resin. By comparison, the degree of crystallinity of untreated UPE/$CaCO_3$ composites appeared higher than stearic acid-treated UPE/$CaCO_3$ composites. This is because treating $CaCO_3$ with stearic acid would reduce the surface energy, thus it cannot act as a strong nucleating species (Papirer et al., 1984). This result is similar to what was reported by Deshmukh et al. (2010a), that untreated $CaCO_3$ composites have higher % crystallinity than stearic acid-treated $CaCO_3$ filled-Poly(butylene terephthalate) composites.

Therefore, the presence of and chemical modification of $CaCO_3$ filler seems to affect the degree of crystallinity of UPE. Filler size and content also affect the % crystallinity of the composites. Table 4.14 lists the degree of crystallinity of 8 wt% filler loading of untreated and stearic acid-treated UPE/$CaCO_3$ composites with various micron sizes.

Table 4.14: DSC data of 8 wt% and different sizes of untreated and stearic acid-treated aragonite $CaCO_3$-filled UPE composites

Untreated UPE/$CaCO_3$ composites								
Size (μm)	**29.84**	**35.06**	**46.30**	**206.55**	**297.94**	**485.84**	**574.81**	**636.87**
$T_d(°C)$	338.78	340.14	341.29	344.76	346.77	347.46	343.07	343.07
ΔH_R(J/g)	192.92	186.30	181.29	176.67	173.5	172.53	162.21	155.53
X_c(%)	51.31	50.63	49.26	48.01	47.15	46.88	44.08	42.26
Stearic acid- treated UPE/$CaCO_3$ composites								
Size (μm)	**29.84**	**35.06**	**46.30**	**206.55**	**297.94**	**485.84**	**574.81**	**636.87**
$T_d(°C)$	344.37	341.89	369.52	342.7	340.14	322.54	345.83	347.17
ΔH_R (J/g)	190.90	172.54	169.77	176.11	166.54	162.21	158.07	154.52
X_c(%)	47.73	46.89	46.13	45.86	45.26	44.08	42.95	41.10
Neat UPE								
$T_d(°C)$	343.06							
ΔH_R (J/g)	136.32							
X_c(%)	34.78							

4.4.3 Thermal conductivity

Thermal conductivity is a measure of a material's ability to conduct heat. In this work, the thermal conductivity was measured by a P.A. Hilton H-940 machine. Each data represents the efficient thermal conductivity measured once steady state is achieved or when the temperature change is not greater than $\pm 1°C$. Each data is the average of three readings taken from three different samples.

Figure 4.36 demonstrates the measured effective thermal conductivity of UPE/$CaCO_3$ (aragonite) composites with different filler sizes and filler contents at 2, 4, 6 and 8 wt%. The figure clearly shows that the thermal conductivities of the composites are higher than the pure UPE matrix. The infusion of aragonite $CaCO_3$ from clam shell particle increases the composites' thermal conductivity and a significant enhancement is achieved by untreated filler at the highest filler content with the finest filler size.

Initially, the thermal conductivity of neat UPE resin was 0.222 W/mK. Introducing 2 wt% coarse filler with size of 636.87 μm increased the thermal conductivity of the composite to 0.2856 W/mK. Replacing the same weight fraction with finer filler increased the thermal conductivity, for example to 0.3980 W/mK, 0.4570 W/mK and 0.4747 W/mK as the filler size reduced to 485.84 μm, 297.94 μm and 206.55 μm, respectively. The finest filler with a size of 29.84 μm improved the thermal conductivity 3 times more than coarser filler with a size of 636.87 μm and almost 4 times more than unfilled UPE matrix. The improvement was tremendous at higher filler loading. At 8 wt% filler content, the thermal conductivity achieved by 29.84 μm particulate-filled composites was 1.23 W/mK, or 5.5 times better than the pure UPE matrix compared to only 2 times higher for the coarser filler size of 636.87 μm.

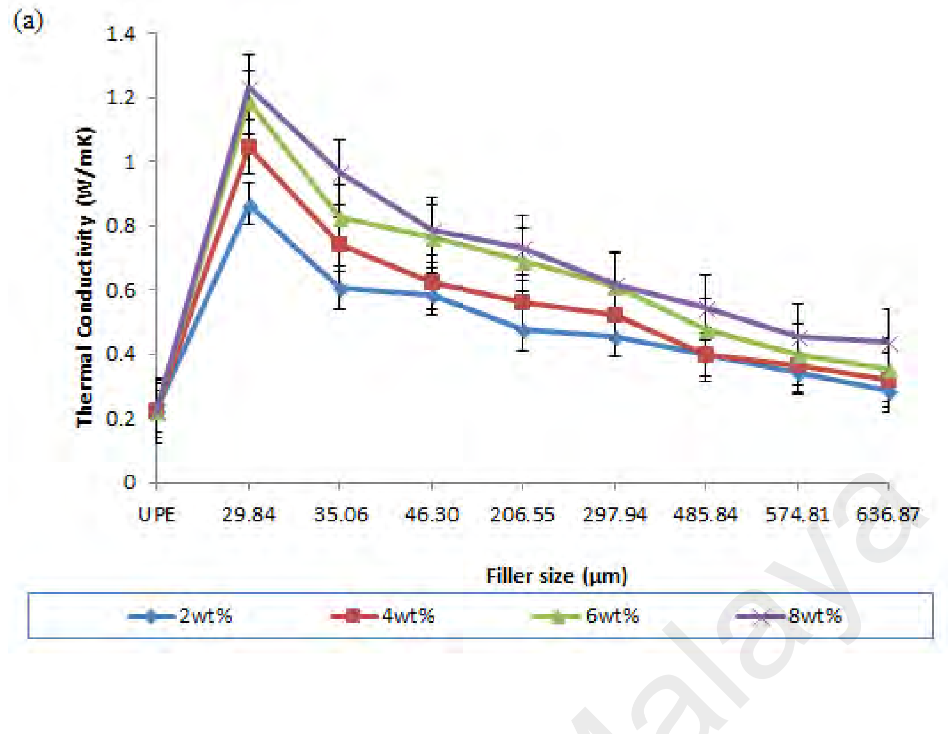

Figure 4.36: Effective thermal conductivity of (a) untreated, and (b) stearic acid-treated UPE/$CaCO_3$ (aragonite) composites of different sizes and filler contents

The efficiency of heat conduction can be improved by reducing the filler size. This may be attributed to the fact that finer particles that have larger interfacial areas tend to come in contact with more resin molecules. With the same filler content, finer filler tends to be well-dispersed and it fulfills the free volume in the matrix phase, providing small distances among the filler, hence improving the filler "bridges" at very low loadings. Better filler dispersion with low average inter-particle distance was observed in finer filler specimens, as shown in Figure 4.37.

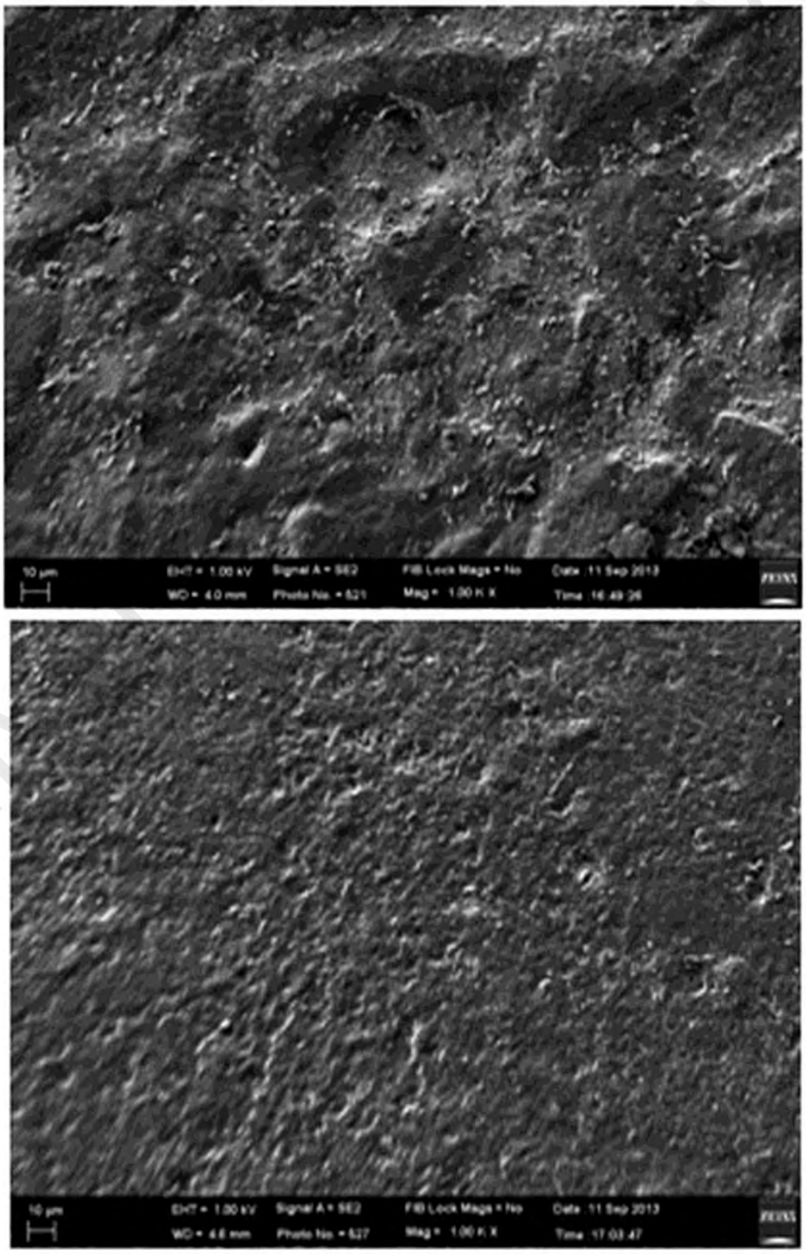

Figure 4.37: Surface morphology by FESEM displaying better filler dispersion in 8 wt% untreated $CaCO_3$ filler with mean particle size of (a) 29.84 µm than (b) 297.94 µm

The effective thermal conductivity of stearic acid-treated UPE/$CaCO_3$ (aragonite) composites, however, is found to be lower than untreated $CaCO_3$, as it is expected that the treated filler is well-dispersed in the polymer matrix. This result is quite similar to what Deshmukh et al. (2010a) reported. Including $CaCO_3$ filler in the polymer increases the % crystallinity more than unfilled polymer matrix, because $CaCO_3$ acts as a nucleating agent during the crystallization of the composites. However, coating the $CaCO_3$ with stearic acid may reduce the surface energy of the particles, hence reducing the performance as a nucleating agent (Deshmukh et al., 2010a; Deshmukh et al., 2010b). As a result, the effective thermal conductivity of stearic acid-treated aragonite $CaCO_3$ filler is lower than untreated UPE/$CaCO_3$ composites.

This result is somewhat interesting for untreated aragonite $CaCO_3$ because as Ebadi-Dehaghani and Nazempour (2012) found, by applying 15 wt% nano-sized $CaCO_3$ to polypropylene (PP), the thermal conductivity improves only up to 64%, which is far less than the 540% improvement in this study. They obtained 0.22 W/mK for neat PP and 0.36 W/mK for 15 wt% nano $CaCO_3$. According to King et al. (2008), composites with thermal conductivity ranging from 1 to 30 W/mK can be applied as heat sinks in electrical or electronic systems. Therefore, higher filler loading, which is normally more than 30 vol%, was applied to achieve the required level of thermal conductivity. Rather than using high filler content to achieve the required level, only 8 wt% filler content of micron-sized $CaCO_3$ was infused into the UPE polymer matrix in this study. The results from this study may be valuable, because infusing high filler content could increase the heat conductivity; nonetheless, at the same time it contributes to processing problems, such as the possibility of extrusion and injection molding, and the likelihood of altering the mechanical behavior and density (King et al., 2008).

The thermal conductivity of particulate-filled polymer composites is also influenced by the particulate shape (Chiang et al., 2005; Tekce et al., 2007). Basically, the higher the aspect ratio of the filler, the better the polymer composites can conduct heat. This is because higher aspect ratio filler can easily build filler “bridges” in the polymer matrix. Good filler interconnection then produces better thermal conductivity. Figure 4.38 illustrates that at low filler loading better filler interconnections are produced by higher aspect ratio particles. This may be the reason why aragonite $CaCO_3$ filler applied in this current study yields higher thermal conductivity than commercial $CaCO_3$ filler even with coarser filler size. Table 4.15 represents the average effective thermal conductivity values of untreated and 1 wt% stearic acid-treated UPE/$CaCO_3$ composites with different filler sizes and filler loadings.

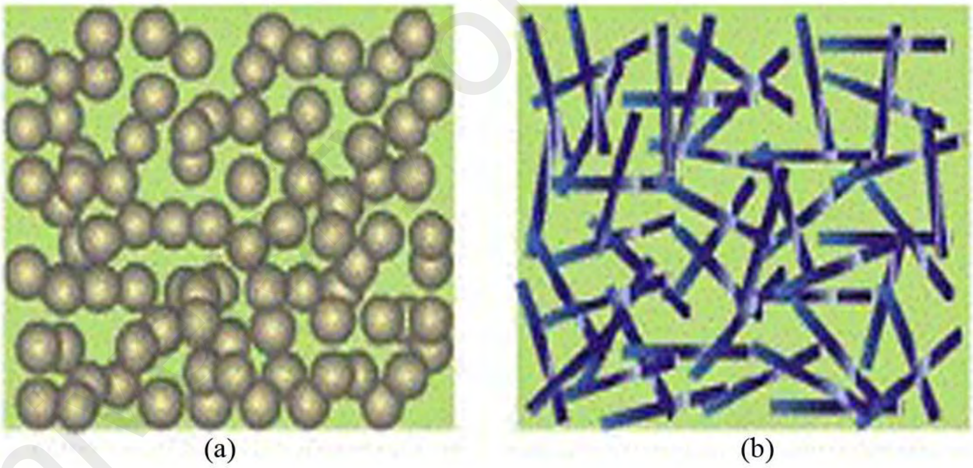

Figure 4.38: Schematic illustrations ofbetter filler interconnections produced by higher aspect ratio particles (fiber/wire) than spherical fillers
(Chiang et al., 2005)

Table 4.15: Effective thermal conductivity of untreated and stearic acid-treated $CaCO_3$-filled unsaturated polyester (UPE) with different sizes and filler loadings

Effective thermal conductivity of untreated UPE/$CaCO_3$ composites (W/mK) ± Standard error (W/mK)								
Size (µm) Weight fraction (wt%)	**29.84**	**35.06**	**46.30**	**206.55**	**297.94**	**485.84**	**574.81**	**636.87**
2	0.8673 ±0.0007	0.6062 ±0.0003	0.5854 ±0.0002	0.4747 ±0.0004	0.4570 ±0.0006	0.3980 ±0.0005	0.3410 ±0.0001	0.2856 ±0.0004
4	1.0470 ±0.0002	0.7400 ±0.0005	0.6240 ±0.0003	0.5623 ±0.0004	0.5245 ±0.0003	0.3960 ±0.0003	0.3636 ±0.0002	0.3180 ±0.0006
6	1.1845 ±0.0003	0.8277 ±0.0003	0.7658 ±0.0004	0.6930 ±0.0003	0.6130 ±0.0006	0.4767 ±0.0003	0.3987 ±0.0003	0.3515 ±0.0005
8	1.2300 ±0.0004	0.9656 ±0.0003	0.7850 ±0.0003	0.7280 ±0.0005	0.6182 ±0.0001	0.5450 ±0.0001	0.4561 ±0.0004	0.4386 ±0.0002
Effective thermal conductivity of stearic acid-treated UPE/$CaCO_3$ composites(W/mK) ± Standard error (W/mK)								
2	0.5468 ±0.0001	0.4695 ±0.0001	0.4402 ±0.0002	0.3974 ±0.0002	0.3852 ±0.0001	0.3275 ±0.0001	0.3029 ±0.0001	0.2775 ±0.0001
4	0.5838 ±0.0003	0.4695 ±0.0002	0.4403± 0.0002	0.4118 ±0.0001	0.3867 ±0.0002	0.3481 ±0.0002	0.3216 ±0.0001	0.3198 ±0.0002
6	0.6595 ±0.0002	0.5246 ±0.0001	0.4893 ±0.0001	0.4880 ±0.0002	0.4351 ±0.0001	0.4099 ±0.0001	0.4095 ±0.0002	0.3823 ±0.0002
8	0.6651 ±0.0004	0.5593± 0.0001	0.5185 ±0.0001	0.5150 ±0.0002	0.4809 ±0.0005	0.4711 ±0.0001	0.4689 ±0.0001	0.4279 ±0.0001

Effective thermal conductivity of neat UPE: 0.2220 (W/mK) ±0.0001W/mK

4.4.4 Specific heat capacity

Specific heat capacity is the amount of heat required for 1 kg of material to increase by 1°C. In this work, the enthalpy, or heat of fusion of the composites was measured by DSC. The test was performed at a heating rate of 10°C/min ata temperature range of 20-500°C in nitrogen atmosphere. The samples' heat capacity values were taken at 23°C by applying equation 3.10. Figure 4.39 shows the specific heat capacity of UPE/$CaCO_3$ (aragonite) composite samples with different filler sizes and filler contents.

Figure 4.39(a) indicates that the specific heat of untreated and stearic acid-treated $CaCO_3$ at 23°C with various micron-sizes of UPE/$CaCO_3$ (aragonite) composites at 8 wt% filler content. The specific heat of the UPE/$CaCO_3$ composites is lower than that of neat UPE. However, at similar filler content (8 wt%), the specific heat is higher for the coarser particles compared to finer particles filled in UPE resin. The neat UPE measured in this study has a specific heat content of 1.87 J/g°C, which is a similar value to that reported by Bastiurea et al. (2014). Adding 8 wt% of micron-sized $CaCO_3$ reduces the specific heat content of any filler size. For untreated $CaCO_3$ filler, the maximum specific heat found is 1.74 J/g°C at mean diameters of 574.81 µm and 636.87 µm, whereas the minimum value is 1.34 J/g°C for 29.84 µm mean diameter filler size. This shows that filler size influences the specific heat of particulate-filled polymer composites.

Besides, untreated UPE/$CaCO_3$ composites always exhibit higher specific heat than stearic acid-treated UPE/$CaCO_3$ composites. For example, for UPE/$CaCO_3$ composites with 636.87µm mean diameter, the specific heat is 1.74 J/g°C and 1.05 J/g°C for untreated and stearic acid-treated composites, respectively. However, with finer filler size, the difference in specific heat between untreated and treated filler composites becomes narrower. At 29.84 µm filler size, the specific heat of untreated composites is 1.34 J/g°C and 1.22 J/g°C for stearic acid-treated composites. This means that modifying the $CaCO_3$ surface with 1 wt% stearic acid would reduce the specific heat of UPE/$CaCO_3$ composites.

Figure 4.39(b) shows the specific heat content of untreated $CaCO_3$ with different filler loadings and 29.84 µm mean diameter in the UPE matrix. The result indicates that the specific heat of untreated UPE/$CaCO_3$ composites decreases gradually with filler increment. There is no change in the specific heat as 2 wt% of 29.84 µm filler is introduced into the UPE resin. At 4 wt% $CaCO_3$ content, the specific heat is reduced to 1.43 J/g°C. This can be explained by the fact that the specific heat of $CaCO_3$ is less than that of UPE. The specific heat of $CaCO_3$ is 0.9 J/g°C (Bastiurea et al., 2014). Adding a filler with a lower specific heat value into the polymer resin would reduce the composites' specific heat. Then there would be very small reductions in specific heat as

$CaCO_3$ particle is added to the UPE resin. For example, the specific heat of 6 wt% UPE/$CaCO_3$ composites is 1.42 J/g^{o}C. Adding 8 wt% filler content decreases the specific heat to 1.34 J/g^{o}C. Table 4.16 lists the specific heat of 8 wt% filler loading of untreated and stearic acid-treated UPE/$CaCO_3$ composites of various micron sizes in SI units (J/kg^{o}C).

Table 4.16: Specific heat (C_p) of 8 wt% and different sizes of untreated and stearic acid-treated aragonite $CaCO_3$-filled UPE composites

	Size (µm)	**29.84**	**35.06**	**46.30**	**206.55**	**297.94**	**485.84**	**574.81**	**636.87**
C_p (J/kg^{o}C)	**Untreated**	1338	1232	1430	1607	1646	1669	1739	1739
	Stearic acid-treated	1218	1131	1420	1108	1126	1144	1318	1052
	UPE	1870							

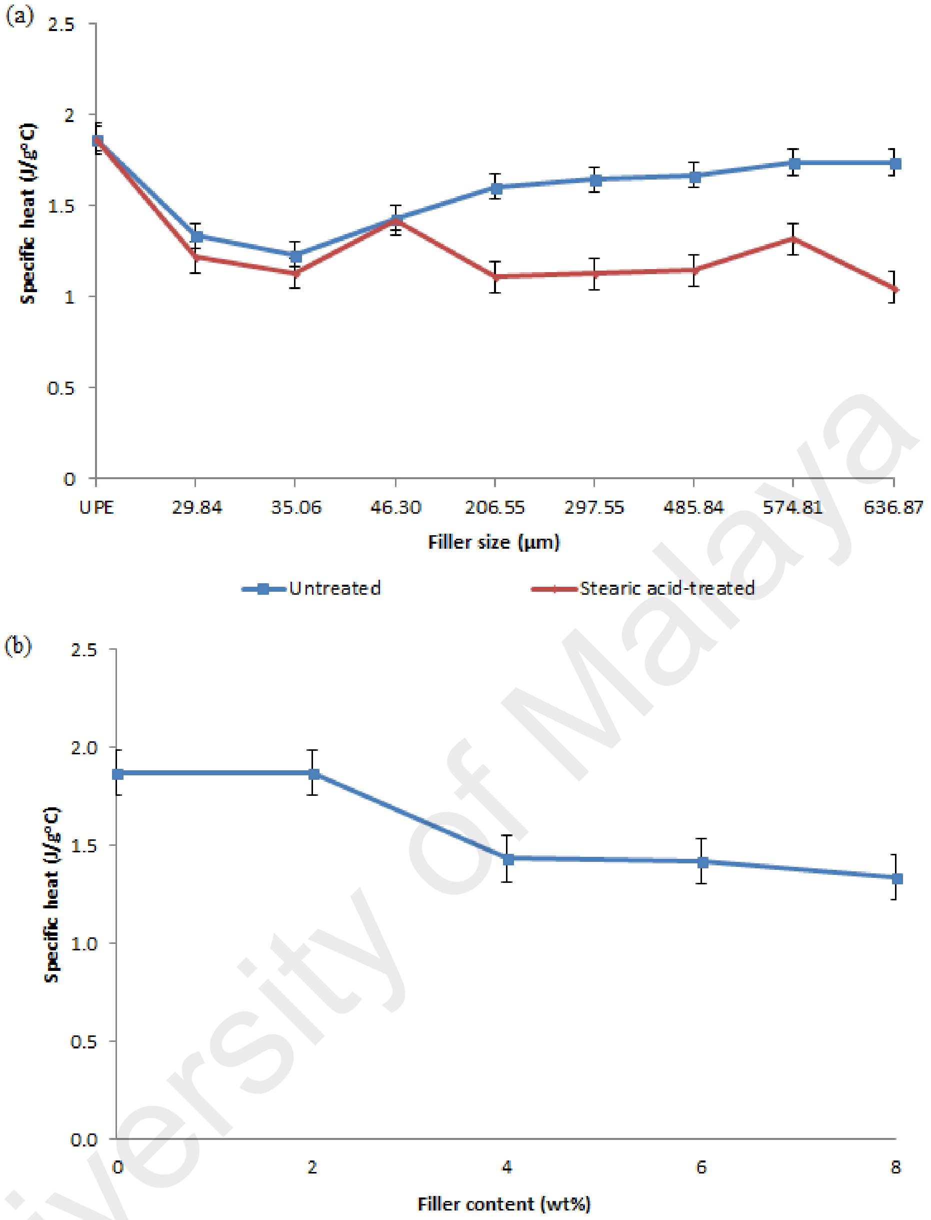

Figure 4.39: Specific heat of (a) various filler sizes of untreated and stearic acid-treated $CaCO_3$ at 8 wt% and (b) various filler content of 29.84 µm mean diameter untreated UPE/$CaCO_3$ (aragonite) composites

4.4.5 Thermal diffusivity

Thermal diffusivity is the speed of heat propagating by conduction during changes in temperature. Materials with high thermal diffusivity are able to propagate heat faster than materials with lower thermal diffusivity. In this work, the thermal diffusivity is calculated using equation 3.12. The equation shows that the thermal diffusivity is related to the sample's thermal conductivity, specific heat capacity and density.

The thermal diffusivity value's dependence on filler content and filler size is presented in Figure 4.40. Figure 4.40 (a) shows the thermal diffusivity of neat UPE, untreated UPE/$CaCO_3$ and stearic acid-treated UPE/$CaCO_3$ composites of various filler sizes and a similar filler loading of 8 wt%. The thermal diffusivity of polymeric materials is relatively low. Neat UPE has a thermal diffusivity of $09829 \times 10^{-7} m^2/s$. Adding $CaCO_3$ filler to the UPE resin increases the heat diffusivity of the composites with all filler sizes. Adding 8 wt% of 29.84 μm mean diameter untreated $CaCO_3$ filler increases the thermal diffusivity by 7.5 times that of unfilled UPE resin to $7.6247 \times 10^{-7} m^2/s$. A 4.6 increase, or $4.4998 \times 10^{-7} m^2/s$ thermal diffusivity was gained over neat UPE resin as 29.84 μm stearic acid-treated $CaCO_3$ was infused into UPE. This finding is similar to unmodified $CaCO_3$, which has higher thermal diffusivity than stearic acid-treated $CaCO_3$ filled in polyolefin resin (Jakubowska & Sterzynski, 2012). This is not surprising, as Jakubowska and Sterzynski (2012) found the thermal diffusivity to be higher in composites with larger agglomerates. As a result, higher thermal diffusivity is attained with fine untreated $CaCO_3$ than stearic acid-treated UPE/$CaCO_3$ composites.

However, as the filler size is greater than 206.55 μm, the thermal diffusivity of the stearic acid-treated filler is higher than untreated filler. At this filler size, the agglomerate is not the main concern. This signifies that for coarser filler of 206.55 μm and above, stearic acid treatment may increase the thermal diffusivity of UPE/$CaCO_3$ composites.

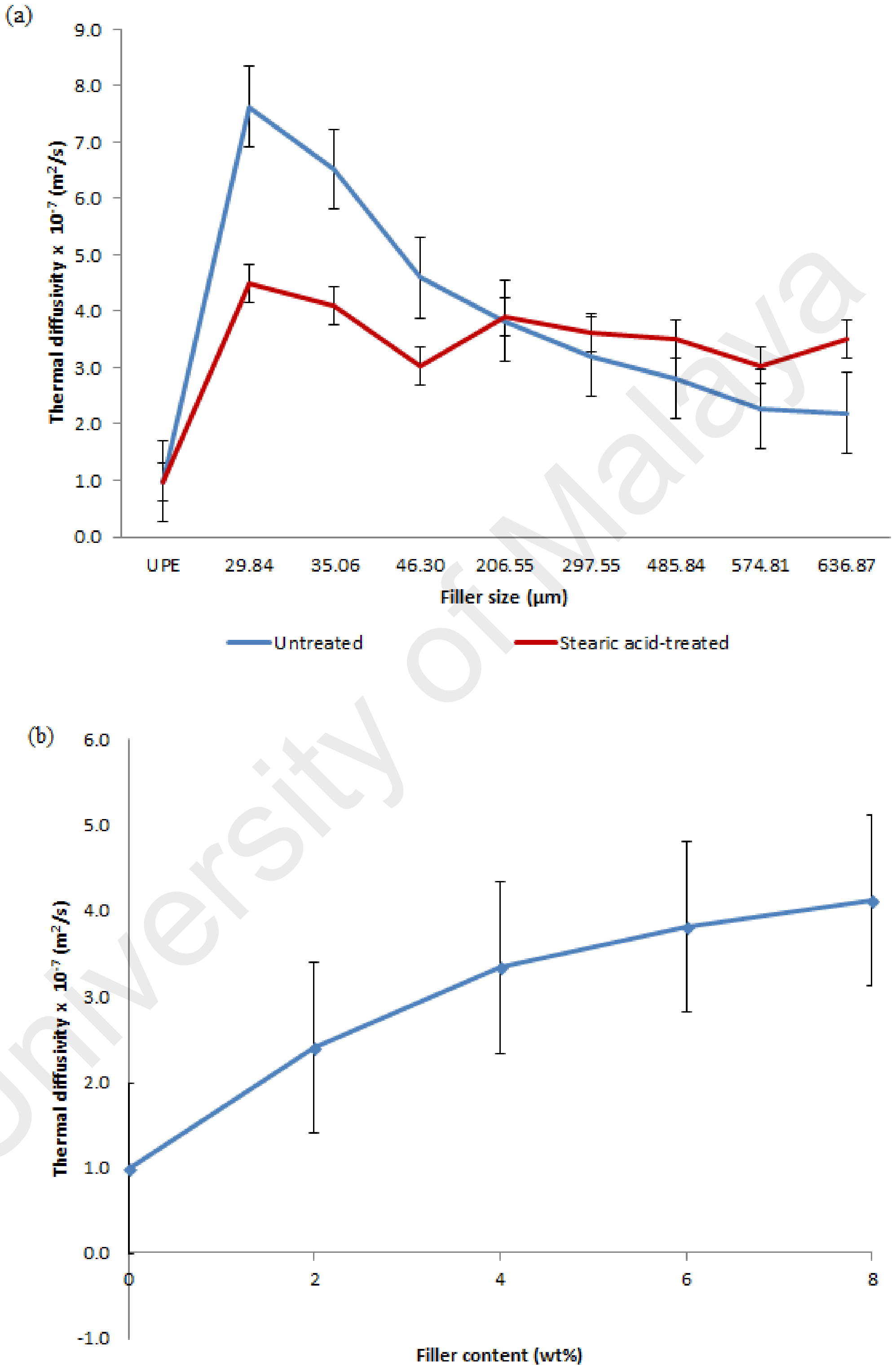

Figure 4.40: Thermal diffusivity of (a) various filler sizes of untreated and stearic acid-treated $CaCO_3$ at 8 wt% and (b) various filler content with 29.84 µm mean diameter untreated UPE/$CaCO_3$ (aragonite) composites

Introducing filler into the UPE matrix results in a higher thermal diffusivity value compared with unfilled UPE matrix. Adding more $CaCO_3$ filler content to the UPE matrix rapidly increases the thermal diffusivity. Figure 4.40 (b) shows that the increment of thermal diffusivity is linear with filler content. Adding 2 wt% $CaCO_3$ from *Polymesoda bengalensis* shell with mean diameter size of 29.84 µm increases the thermal diffusivity to $2.3951 \times 10^{-7} m^2/s$, representing a 2.4 increase over neat UPE. The maximum thermal diffusivity is gained at 8 wt% filler loading, which indicates the value is $4.123 \times 10^{-7} m^2/s$ or 4.2 times higher than unfilled UPE matrix. The improvement in thermal diffusivity means that adding $CaCO_3$ filler into UPE up to 8 wt% accelerates the cooling process, having a positive effect on the ability to conduct heat rapidly. This ability is very important in a wide range of applications, especially in the production of electronic packaging (Weidenfeller et al., 2005). This value, however, is very low, as Weidenfeller et al. (2005) reported that the significant thermal diffusivity value for electronic packaging must be higher than $1.2\, m^2/s$. It is expected that the thermal diffusivity value can be raised to over $1.2\, m^2/s$ by adding more than 30 wt% $CaCO_3$ and by assuming the relationship between thermal diffusivity and filler content is linear. Table 4.17 lists the thermal diffusivity of 8 wt% and different sizes of untreated and stearic acid-treated $CaCO_3$-filled UPE composites.

Table 4.17: Thermal diffusivity, α of 8 wt% and different sizes of untreated and stearic acid-treated aragonite $CaCO_3$-filled UPE composites

	Size (µm)	**29.84**	**35.06**	**46.30**	**206.55**	**297.94**	**485.84**	**574.81**	**636.87**
α ($\times10^{-7}$ m^2/s)	**Untreated UPE/$CaCO_3$ composites**	7.6247	6.5199	4.5944	3.8202	3.1961	2.8000	2.2690	2.1933
	Stearic acid-treated UPE/$CaCO_3$ composites	4.4998	4.1003	3.0368	3.8955	3.6070	3.4978	3.0404	3.5039
	Neat UPE	0.9829							

CHAPTER 5: POTENTIAL APPLICATIONS

5.1 Introduction

This chapter presents the potential applications of clam shell particle from a local seafood resource, which is *Polymesoda bengalensis,* locally known as *lokan*. The first part identifies the potential applications of *Polymesoda bengalensis* clam shell particle in the form of aragonite and aragonite $CaCO_3$ infused in unsaturated polyester (UPE) resin. The experimental results from this study are compared with other results from literature. The second part of the chapter lists other potential applications of aragonite $CaCO_3$ particle and its composites. No comparison is done, as all the information is collected from other literature and from previous work done by the researcher.

5.2 Potential applications of aragonite $CaCO_3$ particle and UPE/$CaCO_3$ (aragonite) composites

1) Scaffold material for bone repair

This study demonstrated that the clam shell of *Polymesoda bengalensis* is comprised of $CaCO_3$ in aragonite form. This polymorph is in rod-like crystal form. Aragonite is a useful biomedical material because it is denser than calcite (commercial $CaCO_3$) and can be integrated into, and mend and replace bones (Stupp & Braun, 1997). This valuable polymorph of natural $CaCO_3$ is used to produce scaffolds to repair bone (Awang-Hazmi et al., 2007). Nanocrystalline aragonite $CaCO_3$ facilitates osteoblast proliferation, differentiation, and adhesion without apparent toxicity (Shafiu Kamba & Zakaria, 2014). Impregnation with hyaluronic acid (HA) has been found to enhance the aragonite-based scaffold properties for the regeneration of cartilage and bone in an animal model (Kon et al., 2014). This can be achieved by introducing the drilled channel for the HA impregnation medium into the aragonite scaffold that allows young hyaline cartilage regeneration. $CaCO_3$ particles dispersed in liquid media can be a good inductors of hydroxyapatite coating growth on the titanium surface compared to CaCO3 film as precoating (Cruz et al, 22016). As a result, such scaffold could be useful for treating both chondral and osteochondral defects in humans.

2) Biomedical applications

Among numerous biomaterials used for tissue engineering, polyesters have been well-documented for their excellent biodegradability, biocompatibility and nontoxicity (Jiao & Cui, 2007), where $CaCO_3$ is the most widely used filler in polyester (Kandelbauer et al., 2014). Other studies have shown that aragonite $CaCO_3$ is a biocompatible, biodegradable and osteoconductive material (Awang-Hazmi et al., 2007; Liao et al., 2000). Hanna et al. (2011) studied the characterization of different types of ceramic filler infused into UPE resin. According to their study, $CaCO_3$ particle with less than 53 µm size and in the range of 3-15 wt% exhibited the best mechanical properties for biomaterial application compared with other fillers, such as CaO, $MgCO_3$ and MgO. Table 5.1 presents a comparison of mechanical properties between the current study and the results reported by Hanna et al. (2011). The outcome achieved with 29.84 µm $CaCO_3$ filler size was selected, because this size generally yields superior resultsover other filler sizes.

Table 5.1: Comparison of the mechanical properties of untreated UPE/$CaCO_3$ and stearic acid-treated UPE/$CaCO_3$ composites with commercial UPE/$CaCO_3$ for biomedical applications

	UPE/$CaCO_3$ for biomedical applications (Hanna et al., 2011)	***Untreated UPE/$CaCO_3$ composites (current study)**	***Stearic acid-treated UPE/$CaCO_3$ composites (current study)**
Tensile strength (MPa)	57.6828 (3 wt%)	29.32 (8 wt%)	37.53 (8 wt%)
Tensile modulus (MPa)	5706.18 (15 wt%)	1982.10 (8 wt%)	2053.02 (8 wt%)
Compression strength (MPa)	124.0965 (9 wt%)	145.56 (8 wt%)	151.55 (8 wt%)
Flexural strength (MPa)	97.864 (15 wt%)	127.39 (2 wt%)	122.42 (8 wt%)
Flexural modulus (MPa)	4890.928 (15 wt%)	4644.48 (8 wt%)	4866.71 (8 wt%)

*The values are produced for 29.84 µm UPE/$CaCO_3$ aragonite.
*The value in brackets ( ) means the $CaCO_3$ content in wt% that yielded the maximum mechanical property values.

Table 5.1 shows that the $CaCO_3$ from *Polymesoda bengalensis* clam shell yields mechanical properties comparable to commercial $CaCO_3$-filled UPE resin. Higher compressive strength and flexural modulus values are achieved with the UPE/$CaCO_3$ (aragonite) composites in this study. The most noticeable weakness is these composites' lower tensile strength and tensile modulus. However, it is expected that by adding filler content up to 15 wt% as Hanna el at. (2011) did, both tensile strength and tensile modulus may be quite similar. This might be achievable by assuming the improvement is linear as filler content is higher and the treatment successfully disperses the filler homogeneously in the UPE resin.

3) Automobile body filler

UPE/$CaCO_3$ (aragonite) composites can also be applied as automobile body filler andare known as car putty. Commercial UPE repair resin contains 33-40 wt% UPE resin, 10-20 wt% styrene, and 45-57 wt% inorganic fillers. The fillers are made up of hollow glass microspheres, talc, magnesium carbonate, calcium carbonate, fumed silica, glass fibers and other minerals. $CaCO_3$ comprises 5-15 wt%, the second highest after talc (Andrews et al., 2009). Table 5.2 lists the flexural properties of cured commercial repair resin as reported by Andrews et al. (2009) and UPE/CaCO$_3$ composites determined in this current study. Andrews et al. (2009) studied the car putties produced by Bondo Corporation, Atlanta. Bondo is a brand for fillers and other accessories such as putties and glazes, undercoatings and tools for automotive, household and marine. Other results from thermogravimetric analysis, rheology and viscosity analysis and dynamic mechanical analysis are not described because those properties are not studied in this work.

Table 5.2: Flexural properties of commercial UPE repair resin (car putty) and aragonite CaCO$_3$ with 29.84 μm-filled UPE composites

Flexural properties of commercial UPE repair resin (Andrews et al., 2009)			**Flexural properties of UPE/CaCO$_3$ at filler mean diameter size of 29.84 μm (current study)**				
Bondo Type	**Flexural Modulus (GPa)**	**Flexural Strength (MPa)**	**Filler content (wt%)**	**Flexural Modulus (GPa) (Untreated)**	**Flexural Strength (MPa) (Untreated)**	**Flexural Modulus (GPa) (Stearic acid-treated)**	**Flexural Strength (MPa) (Stearic acid-treated)**
***HEX**	0.224 ±0.015	7.7 ± 0.4	2	3.803 ±11.82	127.39 ±2.84	3.946 ±11.08	110.43 ±2.02
***BG**	1.97 ± 0.25	22.4 ± 2.2	4	4.294 ±10.52	118.27 ±2.53	4.671 ±10.20	116.42 ±4.39
***BBF**	0.73 ± 0.04	12.7 ± 0.7	6	4.585 ±7.02	116.13 ±3.67	4.865 ±11.17	117.30 ±3.00
***BAP**	0.89 ± 0.04	12.8 ±1.0	8	4.644 ±13.3	112.25 ±3.04	4.866 ±10.73	122.42 ±1.70
***BBR/ BFR**	3.16 ± 0.09	32.2 ±5.2					

*HEX: Hexion 713-6150, neat resin used in BG, BAP and BBF,
*BG: Bondo Glass,
*BBF: Bondo Body Filler,
*BAP: Bondo All-Purpose Putty,
*BBR/BFR: Bondo Boatyard Resin and Bondo Fiberglass Resin.

The comparison indicates that for as little as 2 wt% aragonite CaCO$_3$ filled into the UPE matrix, the flexural modulus and flexural strength are higher than cured commercial UPE repair resin. Replacing 5-15 wt% CaCO$_3$ in the commercial UPE repair resin with less aragonite CaCO$_3$ from *Polymesoda bengalensis* may be beneficial to enhancing the flexural properties.

4) Electronic packaging

According to King et al. (2008), composites with thermal conductivity ranging from 1 to 30 W/mK can be applied as heat sinks in electrical or electronic systems. In the present work, it was found that these UPE/$CaCO_3$ (aragonite) composites are applicable as heat sinks in electrical or electronic systems since the filler size is reduced to 29.84 µm with filler content of 4 wt% and more. The thermal conductivity obtained with this composite is over 1 W/mK. This value is expected to increase with increasing filler content. It is recommended to infuse 30 wt% $CaCO_3$ filler into this composite in order to increase the thermal diffusivity to above $1.2\, mm^2/s$, which is a significant thermal diffusivity value for electronic packaging (Weidenfeller et al., 2005). Besides, it is expected that reducing the size of $CaCO_3$ in the form of aragonite from the *Polymesoda bengalensis* clam shell to the nano-level might increase the effective heat conductivity of polymeric composites. Table 5.2 shows a comparison of the effective thermal conductivity of commercial calcite $CaCO_3$/PP (Ebadi-Dehaghani & Nazempour, 2012) and aragonite $CaCO_3$ derived from *Polymesoda bengalensis* (current study) filling UPE composites. A similar method was applied to measure the effective thermal conductivity, which is the guarded heat flow meter method.

Table 5.3: Comparison of effective thermal conductivity of PP/$CaCO_3$ (nano-calcite) and UPE/$CaCO_3$ (micro-aragonite) composites

Nano size PP/$CaCO_3$ (Ebadi-dehaghani & Nazempour, 2012)		**29.84 µm untreated UPE/$CaCO_3$ (current study)**	
Filler content (wt%)	**Thermal conductivity (W/mK)**	**Filler content (wt%)**	**Thermal conductivity (W/mK)**
(Neat PP)	0.22	(Neat UPE)	0.22
5	0.23	2	0.87
10	0.27	4	1.05
15	0.36	6	1.18
-	-	8	1.23

Table 5.3 compares the thermal conductivity of commercial calcite PP/$CaCO_3$ composites and UPE/$CaCO_3$ (aragonite) composites. It reveals that aragonite $CaCO_3$ performs better in terms of thermal conduction than commercial calcite $CaCO_3$ even

though the particles are micron sized. Neat PP and UPE have a similar thermal conductivity value of 0.22 W/mK. Adding even a small amount of 2 wt% aragonite $CaCO_3$ to the UPE resin may increase the thermal conductivity more than 15 wt% nano-sized $CaCO_3$/PP composites. It is expected that by increasing the amount of aragonite $CaCO_3$ filler in the matrix and also decreasing the filler size to the nano-level, the efficient thermal conductivity of the composites could be tremendous.

5.3 Other potential applications

1) Removal of heavy metal ions from water

The clam shell of *Polymesoda bengalensis* also has the potential to remove heavy metal ions from polluted water because the shell contains $CaCO_3$ in the form of aragonite polymorph. Aragonite $CaCO_3$ obtained from seafood shells can be used as an agent for removing heavy metal ions, such as cadmium (Cd), zinc (Zn), magnesium (Mg), calcium (Ca) and cobalt (Co) (Köhler et al., 2007). Besides, biogenic aragonite benefits from higher solubility and dissolution rate in water, thus having an advantage in removing heavy metal ions from waste water (Cubillas et al., 2005). The study showed that aragonite from fishery industry waste could be an efficient material for water purification by removing heavy metals from polluted waters.

Compared to calcite, the cadmium uptake capacity of aragonite is almost 2 orders of magnitude higher than calcite $CaCO_3$ in a similar experimental condition (Cubillas et al., 2005). This is due to the capability of aragonite to adsorb much bigger amounts of cadmium on its surface than calcite. Aragonite is also a good sorbent of lead because it can interact with lead (Pb) better than calcite (Godelitsas et al., 2003).

Many research works have indicated the shells from crustaceans, such as crab, shrimp, krill (Wang & Xing, 2007), mussel (Abdou et al., 2008) and clam (Letourneau et al., 1976) contain chitin. Chitin is the second most abundant natural biopolymer after cellulose, which is commonly found as a major component of the supporting tissues of organisms like crustaceans, fungi and insects. Chitin is a main raw material to produce chitosan. Chitin and chitosan can be extracted from natural resources by biological and chemical methods. Both chitin and chitosan can be agents of removing heavy metal ions from water, thus both can be utilized for purifying drinking water. The increasing cost of conventional adsorbents makes polysaccharide-based materials like chitin and chitosan among the most attractive biosorbents for waste water treatment (Crini, 2005). For example, the adsorption capacities of crosslinked chitosan derivatives for Cu(II) and Cd(II) are much higher than conventional adsorbents, such as clays, peat and commercial activated carbons.

The efficiency of chitin and chitosan to remove heavy metal ions from water varies. The sorption capacity of chitosan for Cu(II) ions is four to five times higher than that of chitin (Sağ & Aktay, 2002). In case of removing vanadate anions (VO_4^{3-}), chitosan was found be better than chitin. However, most literature reports that chitosan can adsorb more heavy metal ions more efficiently than other agents owing to (1) high hydrophilicity due to large numbers of hydroxyl groups of glucose units, (2) the presence of a large number of functional groups, (3) the high chemical reactivity of these groups, and (4) the flexible structure of the polymer chain (Crini, 2005). Chitosan can efficiently adsorb Hg(II), Cu(II), Ni(II) (Mckay et al., 1989), As(V) (Kwok et al., 2009) and Ag (Lasko & Hurst, 1999).

Several authors have found that comminuted, ground or powdered shell material has very high heavy metal sorption capacity, which issimilar to, or can even exceed that of chitin, chitosan and other sorbent materials (Köhler et al., 2007; Rae & Gibb, 2003; Yan-jiao, 2011). The effectiveness of shell material in being highly reactive for metal sorption capacities is not only due to the chitin and mineral $CaCO_3$ content, but the sub-micron carbonate structure of the shell material provides an extensive surface area embedded within a complex, multi-component organic matrix (Tudor et al., 2006). A study by Tudor et al. (2006) (Figure 5.1) revealed that the shells of *Mercenaria mercenaria* clam, oyster and lobster are about four orders of magnitude more effective in sequestering lead ions in the first four hours of contact time than either geologic or organic materials, such as calcite, aragonite and chitosan. The adsorption capacity of heavy metal ions such as Cu^{2+}, Cd^{2+}, Zn^{2+} and Pb^{2+} using crayfish carapace micro-aragonite particle is about three times higher than that of chitin and chitosan extracted from crayfish carapace micro-particle (Zheng et al., 2010).

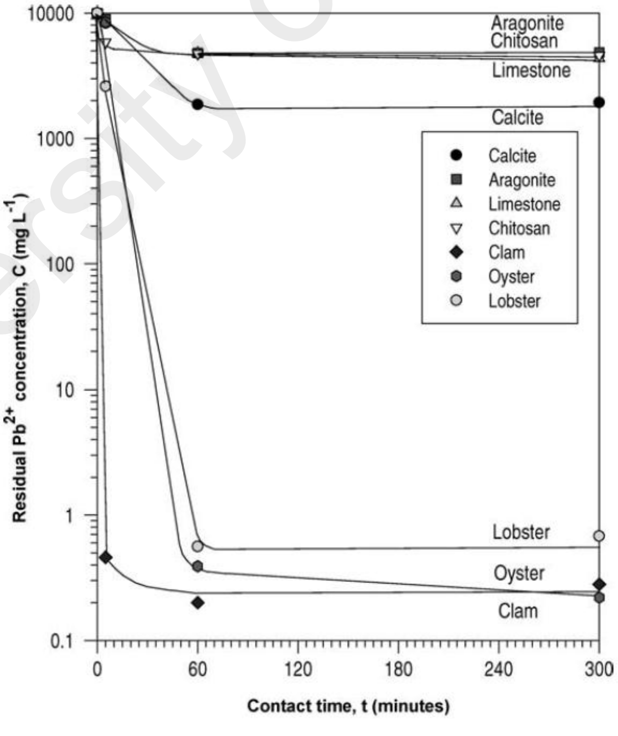

Figure 5.1: Semi-log plot of residual lead concentrations: shells vs geologic carbonates and chitosan as control. Contact time 0-5 hours; Initial Pb concentration = 48.3 mM (10 000 mgL^{-1})

(Tudor et al., 2006)

2) Artificial reefs

An artificial reef is a structure that is submerged in the sea or river and is used to preserve and promote marine life breeding. Thus, by this definition, any materials that are dumped into water can act as artificial reefs. However, common materials for artificial reefs, such as tires and old vehicles can have an adverse impact on the environment if not managed properly. Many studies have shown that concrete is one option for building artificial reefs due to easy construction into various forms and durability (Chou, 1997). Table 5.4 presents a list of research on various shells as replacement material in concrete mix (Falade, 1995; Muthusamy & Sabri, 2012; Sugiyama, 2004; Yusof et al., 2011a), as collected by Othman et al. (2013).

Table 5.4: Various types of shells used as a replacement material in concrete (Othman et al., 2013)

Researchers	Country	Types of shells	Replacement in concrete
Falade (1995)	Nigeria	Priwinkle	Coarse aggregate
Sugiyama (2004)	Japan	Scallop	Coarse aggregate
Yusof et al., (2011)	Malaysia	Clam	Fine aggregate
Muthusamy & Sabri (2012)	Malaysia	Cockle	Coarse aggregate

It was reported that utilizing clam shell particle with sizes below 500 µm produces positive results on compressive strength (Yusof et al., 2011a). The particle acts as filler in the concrete by filling and reducing the number of voids between sand. As a result, the particles between the sand and clam shell achieve excellent interlocking to produce higher compressive strength. Table 5.5 exhibits the concrete mixing proportion of the sample and the compressive strength produced by each sample. The results indicate that at the above-mentioned size of *Polymesoda spp.* particle, the compressive strength increases as the filler content increases. The most obvious increment is achieved at 30 wt% filler, representing a 16% increment compared to concrete without *Polymesoda* *spp.* filler. This proportion also exhibits higher strength than standard concrete for structural applications, which is 17-28 MPa for residential concrete (Collins et al., 2012).

Table 5.5: Concrete mixing proportion and compressive strength of reference sample (without *lokan* particle) and with a different mass fraction of *lokan* particle with size below 500 µm
(Yusof et al., 2011a)

Water/cement ratio: 0.47 **Cement: 3323.5 g** **Water: 1562.05 g**	**Coarse aggregates: 8967.40 g** **Fine aggregates: 4424.20 g**		**Compressive strength (MPa)**
Mass percentage of fine aggregates (%)	**Mass of clam (g)**	**Mass of sand (g)**	
0	0	4424.20	36.95
10	442.42	3981.78	39.71
20	884.84	3539.36	38.04
30	1327.26	3096.94	42.86

Polymesoda spp. clam shell particle can also be used as an alternative material to replace 10 wt% of the total sand composition in mortar for artificial reef construction (Yusof et al., 2011b). Table 5.6 shows the mixing proportion of the reference sample with 10 wt% replacement of the total sand composition in the mortar along with the compressive strength of the mortar. The table indicates that the compressive strength of the mortar can be enhanced when 10 wt% of the total sand content is replaced with clam shell particle. However, the improvement in the compressive strength of mortar is generated by the coarse clam shell particle size. The highest compressive strength was obtained with particles passing through 1.18 mm sieve aperture. The strength was 54.37 MPa, representing 19.54% higher strength than the reference sample with 27.82 MPa compressive strength.

According to a study by Sahari and Mijan (2011), cockle shells not only contribute to enhancing the compressive strength of concrete but also attract marine organisms to settle on it (Sahari & Mijan, 2011). The existence of cockle shells on artificial reefs provides texture to expedite marine organisms on the reef, which is one of the food sources for fish. As a result, fish are attracted to cockle shell reefs more than reefs without cockle shells.

Table 5.6: Mortar mixing proportion and its compressive strength with different clam shell particle sizes
(Yusof et al., 2011b)

Item	Quantity		Clam shell particle through sieve size (µm)	Compressive strength (MPa)
	Reference sample	Sample with 10 wt% of clam shell particle out of total sand		
Sand/Cement volumetric ratio	2	2	Reference sample	27.82
Water/Cement volumetric ratio	0.56	0.56	300	27.47
Cement content	300 kg/m^3	300 kg/m^3	600	28.87
Sand content	600 kg/m^3	540 kg/m^3	850	30.11
Clam shell powder content	0	60 kg/m^3	1180	33.26

Figure 5.2: Comparison of artificial reefs relative to organisms settling on the surface (Sahari & Mijan, 2011)

CHAPTER 6: CONCLUSIONS AND RECOMMENDATIONS

6.1 Introduction

In an effort to investigate the mechanical and thermophysical properties, results from different mean particle diameter sizes and filler contents in untreated and stearic acid-treated calcium carbonate from *lokan* shell are analyzed. In this study, *lokan* shell with the scientific name *Polymesoda bengalensis* was applied as seafood waste in the form of particle into unsaturated polyester (UPE) matrix composites. The motivation behind this research was to reduce waste and to investigate the potential of applying this waste as filler in particulate-filled polymer composites. The three main objectives of this study are:

1. To identify the elemental content and crystal structure of *lokan* shell particle.
2. To investigate the effect of including $CaCO_3$ particle from *lokan* shell-filled unsaturated polyester (UPE) composites of varying sizes and filler concentrations on the mechanical and thermophysical properties.
3. To investigate the effect of modifying the $CaCO_3$ surface with 1 wt% stearic acid on the mechanical and thermophysical properties of UPE/$CaCO_3$ composites.

The crystal structure of *lokan* shell particle was identified by X-ray powder diffraction (XRD), the elemental composition was identified by energy dispersive X-ray (EDX) and the morphology was determined by scanning electron microscope (SEM). The composite samples were successfully fabricated through ultrasonication and open molding method. The samples were degassed for 30 minutes to remove the air bubbles and cured at room temperature for 24 hours. The samples were fabricated according to the filler weight fractions of 2, 4, 6 and 8 wt% with eight different mean filler diameters of 636.87, 574.81, 485.84, 297.94, 206.55, 46.30,35.06 and 29.84 μm. The mechanical properties of the samples were determined using an Instron 4469 universal testing machine and Vickers hardness tester. The heat conductivity was measured by guarded heat flow method using a P.A. Hilton 940 machine. The specific heat content was measured by Differential Scanning Calorimetry (DSC) and the heat diffusivity was determined by applying equation 3.12. Furthermore, the effect of coating the *Polymesoda bengalensis* shell particle with 1 wt% stearic acid was also investigated by comparing the results before and after treatment.

6.2 Conclusions

Some conclusions can be drawn from this study based on the research findings and analyses. The conclusions are divided into four categories based on four research objectives.

1) Elemental content and crystal structure of *lokan* shell particle

The XRD pattern results showed that all peaks matched for calcium carbonate with the entire crystal structure of aragonite. According to the SEM images, the aragonite was in the form of rod-like crystals. The EDX spectroscopy results of elemental content in three different areas showed that the particle contains calcium carbonate and is rich with oxygen and calcium.

2. Effect of including $CaCO_3$ particle from *lokan* shell-filled unsaturated polyester (UPE) composites of varying sizes and filler concentrations on the mechanical and thermophysical properties

i) Effect of filler size and filler loading on the composite's stiffness

The results indicate that including aragonite $CaCO_3$ derived from *lokan* shell particle in all micron sizes (29.84-- 636.87 µm) greatly improved the stiffness of the composites. The stiffness or elastic modulus of UPE/$CaCO_3$ (aragonite) composites appeared to increase with tensile, compressive and flexural loadings more than unfilled or neat UPE resin. The stiffness increased as the filler size decreased, and the filler content increased. Therefore, the maximum stiffness of the composites was acquired at 8 wt% and 29.84 µm mean filler diameter. The stiffness was greatly affected by the filler distribution throughout the polymer matrix. Homogeneous filler distribution in the matrix produced better filler "bridges" or particle interconnection networks in the composites. As a result, the stiffness increased. However, as the filler content increased, the filler tended to agglomerate due to higher surface energy.

ii) Effect of filler size and filler loading on the composite's strength

Adding aragonite $CaCO_3$ particles into the UPE matrix improved the composites' tensile strength and compressive strength. The strength enhanced as the filler size decreased and filler content increased. The strength of the composites was significantly influenced by the interfacial area of the filler. Smaller filler has a larger interfacial area for particle-matrix attachment. Therefore, the strength improved as the filler size decreased. However, the agglomeration of smaller particles owing to higher surface energy might have reduced the interfacial area and thus lowered the efficiency of stress transfer between the particles and matrix.

iii) Effect of filler size and filler loading on the composites' surface hardness and Tabor's number

The surface hardness of the UPE/$CaCO_3$ composites seemingly improved as the filler size decreased and filler content increased. However, for untreated filler samples, a small increment, or insignificant change was observed, except at 8 wt% with 29.84 μm mean diameter UPE/$CaCO_3$ composites. Tabor's number, or the correlation between hardness and ultimate compressive strength of all samples was less than 3 (in the range of 1.8-2.2).

iv) Effect of filler size and filler loading on the composites' thermal conductivity

Adding $CaCO_3$ filler to UPE improved the thermal conductivity of the neat UPE matrix. The filler size and filler content had substantial influence on the efficient thermal conductivity of the composites. The thermal conductivity increased as the filler size decreased and filler content increased. Thus, the thermal conductivity enhanced very much at 8 wt% filler content and the smallest filler size (29.84 μm).

v) Effect of filler size and filler loading on the composites' specific heat capacity

Adding $CaCO_3$ filler to the UPE matrix reduced the specific heat of the neat UPE matrix. The filler size influenced the specific heat of the particulate-filled polymer composites. The composites with coarser filler exhibited higher specific heat capacity than the composites with finer filler**.** Besides, adding more filler was not helpful for increasing the specific heat capacity of UPE/$CaCO_3$ composites.

vi) Effect of filler size and filler loading on the composites' thermal diffusivity

Thermal diffusivity appeared to improve with finer filler size and higher filler content. The maximum thermal diffusivity was achieved with 8 wt% and 29.84 μm mean filler diameter. For filler smaller than 206.55 μm, the untreated filler produced better thermal diffusivity than treated filler composites. The opposite was found for coarser filler.

3. Effect of modifying the $CaCO_3$ surface with 1 wt% stearic acid on the mechanical and thermophysical properties of UPE/$CaCO_3$ composites

i) Effect of treating the $CaCO_3$ surface with 1 wt% stearic acid on the composites' stiffness

Coating aragonite $CaCO_3$ filler with 1 wt% stearic acid could reduce the surface energy and filler agglomeration, hence resulting in a more homogeneous filler distribution. Therefore, in all loading directions (tensile, compressive and flexural), stearic acid-treated filler produced superior stiffness compared to untreated filler $CaCO_3$ filled UPE composites.

ii) Effect of treating the $CaCO_3$ surface with 1 wt% stearic acid on the composites' strength

Treating $CaCO_3$ filler with stearic acid increased the composites' strength more than untreated filler. Better homogeneity of the stearic acid-treated filler in the UPE matrix improved the stress transfer efficiency between filler and matrix. The filler tended to disperse homogeneously, reducing the agglomeration size and thus increasing the total interfacial area for stress transfer. As a result, the strength of the composites increased. However, including aragonite $CaCO_3$ in the UPE matrix was not very helpful in enhancing the flexural strength, except for the smallest filler size (29.84 μm).

iii) Effect of treating the $CaCO_3$ surface with 1 wt% stearic acid on the composites' surface hardness and Tabor's number

Coating the $CaCO_3$ filler with stearic acid softened the composite surface. As a result, the treated composites had lower surface hardness than untreated composites. Consequently, Tabor's number also diminished to less than untreated composites. This was due to the decrease in ductility that occurred because of the limitations with nucleation and movement of dislocations.

iv) Effect of treating the $CaCO_3$ surface with 1 wt% stearic acid on the composites' thermal conductivity

Treating the filler with stearic acid was not helpful to increase the thermal conductivity of the UPE/$CaCO_3$ (aragonite) composites. At similar filler content and filler size, the treated $CaCO_3$ filler exhibited lower thermal conductivity than untreated UPE/$CaCO_3$ composites.

v) Effect of treating the $CaCO_3$ surface with 1 wt% stearic acid on the composites' specific heat capacity

Stearic acid-treated UPE/$CaCO_3$ composites always showed lower specific heat capacity at any filler size and filler loading than untreated composites. Therefore, this treatment was not useful for increasing the specific heat capacity.

vi) Effect of treating the $CaCO_3$ surface with 1 wt% stearic acid on the composites' thermal diffusivity

Treating $CaCO_3$ with stearic acid did not have a positive effect on enhancing the thermal diffusivity for filler sizes smaller than 206.55 μm. Therefore, this treatment was effective for coarser filler of 206.55 μm and above.

4. Potential applications of $CaCO_3$ derived from *Polymesoda bengalensis* shells

A comparative study was done on commercial $CaCO_3$ with reports from literature. Aragonite $CaCO_3$ particle obtained from *Polymesoda bengalensis* clam shells has potential as an agent for removing heavy metal ions from water for water purification and as a scaffold for bone repair. As the particle was infused into unsaturated polyester, the composites showed potential to be applied as biomaterials and automobile body fillers, and in electronic packaging. Concrete infused with clam shell particle and with clam shell particle attached to its surface can be used as an artificial reef. This is because utilizing *Polymesoda bengalensis* shell particle as reinforcement in concrete can improve the compressive strength. In addition, the presence of shells in artificial reefs provides texture to expedite marine organisms on the reef.

6.3 Recommendations

The work presented in this research entailed an investigation of the effects of applying different mean diameters of *Polymesoda bengalensis* shell particle on the mechanical and thermophysical properties as the particle was infused into unsaturated polyester resin. The particles were in the micron-size range. Obvious improvements were achieved in composite stiffness (tensile, compressive and flexural loadings) and thermal conductivity. In future, it is recommended to apply nano-size *Polymesoda bengalensis* shell particle because it may display better properties than micron-size filler. For aragonite $CaCO_3$, nano-size powder can be produced through oil-in-water (O/W) microemulsions using a high-pressure homogenizer (HPH) (Kamba et al., 2013).

In this study, modifying the aragonite $CaCO_3$ filler surface with stearic acid produced superior mechanical properties. The purpose of this treatment was to better disperse the filler in the polymer matrix. As a result, the stiffness for all loadings, i.e.

tensile, compressive and flexural, increased rapidly. Not much improvement was gained in terms of the composites' tensile strength. Therefore, for further work it is recommended to use silane solution, which is a reactive treatment. This treatment may improve the strength of the composites because it can produce better particle-matrix adhesion.

Potential applications were discussed upon doing a comparative study with other literature. It is recommended to conduct detailed research with experimentation and costing analyses to ensure that the $CaCO_3$ particle from *Polymesoda bengalensis* shell is worth being applied as a polymer matrix composite reinforcement. In addition, it is also recommended to do research with focus on the one application. Additional research works should be done to produce more relevant data to investigate whether clam shells can indeed be applied as biomaterials and automobile body fillers, and in electronic packaging, removing heavy metal ions from water and in artificial reefs.

REFERENCES

Abdou, E. S., Nagy, K. S., & Elsabee, M. Z. (2008). Extraction and characterization of chitin and chitosan from local sources. *Bioresource Technology, 99*(5), 1359-1367.

Ahmad, F. N., Jaafar, M., Palaniandy, S., & Azizli, K. A. M. (2008). Effect of particle shape of silica mineral on the properties of epoxy composites. *Composites Science and Technology, 68*(2), 346-353.

Al-Sulaiman, F., Mokheimer, E. A., & Al-Nassar, Y. (2006). Prediction of the thermal conductivity of the constituents of fiber reinforced composite laminates. *Heat and Mass Transfer, 42*(5), 370-377.

Al Robaidi, A., Mousa, A., Massadeh, S., Al Rawabdeh, I., & Anagreh, N. (2011). The Potential of Silane Coated Calcium Carbonate on Mechanical Properties of Rigid PVC Composites for Pipe Manufacturing. *Materials Sciences and Applications, 2*, 481.

Andrews, K., Bingham, S., McAninch, I., Greer, C., Sands, J. M., La Scala, J. J., Geng, X., Palmese, G. R., Crisostomo, V., & Suib, S. (2009). Analysis of commercial unsaturated polyester repair resins: DTIC Document.

Agamuthu, P., & Fauziah, S. (2011). Challenges and issues in moving towards sustainable landfilling in a transitory country-Malaysia. *Waste Management & Research, 29*(1), 13-19.

Askeland, D. R., Fulay, P. P., & Wright, W. J. (2011). *The science and engineering of materials*: Nelson Education.

Awang-Hazmi, A., Zuki, A., Noordin, M., Jalila, A., & Norimah, Y. (2007). Mineral composition of the cockle (Anadara Granosa) shells of west coast of peninsular malaysia and it's potential as biomaterial for use in bone repair. *Journal of Animal and Veterinary Advances, 6*(5), 591-594.

Azeem, S., & Zain-ul-Abdein, M. (2012). Investigation of thermal conductivity enhancement in bakelite–graphite particulate filled polymeric composite. *International Journal of Engineering Science, 52*(0), 30-40.

Baltá Calleja, F., & Fakirov, S. (1997). Recent advances in the study and characterization of polymers by microhardness. *Trends in polymer science, 5*(8), 246-249.

Baskaran, R., Sarojadevi, M., & Vijayakumar, C. T. (2011). Mechanical and thermal properties of unsaturated polyester/calcium carbonate nanocomposites. *Journal of Reinforced Plastics and Composites, 30*(18), 1549-1556.

Bastiurea, M., Bastiurea, R., Andrei, G., Dima, D., Murarescu, M., Ripa, M., & Circiumaru, A. (2014). Determination of Specific Heat of Polyester Composite with Graphene and Graphite by Differential Scanning Calorimetry. *Tribology in Industry, 36*(4).

Boyer, H. E., & Gall, T. L. (1985). Metals handbook; desk edition.

Calleja, F. B., & Fakirov, S. (1997). Recent advances in the study and characterization of polymers by microhardness. *Trends in polymer science, 8*(5), 246-249.

Callister, W. D., & Rethwisch, D. G. (2012). *Fundamentals of materials science and engineering: an integrated approach*: John Wiley & Sons.

Cao, Z., Daly, M., Clémence, L., Geever, L. M., Major, I., Higginbotham, C. L., & Devine, D. M. (2016). Chemical surface modification of calcium carbonate particles with stearic acid using different treating methods. *Applied Surface Science*, *378*, 320-329.

Chan, M.-l., Lau, K.-t., Wong, T.-t., Ho, M.-p., & Hui, D. (2011). Mechanism of reinforcement in a nanoclay/polymer composite. *Composites Part B: Engineering, 42*(6), 1708-1712.

Chiang, H.-W., Chung, C.-L., Chen, L.-C., Li, Y., Wong, C., & Fu, S.-L. (2005). Processing and shape effects on silver paste electrically conductive adhesives (ECAs). *Journal of adhesion science and technology, 19*(7), 565-578.

Chisholm, N., Mahfuz, H., Rangari, V. K., Ashfaq, A., & Jeelani, S. (2005). Fabrication and mechanical characterization of carbon/SiC-epoxy nanocomposites. *Composite Structures, 67*(1), 115-124.

Cho, J., Joshi, M. S., & Sun, C. T. (2006). Effect of inclusion size on mechanical properties of polymeric composites with micro and nano particles. *Composites Science and Technology, 66*(13), 1941-1952.

Chou, L. (1997). Artificial reefs of Southeast Asia-do they enhance or degrade the marine environment? *Environmental monitoring and assessment, 44*(1-3), 45-52.

Chua, K., Sahid, E. J. M., & Leong, Y. (2011). Sustainable municipal solid waste management and GHG abatement in Malaysia. *ST-4: Green & Energy Management*, 04-02.

Collings, A. F. (2006). Process for treating a solid-liquid mixture: Google Patents.

Collins, P., Koren, L., & Hall, W. (2012). *Concrete*: Phaidon Incorporated Limited.

Crini, G. (2005). Recent developments in polysaccharide-based materials used as adsorbents in waste water treatment. *Progress in polymer science, 30*(1), 38-70.

Cruz, M. A. E., Ruiz, G. C., Faria, A. N., Zancanela, D. C., Pereira, L. S., Ciancaglini, P., & Ramos, A. P. (2016). Calcium carbonate hybrid coating promotes the formation of biomimetic hydroxyapatite on titanium surfaces. *Applied Surface Science*, *370*, 459-468.

Cubillas, P., Köhler, S., Prieto, M., Causserand, C., & Oelkers, E. H. (2005). How do mineral coatings affect dissolution rates? An experimental study of coupled $CaCO_3$ dissolution—$CdCO_3$ precipitation. *Geochimica et Cosmochimica Acta, 69*(23), 5459-5476.

Cubillas, P., Köhler, S., Prieto, M., Chaïrat, C., & Oelkers, E. H. (2005). Experimental determination of the dissolution rates of calcite, aragonite, and bivalves. *Chemical Geology, 216*(1), 59-77.

Demjén, Z., Pukanszky, B., & Nagy, J. (1998). Evaluation of interfacial interaction in polypropylene/surface treated $CaCO_3$ composites. *Composites Part A: Applied Science and Manufacturing, 29*(3), 323-329.

Deshmukh, G. S., Pathak, S. U., Peshwe, D. R., & Ekhe, J. D. (2010). Effect of uncoated calcium carbonate and stearic acid coated calcium carbonate on mechanical, thermal and structural properties of poly(butylene terephthalate) (PBT)/calcium carbonate composites. *Bulletin of Materials Science, 33*(3), 277-284.

Deshmukh, S. P., Rao, A. C., Gaval, V. R., & Mahanwar, P. A. (2011). Mica-filled PVC composites: effect of particle size, filler concentration, and surface treatment of the filler, on mechanical and electrical properties of the composites. *Journal of Thermoplastic Composite Materials*, *24*(5), 583-599.

Do, V., Budha, P.B. & Daniel, B.A. 2012. *Polymesoda bengalensis*. The IUCN Red List of Threatened Species 2012.

do Nascimento, E. M., Eiras, D., & Pessan, L. A. (2016). Effect of thermal treatment on impact resistance and mechanical properties of polypropylene/calcium carbonate nanocomposites. *Composites Part B: Engineering*, *91*, 228-234.

Dong, Y., Chaudhary, D., Ploumis, C., & Lau, K.-T. (2011). Correlation of mechanical performance and morphological structures of epoxy micro/nanoparticulate composites. *Composites Part A: Applied Science and Manufacturing, 42*(10), 1483-1492.

Douce, J., Boilot, J.-P., Biteau, J., Scodellaro, L., & Jimenez, A. (2004). Effect of filler size and surface condition of nano-sized silica particles in polysiloxane coatings. *Thin Solid Films, 466*(1–2), 114-122.

Ebadi-Dehaghani, H., & Nazempour, M. (2012). Thermal conductivity of nanoparticles filled polymers. In A. Hashim (Ed.), *Nanotechnology and Nanomaterials, "Smart Nanoparticles Technology"*: InTech, Rijeka, Croatia.

Ebadi-Dehaghani, H., Reiszadeh, M., Chavoshi, A., Nazempour, M., & Vakili, M. (2014). The effect of zinc oxide and calcium carbonate nanoparticles on the thermal conductivity of polypropylene. *Journal of Macromolecular Science, Part B, 53*(1), 93-107.

Elleithy, R. H., Ali, I., Ali, M. A., & Al-Zahrani, S. (2010). High density polyethylene/micro calcium carbonate composites: A study of the morphological, thermal, and viscoelastic properties. *Journal of applied polymer science, 117*(4), 2413-2421.

Falade, F. (1995). An investigation of periwinkle shells as coarse aggregate in concrete. *Building and Environment, 30*(4), 573-577.

Farris, R. (1968). The influence of vacuole formation on the response and failure of filled elastomers. *Journal of Rheology, 12*, 315.

Fekete, E., Móczó, J., & Pukánszky, B. (2004). Determination of the surface characteristics of particulate fillers by inverse gas chromatography at infinite dilution: a critical approach. *Journal of colloid and interface science, 269*(1), 143-152.

Fischer, J. E., & Gogotsi, Y. (2006). *Carbon nanotubes: structure and properties*: CRC Press, Boca Raton, USA.

Fontana, M. G. (2005). *Corrosion engineering*. Tata McGraw-Hill Education.

Frormann, L., Iqbal, A., & Abdullah, S. A. (2008). Thermo-viscoelastic behavior of PCNF-filled polypropylene nanocomposites. *Journal of applied polymer science, 107*(4), 2695-2703.

Fu, S.-Y., Feng, X.-Q., Lauke, B., & Mai, Y.-W. (2008). Effects of particle size, particle/matrix interface adhesion and particle loading on mechanical properties of particulate–polymer composites. *Composites Part B: Engineering, 39*(6), 933-961.

Garrett, R. H., & Grisham, C. M. (2005). Biochemistry, Thomson Learning. *Inc., Stamford, Conn*.

Gent, A. (1980). Detachment of an elastic matrix from a rigid spherical inclusion. *Journal of Materials Science, 15*(11), 2884-2888.

Ghari, H. S., & Jalali-Arani, A. (2016). Nanocomposites based on natural rubber, organoclay and nano-calcium carbonate: Study on the structure, cure behavior, static and dynamic-mechanical properties. *Applied Clay Science*, *119*, 348-357.

Gittings, J. P., Bowen, C. R., Dent, A. C. E., Turner, I. G., Baxter, F. R., Cartmell, S., & Chaudhuri, J. (2009). Influence of porosity on polarisation and electrical properties of hydroxyapatite based ceramics. *Ferroelectrics*, *390*(1), 168-176

Godelitsas, A., Astilleros, J. M., Hallam, K., Harissopoulos, S., & Putnis, A. (2003). Interaction of calcium carbonates with lead in aqueous solutions. *Environmental science & technology, 37*(15), 3351-3360.

Gomari, K., Hamouda, A., & Denoyel, R. (2006). Influence of sulfate ions on the interaction between fatty acids and calcite surface. *Colloids and Surfaces A: Physicochemical and Engineering Aspects, 287*(1), 29-35.

Gosling, E. (2003). Reproduction, settlement and recruitment. *Bivalve molluscs: biology, ecology and culture. Fishing news books, Blackwell, Oxford*, 131-168.

Hamli, H., Idris, M., Hena, M. A., & Wong, S. (2012). Taxonomic study of edible bivalve from selected division of Sarawak, Malaysia. *International Journal of Zoological Research, 8*(1), 52-58.

Hanna, W. A., Gharib, F. E., & Marhoon, I. I. (2011). Characterization of ceramic filled polymer matrix composite used for biomedical applications. *Journal of Minerals and Materials Characterization and Engineering, 10*(12), 1167.

Hashim, R. (1993). *Sumber makanan pesisir laut Sabah*. Selangor, Malaysia: Dewan Bahasa dan Pustaka.

He, D., & Jiang, B. (1993). The elastic modulus of filled polymer composites. *Journal of applied polymer science, 49*(4), 617-621.

He, H., Li, K., Wang, J., Sun, G., Li, Y., & Wang, J. (2011). Study on thermal and mechanical properties of nano-calcium carbonate/epoxy composites. *Materials & Design, 32*(8), 4521-4527.

Henderson, P., & Wallace, A. (1989). Hardness and creep of cross-linked polyethylene. *Polymer, 30*(12), 2209-2214.

Holme, N. A. (1995). Conservation of marine molluscs in the British Isles. *The Conservation Biology of*, 29.

Horrocks, A. R., & Price, D. (2001). *Fire retardant materials*: Woodhead Publishing.

Hu, Z., Zen, X., Gong, J., & Deng, Y. (2009). Water resistance improvement of paper by superhydrophobic modification with microsized $CaCO_3$ and fatty acid coating. *Colloids and Surfaces A: Physicochemical and Engineering Aspects,351*(1-3), 65-70.

Huda, M. S., Drzal, L. T., Mohanty, A. K., & Misra, M. (2006). Chopped glass and recycled newspaper as reinforcement fibers in injection molded poly (lactic acid)(PLA) composites: a comparative study. *Composites Science and Technology, 66*(11), 1813-1824.

Islam, K. N., Bakar, M. Z. B. A., Ali, M. E., Hussein, M. Z. B., Noordin, M. M., Loqman, M., Miah, G., Wahid, H., & Hashim, U. (2012). A novel method for the synthesis of calcium carbonate (aragonite) nanoparticles from cockle shells. *Powder Technology*.

Ichetaonye, S. I., Ichetaonye, D. N., & Tenebe, O. G. (2016). Study of Mechanical and Micro-Structural Effect on Alkaline Treated Sponge Gourd (Luffa aegyptiaca) Fibre Epoxy Composite. *Modern Mechanical Engineering*, *6*(01), 1

Islam, K. N., Bakar, M. Z. B. A., Noordin, M. M., Hussein, M. Z. B., Rahman, N. S. B. A., & Ali, M. E. (2011). Characterisation of calcium carbonate and its polymorphs from cockle shells (Anadara granosa). *Powder Technology, 213*(1), 188-191.

Jakubowska, P., & Sterzynski, T. (2012). Thermal diffusivity of polyolefin composites highly filled with calcium carbonate. *Polimery, 57*(4), 271-275.

Jeong, S.-B., Yang, Y.-C., Chae, Y.-B., & Kim, B.-G. (2009). Characteristics of the treated ground calcium carbonate powder with stearic acid using the dry process coating system. *Materials transactions, 50*(2), 409.

Jerabek, M., Major, Z., Renner, K., Móczó, J., Pukánszky, B., & Lang, R. W. (2010). Filler/matrix-debonding and micro-mechanisms of deformation in particulate filled polypropylene composites under tension. *Polymer, 51*(9), 2040-2048.

Ji, X. L., Jing, J. K., Jiang, W., & Jiang, B. Z. (2002). Tensile modulus of polymer nanocomposites. *Polymer Engineering & Science, 42*(5), 983-993.

Jiang, L., Lam, Y., Tam, K., Chua, T., Sim, G., & Ang, L. (2005). Strengthening acrylonitrile-butadiene-styrene (ABS) with nano-sized and micron-sized calcium carbonate. *Polymer, 46*(1), 243-252.

Jiao, Y.-P., & Cui, F.-Z. (2007). Surface modification of polyester biomaterials for tissue engineering. *Biomedical Materials, 2*(4), R24.

Jones, D. R. H., & Ashby, M. F. (2012). *Engineering materials 2: an introduction to microstructures and processing*. Butterworth-Heinemann.

Kamba, A. S., Ismail, M., Ibrahim, T. A. T., & Zakaria, Z. A. B. (2013). Synthesis and characterisation of calcium carbonate aragonite nanocrystals from cockle shell powder (anadara granosa). *Journal of Nanomaterials, 2013*, 5.

Kandelbauer, A., Tondi, G., Zaske, O. C., & Goodman, S. H. (2014). 6 - Unsaturated polyesters and vinyl esters. In H. Dodiuk & S. H. Goodman (Eds.), *Handbook of Thermoset Plastics (Third Edition)* (pp. 111-172). Boston: William Andrew Publishing.

Kaundal, R., Patnaik, A., & Satapathy, A. (2012). Effect of SiC particulate on short glass fiber reinforced polyester composite in erosive wear environment. *Walailak Journal of Science and Technology (WJST), 9*(1), 49-64.

Kaymakci, A., & Ayrilmis, N. (2014). Investigation of correlation between Brinell hardness and tensile strength of wood plastic composites. *Composites Part B: Engineering, 58*, 582-585.

King, J. A., Barton, R. L., Hauser, R. A., & Keith, J. M. (2008). Synergistic effects of carbon fillers in electrically and thermally conductive liquid crystal polymer based resins. *Polymer composites, 29*(4), 421-428.

Kiss, A., Fekete, E., & Pukánszky, B. (2007). Aggregation of $CaCO_3$ particles in PP composites: Effect of surface coating. *Composites Science and Technology, 67*(7), 1574-1583.

Köhler, S. J., Cubillas, P., Rodríguez-Blanco, J. D., Bauer, C., & Prieto, M. (2007). Removal of cadmium from waste waters by aragonite shells and the influence of other divalent cations. *Environmental science & technology, 41*(1), 112-118.

Kon, E., Filardo, G., Robinson, D., Eisman, J., Levy, A., Zaslav, K., Shani, J., & Altschuler, N. (2014). Osteochondral regeneration using a novel aragonite-hyaluronate bi-phasic scaffold in a goat model. *Knee Surgery, Sports Traumatology, Arthroscopy, 22*(6), 1452-1464.

Krämer, H. (1992). Polyester Resins, Unsaturated. *Ullmann's encyclopedia of industrial chemistry*.

Krupa, I., Cecen, V., Tlili, R., Boudenne, A., & Ibos, L. (2008). Thermophysical properties of ethylene–vinylacetate copolymer (EVA) filled with wollastonite fibers coated by silver. *European Polymer Journal, 44*(11), 3817-3826.

Krupa, I., & Chodák, I. (2001). Physical properties of thermoplastic/graphite composites. *European Polymer Journal, 37*(11), 2159-2168.

Kumlutaş, D., Tavman, I. H., & Turhan Çoban, M. (2003). Thermal conductivity of particle filled polyethylene composite materials. *Composites Science and Technology, 63*(1), 113-117.

Kwok, K. C., Lee, V. K., Gerente, C., & McKay, G. (2009). Novel model development for sorption of arsenate on chitosan. *Chemical engineering journal, 151*(1), 122-133.

Lam, C.-K., Cheung, H.-y., Lau, K.-t., Zhou, L.-m., Ho, M.-w., & Hui, D. (2005). Cluster size effect in hardness of nanoclay/epoxy composites. *Composites Part B: Engineering, 36*(3), 263-269.

Lange, F., & Radford, K. (1971). Fracture energy of an epoxy composite system. *Journal of Materials Science, 6*(9), 1197-1203.

Lasko, C. L., & Hurst, M. P. (1999). An investigation into the use of chitosan for the removal of soluble silver from industrial waste water. *Environmental science & technology, 33*(20), 3622-3626.

Lau, K.-T., Shi, S.-Q., Zhou, L.-M., & Cheng, H.-M. (2003). Micro-hardness and flexural properties of randomly-oriented carbon nanotube composites. *Journal of Composite Materials, 37*(4), 365-376.

Lauke B. (2015) Effect of particle size distribution on fracture toughness of polymer composites considering plastic void growth after particle debonding. *Mechanics Research Communications*; 66: 1-6.

Lent, C. M. (1969). Adaptations of the ribbed mussel, Modiolus demissus (Dillvvyn), to the intertidal habitat. *American Zoologist, 9*(2), 283-292.

Letourneau, D., Deven, J., & Manocha, M. (1976). Structure and composition of the cell wall of Choanephora cucurbitarum. *Canadian journal of microbiology, 22*(4), 486-494.

Liao, H., Mutvei, H., Sjöström, M., Hammarström, L., & Li, J. (2000). Tissue responses to natural aragonite (Margaritifera shell) implants in vivo. *Biomaterials, 21*(5), 457-468.

Mareri, P., Bastide, S., Binda, N., & Crespy, A. (1998). Mechanical behaviour of polypropylene composites containing fine mineral filler: Effect of filler surface treatment. *Composites Science and Technology, 58*(5), 747-752.

Marschall, H., Morch, K., Keller, A., & Kjeldsen, M. (2003). Cavitation inception by almost spherical solid particles in water. *Physics of Fluids, 15*(2), 545-553.

Mckay, G., Blair, H. S., & Findon, A. (1989). Equilibrium studies for the sorption of metal-ions onto chitosan. *Indian Journal of Chemistry Section a-Inorganic Bio-Inorganic Physical Theoretical & Analytical Chemistry, 28*(5), 356-360.

Mehrjerdi, A. K., Adl-Zarrabi, B., Cho, S. W., & Skrifvars, M. (2013). Mechanical and thermo-physical properties of high-density polyethylene modified with talc. *Journal of applied polymer science, 129*(4), 2128-2138.

Michler, G. H., & von Schmeling, H.-H. K.-B. (2013). The physics and micro-mechanics of nano-voids and nano-particles in polymer combinations. *Polymer*.

Mihajlović, S., Sekulić, Ž., Daković, A., Vučinić, D., Jovanović, V., & Stojanović, J. (2009). Surface properties of natural calcite filler treated with stearic acid. *Ceram. Silik, 53*, 268-275.

Mishra, S., Sonawane, S., & Singh, R. (2005). Studies on characterization of nano $CaCO_3$ prepared by the in situ deposition technique and its application in PP-nano $CaCO_3$ composites. *Journal of Polymer Science Part B: Polymer Physics,* 43(1), 107-113.

Móczó, J., Fekete, E., & Pukánszky, B. (2002). Acid-base interactions and interphase formation in particulate-filled polymers. *The Journal of Adhesion, 78*(10), 861-875.

Moczo, J., & Pukanszky, B. (2008). Polymer micro and nanocomposites: structure, interactions, properties. *Journal of Industrial and Engineering Chemistry, 14*(5), 535-563.

Muthusamy, K., & Sabri, N. (2012). Cockle shell: a potential partial coarse aggregate replacement in concrete. *International Journal of Science, Enviroment and Technology, 1*, 260-267.

Nakamura, Y., Yamaguchi, M., Okubo, M., & Matsumoto, T. (1992). Effect of particle size on mechanical properties of epoxy resin filled with angular-shaped silica. *Journal of applied polymer science,* 44(1), 151-158.

Ng, P. K., & Sivasothi, N. (1999). *A guide to the Mangroves of Singapore: 1: the ecosystem & plant diversity. The ecosystem and plant diversity*: Singapore Science Centre.

Othman, N. H., Bakar, B. H. A., Don, M., & Johari, M. (2013). Cockle shell ash replacement for cement and filler in concrete. *Malaysian Journal of Civil Engineering, Penang: University Sains Malaysia*.

Otterstedt, J.-E., & Brandreth, D. A. (1998). *Small particles technology*: Springer.

Ou, Y., Yang, F., & Yu, Z. Z. (1998). A new conception on the toughness of nylon 6/silica nanocomposite prepared via in situ polymerization. *Journal of Polymer Science Part B: Polymer Physics, 36*(5), 789-795.

Papirer, E., Schultz, J., & Turchi, C. (1984). Surface properties of a calcium carbonate filler treated with stearic acid. *European Polymer Journal, 20*(12), 1155-1158.

Patnaik, A., Abdulla, M., Satapathy, A., Biswas, S., & Satapathy, B. K. (2010). A study on a possible correlation between thermal conductivity and wear resistance of particulate filled polymer composites. *Materials & Design, 31*(2), 837-849.

Pechenik, J. A. (2005). *Biology of the invertebrates*: McGraw-Hill, Higher Education.

Penczek, P., Czub, P., & Pielichowski, J. (2005). Unsaturated polyester resins: chemistry and technology. *Crosslinking in Materials Science*, 405-405.

Pierson, H. O. (1993). Handbook of carbon, graphite, diamonds and fullerenes: processing, properties and applications. *Noyes Publications, Park Ridge*.

Plaziat, J. (1984). Mollusk distribution in the mangal. *Hydrobiology of the mangal: the ecosystem of the mangrove forests. Junk, Boston*, 111-143.

Pokroy, B., Fieramosca, J., Von Dreele, R., Fitch, A., Caspi, E., & Zolotoyabko, E. (2007). Atomic structure of biogenic aragonite. *Chemistry of materials, 19*(13), 3244-3251.

Poutiers, J. (1998). Gastropods. *FAO Species Identification Guide for Fishery Purposes. The Living Marine Resources of the Western Central Pacific, 1*, 363-648.

Pukanszky, B. (1990). Influence of interface interaction on the ultimate tensile properties of polymer composites. *Composites, 21*(3), 255-262.

Pukanszky, B. (1995). Particulate filled polypropylene: structure and properties *Polypropylene structure, blends and composites* (pp. 1-70): Springer.

Pukanszky, B., & Vörös, G. (1993). Mechanism of interfacial interactions in particulate filled composites. *Composite Interfaces, 1*(5), 411-427.

Radford, K. (1971). The mechanical properties of an epoxy resin with a second phase dispersion. *Journal of Materials Science, 6*(10), 1286-1291.

Rae, I., & Gibb, S. (2003). Removal of metals from aqueous solutions using natural chitinous materials. *Water science and technology, 47*(10), 189-196.

Reis, J. M. L. D. (2012). Effect of temperature on the mechanical properties of polymer mortars. *Materials Research,15*(4), 645-649.

Rothon, R. N. (2007). *Paper I: The high performance fillers market and the position of precipitated calcium carbonate and silica.* Paper presented at the Proceedings of High Performance Filler 2007, Hamburg, Germany.

Sağ, Y., & Aktay, Y. (2002). A comparative study for the sorption of Cu (II) ions by chitin and chitosan: Application of equilibrium and mass transfer models. *Separation science and technology, 37*(12), 2801-2822.

Sahari, F., & Mijan, N. A. (2011). *Cockle Shell As An Alternative Construction Material For Artificial Reef.* Paper presented at the Proceedings of 3rd International Conference on Applied and Creative Arts, Faculty of Applied and Creative Arts, UNIMAS, Kuching, Sarawak.

Schwartz, J., & Söderholm, K. J. (2004). Effects of filler size, water, and alcohol on hardness and laboratory wear of dental composites. *Acta Odontologica Scandinavica, 62*(2), 102-106.

Semakina, O. K., Phomenko, A. N., Leonteva, A. A., & Rymanova, I. E. (2015). Research of surface properties of fillers for polymers. *Procedia Chemistry,15*, 79-83.

Severini, F., & Gallo, R. (1985). Differential scanning calorimetry study of the thermal decomposition of peroxides in the absence of a solvent. *Journal of Thermal Analysis and Calorimetry, 30*(4), 841-847.

Shafiu Kamba, A., & Zakaria, Z. A. B. (2014). Osteoblasts growth behaviour on bio-based calcium carbonate aragonite nanocrystal. *BioMed research international, 2014*.

Shi, H., Villegas, I. F., & Bersee, H. E. (2017). Analysis of void formation in thermoplastic composites during resistance welding. *Journal of Thermoplastic Composite Materials*, *30*(12), 1654-1674.

Shi, X., Bertóti, I., Pukánszky, B., Rosa, R., & Lazzeri, A. (2011). Structure and surface coverage of water-based stearate coatings on calcium carbonate nanoparticles. *Journal of colloid and interface science,362*(1), 67-73.

Shimpi N, Mali A, Hansora D, Mishra S. (2015) Synthesis and surface modification of calcium carbonate nanoparticles using ultrasound cavitation technique. *Nanoscience and Nanoengineering*, 3(1), 8-12.

Singh, R., Zhang, M., & Chan, D. (2002). Toughening of a brittle thermosetting polymer: effects of reinforcement particle size and volume fraction. *Journal of Materials Science, 37*(4), 781-788.

Sofian, N., Rusu, M., Neagu, R., & Neagu, E. (2001). Metal powder-filled polyethylene composites. V. Thermal properties. *Journal of Thermoplastic Composite Materials, 14*(1), 20-33.

Spanoudakis, J., & Young, R. (1984). Crack propagation in a glass particle-filled epoxy resin. *Journal of Materials Science, 19*(2), 473-486.

Stewart, R. (2004). Plastics USA preview. *Plastics Engineering, 60*(8), 22-27.

Stupp, S. I., & Braun, P. V. (1997). Molecular manipulation of microstructures: biomaterials, ceramics, and semiconductors. *Science, 277*(5330), 1242-1248.

Sudar, A., Moczo, J., Voros, G., & Pukanszky, B. (2007). The mechanism and kinetics of void formation and growth in particulate filled PE composites. *Expr Pol Lett, 1*(11), 763-772.

Sugiyama, M. (2004). *The compressive strength of concrete containing tile chips, crushed scallop shells, or crushed roofing tiles.* Paper presented at the Proc of the International Conference on Sustainable Waste Management and Recycling: Construction Demolition Waste.

Sumita, M., Shizuma, T., Miyasaka, K., & Ishikawa, K. (1983). Effect of reducible properties of temperature, rate of strain, and filler content on the tensile yield stress of nylon 6 composites filled with ultrafine particles. *Journal of Macromolecular Science, Part B: Physics, 22*(4), 601-618.

Suprapakorn, N., Dhamrongvaraporn, S., & Ishida, H. (1998). Effect of $CaCO_3$ on the mechanical and rheological properties of a ring-opening phenolic resin: Polybenzoxazine. *Polymer composites, 19*(2), 126-132.

Suwanprateeb, J. (2000). Calcium carbonate filled polyethylene: correlation of hardness and yield stress. *Composites Part A: Applied Science and Manufacturing, 31*(4), 353-359.

Švehlová, V., & Polouček, E. (1987). About the influence of filler particle size on toughness of filled polypropylene. *Die Angewandte Makromolekulare Chemie, 153*(1), 197-200.

Švehlová, V., & Polouček, E. (1994). Mechanical properties of talc-filled polypropylene. Influence of filler content, filler particle size and quality of dispersion. *Die Angewandte Makromolekulare Chemie, 214*(1), 91-99.

T'Joen, C., Park, Y., Wang, Q., Sommers, A., Han, X., & Jacobi, A. (2009). A review on polymer heat exchangers for HVAC&R applications. *International journal of refrigeration, 32*(5), 763-779.

Tabor, D. (1951). The hardness of metals, Clarendon. *New York*.

Tae, G. H., & Choi, E. S. (2012). *Time Dependent Behavior of Polymer Concrete Using Unsaturated Polyester Resin*: INTECH Open Access Publisher.

Taylor, J. D., & Layman, M. (1972). The mechanical properties of bivalve (Mollusca) shell structures. *Palaeontology, 15*(1), 73-87.

Tekce, H. S., Kumlutas, D., & Tavman, I. H. (2007). Effect of particle shape on thermal conductivity of copper reinforced polymer composites. *Journal of Reinforced Plastics and Composites, 26*(1), 113-121.

Teng, H. (2010). Stiffness properties of particulate composites containing debonded particles. *International Journal of Solids and Structures, 47*(17), 2191-2200.

Thio, Y., Argon, A., & Cohen, R. (2004). Role of interfacial adhesion strength on toughening polypropylene with rigid particles. *Polymer, 45*(10), 3139-3147.

Tudor, H. E., Gryte, C. C., & Harris, C. C. (2006). Seashells: detoxifying agents for metal-contaminated waters. *Water, air, and soil pollution, 173*(1-4), 209-242.

Uddin, M. F. (2009). Effect of nanoparticle dispersion on mechanical behavior of polymer matrix and their fiber reinforced composites. *Thesis (Ph.D) Purdue University*.

Unal, H., Mimaroglu, A., & Arda, T. (2006). Friction and wear performance of some thermoplastic polymers and polymer composites against unsaturated polyester. *Applied Surface Science, 252*(23), 8139-8146.

V., D., P.B., B., & B.A., D. (2012). *Polymesoda bengalensis. IUCN Red list of threatened species. Version 2013.2.* from http://www.iucnredlist.org

Verbeek, C. (2003). The influence of interfacial adhesion, particle size and size distribution on the predicted mechanical properties of particulate thermoplastic composites. *Materials Letters, 57*(13), 1919-1924.

Verdonck, E., Schaap, K., & Thomas, L. C. (1999). A discussion of the principles and applications of modulated temperature DSC (MTDSC). *International journal of pharmaceutics, 192*(1), 3-20.

Vollenberg, P., & Heikens, D. (1989). Particle size dependence of the Young's modulus of filled polymers: 1. Preliminary experiments. *Polymer, 30*(9), 1656-1662.

Wang, M., Berry, C., Braden, M., & Bonfield, W. (1998). Young's and shear moduli of ceramic particle filled polyethylene. *Journal of Materials Science: Materials in Medicine, 9*(11), 621-624.

Wang, X., & Xing, B. (2007). Importance of structural makeup of biopolymers for organic contaminant sorption. *Environmental science & technology, 41*(10), 3559-3565.

Weidenfeller, B., Höfer, M., & Schilling, F. R. (2004). Thermal conductivity, thermal diffusivity, and specific heat capacity of particle filled polypropylene. *Composites Part A: Applied Science and Manufacturing, 35*(4), 423-429.

Weidenfeller, B., Höfer, M., & Schilling, F. R. (2005). Cooling behaviour of particle filled polypropylene during injection moulding process. *Composites Part A: Applied Science and Manufacturing, 36*(3), 345-351.

Wilbur, K. M. (1964). Shell formation and regeneration *Physiology of mollusca* (Vol. 1, pp. 243-282): Academic Press.

Wood, E., & Wells, S. (1995). The shell trade: a case for sustainable utilization. *The Conservation Biology of Molluscs. Occasional Paper of the IUCN Species Survival Commission No, 19*, 41-52.

Wypych, G. (2016). *Handbook of fillers*. Elsevier.

Yan-jiao, G. (2011). *Cadmium and cobalt removal from heavy metal solution using oyster shells adsorbent.* Paper presented at the Consumer Electronics, Communications and Networks (CECNet), 2011 International Conference on.

Yang, K., Yang, Q., Li, G., Sun, Y., & Feng, D. (2006). Morphology and mechanical properties of polypropylene/calcium carbonate nanocomposites. *Materials Letters, 60*(6), 805-809.

Yap, C., & Cheng, W. (2009). Heavy metal concentrations in Nerita lineata: the potential as a biomonitor for heavy metal bioavailability and contamination in the tropical intertidal area. *Marine Biodiversity Records, 2*, e46.

Yusof, M., Ujai, S. J., Sahari, F., Taib, S., & Noor Mohamed, N. (2011a). Application of Clam (*Lokan*) Shell as Beach Retaining Wall. *Proceeding of EnCon, 2011*.

Yusof, M., Mok, Z. Y., Junaidi, E., Taib, S. N. L., & Abdullah, M. O. (2011b). Study of application of clam shell for artificial reef. *Proceeding of EnCon 2011.*

Yusoff, N. A. M., & Long, S. M. (2011). Preliminary study on the accumulation of heavy metal concentration in edible mollusk from Sungai Sematan estuary. *Research Bulletin Faculty of Resource Science and Technology Universiti Malaysia Sarawak, 1*(April 2011), 2.

Zaske, O., & Goodman, S. (1986). Handbook of thermoset plastics. *by SH Goodman*.

Zhang, P., Li, S., & Zhang, Z. (2011). General relationship between strength and hardness. *Materials Science and Engineering: A, 529*, 62-73.

Zhang, Q., Tian, M., Wu, Y., Lin, G., & Zhang, L. (2004). Effect of particle size on the properties of $Mg(OH)_2$-filled rubber composites. *Journal of applied polymer science, 94*(6), 2341-2346.

Zhang, S., Cao, X., Ma, Y., Ke, Y., Zhang, J., & Wang, F. (2011). The effects of particle size and content on the thermal conductivity and mechanical properties of Al_2O_3/high density polyethylene (HDPE) composites. *EXPRESS POLYMER LETTERS, 5*(7), 581-590.

Zhao, H., & Li, R. K. (2006). A study on the photo-degradation of zinc oxide (ZnO) filled polypropylene nanocomposites. *Polymer, 47*(9), 3207-3217.

Zhao, L., Zhang, Y., Miao, Y., & Nie, L. (2016). Controlled synthesis, characterization and application of hydrophobic calcium carbonate nanoparticles in PVC. *Powder Technology*, *288*, 184-190.

Zheng, X., Li, B., Zhu, B., Kuang, R., Kuang, X., Xu, B., & Ma, M. (2010). Crayfish carapace micro-powder (CCM): A novel and efficient adsorbent for heavy metal ion removal from waste water. *Water, 2*(2), 257-272.

LIST OF PUBLICATIONS AND PAPERS PRESENTED

Academic Journals

Mahshuri, Y., & Amalina, M. (2014). Hardness and compressive properties of calcium carbonate derived from clam shell filled unsaturated polyester composites. *Materials Research Innovations, 18*(S6), S6-291-S296-294. (ISI/Scopus publication – IF:0.321)

Mahshuri, Y., Amalina, M., & Nurnadhiah Nadhirah, C. (2014). Thermal conductivity of calcium carbonate filled with unsaturated polyester composites with different filler sizes. *Materials Research Innovations, 18*(S6), S6-340-S346-344. (ISI/Scopus publication – IF:0.321)

Damia, M., Amalina, M., & Mahshuri, Y. (2014). Crystalline properties of polylactide acid-filled aragonite $CaCO_3$ derived from *Polymesoda bengalensis(lokan)* shell. *Materials Research Innovations, 18*(S6), S6-95-S96-99. (ISI/Scopus publication – IF:0.321)

Yusof, M., & Muhammad Afifi, A. (2014). Effect of filler size on flexural properties of calcium carbonate Derived from clam shell filled with unsaturated polyester composites. *Key Engineering Materials, 594*, 57-62 (Scopus publication-SJR:0.19)

Conference/Conference Publications

Mahshuri, Y., & Amalina, M. Hardness and compressive properties of calcium carbonate derived from clam shell filled unsaturated polyester composites. International Conference on the Science and Engineering of Materials (ICoSEM 2013) attended on 13th-14th November 2013, Kuala Lumpur, Malaysia.

Mahshuri, Y., Amalina, M., & Nurnadhiah Nadhirah, C. Thermal conductivity of calcium carbonate filled with unsaturated polyester composites with different filler sizes. International Conference on the Science and Engineering of Materials (ICoSEM 2013) attended on 13th-14th November 2013, Kuala Lumpur, Malaysia.

Damia, M., Amalina, M., & Mahshuri, Y. Crystalline properties of polylactide acid-filled aragonite $CaCO_3$ derived from Polymesoda bengalensis (*lokan*) shell. International Conference on the Science and Engineering of Materials (ICoSEM 2013) attended on 13th-14th November 2013, Kuala Lumpur, Malaysia.

Yusof, M., & Muhammad Afifi, A. Effect of filler size on flexural properties of calcium carbonate Derived from clam shell filled with unsaturated polyester composites. Conference on Advanced Material Engineering & Technology (ICAMET2013) attended on 28th-29th November 2013, Bandung, Indonesia.